



Determination of the effect of mineralogy and texture on the geomechanical parameters of metamorphic rocks

Par

Mahdi Askaripour

**Sous la supervision du prof. Ali Saeidi, et la co-supervision du prof. Alain Rouleau
et du Dr. Patrick Mercier-Langevin**

**Thèse présentée à l'Université du Québec à Chicoutimi dans le cadre du programme
offert conjointement avec l'Université du Québec à Montréal en vue de l'obtention du
grade de Philosophiæ Doctor (Ph. D.) en science de la terre et de l'atmosphère**

Soutenue le 4 mai 2022

Jury:

Réal Daigneault, Professeur, Département des sciences appliquées, Université du Québec à Chicoutimi, Président du Jury

Abtin Jahanbakhshzadeh, PhD, Assistant de recherche, Polytechnique Montréal, Membre externe

Abbas Kamali Bandpay, PhD, Département des sciences appliquées, Université du Québec à Chicoutimi, Membre interne.

Québec, Canada

© Mahdi Askaripour 2022

RÉSUMÉ

Au cours des dernières décennies, l'amélioration des méthodes d'extraction, l'augmentation importante de la demande mondiale en métaux et le cours favorable du marché des métaux ont conduit l'industrie minière à exploiter des gisements de minerai à des profondeurs de plus en plus importantes, jusqu'à quelques milliers de mètres sous la surface dans certains cas. La probabilité de rupture des massifs rocheux, et plus particulièrement l'apparition d'événements violents et potentiellement dangereux tels que des coups de terrain, augmente lorsqu'une excavation souterraine est plus profonde. Ce risque accru d'instabilité de la roche est dû à plusieurs facteurs, incluant les caractéristiques inhérentes de la roche ainsi que les conditions externes à savoir, l'ampleur des contraintes in situ, les perturbations dynamiques, les séquences d'excavation et les structures géologiques. La texture joue un rôle très important dans les paramètres de résistance des roches, qui sont parmi les facteurs les plus critiques dans la stabilité des structures souterraines. À l'exception de certaines roches sédimentaires et volcano-sédimentaires, les roches primaires sont en général relativement homogènes, alors que les roches métamorphisées et déformées ont tendance à avoir des caractéristiques hétérogènes qui influencent leur comportement sous des contraintes élevées. La minéralogie des roches métamorphiques change en fonction du degré de métamorphisme alors que la texture varie en fonction de l'intensité de la déformation. Par conséquent, il est crucial de comprendre les interactions entre les propriétés pétrophysiques et les propriétés mécaniques des roches métamorphiques. Cette étude présente des méthodes pour l'analyse de l'impact de la composition, de la texture et de la minéralogie sur les paramètres géomécaniques des roches métamorphiques. Des outils statistiques sont développés pour palier le faible nombre d'échantillons ayant été soumis à la fois à des tests géomécaniques et à une étude pétrographique sur lames minces.

La mine d'or Westwood, située dans le nord-ouest du Québec, a été choisie comme étude de cas, car ses opérations s'étendent de près de la surface jusqu'à environ 2 000 m de profondeur, avec un potentiel d'exploitation à plus grande profondeur. Les coups de terrain avec projection de roches (« *rockburst* ») ont été enregistrés à Westwood à

différentes profondeurs dans des roches présentant des caractéristiques minéralogiques et texturales contrastées. Dans cette étude, une méthode entièrement nouvelle a tout d'abord été développée pour déterminer la composition minéralogique d'un grand nombre d'échantillons. A cet effet, une étude de lames minces a permis d'établir la minéralogie d'un groupe d'échantillons représentatifs des principales lithologies présentes à la mine. D'autres groupes d'échantillons ont été statistiquement regroupés en fonction de caractéristiques minéralogiques similaires et assignés à des lithologies spécifiques. Cette méthode a permis de classer tous les échantillons selon leur minéralogie. Ensuite, une analyse en composantes principales (ACP) a été utilisée pour déterminer les minéraux métamorphiques ayant la plus grande influence sur la mécanique des roches. Les échantillons utilisés dans l'étude ont été classés en deux groupes, l'un mafique et l'autre felsique. Des essais géomécaniques ont été réalisés en laboratoire. Plus de 1 300 essais de charges ponctuelle (PLT), l'une axiale et l'autre diamétrale, ont été effectués sur les échantillons. Des analyses de l'impact des minéraux métamorphiques sur l'indice de charge ponctuelle (PLI) ont été effectuées par des calculs de régression en composantes principales (PCR). Dans l'étude de l'effet de la minéralogie sur les roches mafiques et felsiques, il est ressorti que le quartz a l'effet le plus élevé sur le PLI axial et diamétral des roches mafiques. Les résultats montrent également que le quartz, l'épidote, l'amphibole et le feldspath sont les minéraux qui peuvent augmenter le PLI axial dans les roches felsiques. Le contraire est observé pour les minéraux tels que la séricite (mica blanc très fin) et le mica blanc (paillettes de muscovite), qui ont plutôt un effet négatif. L'épidote, l'amphibole et le feldspath ont un effet positif sur le PLI axial et diamétral de la roche mafique. Par contre, la chlorite et le mica blanc ont un effet négatif sur le PLI axial et diamétral dans les roches mafiques. De plus, les minéraux qui ont un effet positif sur les essais axiaux ont un effet moins positif sur les essais diamétraux. Les minéraux qui ont un effet négatif sur les essais axiaux ont un effet plus négatif sur les essais diamétraux à cause de la schistosité, qui est une forte anisotropie planaire due à un alignement préférentiel des minéraux métamorphiques.

L'effet des minéraux métamorphiques des roches volcaniques sur la résistance à la compression uniaxiale (UCS) et la résistance à la traction a également été évalué, même

lorsque des échantillons de carottes de haute qualité n'étaient pas disponibles. Une nouvelle approche pour déterminer la relation entre les propriétés des roches et la minéralogie a été développée. Suite à des essais expérimentaux sur un nombre restreint d'échantillons, la méthode inverse de la fonction de distribution cumulative (CDF^{-1}) a été utilisée pour générer suffisamment de données UCS et de résistance à la traction pour effectuer une analyse statistique. Cette méthode génère des données virtuelles à partir de la valeur réelle des données sur la fonction de distribution de probabilité et l'inverse de sa fonction de distribution cumulative. La régression linéaire entre les paramètres géomécaniques et la minéralogie des roches métamorphiques a été examinée à l'aide de deux méthodes statistiques multivariées, l'analyse en composantes principales (ACP) et la régression en composantes principales (PCR) pour les données UCS et celles générées par la résistance à la traction. La CDF^{-1} semble être une méthode efficace pour augmenter le nombre de données géomécaniques en l'absence de données d'essais suffisantes. La comparaison des résultats de plusieurs variables montre que le quartz, l'amphibole, le feldspath et l'épidote ont des effets positifs sur la résistance à la traction et l'UCS, tandis que la chlorite, la séricite et le mica blanc ont des effets négatifs sur les deux tests. Ainsi, l'interaction entre les minéraux et les paramètres géomécaniques de la roche là où il n'y avait pas suffisamment d'échantillons a été déterminée. Les deux techniques, la nouvelle méthodologie proposée et l'inverse de la fonction de distribution cumulative pourraient s'appliquer afin de générer plus de données pour les paramètres géomécaniques et la minéralogie de la roche en fonction de la base de données initiale.

Mots clés: Les coups de terrain, Instabilité du massif rocheux, Paramètres de texture de la roche, Minéralogie, Analyses statistiques

ABSTRACT

In the last few decades, improvements in mining methods, major increases in global demand for metals, and favorable metal prices has led the industry in mining ore deposits at increasingly greater depths below the surface, i.e. up to a few thousand meters in some cases. The probability of rock mass failure, and more particularly violent and potentially dangerous events such as rockbursts, increases when an underground excavation is carried out in deeper excavation. This increased risk of rock instability is due to several factors, including inherent qualities of rock and external conditions, such as the magnitude of in-situ stresses, dynamic disturbances, excavation sequence, and geological structures. The texture of the rocks plays a very important role in their strength parameter, which is one of the most critical factors in the stability of the underground structures. Primary rock types are generally relatively homogeneous, whereas rocks that were metamorphosed and deformed tend to have heterogeneous characteristics that influence their behavior under major stress. The mineralogy of metamorphic rocks changes according to the degree of metamorphism. Therefore, it is crucial to understand the interactions between petrophysical properties and mechanical properties of metamorphic rocks. This work presents an approach to investigating the different effects of metamorphic rock minerals on the state of the geomechanical parameters of rock by employing different statistical methods.

The Westwood gold mine, situated in northwestern Québec, was selected as a case study as mining operations extend from near surface down to about 2,400 m below surface, with potential for mining at greater depth. Rockbursts have been recorded at Westwood at different depths in rocks that show contrasting mineralogical and textural characteristics. In this study, firstly, an entirely new method for determining the mineralogy composition of a large number of samples was developed. For this purpose, thin section study was used to establish the mineralogy of a group of selected samples representative of the principal lithologies present at the mine; other groups of samples were statistically grouped based on similar mineralogical characteristics and assigned to specific lithologies. This method made it possible to classify all the samples according to their mineralogy. Following that, principal component analysis (PCA) was used to determine the metamorphic minerals having the greatest influence on rock

mechanics. The samples used in the study, were classified into mafic and felsic groups. Geomechanical tests were conducted in the laboratory. Then, more than 1,300 axial and diametrical point load tests (PLT) were done on the samples. Analyses of the impact of metamorphic minerals on point load index (PLI) were carried out through principal component regression (PCR) calculations. In the study of the effect of mineralogy on mafic and felsic rocks, it was found that quartz has the highest effect in axial and diametrical PLI in mafic rocks. The results show that quartz, epidote, amphibole, and feldspar are the minerals that can increase the axial PLI in felsic rocks, whereas sericite and white mica have a negative effect on felsic rocks axial PLI. Epidote, amphibole and feldspar have the positive effect on axial and diametrical PLI of mafic rock. On the other hand, chlorite and white mica have a negative effect on the axial and diametrical PLI in mafic rocks. In addition, minerals that have a positive effect on the axial test have a less positive effect on the diametrical test. The minerals that have a negative effect on the axial test have a more negative effect on the diametrical tests because of the effect of schistosity (strong planar anisotropy due to a preferential alignment of metamorphic minerals) on diametrical PLT.

The effect of metamorphic minerals in volcanic rocks on the uniaxial compressive strength (UCS) and tensile strength where high-quality core samples were not available was also evaluated. A new approach in determining the relationship between rock properties and mineralogy has been developed. Geomechanical tests were conducted in the laboratory. After experimental tests on a restricted set of samples, the inverse of cumulative distribution function method (CDF^{-1}) was used to generate sufficient UCS and tensile strength data to perform statistical analysis. This method generates virtual test results based on the probability distribution function and its inverse of the cumulative distribution function. In order to find the relationship between geomechanical parameters and mineralogy of metamorphic rocks, linear regression is examined by using two multivariable statistical methods, principal component analysis (PCA) and principal component regression (PCR) of the UCS and tensile strength generated data. The CDF^{-1} appears to be an effective method to increase the number of the geomechanical data in the absence of enough test data. The comparison of the results of multiple variables shows that quartz, amphibole, feldspar, and epidote have

positive effects on both tensile strength and UCS, while chlorite, sericite, and white mica have negative effects on both tests. So, the interaction between minerals and geomechanical parameters of rock where enough samples didn't exist, was determined.

Keywords: Rockburst, Rock mass instability, Rock texture parameters, Mineralogy, Statistical analysis

TABLE OF CONTENTS

RÉSUMÉ	ii
ABSTRACT	v
TABLE OF CONTENTS.....	viii
LIST OF TABLES.....	xii
LIST OF FIGURES	xv
LIST OF ABBREVIATION	xvii
LIST OF SYMBOLS	xix
DEDICATION.....	xxi
ACKNOWLEDGMENTS.....	xxii
Chapter 1: Introduction.....	1
1.1 Problem statement	4
1.2 Research objective.....	6
1.3 Research methodology	7
1.4 Originality and contribution	9
1.5 Thesis outline.....	10
1.6 References.....	12
Chapter 2: Rockburst in underground excavations: A review of mechanism, classification, and prediction methods	13
2.1 Introduction	14
2.2 Classification of Rockburst	17
2.3 Rockburst Mechanism.....	30
2.3.1 Strainburst	32
2.3.2 Pillar burst	34
2.3.3 Fault-Slip Rockburst	34
2.3.4 Mechanism of coal- gas compound dynamic disasters	38
2.3.4.1 Mechanism of rockburst-induced outburst dynamic disaster	38
2.3.4.2 Mechanism of outburst-induced rockburst dynamic disaster	39
2.3.4.3 Mechanism of outburst and rockburst coupling dynamic disaster.....	39
2.4 Rockburst prediction methods.....	40
2.4.1 Stress Methods	41
2.4.1.1 Rock Brittleness Coefficient.....	42
2.4.1.2 Mean Stress (Tao Discriminant Index) (α)	44
2.4.1.3 Strength Index.....	46
2.4.1.4 Stress Index.....	46
2.4.1.5 Tangential Stress.....	47
2.4.1.6 Turchaninov Method.....	48
2.4.1.7 Failure Duration Index (Dt)	48
2.4.1.8 Grimstad and Barton Classification	49

2.4.1.9 Five Factors	50
2.4.1.10 Hoek and Brown Classification	50
2.4.1.11 Rock Mass Index (RMI)	51
2.4.2 Energy Methods	52
2.4.2.1 Elastic Strain Energy Index	53
2.4.2.2 Linear Elastic Energy and Burst Potential Index (BPI)	54
2.4.2.3 Rock Mass Integrity Coefficient	57
2.4.2.4 Seismic Energy	57
2.4.2.5 Excess Shear Stress (ESS)	60
2.4.2.6 Fractional Energy Release Rate (FERR)	60
2.4.2.7 Burst Efficiency Ratio	61
2.4.3 Other Rockburst Prediction Methods	62
2.4.4 Literature Review on Stress, Energy, and numerical Methods of Rockburst Prediction	67
2.4.5 Discussion	76
2.5 Summary and Conclusion	79
2.6 References	82
Chapter 3: A review on relationship between texture characteristic and mechanical properties of rock	94
3.1 Introduction	95
3.2 Rock textural characteristics	96
3.2.1 Primary structure	107
3.2.2 Secondary structures	107
3.3 Relationships between rock textural characteristics and mechanical properties	112
3.3.1 Mineral composition	113
3.3.2 Grain size, density, and porosity	117
3.3.3 Texture coefficient (TC)	125
3.3.4 Rock anisotropy	127
3.4 Failure criteria of anisotropic rocks	129
3.5 Discussion	138
3.6 Summary and Conclusion	141
3.7 References	142
Chapter 4: Evaluation of the effect of mineralogy on the point load compressive strength of rock	154
4.1 Introduction	154
4.2 Westwood mine	157
4.3 Methodology	161
4.3.1 Assessment of borehole logging data	163
4.3.2 Assessment of rock mineralogy	164
4.3.3 Assignment of thin section results to borehole units	167
4.3.4 Point load test (PLT)	167
4.3.5 Determination of the effect of minerals on PLT by multivariable statistical analysis	168

4.3.5.1 Step 1: Evaluation of most significant independent variable (minerals) through the database by PCA	169
4.3.5.2 Step 2: Evaluation of the effect of mineral composition of rock on the point load compressive strength of rock by PCR.....	169
4.4 Data preparation	171
4.4.1 Point load compressive strength of rock	172
4.4.2 Prerequisite to multivariable statistical analysis	176
4.4.2.1 Linearity testing	176
4.4.2.2 Multicollinearity verification.....	177
4.5 Results and discussion.....	179
4.5.1 Determination of the most important variables.....	179
4.5.2 Determination of the effect of each mineral on point load index by PCR analysis	186
4.6 Conclusion.....	188
4.7 References	189
Chapter 5: Effects of mineral composition on geomechanical parameters of hydrothermally altered volcanic rocks	193
5.1 Introduction	193
5.2 Westwood Mine.....	196
5.3 Methodology	197
5.3.1 Assessment of rock mineralogy	199
5.3.2 Uniaxial compressive strength test (UCS) and Brazilian test	201
5.3.3 Methods of random sampling generation	202
5.3.4 Determination of the effect of minerals on UCS and tensile strength by multivariable statistical analysis.....	203
5.4 Data preparation	204
5.4.1 Laboratory test data for UCS and tensile strength of intact rock	204
5.4.2 Creation of additional data.....	204
5.4.3 Prerequisite to multivariable statistical analysis	219
5.5. Results and discussion.....	221
5.5.1 Determination of the most important variables.....	221
5.5.2 Determination of the effect of each mineral on UCS and tensile strength of rock	228
5.6 Evaluation of model performance	230
5.7 Conclusion.....	231
5.8 References	232
Conclusion	235
Assessing the effect of metamorphic minerals on axial and diametrical point load index using a new mineral assignment method.....	235
Assessing the mineral composition effect on UCS, tensile strength, and PLI.....	236
Perspectives for future research.....	237
APPENDIX I: SUPPORTING INFORMATION FOR CHAPTER 4.....	238

LIST OF PUBLICATIONS	244
JOURNAL PAPERS	244
CONFERENCE PAPERS	244

LIST OF TABLES

Table 2 1. Classification of rockburst proposed by Ortlepp and Stacey (1994).	19
Table 2 2. Classification of rockburst (Hedley, 1992).	22
Table 2 3. Rockbursts and their properties (Li et al., 2017).	25
Table 2 4. Likelihood of strainburst based on the level of deviatoric stress (Castro et al., 2012).	33
Table 2 5. Rockburst intensity based on the brittleness coefficient (Wang & Park, 2001).	42
Table 2 6. Rockburst intensity based on the brittleness coefficient (Zhang et al., 2003).	43
Table 2 7. Rockburst intensity based on the brittle deformation coefficient (Neyman, et al., 1972).	43
Table 2 8. Rockburst intensity based on the rock brittleness index (Tang & Wang, 2002). ..	44
Table 2 9. Rockburst intensity based on the Tao discriminant index (Tao, 1988).	45
Table 2 10. Rockburst intensity classification (Hou & Wang, 1989).	45
Table 2 11. Rockburst intensity classification (Grimstad, 1999).	45
Table 2 12. Rockburst intensity based on the strength index (Hawkes, 1966).	46
Table 2 13. Value of stress index for prediction of rockburst (Yoon, 1994).	47
Table 2 14. Tangential stress criterion (Wang et al., 1998).	47
Table 2 15. Rockburst prediction value based on Russenes method (Russenes, 1974).	48
Table 2 16. Rockburst prediction values based on the Turchaninov scholar (Turchaninov et al., 1972).	48
Table 2 17. Rockburst intensity based on the failure duration index (Wu & Zhang, 1997) ...	49
Table 2 18. Rockburst intensity classification based on the Grimstad and Barton method (Grimstad & Barton, 1993).	49
Table 2 19. Five factors (Zhang & Fu, 2008).	50
Table 2 20. Rockburst intensity based on the Hoek and Brown classification (Hoek & Brown, 1980)	51
Table 2 21. Rockburst intensity based on the R _{Mi} (Palmstrom, 1995).	52
Table 2 22. Energy index value (Kidybiński, 1981).	53
Table 2 23. Rockburst intensity based on the linear elastic energy (Wang & Park, 2001).	54
Table 2 24. BIM indicative values and risk of violent rupture (Aubertin et al., 1994).	56
Table 2 25. Rockburst prediction tendency based on the rock integrity coefficient (Yoon, 1994).	57
Table 2 26. Rockburst classification based on the logarithm of radiant energy (Spottiswoode & McGarr, 1975)	58
Table 2 27. Rockburst intensity quantitative classification criteria based on radiated energy with rock mass failure intensity (Chen et al., 2013).	59
Table 2 28. Rockburst intensity based on the burst efficiency ratio (Singh, 1989).	62
Table 2 29. Prediction of ground conditions for tunneling (Goel & Jethwa, 1995) (u_a is the tunnel closure/deformation, a is the tunnel radius in m, u_a/a is the normalised tunnel convergence in %, N is the stress free Q , J_r is the Barton's joint toughness number and J_a is the Barton's joint alternation number).	63
Table 2 30. Original and modified criterion (Zhao et al., 2017).	65
Table 2 31. RQD classification (Tang, 2000).	66
Table 2 32. Rockburst occurrence based on the energetic rockburst indicator (Tajduš et al., 1997).	67
Table 2 33. Rockburst hazard based on the SED, B_i , and UCS (Lee et al., 2004)	73
Table 3 1. Classifications of rock characteristics (Williams et al., 1982).	96
Table 3 2. Rock textural parameters	98
Table 3 3. Grain Shape Characterization Methods (Cox, 2008).	102

Table 3 4. Summary of the basic microstructural parameters measured by the petrographic image analysis of thin sections (Adopted from Howarth and Rowlands; 1986 Prikrýl, 2006).	103
Table 3 5. Degree of weathering of the rock (Hack and Price, 1997)	106
Table 3 6. Anisotropy classification according to uniaxial compressive strength for different fine-grained rocks (Ramamurthy, 1993).	109
Table 3 7. Anisotropy classification according to point load index (ISRM, 1985)	110
Table 3 8. Anisotropy classification according to ultrasonic wave velocity (Tsidzi, 1997). 110	
Table 3 9. Suggested classes for the classification of anisotropic rocks (Saroglou and Tsiambaos, 2007,a)	112
Table 3 10. Linear regression equations between mechanical properties and quartz-to- feldspar ratio (QFR) (σ_c , I_s50 , and σ_t are in Mpa)	114
Table 3 11. Regression equations between mechanical properties and some aspect of rock texture characteristics.....	115
Table 3 12. Some significant multiple regression equations (Ündül,2016) (C_{plg} . is plagioclase content in %, C_{amf} . is amphibole content in %, C_{GrM} . is groundmass content for all types of composition in %, M_{felds} . is the mass fraction of total feldspar minerals in %, M_q . is the mass fraction of quartz in %. n_t is total porosity, F_{opa} . is Feret's diameter of opaque minerals in mm, F_{bio} . is Feret's diameter of biotite in mm, LOI is loss-on-ignition values in %, E is Young's modulus (Gpa), and UCS is the uniaxial compressive strength of rock in Mpa).....	116
Table 3 13. Relationship between some aspects of rock texture (Ulusay et al.,1994) (Unit weight in KN/m^3 , point load index in MPa, quality index in %, porosity in %, uniaxial compressive strength in MPa, Young's Modulus in (GPa), mean grain size in mm, all petrographic characteristics given as independent variables are in percent).....	118
Table 3 14. Regression equations of mechanical properties and mean grain size. (σ_c is unconfined compressive strength in MPa; σ is compressive strength in MPa; D_{mean} is the mean grain size of all consisting minerals in mm; $D_{meanquartz}$, $D_{meanplagioclase}$, and D_{meank} – feldsparmean are respectively the mean grain sizes of quartz, plagioclase, and K-feldspar minerals in mm; P is the confining pressure in MPa; a and b are empirically determined constants that depend on mean grain size.).....	119
Table 3 15. Empirical equations for prediction mechanical properties (Shakoor and Bonelli, 1991) (uniaxial compressive strength in psi, density in pcf, tensile strength in psi, Young's modulus $\times 10^6$ in psi, absorption in %, total pore volume in cc/gm, sutured contacts in %)	121
Table 3 16. Regression analysis of core samples in the Krishna-Godavari and Gauvery basins (Chatterjee and Mukhopadhyay, 2001) (Uniaxial compressive strength in Mpa, Dry density in kg/m^3 , Tensile strength in MPa, effective porosity in %, Young's modulus in GPa)	122
Table 3 17. Prediction model of multiple regression for physical and mechanical indexes (Tamrakar et al., 2006) (SHH is Schmidt hammer hardness, UCS is uniaxial compressive strength in MPa, DOI is the degree of induration, PLI is point load index in Mpa, porosity in %, G-C in %, G-V in %, Cc in %, E_s is Secant modulus in GPa, E_t is the tangent modulus in GPa. P_{dry} is dry density in Kg/m^3 , and P_{sat} is saturated density in Kg/m^3 .)	123
Table 3 18. Linear regression between mechanical properties and some aspects of crock texture (Ündül, 2016) (M_g is the mass fraction of quartz (%), n_t is total porosity, CGrM is the groundmass content for all types of compositions, C_{grm1} is the groundmass content values obtained only from the specimen of andesitic composition, ν is Poisson's ration, E is Young's modulus (GPa), C_{grm2} is groundmass content values obtained only from the specimen of rhyodacite composition, A_{ngopa} . is the angularity of opaque minerals, F_{opa} . is Feret's diameter of opaque minerals (mm), F_{bio} is Feret's diameter of biotite (mm),	

P_{opa} . is the perimeter of opaque minerals, LOI is an indicator of the weathering stage of rock(%), and UCS is uniaxial compressive strength (MPa).....	124
Table 3 19. Linear regression equations between unconfined compressive strength and texture coefficient (σ_{cis} unconfined compressive strength in MPa; σ_t is indirect tensile strength in MPa; TC is texture coefficient).....	126
Table 3 20. Classification of widely used anisotropic failure criteria (Ambrose, 2014)	132
Table 3 21. List of material constants included in the initial and modified criteria	134
Table 3 22. Mathematical and empirical continuous criteria based on Ambrose (2014), Duveau, Shao, and Henry (1998), and Dehkordi (2008).	140
Table 4 1. Description of the lithological units sampled by the boreholes.....	159
Table 4 2 Mineralogy of samples (All minerals in %, Q is quartz, Chl is chlorite, Car is carbonate, Ser is sericite, Epi is epidote, Amp is amphibole, Plag is plagioclase, Feld is feldspar, Bi is biotite, WM is white mica, Gar is garnet, Apa is apatite, Tou is tourmaline.....)	166
Table 4 3. Number of PLT in each unit of boreholes	172
Table 4 4. Eigenvalue and total variance of extracted components for felsic rocks	180
Table 4 5. Eigenvalue and total variance of extracted components for mafic rocks	180
Table 4 6. Factor loading number for felsic rocks	181
Table 4 7. Factor loading number for mafic rocks.....	183
Table 4 8. Eigenvalue and total variance of extracted components for felsic rocks.....	184
Table 4 9. Eigenvalue and total variance of extracted components for mafic rock.....	184
Table 4 10. Factor loading matrix with Varimax rotation for felsic rock.....	185
Table 4 11. Factor loading matrix with Varimax rotation for mafic rock.....	185
Table 5 1. Mineralogy of samples by thin section study (All minerals in modal %).....	200
Table 5 2. Test of normality.....	205
Table 5 3. Mean and standard deviation of data	205
Table 5 4. Detailed information about generated samples.....	215
Table 5 5. Eigenvalue and total variance of extracted components for felsic rocks.....	223
Table 5 6. Eigenvalue and total variance of extracted components for mafic rocks	223
Table 5 7. Factor loading number for felsic rocks	224
Table 5 8. Factor loading number for mafic rocks.....	226
Table 5 9. Eigenvalue and total variance of extracted components for felsic rocks.....	226
Table 5 10. Eigenvalue and total variance of extracted components for mafic rocks	227
Table 5 11. Factor loading matrix with Varimax rotation for felsic rock.....	228
Table 5 12. Factor loading matrix with Varimax rotation for mafic rock.....	228
Table 5 13. Results of performance analysis of different models.....	230
Table A I. Results of uniaxial compressive strength and Young's modulus of felsic rock....	238
Table A II. Results of uniaxial compressive strength and Young's modulus of mafic rocks	240

LIST OF FIGURES

Figure 1 1. Simplified geological map of Bousquet formation (Mercier-Langevin et al, 2007)...	2
Figure 2 1. Modes of rock mass instability as a function of GSI and the ratio of maximum far-field stress (Adapted from Hoek & Brown, 1980).	16
Figure 2 2. (a) Strainburst, (b) buckling, (c) ejection, and (d) collapsed arch schematic (Ortlepp & Stacey, 1994).....	21
Figure 2 3. (a) Tensile cracking and spalling, (b) tensile cracking and toppling, (c) tensile cracking and sliding, (d) buckling and breaking, (e) tensile shearing and bursting, and (f) arc shearing and bursting (Li et al., 2017).....	24
Figure 2 4. Schematic sketch of rockburst (Zhang et al., 2003)	30
Figure 2 5. Rock mass failure modes under low and high confinement (Diederichs, 1999). .	32
Figure 2 6. Schematic representation of rockburst potentials (Castro et al., 2012).	33
Figure 2 7. Schematic of pillar burst (Sainoki & Mitri, 2017).....	34
Figure 2 8. The complete stress-strain curve (Kidybiński, 1981).....	53
Figure 2 9. Typical stress-strain curve for loading and unloading during uniaxial compression test (Singh, 1988).	55
Figure 2 10. Determination of BIM with uniaxial compression tests (Aubertin et al., 1994). 56	56
Figure 2 11. Prediction of squeezing ground condition (Goel, 1994).....	64
Figure 3 1. Measurements of crystal or grain size by analytical methods (Higgins, 2006).....	105
Figure 3 2. Classification of anisotropy for transversely isotropic rocks (After Singh et al., 1989; β is foliation angle, and σ_c is uniaxial compressive strength of rock).....	108
Figure 3 3. Minimum and maximum orientation of UCS of anisotropic intact rock.....	109
Figure 3 4. Main work on the effect of rock mineralogy on the geomechanical parameters of rock.....	114
Figure 3 5. Correlation between the UCS of Ranyah sandstone and angle of oreintation β (AL-Harhi,1998).....	127
Figure 3 6. Single plane-of-weakness theory (reproduced from Saroglou and Tsiambaos 2007,b).....	133
Figure 3 7. Diagram of strength variation versus β (a) original Jaeger’s criterion (b) extended Jaeger’s criterion (Adapted from Tien and Kuo, 2001).....	134
Figure 4 1. Westwood mine location.....	157
Figure 4 2. Methodology used to evaluate the effect of rock mineral composition on the point load compressive strength of rock.....	162
Figure 4 3. Proposed rock characteristic chart.....	164
Figure 4 4. Thin section photomicrographs of rock samples.....	165
Figure 4 5. Assignment of thin section results to each intact rock sample.....	167
Figure 4 6. Simple schematic of the applied multivariable statistical method.....	169
Figure 4 7. Distribution of axial and diametrical point load indexes.....	175
Figure 4 8. Scatter plot matrix of chlorite – white mica for linearity testing.....	177
Figure 4 9 Variance of inflection factor of all variables prior to PCA.....	178
Figure 5 1 Westwood mine location (IAMGOLD Corporation).....	196
Figure 5 2 Methodology used to assess the effect of rock mineral composition on the UCS and tensile strength of rock.....	198
Figure 5 3. Thin section photomicrographs of rock samples (A and B are graphs observed under polarized trnamitted light;normal transmitted light of felsic rock; C and D are graph presented under polarized trnamitted light normal transmitted light of mafic rock).....	201
Figure 5 4. Q-Q plot of laboratory data of felsic and mafic rocks.....	208
Figure 5 5. Histogram of laboratory tests data of mafic and felsic rocks.....	210
Figure 5 6. Probability density function and cumulative distribution function of variables... 214	214
Figure 5 7. Histograms and Q-Q plots of generated values of variables by CDF ⁻¹ method.....	218

Figure 5 8. Scatter plot matrix of Chlorite and white mica (sericite and muscovite) for linearity testing (Chl and WM) in %219
Figure 5 9. Variance of inflection factor of all variables prior to PCA.....221

LIST OF ABBREVIATION

BPI	Burst Potential Index (%)
BIM	Brittleness Index Modified
SRF	Stress Reduction factor
ERR	Energy Release Rate (KJ m^{-3})
FERR	Fractional Rnergy Release Rate
LESR	Limit Rnergy Storage Rate
LERR	Local Rnergy Release Rate
LDA	Linear Discriminant Analysis
PLSDA	Partial Least-Squares Discriminant Analysis
KNN	K-Nearest Neighbor
ABC	Artificial Bee Colony
SGB	Gradient Boosting Methods
CT	Classification Tree
RF	Random Forest
RBERR	Rockburst Rnergy Release Rate
RQD	Rock Quality Designation
QDA	Quadratic discriminant Analysis
NB	Naïve Bayes
MLPNN	Multilayer Perceptron Neural Network
SVM	Support Vector Machine
GBM	Gradient-Boosting Machine
UCS	Uniaxial Compressive Strength
PLT	Point Load Test
PLI	Point Load Index
PDF	Probability Density Function
CDF	Cumulative Density Function
CDF^{-1}	Inverse of Cumulative Density Function
PCA	Principal Component Analysis

PCR	Principal Component Regression
RMSE	Root Mean Square Error

LIST OF SYMBOLS

$2a$	Length of the flaw
B	Tunnel span or diameter
b_i	Inclined angle of the flaw
B_i	Rock brittleness coefficient
C	Cohesion static fraction
D_t	Failure duration index
C_g	Competency factor
E	Young's modulus (GPa)
E_k	Energy accumulated in the rock mass (KJ m^{-3})
E_n	Energy generated by the tremor in the rock mass
E_R	Stain energy retain
E_D	Permanent strain energy
E_k^0	Energy necessary for initiating the rockburst
E_t	Energy of rock fragments after failures
S	Turchaninov index
S_i	Stress index
T	Energetic rockburst indicator
T_s	Shear strength of rock mass (Tangential stress)
T_d	Dynamic resistance
U	Total peak strength of rock mass before rock deformation
U_t	Permanent deformation of the rock before the peak
$U_{i \max}$	Peak value of elastic strain energy before brittle failure
$U_{i \min}$	Peak value of elastic strain energy after brittle failure
V_c'	Initial strain energy of the rock mass
V_0^2	Average velocity of broken rock mass ejected to an opening
V_{pr}	Rock elastic wave
V_c	Strain energy of the rock mass
V_j	Volume of broken element j
V_{pm}	Rock mass elastic wave speed

f_a	Factor for scale effect of compressive strength
H	Overburden depth
K	Rock brittleness index
K_u	Brittle deformation coefficient
K_V	Rock mass integrity coefficient
L_{ZV}	Break in rock mass volume (t/m^3)
$\lg(E/J)$	Average logarithm of the radiated energy
N	Rock mass number
Q	Barton classification index
R	Elastic strain energy index
V_i	Total volume of broken element in statistic interval i
W_E	Elastic strain energy accumulated before the rock failure
W_P	Plastic strain energy consumed after rock failure
W_{et}	Elastic strain energy
σ_c	Uniaxial compressive strength of rock mass (MPa)
σ_1	Maximum principal in situ stress (MPa)
σ_2	Intermediate principal stress (MPa)
σ_3	Minimum principal in situ stress (MPa)
σ_t	Tensile strength of rock mass (MPa)
σ_v	Overburden stress (MPa)
σ_n	Normal stress (MPa)
ε_b	Strain after peak
ε_f	Strain before peak
μ	Passion ration of rock
γ	Rock density ($kN \cdot m^{-3}$)
A	Mean stress (Tao discriminant index)
μ_s	Static friction angle
η	Burst efficiency ratio
RS_i	Strength index
RM_i	Rock mass index
ρ_v	Average density of broken rock

DEDICATION

To my spouse, Betisa,

Whose patience, encouragement, and moral support were an inspiration to me
throughout this endeavor.

ACKNOWLEDGMENTS

After years of research, working with a great number of expert scientists, engineers and technicians, this thesis has been finally realized and the work has been greatly valued by the scientific as well as non-scientific community. It is a great pleasure to convey my humble gratitude to all the people involved in building up this thesis.

In the first place, I would like to acknowledge, with a deep sense of gratitude and indebtedness, **Prof. Ali Saeidi**, director of my thesis project, for his valuable suggestions and encouragement. Working with Prof. Saeidi has been a great pleasure. His originality, experience and contributions in the field of geomechanics have absolutely nourished the value of this thesis. An extremely busy professional, Prof. Saeidi has always been available and kind in need. It is an honor for me to earn my graduation under his direction.

I would like to express my special thanks to my co-supervisor, **Prof. Alain Rouleau** for his infinite support, encouragement and all his experience that he shared with me. His incessant perseverance and the trust he confided in me helped me mature from a regular graduate student to an individual capable of multi-tasking research projects. It was my great pleasure to work with him for my graduate studies and gain invaluable experience during these years.

I am extremely grateful to my co-director, **Dr. Patrick Mercier-Langevin** for his supervision, advice, continuous guidance, suggestions, scientific and technical criticisms and constant encouragement. His truly scientific intuition exceptionally inspired and helped me grow as a student, a researcher and a scientist.

To **Dr. Mahdiyeh Seifaddini**, research assistant at UQAC, I would like to express my deepest gratitude for finding time and helping me to carry out laboratory tests. Thank you for your technical support.

This research is financially supported by a research grant from the Natural Sciences and Engineering Research Council of Canada (NSERC) and a research grant provided by the Westwood Mine (IAMGOLD). I would like to thank them for their financial support.

I would like to sincerely thank my wife, **Betisa**, for all her kind support, patience and encouragements during these years, without her support it would be so difficult to finish this step of my life. There are no words to thank you **Betisa**.

I do not know how to express my sincere gratitude to my mother and father, **Zahra and Hossein**, my brother, **Hadi**, my father and mother in-law, **Akram** and **Hassan**, and my sisters in-law, **Parisa** and **Parinaz**, to whom I owe all my success and life. They are those who persistently encourage me whenever I face disappointment. Their encouragements, support and sympathy were the essential driving force for me to deal with challenges and pursue my work. My mother never forgot to call every day to listen to me and give me hope and patience for a brilliant future.

It is a pleasure to express my gratitude wholeheartedly to Prof. Saeidi's family for their warm welcome and kind hospitality in Chicoutimi.

I would like to specifically thank my dear friends, Kavand, Mohammad, Peyman, Vahid, Yavar, Mahsa, Alireza and Behzad. Thank you for the confidence you gave me and for all the shared laughs that made some “heavy days” lighter. I wish you all best of luck in your life.

Finally, I would like to thank everybody who was important to the successful realization of this thesis; I apologize that I could not thank them personally one by one.

Chapter 1: Introduction

With the rapid development of tunnels and underground space engineering, rock mechanics problems related to deep burial and high geostress are becoming increasingly serious. Rock mass instability is particularly problematic in deep underground mines, causing injuries to mine operators and damage to underground workings.

Besides, the rock mass is generally substantially heterogeneous with contrasting types of rocks; therefore, it cannot be regarded as a homogeneous medium. Furthermore, a single rock type can have distinct textural properties (e.g., mineral species, grain size, shape, and orientation). Thus, understanding the influence of rock texture on its geomechanical behavior is crucial.

The Westwood Mine was selected due to its unique features in terms of different metamorphic rock, hard rock quality, and the reports of rock mass instability as rockburst. These aspects allow us to figure out effect of different mineralogy of metamorphic rocks on geomechanical parameters of rock mass. The Westwood gold mine is situated in the Doyon property, which is located 2.5 kilometers east of the former Doyon gold mine in the Bousquet Township, approximately 40 kilometers east of Rouyn-Noranda, and 80 kilometers west of Val d'Or in northwestern Québec, Canada. The Westwood mine is owned and operated by IAMGOLD Corporation and was put into production in 2013 (IAMGOLD, 2019). Three sub-vertical, E-W oriented mineralized corridors are present at the mine and mineralization extends from near surface to a depth of more than 2,400 meters below surface.

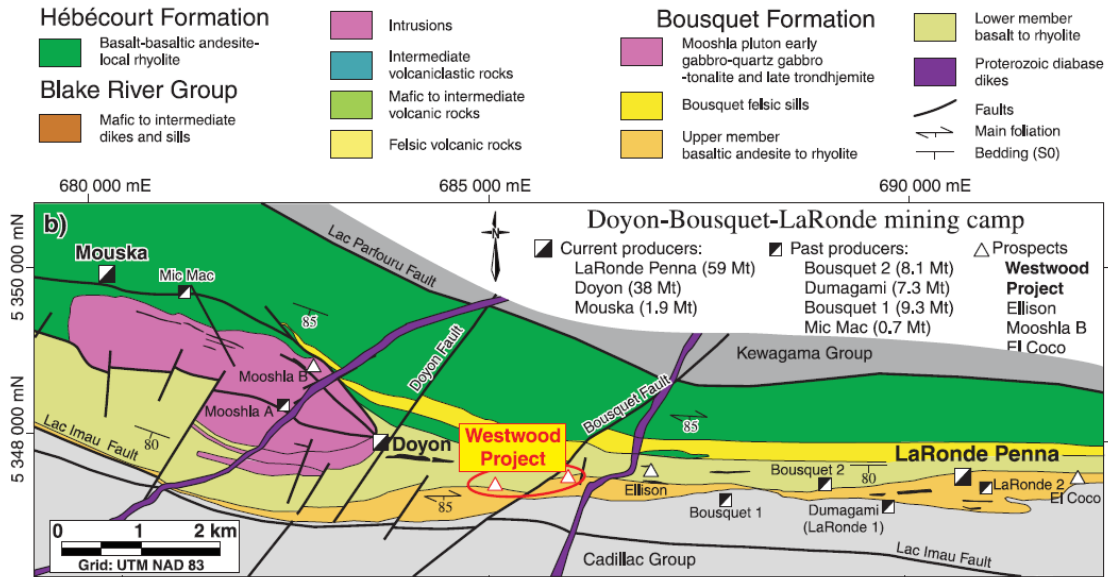


Figure 1. Simplified geological map of Bousquet formation (Mercier-Langevin et al., 2007)

The main focus of Westwood mine in the coming years will be on underground development to increase the number of extraction sectors, on re-excavation in the sectors affected by rockbursts, and development projects to give access to new production areas. The safe development of access drifts and mining stopes is therefore a priority to increase production and ensure the stability of openings and the safety of the workers. However, the geology of Westwood deposit is complex and a major fault named the Bousquet fault is present. Certain mineralized corridors of Westwood mine are located on either side of the Bousquet fault. The rocks hosting the Westwood deposit vary considerably in composition and are complexly intercalated often at the meter scale. The strata are now vertical and lithological contacts are parallel with a penetrative schistosity because of regional deformation. Numerous contact-parallel and high-angle ductile to brittle faults affect the units. All the units were affected to some extent by ore-forming hydrothermal alteration that caused the breakdown of primary minerals, such as feldspar, into phyllosilicates and clays, which were later recrystallized to coarser phyllosilicates and silicate porphyroblasts in a matrix of fine-grained quartz and feldspar. Also, regional metamorphism is transitional from greenschist to lower amphibolites facies, increasing with depth at Westwood. The units are often thin and interleaved, thus creating or generating differential strength in rocks within short distances, thus presenting a day-to-

day challenge for mining operations and causing some rock stability issues (Yergeau, 2015). The geomechanical parameters or geomechanical domains are complex and heterogeneous within the operating zones, thereby making the control of rockburst and the planning of retaining structures difficult. Characterization of the different lithologies and mineralogy of the Westwood deposit is essential to understand the impact of rock quality on the geomechanical parameters of rock and rockbursts.

1.1 Problem statement

The mechanical properties and composition of rocks are commonly used to obtain critical information, such as rock or slope instability, failure mechanism and strength-deformation characteristic assessment. However, much remains to be learned about the influence of the mineralogy of metamorphic rock on its geomechanical behavior. Metamorphic rock refers to the changes in mineral assemblage(s) and texture(s) that result from subjecting a rock to pressures and temperatures that are different from those under which the rock originally formed. As depth increases at Westwood Mine, regional metamorphism shifts from greenschist to lower amphibolites, where the magnitude of in-situ stresses is high and mining operations are increasingly facing the challenge of unstable rock masses, especially the rockburst-type of failure.

Mineral composition is an intrinsic property that influences rock strength. This subject has been studied in recent decades (e.g., Hugman and Friedman, 1979; Bell and Lindsay, 1999; Åkesson et al., 2003; Yusof and Zabidi, 2016). Some of the studies listed above investigated one or very few minerals and therefore did not consider other minerals in rocks, and more particularly minerals of metamorphic rocks. The composition and texture of rock can vary significantly in a single rock mass, which was also overlooked in most studies. Having little knowledge of mineralogy hinders the ability to investigate the mechanical behavior of rock units. In addition, different textures can alter the mechanical properties of rocks with the same chemical and mineral composition. To improve the understanding of rock behavior, and to better know how to analyze rock masses in complex environments, studies on mineral composition and how it affects rock mechanics are important. Such critical information could therefore allow to better estimate the behavior of rock in any underground excavation by evaluating more rock minerals according to their geomechanical properties, such as uniaxial compressive strength (UCS), point load index (PLI), and tensile strength.

The second problem is that high-quality core samples are not always available for laboratory testing to estimate rock strength and elastic parameters. The core sample is an important source of data and it must be complete and in one unbroken piece. However, core samples from underground boreholes are costly and serious issues such as physical

impact of the drilling process or geochemical processes can cast uncertainty on the results. Moreover, collecting samples from all the study sites is sometimes difficult.

The third problem in the study of rock behavior is that thin section analysis would be difficult to perform on all the geomechanical test samples from different excavation sites due to the high cost. In addition, the mineralogy of the samples needs to be determined for geomechanical laboratory tests. Sometimes, the mineralogy of the study site changes due to the intensity of alteration and metamorphic processes (e.g., mineral changes and recrystallization). Thus, the lack of information about the mineralogy could directly affect the estimation of the behavior of the rock in underground excavation. Therefore, determining the sample composition of different mine sites in a simple way is imperative.

The aim of this study is to determine the significant geological parameters that contribute in the geomechanical parameters of the rock in deep hard rock underground mines. This approach can be developed by focusing on rocks with different metamorphic minerals by using the UCS test, point load test, and Brazilian test in conjunction with statistical methods. In addition, a newly developed method is developed to assign the minerals obtained from the thin section study to all selected samples. In the absence of sufficient geomechanical test data, the inverse cumulative distribution function is used in conjunction with statistical analysis (principal component analysis [PCA] and principal component regression [PCR]) to analyze the role of each metamorphic mineral on the mechanical properties of rock. The Westwood underground mine (Québec, Canada) is an excellent case study, where the effect of varying metamorphic grades on the rock mass quality is observed. The general and specific objectives of the thesis are presented in the following section.

1.2 Research objective

The general objective of this research is to determine the effect of rock texture and mineralogy on the geomechanical parameters of intact metamorphic rocks, which are important to the stability of underground structures. The specific objectives of this study are summarized as follows:

- Understand the rockburst mechanism as one of the most important underground stability issues and identify the geomechanical parameters of rock that affect the occurrence of this phenomenon.
- Determine the variations in rock mineralogy and mineral assemblages at different depths in Westwood mine and determine the mineralogy of metamorphic rocks by using thin section study.
- Determine the geomechanical parameters of rock by performing UCS, axial, and diametrical PLI tests, as well as the tensile strength of rocks and their uncertainties for each rock type.
- Develop a new method to predict the mineralogy of each lithological borehole where insufficient data on the mineralogy of the rock are available.
- Determine the effect of rock minerals on the PLI of mafic and felsic metamorphic rocks.
- Determine the effect of rock minerals on the UCS and tensile strength of metamorphic rocks.

1.3 Research methodology

The following procedures describe the methodology used to achieve the objectives of this research. The first step is to conduct two literature reviews. The first one is conducted on the mechanism of rock mass instability in underground excavations. This literature review focuses on one of the main rock mass instability, referred to as rockburst. The mechanisms of rockburst and their classifications were reviewed. Rockburst prediction methods that involve stress and energy methods are also studied. This review helps us identify the important impact of rock parameters on the occurrence of this phenomenon. The detailed methodology of this part is explained in Chapter 2.

A literature review is then conducted on the effect of rock texture on the geomechanical parameters of rock, because the variation of the geomechanical parameters of rock directly impacts rock mass instability. Several parameters determine rock texture, namely, packing density, grain contact, grain shape, mineralogy, and anisotropy. The effects of these parameters on the geomechanical parameters of rock are reviewed. The detailed methodology of this part is explained in Chapter 3.

The next step involves assessing the effects of metamorphic rock minerals on axial and diametrical PLI by using multivariable statistical analysis with a novel method developed to determine the mineralogy of samples. Assessment is accomplished by determining the mineralogy of the rock, assigning the results of thin section studies to all samples, and applying multivariable statistical methods. Multivariable statistical analysis requires the extraction of significant variables due to the large number of input variables. A comparison of the axial and diametrical results of the PLI is performed to determine how metamorphic minerals affected the PLI. Also, the effect of anisotropy on the axial and diametrical PLI is analyzed. The detailed methodology of this part is explained in Chapter 4.

Lastly, the effect of mineralogy of the rock is evaluated on the UCS and the tensile strength of the rock where there are not sufficient geomechanical laboratory data. On the basis of the geomechanical laboratory tests, the inverse cumulative distribution function of obtained geomechanical laboratory results is used to generate enough virtual samples to run multivariable statistical analysis. General multilevel factorial analysis determines

the probability density function of the generated samples. In a subsequent step, multivariable statistical methods are utilized to determine the effect of mineral composition on tensile strength and UCS. The detailed methodology of this part is explained in Chapter 5.

1.4 Originality and contribution

The novelty of this work in terms of the effect of metamorphic rock minerals on the state of the geomechanical parameters of rock is to propose a comprehensive methodology to investigate the significant minerals' combined effects on various modes of mechanical parameters of rock by using different statistical methods.

While the literature is rich in studies that examine the effect of minerals of different rock types on the geomechanical parameters of rock, the literature review indicates that the influence of rock minerals on the geomechanical parameters of rock is limited by the low amount of available geomechanical data from laboratory tests. Previous studies primarily focused on a single mineral's effect, without considering the interactive effects of several minerals within the rock (resulting in variation and instability in the rock mass). Therefore, the aforementioned studies and their corresponding assumptions have a number of drawbacks. A primary problem with such limited studies is that they focus on one or just a few minerals and do not offer much information on other minerals, especially minerals in metamorphic rocks, which are very common in mining environments and other underground excavation works. Most of the studies did not examine how minerals interact with one another or how cumulative influence affects rock strength. As a result, acquiring a comprehensive understanding of how different minerals affect the stability of rock and the geomechanical parameters of the rock seemed challenging. The second problem is that high-quality core samples are not always available for testing rock strength and elastic parameters in the laboratory. The researchers therefore attempted to determine whether the mineralogy is correlated with the mechanical properties of the rock, but insufficient evidence is available for a sufficiently precise regression analysis between geomechanical parameters and rock texture characteristics. Therefore, understanding the interaction between rock texture, petrophysical characteristics, and mechanical properties can be vital for developing geoenvironmental facilities and conducting research. In addition, the mechanical properties of rocks with a given mineral composition can differ according to their texture. The purpose of mineral composition studies is to develop the knowledge and tools needed to understand how rock masses behave in complex environments.

1.5 Thesis outline

This thesis resulted in four scientific journal manuscripts, which are presented in separate chapters (Chapters 2, 3, 4, and 5). Each of these chapters includes an introduction and a conclusion. In addition, a general statement of the problem is accompanied with a brief selected literature review, as well as some of the thesis objectives and outlines as stated in this chapter.

Following the introduction, Chapter 2 presents a summary of the literature review on different modes of underground instability. Rockburst is one of the instability modes of failure that affect the stability of underground excavation in deep mines and especially in metamorphic rocks. The modes of rockburst, such as strain burst, pillar burst, and shear burst, are explained. Then, the mechanism, classification, empirical methods of rockburst prediction, and a comprehensive literature review on a comparison among these methods are presented. This review article was published in *Underground space journal*.

Chapter 3 discusses the relationship between the texture characteristics and the mechanical properties of the rock. The rock texture parameters are explained, and the relationship between the rock texture parameters and mechanical properties of rock such as UCS and tensile strength are discussed. Finally, the failure criteria of anisotropic rocks are explained. This review article was published in *Geotechnics journal* (Askaripour, M., Saeidi, A., Mercier-Langevin, P., Rouleau, A. (2022). A Review of Relationship between Texture Characteristic and Mechanical Properties of Rock. *Geotechnics*, 2(1), 262-296).

Chapter 4 presents an evaluation of the effect of mineralogy of metamorphic rock on axial and diametrical PLI from Westwood mine. Axial and diametrical PLIs of more than 1,300 metamorphic rock specimens from the mine site are carefully measured. The mineralogy of a subset of samples that are representative of the principal lithologies present at the mine is established. The remaining samples are statistically grouped and attributed by using a method developed by the authors to specific lithologies based on similar mineralogical characteristics. The effect of minerals on PLI is then evaluated by PCA and PCR. The results were submitted in *Geomechanics and Engineering journal* (Under journal review).

Chapter 5 presents a new approach that can be utilized to establish a relationship between the geomechanical parameters of rock (UCS and tensile strength) and the

mineralogy of samples at Westwood mine. On the basis of the experimental UCS and tensile strength test, a random sampling method, based on the inverse of cumulative distribution function (CDF^{-1}), is applied to the UCS and tensile strength of the rock to generate enough UCS and tensile strength values for the statistical methods. Then, two multivariable statistical methods, namely, PCA and PCR, are used to figure out the linear regression between the geomechanical parameters and the mineralogy of metamorphic rocks. The results were submitted in International Journal of Mining Science and Technology.

Finally in Chapter 6, conclusions, recommendations and perspectives for future research are presented. In addition to these main body chapters, Appendix I is also included at the end of this thesis providing supplementary information for Chapter 4.

1.6 References

- Åkesson, U., Stigh, J., Lindqvist, J. E., Göransson, M. (2003). The influence of foliation on the fragility of granitic rocks, image analysis and quantitative microscopy. *Engineering Geology*, 68(3-4), 275-288.
- Bell, F. G., Lindsay, P. (1999). The petrographic and geomechanical properties of some sandstones from the Newspaper Member of the Natal Group near Durban, South Africa. *Engineering Geology*, 53(1), 57-81.
- Hugman, R. H. H., Friedman, M. (1979). Effects of texture and composition on mechanical behavior of experimentally deformed carbonate rocks. *AAPG Bulletin*, 63(9), 1478-1489.
- IAMGOLD, (2019), www.iamgold.com/English/operations/westwood/default.aspx.
- Mercier-Langevin, P., Dube, B., Lafrance, B., Hannington, M.D., Galley, A., Moorhead, J., (2007), A group of papers devoted to the LaRonde Penna Au-rich volcanogenic massive sulphide deposit, eastern Blake River Group, Abitibi greenstone belt, Quebec – Preface; *Economic Geology and the Bulletin of the Society of Economic Geologists*.
- Yergeau, D. (2015). “Géologie du gisement synvolcanique aurifère atypique westwood, abitibi, québec”. Ph.D. Dissertation; Université du Québec, Québec, Canada.
- Yusof, N. Q. A. M., Zabidi, H. (2016). Correlation of mineralogical and textural characteristics with engineering properties of granitic rock from Hulu Langat, Selangor. *Procedia Chemistry*, 19, 975-980.

Chapter 2: Rockburst in underground excavations: A review of mechanism, classification, and prediction methods ¹

Abstract

Technical challenges have always been part of underground mining activities, however, some of these challenges grow in complexity as mining occurs in deeper and deeper settings. One such challenge is rock mass stability and the risk of rockburst events. To overcome these challenges, and to limit the risks and impacts of events such as rockbursts, advanced solutions must be developed and best practices implemented. Rockbursts are common in underground mines and substantially threaten the safety of personnel and equipment, and can cause major disruptions in mine development and operations. Rockbursts consist of violent wall rock failures associated with high energy rock projections in response to the instantaneous stress release in rock mass under high strain conditions. Therefore, it is necessary to develop a good understanding of the conditions and mechanisms leading to a rockburst, and to improve risk assessment methods. The capacity to properly estimate the risks of rockburst occurrence is essential in underground operations. However, a limited number of studies have examined and compared yet different empirical methods of rockburst. The current understanding of this important hazard in the mining industry is summarized in this paper to provide the necessary perspective or tools to best assess the risks of rockburst occurrence in deep mines. The various classifications of rockbursts and their mechanisms are discussed. The paper also reviews the current empirical methods of rockburst prediction, which are mostly dependent on geomechanical parameters of the rock such as uniaxial compressive strength of the rock, as well as its tensile strength and elasticity modulus. At the end of this paper, some current achievements and limitations of empirical methods are discussed.

Keywords: Rockburst; Empirical methods; Underground instability; Rockburst prediction methods

¹ Askaripour M, Saeidi A, Rouleau A, Mercier-Langevin P. Underground Space (Online Published).

2.1 Introduction

With a growing demand for mineral resources, the optimization of mining and metals recovery techniques, and the gradual depletion of near surface resources, the industry is mining at increasingly greater depths below surface (Lippmann-Pipke et al., 2011). Underground operations at 2 000 m below surface or more are becoming more and more common, with a few examples at more than 4000 m. One of the most important challenges that underground mining operations must face is the instability of the rock mass (Aydan & Genis, 2001). The shape and type of rock mass instability in deep excavations depend on several factors, including inherent properties of rock, such as strength and brittleness, and external conditions, such as magnitude of in situ stresses, dynamic disturbance, excavation sequence and geological structure (Meng et al., 2017). However, the magnitude of in situ stresses and the quality of rock mass play a significant role in the determination of the rock mass instability in underground excavations. Based on these parameters, nine types of rock mass instability were defined by Hoek and Brown (1980) (Figure. 2.1). The geological strength index (GSI) and a stress parameter (ratio of the maximum principal stress to the uniaxial compressive strength of the rock) are considered in this classification. In low-stress environments, the distribution and the continuity of natural fractures control the failure process in the rock; whereas, in high-stress environments, the failure process is controlled by stress-induced fractures around the excavation zone, which are formed parallel to the excavation walls. In the case of an underground excavation where the magnitude of in situ stresses is relatively high, then slabbing, spalling and zonal disintegration are regarded as the main failure mechanism (Dowding & Andersson, 1986; Martin & Christiansson, 2009; Feng et al, 2012). Thus, rockburst phenomenon is recognized as a specific type of rock mass failure around excavations in hard and brittle rocks and in high-stress environments (the yellow boxes in Figure. 2.1). Although rockbursts must have occurred in mines since the earliest days of underground mining, the first clearly reported cases date from the 18th century. A rockburst was first reported in a tin mine in Britain in 1738, and the first recorded rockburst occurred at a British coal mine in Stafford in 1938. The extreme level of rockburst were announced in 1900 in the Golden Horn area in India, which annihilated the buildings on the ground. Other such event of variable intensity and impact were

reported from mines in Africa, Australia, Canada, China, Chili, Korea, Norway, Russia, Sweden, and the U.S., where important underground excavations and tunnels have been built (Lee et al., 2004; Liu et al., 2015; Ahmed et al., 2017). Rockburst hazard seriously endanger the safety of mine personnel, mine galleries and equipment. In addition, it causes major perturbations to mine development and operations, and can seriously impact on the economic performance of a mine or company. It is therefore primordial to control this issue in underground excavations.

As mentioned, the rockburst may now be a universal problem. The rockbursts usually occur in zones of high magnitude in situ stresses, in hard and brittle rocks. After excavation, the magnitude of in situ stresses and their orientations are perturbed and if the magnitude of induced stresses exceeds the rock strength, cracks are created in the rock and propagate around the underground excavation. Cracks in the rock make it more likely to lose its strength resulting in its failure. There is no consensus on the significant parameters which affect the trigger of a rockburst due to hidden nature of the geological conditions. Nevertheless, a number of research studies have achieved thoughtful and profound results on rockburst mechanisms and their prediction. Zhou et al. (2011) proposed that preexisting cracks in rock are beneficial to the sudden release of energy stored in rock masses. Lu et al. (2018) demonstrated that geological structures, such as faults and joints, bring about sharp stress increase, which may lead to a rockburst. Yang et al. (2017) indicated that high in situ stresses are the main factor that causes strain energy accumulation. Zhu et al. (2010) proposed that a great importance should be attached to rockburst brought by dynamic disturbance during underground mining.

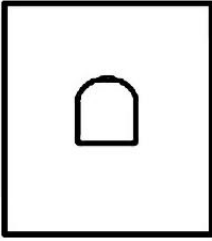
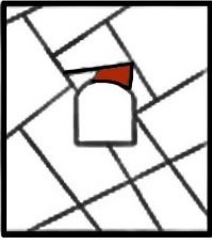
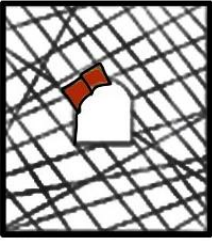
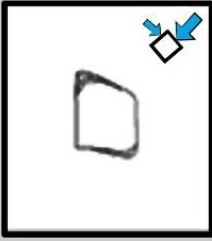
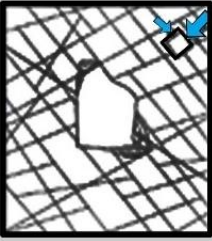
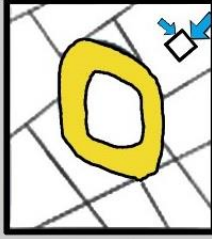
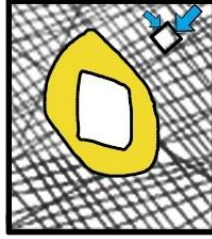
	Massive (GSI >75)	Moderately fractured (50<GSI<75)	Highly fractured (GSI<50)	
Low in situ stress ($\sigma_1/\sigma_c < 0.15$)	 Linear elastic respons.	 Falling or sliding of blocks and wedges.	 Unravelling of blocks from the excavation surface.	$D_1 < 0.4 (\pm 0.1)$
Intermediate in situ stress ($0.4 > \sigma_1/\sigma_c > 0.15$)	 Brittle failure adjacent to excavation boundary.	 Localized brittle failure of intact rock and movement of blocks.	 Localized brittle failure of intact rock and unravelling along discontinuities.	$0.4 (\pm 0.1) < D_1 < 1.1 (\pm 0.1)$
High in situ stress ($\sigma_1/\sigma_c > 0.4$)	 Brittle failure around the excavation.	 Brittle failure of intact rock around the excavation and movement of blocks.	 Squeezing and swelling rocks. Elastic/plastic continuum.	$D_1 > 1.1 (\pm 0.1)$

Figure 2 1. Modes of rock mass instability as a function of GSI and the ratio of maximum far-field stress (Adapted from Hoek & Brown, 1980).

As mentioned above, rockbursts cause substantial damages to underground structures and equipment, and they threaten workers' safety. Thus, this study reviews the global history of rockburst observation in underground excavation and represents some current definitions of rockburst. The recent rockburst classification systems and the underlying rockburst mechanisms are explained as well. Then, this study provides a brief literature review on strainburst, pillar burst, and fault-slip burst. The last part of this paper includes

the introduction of empirical methods of rockburst based on stress and energy methods. Notably, this review paper is based on the utilization of empirical methods of rockburst prediction for several purposes, including the case studies and selection of numerical or intelligent methods.

2.2 Classification of Rockburst

Properly explaining the definitions of rockburst, classification systems, and their mechanism is essential before describing the rockburst prediction methods. As a simple definition of rockburst mechanism, an increase in the tangential stress (σ_{θ}) and a decrease in the radial stress (σ_r) will lead to the release of rock mass elastic energy and the occurrence of a sudden rockburst (Jiang et al., 2010). Several definitions of rockburst have been proposed from the first observation of rockburst at the Kolar gold mine in India and the British coal mine (Cai, 2016). Terzaghi (1946) firstly introduced the definition of rockburst as a sudden separation or falling off of the rock from the tunnel wall due to excessive stress on brittle and hard rocks. Cook (1963) provided the second definition as an uncontrolled disruption of rock associated with a violent release of energy. Obert and Duvall (1967) reported rockburst as any sudden and violent explosion of rock when the amount of stress exceeds the strength of rock mass. They mentioned that rockburst occurs when the uniaxial compressive strength (UCS) of the rock is between 100 and 400 MPa and its elasticity modulus is between 40 and 90 GPa. Russenes (1947) stated that any kind of rock mass failure, such as spalling, ejection, and fracture face, is regarded as rockburst. Blake (1972) suggested that rockburst is a sudden separation and expulsion of rock from its surrounding due to the release of rock energy. Tan (1988) mentioned that not all rock failures are necessarily rockburst. Only the ejection of rock is a rockburst, and the other types of rock failure are due to the brittle fracture phenomenon. From 1980 to 2009, all rockburst definitions focused on the ejection of rock mass when the rock energy is released (Gill et al., 1993; Hedley, 1992; Tao, 1988; Kaiser et al., 1996; Ortlepp & Stacey, 1994; Singh & Goel, 1999; Wang & Park, 2001; Guo & Yu, 2002; Blake, 2003; He, 2005; Zhou et al., 2017). Dietz et al. (2018) defined rockburst as a sudden and violent movement of rock in high-stress environments. All definitions of rockburst seem to be based on the fact that the rock's

elastic energy is suddenly released due to perturbation of the magnitude of in situ stresses during the excavation.

The objective of rockburst classification is to determine the rockburst mechanism in the underground excavation. Rockburst was first classified in 1950 based on its origin (Colson, 1950). Rockburst should be classified in different types based on its intensity, seismicity, the shape of the ejected rock, and others. The rockburst classification is generally categorized into three groups. The first one is a classification based on rockburst type (features of failure plane observed in underground excavation). The second is based on rockburst intensity, and the last one is based on rockburst's triggered mechanism and evaluation of seismic events (Kaiser et al., 1996; Ortlepp & Stacey, 1994). Kaiser et al. (1996) highlighted that changing rock massive volume, tunnel wall deformation, and rock-throwing intensity can be used as the three main criteria for the rockburst classification. In 1996, the rockburst classification included new phenomena: strainburst, slip/fault rockburst, and the combination of two mechanisms (Tang, 2000). Ortlepp and Stacey (1994) classified rockburst on the basis of the source and damage mechanisms. The advantage of this classification is that the type of rockburst was clearly defined on the basis of the energy source and damage mechanisms (Zhou et al., 2018). There are some differences between source damage and mechanism damage. The energy source provides sufficient energy for triggering the rockburst event. This energy can be provided by stored elastic energy in the rock or a seismic event. For example, buckling damage is due primarily to the strain energy stored in the "plates" subjected to buckling. Moreover, the location and source of damage can be coincident or not. In other words, when the location and source of damage are coincident, rockburst occurs in an area where energy was stored. In the case of buckling rockburst, the source of energy is elastic energy which is stored in the rock. However, when the location and source of damage are not coincident, the energy that triggers the rockburst may originate from a seismic event, in which the source of hypocenter may be some distance away from the damage location. For example, when a shear rockburst occurs the energy source may come from a blasting event located far from the location of the ejection damage. Regarding to classification of Ortlepp and Stacey (1994), the location and source of damage are coincident for the first three classes (strain bursting, buckling, and face crush). However,

in the last two classes, the rockburst mechanism includes a shear failure on a plane that could reach hundreds of meters (Ortlepp & Stacey, 1994). Table 2.1 represents the rockburst classification with respect to the seismic events in a tunnel.

Table 2 1. Classification of rockburst proposed by Ortlepp and Stacey (1994).

Seismic event	Postulated source mechanism	First motion from seismic record	Richter magnitude, M
Strain-bursting	Spalling rockburst with a severe ejection of fragments	Usually undetected, could be implosive	-0.2-0
Buckling	Outward expulsion of pre-existing larger slabs parallel to the opening	Implosive	0-1.5
Face crush	Violent expulsion of rock from the tunnel face	Implosive	1.0-2.5
Shear failure	Violent propagation of shear fracture through the intact rock mass	Double-couple shear	2.0-3.5
Fault-slip	Severe renewed movement on existing fault	Double-couple shear	2.5-5.0

Ortlepp and Stacey (1994) categorized rockburst into the four groups on the basis of the damage mechanism, namely, strainburst, buckling, ejection, and arch collapse. Strainburst likely occurs in massive rock masses rather than the jointed or fractured ones, where thin and very sharp edge fragments of the rock are violently separated from the rock mass. The orientation of in situ stresses and the geometry of excavation are

significant factors in determining the location of fragments. Strainburst can occur when the magnitude of field stresses is as low as 15% of the UCS of rock (Singh, 1987). Thus, the occurrence of high-magnitude in situ stresses is not required for strainburst. From the observations of Broch and Sørheim (1984), the probability of rockburst in the form of strainburst increases as the rock mass strength increases. In addition, when a machine-excavated method is used, the probability of strainburst occurrence is more likely to be higher than when using the drill and blast methods. Chen et al. (2013) reported that the strainburst may cause the rocks to be brittle and non-brittle, such as limestone and shale. Moreover, buckling occurs anywhere around the perimeter of the excavation opening, depending on the type of geological structures. This mechanism likely occurs in transverse rocks. The stored energy in a massive rock mass can indicate the buckling potential, whereas some other sources of energy, for example, the wave of the blasting, can cause buckling. The ejection type of rockburst is defined as the ejection of the portion of tunnel hanging or footwall associated with the shock wave. The presence of joints or fractures affects the shape of the ejected block of rocks. The collapsed arch should be considered as the sub-level of the ejection type of the rockburst. This type of rockburst occurs at the geological structure or induced fractures. Figure 2.2 shows such types of rockburst.

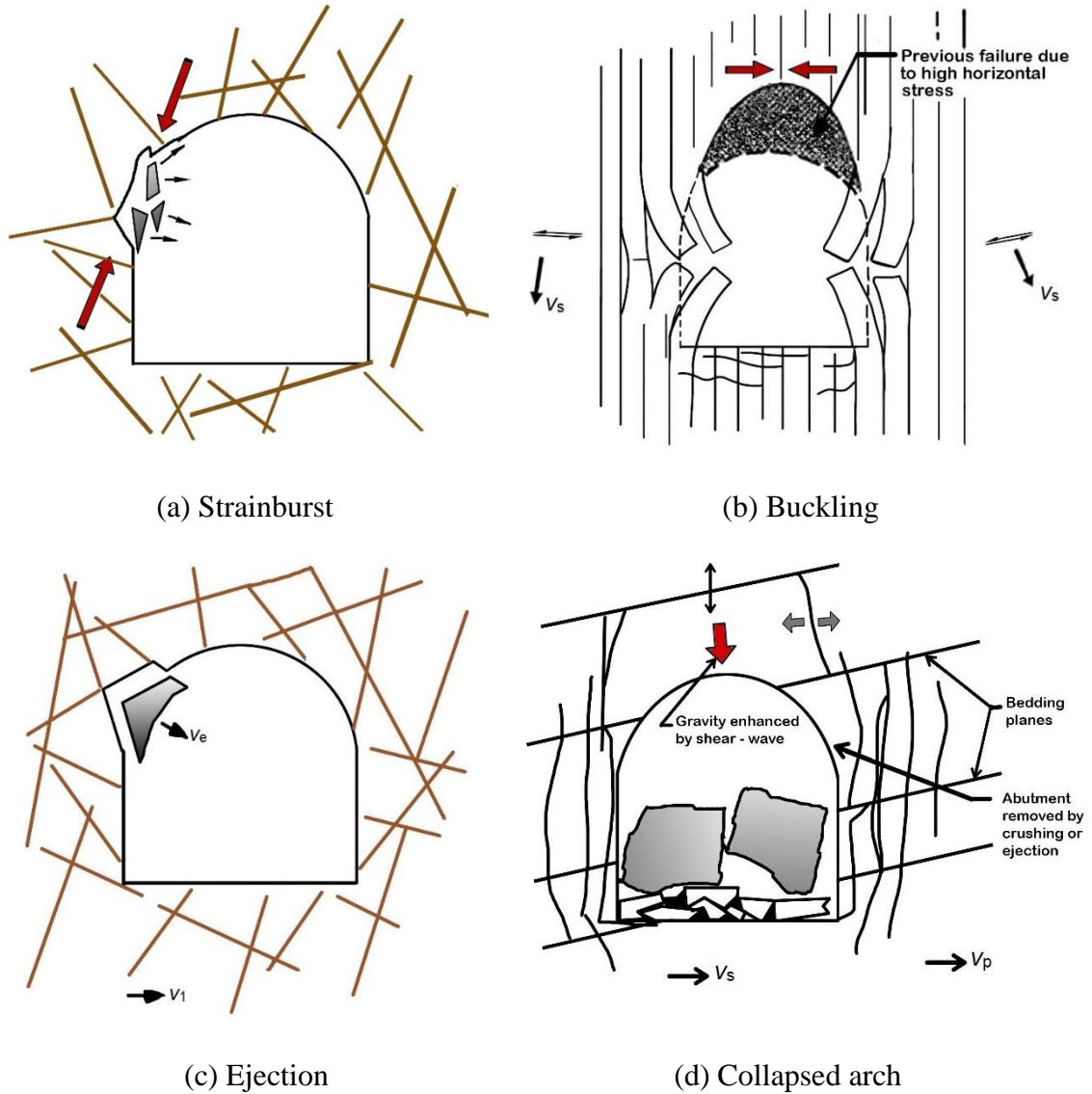


Figure 2.2. (a) Strainburst, (b) buckling, (c) ejection, and (d) collapsed arch schematic (Ortlepp & Stacey, 1994).

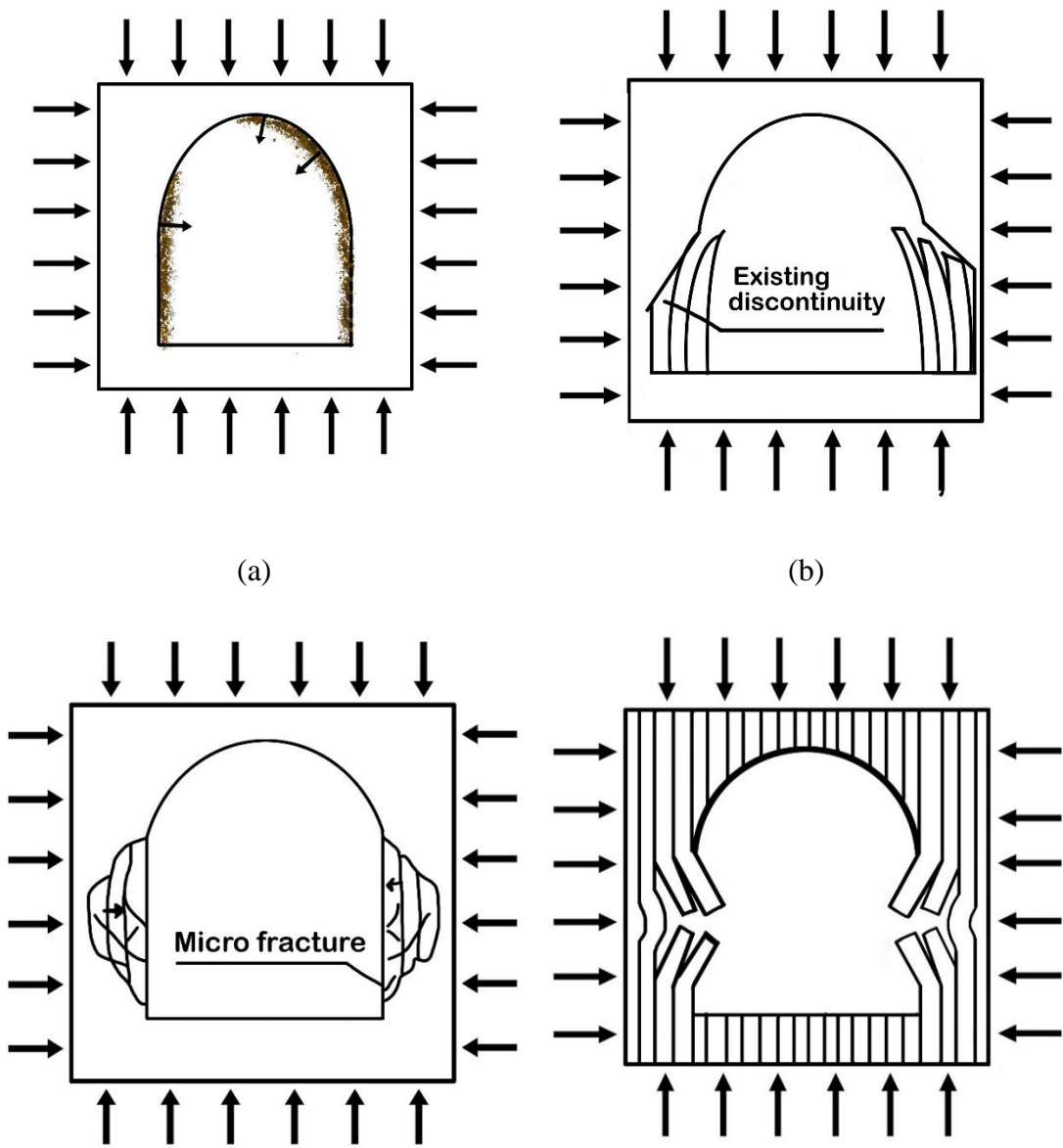
Hedley proposed another rockburst classification system and classified it into three groups: (a) inherent burst, (b) induced burst, and (c) fault-slip burst (Table 2.2) (Hedley, 1992). However, this classification has significant disadvantages because the geomechanical nature of rockburst is not adequately considered, and this classification is not capable of describing the rockburst process mechanism.

Table 2 2. Classification of rockburst (Hedley, 1992).

Rockburst type	Definition
Inherent burst	Magnitudes of in situ stresses are high enough to cause failure in the initial step of excavation
Induced burst	The remaining stresses after the excavation on the pillar
Fault-slip burst	Existing major geological structure

Kaiser et al. (1996) proposed a rockburst classification based on self-initiated and remotely triggered mechanisms. The former refers to those that occur during the excavation; whereas, the latter refers to those that occur after the excavation by a dynamic load added up to the stored energy around the excavation area. Moreover, Kaiser (2009) proposed another classification of rockburst, namely, strainburst, fault-slip burst, and pillar burst. Misich and Lang (2001) defined another rockburst classification based on the time between the unloading and the start of the rockburst. This classification was also based on the source and damage mechanisms of rockburst. Tang (2000) considered three major types of rockburst, namely, strainburst, fault-slip burst, and the combination of the two mechanisms. The strainburst and fault-slip burst are likely to occur underground in a large and deep scale in the excavation area. However, he stated that the most common type of rockburst in a tunnel should be considered strainburst. He et al. (2015) mentioned that strainburst and pillar burst occur in a high-stress environment; whereas, the fault-slip burst occurs in major geological structures far away from the location of underground excavation. Recently, Li et al. (2017) proposed a highly comprehensive classification of rockburst. They used several geological and mechanical rockburst analyses in Chinese mines by considering the rockburst mechanism, severity, and type. Then, they proposed six geomechanical rockburst types based on the failure mechanism as follows: (1) tensile cracking and spalling, (2) tensile cracking and toppling, (3) tensile cracking and sliding, (4) tensile shearing and bursting, (5) buckling and breaking, and (6) arc shearing and bursting. Figure 2.3 depicts the aforementioned six types of rockburst. The rockburst mechanism will be discussed further in Section 2.2. As mentioned earlier, the basic

classification system classifies the rockburst as strainburst and fault/slip burst. Hence, tensile cracking and spalling are referred to as strainburst, and tensile cracking sliding type is referred to as the slip/fault burst. The other four geomechanical types of rockburst, proposed by Li et al. (2017) cannot be regarded as either strainburst or slip-fault burst due to the combination of initial crack mechanism and the development of micro-cracks in intact rocks. Table 2.3 shows the properties of six geomechanical types of rockburst.



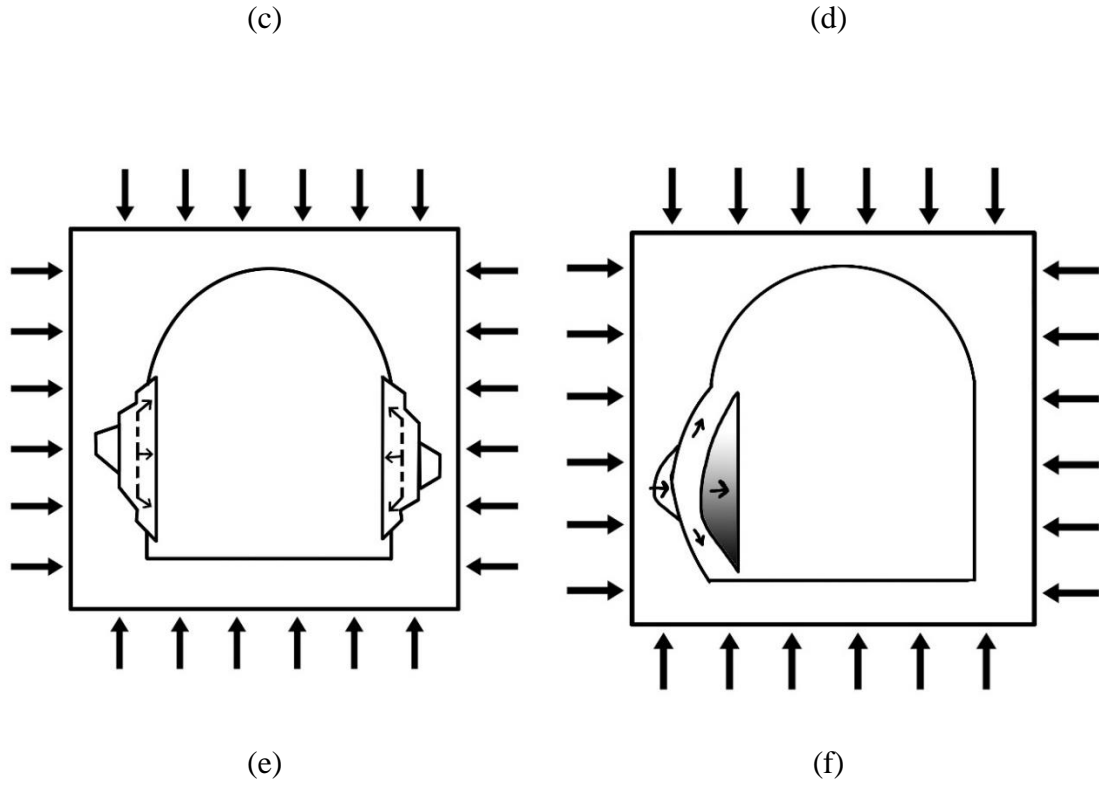


Figure 2.3. (a) Tensile cracking and spalling, (b) tensile cracking and toppling, (c) tensile cracking and sliding, (d) buckling and breaking, (e) tensile shearing and bursting, and (f) arc shearing and bursting (Li et al., 2017).

Table 2 3. Rockbursts and their properties (Li et al., 2017).

Characteristic	Tensile cracking and spalling	Tensile cracking and toppling	Tensile cracking and sliding	Buckling and breaking	Tensile shearing and bursting	Arc shearing and bursting
Structure of rock masses	Existing micro-fractures parallel to the free surface	Layered structure	Layered or massive with an existing fracture zone	Layer or layer-like	Intact or massive	Intact or massive
Cracking property	Tensile	Tensile	Tensile and shear	Tensile	Tensile, shear, and tensile-shear	Tensile and shear
Failure plane	Flat or conchoidal with step-like boundaries	Irregular or stepped	Stepped or curved	Stepped or conchoidal	Stepped or arc-like	Elliptical or dome-like
Energy release	Negligible	Little	Moderate	Moderate	Large	Large or very large

As mentioned earlier, the other rockburst category is based on intensity. The intensity grade varies from low to high; however, these grades would be different for each classification. Russenes (1974) proposed the first classification based on the severity of rockburst and categorized the rockburst into four groups: none, weak, moderate, and severe rockburst. Tan (1992) also proposed another rockburst classification system based on the intensity, where many laboratory tests were conducted considering the geomechanical characteristic and the failure type and shape. Thus, the rockburst magnitude was classified into none, weak, moderate, and severe. Moreover, Brauner (1994) proposed a rockburst classification system with three categories based on the

extent of rock destruction. Kaiser et al. (1996) found that rockbursts could be classified into minor, moderate, and major groups. According to this study, the intensity of rockburst should be derived from empirical evidence, the depth of the damage zone in the rock mass, and geometric considerations. Chen et al. (2013) proposed a quantitative rockburst evaluation method based on the radiated energy of rockburst, which could be recorded through microseismic technique. Zhang and Dai (2017) proposed four rockburst intensity grades, from grade I (no intense) to IV (extremely intense rockburst) based on the index distance and uncertainty measure.

In coal mines, coal-gas explosion represents an extra type of rockburst that can cause serious dynamic disasters in deep mining (Li et al., 2015; Zhu et al., 2016). Coal-gas outbursts and rockbursts usually occur independently. However, increasing mining depth in recent years has caused these two dynamic disasters to coexist, be mutually induced, and combined, resulting in new types of dynamic disasters called coal-gas compound dynamic disasters (Pan, 2016; Sun & Li, 2011).

Asvershin (1959) studied the question whether gas explosions cause rockbursts, or rockburst causes gas explosions, or whether both can occur at the same time. Shepherd et al. (1981) classified coal and rock dynamic disasters into the coal and gas outbursts, bumps or rockburst and outburst from the floor or roof strata. The international classification of coal and rock dynamic disasters developed by Dechelette et al. (1984) comprises coal (rock) and gas outbursts, gas outbursts, rockbursts, and mine tectonic phenomena. Zhang (1991) studied the mechanisms of coal and gas outbursts, and rockbursts, established the occurrence criteria for each disaster, and then developed the unified stability-losing theory of the two types of disasters. Li et al. (2005, 2007) discussed how coal-gas outbursts are induced by rockburst and developed the correlation between rockburst and gas outbursts in deep mining. As a result, they suggested high gas pressure would play a very significant role in the triggering of a rockburst. Fisher (2013) investigated the effect of gas emissions on rockburst. As he pointed out, high-pressure gas triggers rockbursts by extending the plastic disturbed zone. Cao et al. (2015) developed an evaluation system for coal and rock dynamic disasters, in which the dynamic disasters are divided into typical and atypical disasters based on the unified energy equation and the concept of degrees of gas participation in coal and rock dynamic

disasters. Typical dynamic disasters are coal and gas explosions and rockbursts, while atypical dynamic disasters are coal-gas impacts and coal-gas extrusions. In the case of atypical dynamic disasters, burst tendency is the primary classification indicator. If the coal samples burst, the type of disaster is coal-gas impact, otherwise, it is coal-gas extrusion. Compound dynamic disasters may also exhibit a low index phenomenon, that is, coal and rock without burst tendency may still produce a rockburst disaster under the influence of gas outbursts. Pan (2016) classified coal and rock dynamic disasters according to the relative release of gas internal energy and coal-rock elastic energy as follows: coal and gas outburst, outburst-rockburst compound disaster, and rockburst compound disaster. Such classification represents a significant improvement relative to the previous classifications. However, compound dynamic disasters are determined by the relative amount of two energy types released, without considering the order in which the energy types are released, which does not allow to take into account mutual induction and mutual transformation between coal and gas outburst and rockburst. The researches of Fisher (2013) and Li et al. (2015) show that the expansion energy of high-pressure gas desorption has a positive effect on triggering rockbursts. Therefore, it appears that a gas outburst can induce or increase the likelihood of a rockburst, which is caused by the dynamic energy released from the gas pressure, leading to a new classification of coal and rock dynamic disasters as follows: (1) Rockburst-induced outburst dynamic disaster means that (coal and) gas outburst is induced by the rockburst in a short time; (2) Outburst-induced rockburst dynamic disaster means that rockburst is induced by the (coal and) gas outburst in a short time; (3) Outburst and rockburst coupling dynamic disaster means that (coal and) gas outburst and rockburst occur at the same time and coexist each other (Wang & Du, 2019). There is no indication of a chronological sequence between these events.

Besides classification of coal and rock dynamic disaster, there is another phenomenon known as coal bumps. This is a dynamic phenomenon, which will cause sudden and severe damage to underground mining. It basically involves the release of elastic deformation energy from the surrounding rock mass of a mining tunnel, characterized by loud noises and the projection of large quantities of rock or coal mass. In general, coal bumps are characterized by the following features: (1) There are no clear macro-

precursors to coal bumps; (2) They cannot be predicted in terms of magnitude, location, and likelihood of occurrence; (3) Other dynamic disasters can also co-occur, such as gas eruptions, gas explosions, and water inflow (Jiang et al., 2014). Phillips (1944) categorized the coal mine bumps as either pressure or shock bumps. A pressure bump occurs when a strong or brittle pillar in a developed area is statically stressed past the failure strength of the coal. A shock bump is caused by dynamic loading of the coal through either dramatic change in the stress distribution within the overlying strata or by an abrupt loading of the coal ahead of the face resulting from dynamic roof rock failure. Spalding (1948) explains that certain types of rock bumps can be classified as ring, shear, or pillar bumps. Holland (1954) indicated that many shock bumps in a mine were actually caused by coal mined under high static loads. As a result of this study, bumps previously thought to be caused by dynamic loading are actually the result of local variations in mine geology and coal properties or improper mine design and sequencing, which created zones of high stress. Zanski et al. (1964) concluded that bumps are classified into seam, roof, and floor bumps based on where they occur. According to Qian & Zhou (2011), coal bumps can be divided into sliding coal bumps resulting from fault slips and strain energy bumps resulting from coal mass failures. In terms of geological conditions specific to a site, coal bumps can be classified into three categories based on their patterns and associated factors (Jiang et al., 2017): **Type I:** Material failure is the cause of coal bumps. Cracks can form, develop, spread, penetrate, and propagate during the excavation of tunnels or longwall panels. As the surrounding rock or coal mass reaches its maximum strength, coal bump can occur. **Type II:** Coal bumps are caused by hard roofs or floors. There can often be large stiffness differences between roof/floor strata and coal seams when coal bumps occur (Rostami et al., 2015). During mining, the hard roof or floor may release accumulated strain energy instantly. The coal may develop coal bumps or move horizontally toward the tunnel in this case. **Type III:** Coal bumps are caused by tectonic structures. During the long-term evolution of rock strata characterized by strong tectonic structures, a huge amount of elastic energy can accumulate in the regions adjacent to the tectonic structures. Mining nearby may also reactivate faults, resulting in coal bumps. In practice, high in situ stress may result in fault reactivation, release of high pressure and

coal bumping as mining proceeds. The degree of damage caused by coal bumps of Types II and III is greater than that caused by Type I. (Jiang et al., 2017).

As mentioned before, the classification of rockburst evaluates not only the intensity of rockburst but also the type and shape of the failure zones. However, obtaining additional information about the mechanism of rockburst provides complete and comprehensive information on the rockburst issue in the underground excavations. In the next section, the mechanism of rockburst will be discussed and reviewed.

As the discussion on this section, rockburst classification is typically used to determine how they occur. Several distinct types of rockbursts have been identified based on the rockburst phenomenon, the rockburst mechanism, the rockburst energy and stress, the scale and location of rockbursts, and the cause and effect of rockbursts. Rockburst classification methods such as those mentioned above have been widely used by mining and geotechnical engineers owing to their simplicity and flexibility. However, even when they share the same methodology, the different evaluation indices can generate results that are conflicting. Rockbursts were first classified based on shape and rock-projection intensity, such as the classifications by Russenes (1974), Brauner (1994), Tan (1992), and Kaiser et al. (1996). One shortcoming of such classifications is that they do not consider underlying mechanisms, seismic events, and rockburst shape. Furthermore, there is no sufficient information about fault slip burst. The classification of Kaiser et al. (1996) has the advantage of considering two significant mechanisms of rockburst, such as self-initiated or remotely triggering, as well as its intensity. More recent classifications are based on the idea that rockburst events should be categorized based on the mechanism and severity (e.g., Tang, 2000; Kaiser, 2009; He et al., 2015). One of the best rockburst classifications, by Li et al. (2017), defined six classes of rockbursts and their mechanisms. The advantage of that classification is that the different types of rockburst are described according to their failure plane, type of cracking (tensile or shear), and amount of energy released. By combining this classification with mine staff observations and the recorded seismic data of a mine, the best classification of rockbursts can be determined for a mine site. Moreover, according to this classification of rockburst, it is possible to categorize rockburst predictions into two categories: short-term ones, which can be used during the life of a project, and long-term ones, which are useful at the design

stage. The short-term prediction of rockbursts primarily relies on field monitoring but also includes micro-seismic, electromagnetic, drilling cutting, micro-gravity, and infrared thermal imaging. After underground development is complete, short-term rockburst prediction methods can be used. It is only possible to install monitoring equipment in underground excavations after tunneling or drifting underground. The design stage of future excavations should use a long-term rockburst prediction method in order to avoid areas with high rockburst hazard during excavation. A long-term rockburst prediction is based on both rockburst potential and field conditions. Scholars have proposed several indicators to best evaluate burst potential. These methods will be discussed in Section 2.4.

As robust and complete a classification schemes can be, rockbursts evaluation and classification depend on engineers' evaluation and access to data for each specific case (e.g., length, shape, and intensity) and there is a human factor that cannot be eliminated in classifying rockbursts. This implies that a similar environment or event may lead to different measures depending on how the classification was made, and by whom. Thus, the proposed method for unified rockburst classification needs to be implemented in future research.

2.3 Rockburst Mechanism

When the accumulated strain energy exceeds the energy storage limit of the rock mass, excessive energy will be released suddenly, and the rock mass around the opening will be violently ejected from the rock mass domain, as shown in Figure. 2.4.

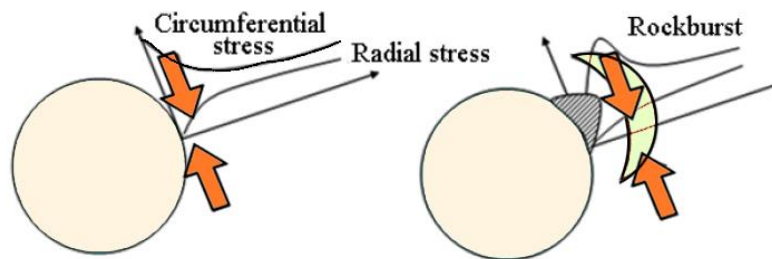


Figure 2.4. Schematic sketch of rockburst (Zhang et al., 2003)

The aspects of rockburst mechanisms are defined by two main mechanisms: damage and source mechanisms. The latter causes the seismic event, and the hypocenter of the source mechanism can be far away from the location of the damage. The former directly causes the damage, and its location is identical to the damage site (Ortlepp & Stacey, 1994). From the studies in the Canadian hard rock mines on rockburst hazards, the rockburst damage mechanisms depend on the level of underground confinement (Kaiser et al., 2000). Accordingly, the rockburst mechanism could be classified into three groups, namely, strainburst, pillar burst, and fault-slip burst. Strainburst occurs under low-confinement conditions (reducing the radial stresses and increasing the tangential stresses), whereas the pillar burst occurs at the boundary between low and high confinement conditions. Moreover, the fault-slip rockburst occurs in high confinement conditions. Figure 2.5 shows the classification of rock mass failure modes developed based on the level of underground confinement. The above-mentioned modes of underground instability and their corresponding desired occurrence conditions (low and/or high confinement conditions) are in accordance with the elementary rockburst classification proposed by Board (1996).

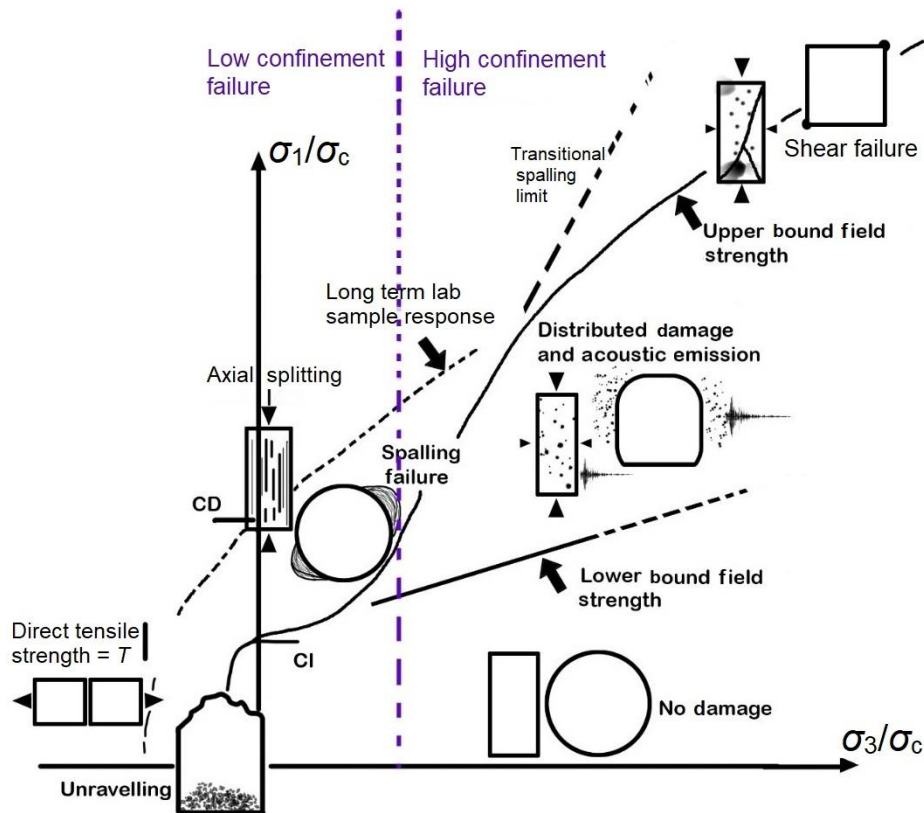


Figure 2.5. Rock mass failure modes under low and high confinement (Diederichs, 1999).

2.3.1 Strainburst

As mentioned before, the rockburst is classified into three groups, as shown in Figure 2.6 (Castro et al., 2012). Rock mass damage at low-confinement conditions can be generally divided into two categories: (1) stress-induced failure with slabbing and spalling failure plane and (2) structurally controlled gravity-driven failures (Kaiser et al., 2000). However, the first group is demonstrated as strainburst depending on the range of deviatoric stresses. According to the strainburst mechanism (decreasing the radial stress and increasing the tangential stress), rock mass failure develops on the perimeter of the excavation under low-confinement conditions. Under a low-confinement condition, the fractures intend to extend in the direction of the major induced stress and develop sub-parallel to the excavation boundary when the rock is exposed to the compressive loads (Diederichs, 1999). Strainburst likely develops by the stress-induced spalling and slabbing failure. An important characteristic of strainburst is that no damaging vibration occurs prior to rock failure. Damaging vibration is generated during and after bursting.

The deviatoric stress level was defined to evaluate the strainburst severity and rock mass damage around the excavation zone (Castro et al., 2012), as shown in Table 2.4.

Table 2 4. Likelihood of strainburst based on the level of deviatoric stress (Castro et al., 2012).

$\sigma_1 - \sigma_3/UCS$	Rock mass damage	Likelihood of strainburst
0.35	No to minimum	No
0.35–0.45	Minimum	No
0.45–0.6	Moderate	Minor
0.60–0.7	Moderate to major	Moderate
>0.7	Major	High

Notably, the deviatoric stress only considers the induced principal stresses and the UCS of intact rock. However, the ground stress cannot represent the potential energy release driven by the loading system, given that the potential energy release depends on the loading stiffness (loading stiffness is the degree to which an object resists its deformation in an applied load) (Duan et al., 2019).

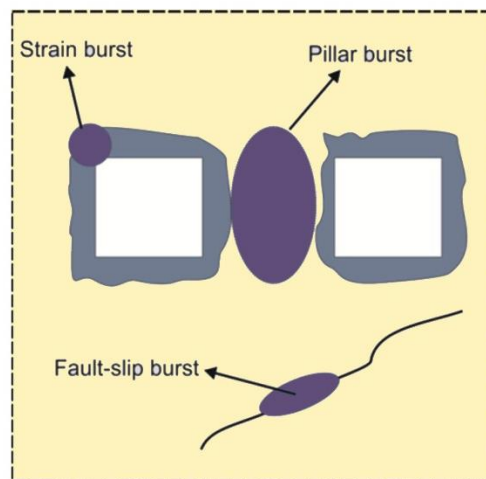


Figure 2 6. Schematic representation of rockburst potentials (Castro et al., 2012).

2.3.2 Pillar burst

In deep underground hard rock mines, pillars have the potential to cause rockburst because of the high strain energy stored within them and the brittle characteristics of the rock mass (Sainoki & Mitri, 2017; Hauquin et al., 2018). Pillar burst occurs under a low to moderate confinement condition (Figure 2.7). Based on the pillar's width to height ratio (W/H), several confinement conditions develop in its core. With low W/H (approximately < 1.0), no or little confining stress is developed within the pillar. The confining stress increases as this ratio increases, resulting in two failure processes: surface spalling along the skin of the pillar and in the core of the pillar. The first mechanism is related to the occurrence of strainburst around drifts and stopes, and the second one is related to the development of short tensile cracks and their subsequent coalesce along the plane of induced shear stress. Many informative articles about the mechanism and effect of several parameters on pillar burst exist. However, these articles only focused on the strainburst and fault-slip burst.

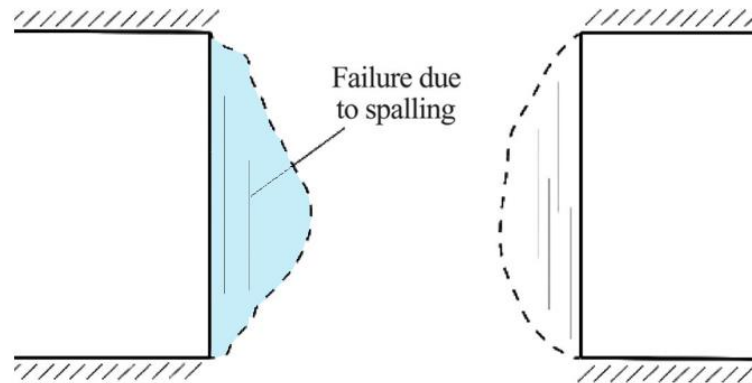


Figure 2.7. Schematic of pillar burst (Sainoki & Mitri, 2017).

2.3.3 Fault-Slip Rockburst

Fault-slip or shear burst occurs under high confinement conditions and is triggered by stope extraction, drift development, and production blasting, which reactivated the pre-existing faults or formed the seismically active structural zones. The determination of strainburst or pillar burst is less complex than that of the fault-slip burst due to two main reasons. First, the determination of the physical and mechanical properties of the fault surface through laboratory and numerical studies could be very challenging. Second, the

evaluation of stress re-distribution around the excavation opening could be a complicated task. Several friction models of fault-slip have been proposed to simulate the dynamic behavior of shear sliding, such as static-dynamic friction, velocity-dependent, slip-weakening, and rate and state-dependent models, to find a way to obtain the properties of fault (Sainoki & Mitri, 2014). Moreover, four vital factors can affect fault-induced slip in underground excavations. The first factor is called unclamping, which occurs on two scales: (1) the local unclamping as a result of overlapping the induced tensile stress field with a nearby pre-existing geological fault and (2) the regional unclamping, which occurs when the extension and size of mining excavation are sufficiently large. The difference between local and regional unclamping is that in regional mechanisms, slip is far away from the free face. The second important factor is daylight, which becomes vital when the actual underground excavation intersects a geological fault. In this situation, enough surface is provided for the fault to move toward the excavation area, and a considerable amount of energy is released, which could be accompanied by a large seismic event. The other important factor is stress rotation caused by perturbation of in situ stresses after excavation. In this situation, the major induced stress can switch from normally orientation to parallel with the fault plane. Finally, pillar shear is the last vital factor that contributes to fault-slip. Pillars can inhibit the displacement of the rock mass on one side of the fault and can also move freely on the other side. However, the dynamic behavior of fault-slip burst has not been fully understood, because the effect of physical characteristics of faults and the uncertainty of scale effect have not yet been completely investigated. Vasak et al. (2008) reported that the majority of microseismic events during mining excavation did not occur immediately after the stope excavation. Dowding and Andersson (1986) reported that with the increasing depth of excavation and the width and area of production face, the possibility of fault-slip burst also increases. However, the shear bursts occurred along with a new or major pre-existing geological structure. Zhang and Fu (2008) used a continuous numerical model to analyze the effect of the fault on the occurrence of rockbursts in the tunnel. Sainoki and Mitri (2014) proposed dynamic modeling of fault-slip with Barton's shear strength. To this end, Barton's shear strength was inputted into the FLAC3D to analyze the effect of the fault-slip on underground excavation. The results demonstrated that the fault roughness has a

significant effect on the seismic events. The chance of seismic events increases as the fault surface roughness increases. Moreover, the fault surface roughness affects the seismic moment and radiated energy. Sainoki and Mitri (2016) conducted a numerical analysis on dynamic behavior of fault in underground mines. The results showed that the fault friction angle has a significant effect on the maximum dynamic shear displacement during the stope excavation process, including the mining depth and position of fault with respect to the orebody. However, the stiffness and dilation angle of the fault shows no significant effect on the maximum dynamic shear displacement. Moreover, the fault position and friction angle have an influence on the seismic moment and the released energy of fault-slip. Then, they employed the finite-difference code of FLAC3D to conduct a numerical evaluation of fault-slip bursts using stress waves generated by stope production blast. Based on the obtained results, the reduction of normal stress on the fault is beneficial for the fault to slip over the fault plane. Furthermore, the blasting sequence has an important effect on the seismic moment and the released energy during the fault-slip. Meng et al. (2016) studied the prediction of fault-slip burst by using the experimental method. Based on the obtained results, the normal stress increases as the b -value decreases (the b -value reflects the proportion of large-magnitude earthquakes relative to small-magnitude ones). Hence, the risk of the rockburst induced by dynamic shear failure increases. A lower b -value is associated with a high rockburst probability and intensity. Sainoki et al. (2017) investigated the relationship of the fault-slip potential with the shearing of fault asperities. The numerical modeling was utilized (by FLAC3D software) to understand the relationship between the D and H parameters of an excavation area (D is the distance between the fault and orebody, and H is the height of the mined-out core). The results indicate that the potential for fault-slip burst drastically increases by increasing the value of H . Moreover, the potential of fault-slip burst does not increase when D is small because the entire accumulated strain energy is released when the distance between the fault and orebody is shortened. Moreover, the seismic moment and radiated seismic energy increase when the ratio of D and H decreases. Then, they estimated the extent of damage around an underground opening induced by seismic waves from mining fault-slip. To this end, the failure of rock mass under biaxial stress condition was considered, and the model examined ran under static and dynamic

conditions. Two methodologies were applied to assess the extent of damage caused by the seismic wave propagation. The first one is the ratio of plastic strain increment to elastic strain limit, and the second is a variation of plastic strain energy density. Moreover, effective shear and volumetric strain increment were tested. According to the results, volumetric strain increment is adequately accurate in determining the extent of damage near the stope wall; whereas, the effective shear strain can be used to estimate the extent of damage in the backfill. Moreover, the damage assessment method with plastic strain energy can be applied for detecting damage in an extensive area caused by seismic waves and fault movements. Furthermore, Sainoki et al. (2017) studied the characterization of a seismic fault-slip through numerical modeling and the influence of mining activity on the reactivation of a footwall fault. They demonstrated that the volume of ore extracted before mining activity significantly affects the degree of clamping of the fault. They also showed that the shear movement on the fault is not the only cause of rockburst. The main reason is the stress changes induced by the slip. Meng et al. (2017) studied the significant factors affecting the fault-slip burst in deeply hard rock tunnels. The inherent properties of rock, such as strength and brittleness, and external environmental conditions, such as the magnitude of in situ stresses, dynamic disturbance, excavation sequence, and geological structure, influence the intensity of rockburst. Three different samples were examined, and the influences of the rock type, the normal stress, the surface morphology, the infilling, and shear history on fault-slip rockburst were investigated to evaluate these factors. The results show that rockburst occurs rapidly under following granite joint scenarios: stress drops after the peak stress and during the stick-slip period. In addition to the stress drop after the peak, stress and average stress drop during stick slip represent a linear relationship with normal stress. The value of average stress and stress drop increases with increasing the normal stress, which is associated with increased probability and intensity of fault burst. Moreover, they showed that the surface morphology also affects the intensity of fault burst. Another important result is the reduced probability of fault burst due to release of energy with reducing previous shearing events. One of the significant issues in underground excavation is the control and prediction of rockburst. The prediction methods are usually employed to decrease the rockburst damage to the tunnel or excavation zone. The prediction methods

are often used for the strainburst rather than the pillar burst or shear burst, because the geological and geomechanical parameters of rock can be extracted easily for the prediction of rockburst than that of pillar burst or shear burst. The numerical analysis is normally used to analyze the pillar burst and shear burst. In general, the prediction methods are classified into the experimental, empirical, intelligent, and analytical methods. In this study, the empirical methods of rockburst prediction will be classified into three groups: stress, energy, and other methods of rockburst prediction. The other classification methods are referred to as the methods that are less important in the application for predicting rockburst in underground excavation or they have several indicators for rockburst prediction. As a brief description of the next section, the empirical methods of rockburst prediction will be explained, and the rockburst criteria with their corresponding definitions will be represented. Then, a comprehensive review of literature on the rockburst prediction methods will be presented.

2.3.4 Mechanism of coal- gas compound dynamic disasters

According to the classification of coal-gas compound dynamic presented in Section 2.2, and to understand the mechanism of coal-gas compound dynamic disasters in a systematic way, it is necessary to clarify all aspects of each classification that was proposed by Wang and Du (2019). In coal and rock dynamic disasters, energy dissipation and release play a major role. Therefore, energy dissipation can be used to explain mechanisms of dynamic disasters.

2.3.4.1 Mechanism of rockburst-induced outburst dynamic disaster

After a rockburst occurs, the elastic energy released from the burst acts as kinetic energy, promoting the development of cracks and fissures in gas-containing coal (Brady & Brown, 1993). Gas desorption and expansion occur simultaneously. In the absence of sufficient gas pressure, gas expansion energy is insufficient for the ejection of coal and it simply refers to the occurrence of gas outburst (abnormal emission). However, coal is prone to spall fracture under conditions of higher gas pressure. The coal and gas outburst occurs when a large amount of desorption gases accumulate in fractures and eventually burst in the form of a pressurized storm when they come into contact with broken coal. In contrast, after the occurrence of rockburst, the stress state of coal changes, with cracks

and fissures expanded, resulting in reduced ability of coal to resist deformation (Jiang et al., 2017). In addition, crack growth increases the stress potential of coal. In consequence, the coal body is more likely to attain the unstable state of outburst, increasing the likelihood of a coal and gas eruption.

2.3.4.2 Mechanism of outburst-induced rockburst dynamic disaster

By assuming that the outburst is triggered by mining disruption at a certain time, the outburst may induce rockburst by a number of ways:

(1) Outburst disasters involve desorption and expansion of gas, as well as failure of a coal or rock structure, which releases energy similar to mine seismic energy and the stress waves will be generated as a result of this transmission of energy. Due to the disturbance of the propagation medium caused by the stress wave, this process is regarded as that of dynamic loading. Whenever the stress wave interacts with the surrounding rock, it increases the load of the rock. As a result of the propagation of internal cracks and friction sliding between floor and roof, the surrounding rock loses its bearing capacity, eventually resulting in a failure.

(2) Coal bodies are thrown out with the subsidence of the roof during an outburst disaster, which results in further instability of coal and rock mass. With the redistribution of surrounding rock stress, the limit storage energy of the coal-rock system is reduced; meanwhile, elastic energy is transferred and released. In conjunction with the above factors, the unstable equilibrium state of the coal-rock deformation system is intensified, which may cause the roof rock to rupture and collapse, causing a rock burst.

(3) The coal-gas two-phase flow from an outburst hole is ejected at a certain velocity after an outburst disaster. In the tunnel space, the gas can be impacted and disturbed. Consequently, the coal and rock may become unstable due to the impact of airflow.

2.3.4.3 Mechanism of outburst and rockburst coupling dynamic disaster

Both coal and gas outbursts can happen in coal mines in addition to rockbursts. Unstability created by mining activity or natural events can induce the release of elastic

energy leading to such bursts. Desorbed gas accumulated in the pores and fissures of coal has tensile destructive effects and spurts with broken coal into a pressurized storm, which results in the coal and gas explosion. A combined dynamic disaster can happen if coal and rock are elastically deformed and gas is stored and released simultaneously, with outburst and rockburst coexisting and combining.

2.4 Rockburst prediction methods

Rockburst prediction has always been a challenge worldwide and is one of the most significant ways of preventing and controlling rock failure in underground openings or tunnel excavations (Li et al., 2017). Different methods for prediction of rockburst have been studied since 1960. Up to this date, researchers try to develop, modify, and verify the prediction methods through experimental tests, numerical modeling, and intelligent methods. The rockburst prediction methods are classified into three main groups: (1) regional, (2) local, and (3) current prediction. Regional prediction indicates the likelihood of rockburst based on the natural conditions of rock. The lithology of the strata, physical, and mechanical properties of the rock mass, depth, thickness and layer dip, and structural and tectonic patterns are the significant contributing factors. The local prediction can be used in regions within the rock mass, which are subjected to rockburst risk. Depth and thickness of rock mass and the influence of previous mining activities, such as pillar remaining and rib edges, are the significant factors of local rockburst prediction (Ptáček, 2017). The current prediction is defined as the activities performed in underground mining to determine the regions of strata with a stress concentration (Talka et al., 2005). Prediction methods can also be classified into analytical, experimental, intelligent, laboratory, and numerical methods. Empirical methods of rockburst prediction are divided into two main groups, namely, the stress and energy methods. The former refers to those methods that consider the magnitude of induced stresses and the geomechanical parameters of rock. By contrast, the latter refers to those methods which consider the stored elastic energy of rock mass (Cook, 1963). The empirical methods rank the rockburst based on the intensity level as no, light, medium, and severe or strong rockburst. No rockburst resembles the condition within which no sounds of rockburst and no rockburst activity are expected to occur. Light rockburst is used where the

surrounding rock mass is deformed, cracked, or rib-spalled, and a weak sound or no ejection phenomenon exists. Medium rockburst defines the conditions where the surrounding rock mass is deformed and fractured, and a considerable number of rock chips are ejected. In these cases, a light and sudden destruction occurs, accompanied by crisp crackling often in surrounding rock. Last, severe rockburst is considered in situations where the surrounding rock mass bursts severely and is ejected suddenly into the opening void, accompanied by a continuous strong burst, roaring sound, air spray, and storm phenomena. Moreover, a rapid expansion of rockburst to the depth of surrounding rock is expected to occur. In the following sections, all the stress and energy methods of rockburst prediction will be reviewed. These methods will be explained, and their application and importance in prediction of rockburst in underground excavations will be studied.

2.4.1 Stress Methods

Empirical stress estimation constitutes the most widely used category of methods for rockburst prediction and prevention in underground mining; it employs various indices and indicators to characterize the rock mass. The geomechanical parameters of intact rock and the magnitude of in situ or induced stresses are key factors indicating the severity of rockburst in such methods. These methods have shown to be easy to use while making an acceptable rockburst prediction in deep underground environments (Gong & Li, 2007).

Some very early observations can help get an idea of rock mass properties such as drill core description. For example, core discing represents a useful source of information to estimate and locate potentially overstressed areas. The pre-loading of a rock mass has consequences on rock stress evaluation. As a result of boring holes to obtain cores, stress concentrations occur directly at the coring bit/rock interface. When the core is drilled, the annular groove causes the in situ stresses to redistribute, leading to high induced stresses throughout the core. A core can thus be significantly damaged because of the sudden release of that stress, which can further be exacerbated by rock anisotropy. High in situ stress and brittle rock can result in 'core discing', where the core appears as thin 'poker chips'. In extreme cases, the discs can become so thin that they resemble *milles*

feuilles, or *flaky pastry*. The presence of discing in cores is often interpreted as evidence for high-stress zones (Fairhurst, 2003). Understanding overstressed areas could enable us to consider that the rockbursts are perhaps more likely to occur in specific areas. Let us now turn our attention to stress methods and rockburst prediction. The most common empirical stress methods and their applications are reviewed as follows.

2.4.1.1 Rock Brittleness Coefficient

Brittleness of rock, as one of the significant properties of rock, is considered an index to determine the intensity of rockburst in an underground excavation. From a mechanical point of view, brittleness is a reduction of strength derived from the bond between the grains. According to the experimental results and site investigation, the rock brittleness coefficient is defined as the ratio of UCS to the tensile strength of intact rock as follows (Qiao & Tian 1998; Chen et al., 2013):

$$B_i = \frac{\sigma_c}{\sigma_t}, \quad \text{Eq. 2 1}$$

Where σ_c is uniaxial compressive strength of the rock and σ_t is tensile strength of the rock. The both values are in MPa.

Table 2 5. Rockburst intensity based on the brittleness coefficient (Wang & Park, 2001).

Rock Brittleness Coefficient	Risk of violent rupture
No rockburst	$B_i > 40$
Weak rockburst	$26.7 < B_i < 40$
Moderate rockburst	$14.5 < B_i < 26.7$
Strong rockburst	$B_i < 14.5$

Moreover, Zhang et al. (2003) mentioned the other classification of rockburst based on the rock brittleness coefficient (Table 2.6). Based on their classification, the possibility of rockburst increases as the rock brittleness coefficient ratio increases.

Table 2 6. Rockburst intensity based on the brittleness coefficient (Zhang et al., 2003).

Rock Brittleness Coefficient	Risk of violent rupture
No rockburst	$B_i < 10$
Weak rockburst	$10 < B_i < 18$
Strong rockburst	$B_i > 18$

In terms of accumulated energy, the brittle deformation coefficient (K_u) is defined as:

$$K_u = \frac{U}{U_t}, \quad \text{Eq. 2 2}$$

where U is the total peak strength of rock before rock deformation (in %), and U_t is the permanent deformation of rock before the peak or elastic deformation (in %) (Neyman, et al., 1972). Moreover, brittle deformation coefficient is defined as the ratio of the tensile strength of rock to the maximum in situ stress component as follows:

$$K_u = \frac{\sigma_t}{\sigma_1}. \quad \text{Eq. 2 3}$$

Table 2.7 shows the intensity of rockburst based on the brittle deformation coefficient.

Table 2 7. Rockburst intensity based on the brittle deformation coefficient (Neyman, et al., 1972).

Brittle deformation coefficient	Rockburst intensity
$K_u \leq 2$	No rockburst
$2 < K_u \leq 6$	Light rockburst
$6 < K_u \leq 9$	Medium rockburst
$K_u > 9$	Strong rockburst

Tang and Wang introduced another definition of rock brittleness as follows (Tang & Wang, 2002):

$$K = \frac{\sigma_c \varepsilon_f}{\sigma_t \varepsilon_b}, \quad \text{Eq. 2.4}$$

Where σ_c is the compressive strength of the rock, σ_t is the tensile strength of rock, ε_f is the strain before the peak, and ε_b is the strain after the peak. Table 2.8 shows the intensity of rockburst as a function of the rock brittleness index.

Table 2.8. Rockburst intensity based on the rock brittleness index (Tang & Wang, 2002).

Rock brittleness index	Risk of violent rupture
No rockburst	$K \leq 20$
Light rockburst	$20 < K \leq 75$
Medium rockburst	$75 < K \leq 130$
Strong rockburst	$K > 130$

2.4.1.2 Mean Stress (Tao Discriminant Index) (α)

This index is based on the stress reduction factor in Q system (Barton's classification) and defined as the ratio of UCS of rock to the maximum principal in situ stress (Grimstad, 1999; Tao, 1988) as follows:

$$\alpha = \frac{\sigma_c}{\sigma_1}, \quad \text{Eq. 2.5}$$

Where σ_c is uniaxial compressive strength of the rock and σ_1 is maximum in situ stress. Table 2.9 presents the rockburst classification based on the mean stress index.

Table 2 9. Rockburst intensity based on the Tao discriminant index (Tao, 1988).

Mean Stress	Risk of violent rupture
No rockburst	$\alpha > 14.5$
Weak rockburst	$5.5 < \alpha \leq 14.5$
Moderate rockburst	$2.5 < \alpha \leq 5.5$
Strong rockburst	$\alpha \leq 2.5$

Hou and Wang (1989) introduced another classification or rockburst based on Eq. (5), as shown in Table 2.10.

Table 2 10. Rockburst intensity classification (Hou & Wang, 1989).

Mean stress	Risk of violent rupture
No rockburst	$\alpha \leq 0.30$
Weak rockburst	$0.30 < \alpha \leq 0.37$
Moderate rockburst	$0.37 < \alpha \leq 0.62$
Strong rockburst	$\alpha > 0.62$

Grimstad (1999) introduced another rockburst classification based on the mean stress as shown in Table 2.11.

Table 2 11. Rockburst intensity classification (Grimstad, 1999).

Mean stress	Risk of violent rupture
No rockburst	$\alpha > 5$
Weak rockburst	$5 \leq \alpha < 3$
Moderate rockburst	$3 \leq \alpha < 2$
Strong rockburst	$\alpha < 2$

2.4.1.3 Strength Index

Hawkes (1966) defined for the first time the strength index as one of the empirical methods of rockburst prediction. The rock mass strength index (RS_i) is defined as:

$$RS_i = \frac{3\sigma_1}{\sigma_c}, \quad \text{Eq. 2 6}$$

Where σ_1 is the magnitude of maximum principal stress, and σ_c is UCS of rock. Table 2.12 shows the intensity of the rockburst based on the strength index.

Table 2 12. Rockburst intensity based on the strength index (Hawkes, 1966).

Strength index	Risk of violent rupture
$RS_i < 0.2$	Low rockburst
$0.2 < RS_i \leq 0.4$	Significant rockburst
$0.4 < RS_i \leq 0.6$	High rockburst
$0.6 < RS_i \leq 0.8$	Very high rockburst
$0.8 < RS_i \leq 1.0$	Dangerously high rockburst
$RS_i > 1.0$	Unstable

2.4.1.4 Stress Index

The stress index (S_i) is defined as the ratio of the UCS of the rock to the vertical component of in situ stress (Yoon, 1994), which is written as

$$S_i = \frac{\sigma_c}{\sigma_v}. \quad \text{Eq. 2 7}$$

Table 2.13 shows the intensity of rockburst based on the stress index.

Table 2 13. Value of stress index for prediction of rockburst (Yoon, 1994).

Stress index	Risk of violent rupture
$S_i \leq 2.5$	Heavy rockburst
$2.5 < S_i \leq 5$	Mild rockburst

2.4.1.5 Tangential Stress

The Tangential stress criteria are defined as the ratio of tangential stress around the excavation opening to UCS of rock (Wang et al., 1998; Hoek & Brown, 1980) as follows:

$$T_s = \frac{\sigma_\theta}{\sigma_c}. \quad \text{Eq. 2 8}$$

Table 2.14 presents the rockburst intensity based on the tangential stress.

Table 2 14. Tangential stress criterion (Wang et al., 1998).

Tangential stress	Risk of violent rupture
$T_s < 0.3$	No rockburst
$0.3 \leq T_s < 0.5$	Weak rockburst
$0.5 \leq T_s < 0.7$	Strong rockburst
$T_s \geq 0.7$	Violent rockburst

Russenes (1974) introduced another empirical method to evaluate the risk of rockburst. This criterion is based on the relation of tangential stress and the strength of the rock. The method is defined as the ratio of the maximum tangential stress surrounding the rock to the UCS of rock. Table 2.15 shows the rockburst intensity based on the Russenes criterion.

Table 2 15. Rockburst prediction value based on Russenes method (Russenes, 1974).

Russenes Method	Risk of violent rupture
$\frac{\sigma_{\theta}}{\sigma_c} < 0.2$	No rockburst
$0.2 \leq \frac{\sigma_{\theta}}{\sigma_c} < 0.30$	Light rockburst
$0.3 \leq \frac{\sigma_{\theta}}{\sigma_c} < 0.55$	Medium rockburst
$\frac{\sigma_{\theta}}{\sigma_c} \geq 0.55$	Violent rockburst

2.4.1.6 Turchaninov Method

Turchaninov et al. (1972), defined the Turchaninov criterion to measure the rockburst intensity. This criterion is defined as

$$S = \frac{\sigma_{\theta} + \sigma_1}{\sigma_c} . \quad \text{Eq. 2 9}$$

Table 2.16 represents the rockburst intensity based on the Turchaninov criterion.

Table 2 16. Rockburst prediction values based on the Turchaninov scholar (Turchaninov et al., 1972).

Turchaninov method	Risk of violent rupture
$S < 0.3$	No rockburst
$0.3 \leq S < 0.5$	Rockburst probably
$0.5 \leq S < 0.8$	Rockburst surely
$S \geq 0.8$	Violent rockburst

2.4.1.7 Failure Duration Index (Dt)

Wu and Zhang (1997) defined the failure duration index during the coal specimen. This index is expressed as the time taken for a coal specimen to break down from the

peak strength to the complete failure while compressed uniaxially. Table 2.17 shows the rockburst tendency based on the failure duration index.

Table 2 17. Rockburst intensity based on the failure duration index (Wu & Zhang, 1997)

Failure duration index	Risk of violent rupture, D_t (ms)
None rockburst	D_t is larger than 500
Medium rockburst	D_t is between 500 and 50
Strong rockburst	D_t is lower than 50

2.4.1.8 Grimstad and Barton Classification

Grimstad and Barton (1993) introduced a criterion for rockburst prediction. They gathered data from measurement of the in situ stresses and strength of samples and could find some relationship that confirms the equations of Russenes (1974) and Hoek & Brown (1980). This criterion is defined as the ratio of UCS of rock to the maximum principal stress and the ratio of the maximum tangential stress to the UCS of rock. Table 2.18 shows the rockburst intensity based on the Grimstad and Barton classification.

Table 2 18. Rockburst intensity classification based on the Grimstad and Barton method (Grimstad & Barton, 1993).

Stress class	Description of potential induced stress	$\frac{\sigma_c}{\sigma_1}$	$\frac{\sigma_\theta}{\sigma_c}$
1	Low stress, near surface, open joints	>200	<0.01
2	Medium stress, favorable stress conditions	200–10	0.01–0.3
3	High stress, very tight structure, usually beneficial to blasting except for wall	10–5	0.3–0.4
4	Moderate spalling after > 1 h	5–3	0.5–0.65

5	Spalling and rockburst after a few minutes	3–2	0.65–1
6	Heavy rockburst and immediate strain failure	<2	>1

2.4.1.9 Five Factors

Zhang and Fu (2008) proposed a five-factor criterion as a compressive criterion for the prediction of rockburst. This criterion considers five involved parameters of rockburst shown in Table 2.19.

Table 2 19. Five factors (Zhang & Fu, 2008).

	No rockburst	Light rockburst	Medium rockburst	Strong rockburst
$\frac{\sigma_c}{\sigma_1}$	≤ 0.15	0.15–0.2	0.2–0.4	> 0.4
$\frac{\sigma_\theta}{\sigma_c}$	≤ 0.2	0.2–0.3	0.3–0.55	> 0.55
$\frac{\sigma_c}{\sigma_t}$	< 15	15–18	18–22	> 22
W_{et}	< 2	2–3.5	3.5–5	> 5
K_u	≤ 0.55	0.55–0.60	0.60–0.80	> 0.80

Note: σ_1 is the maximum in situ stress, σ_θ is tangential stress, σ_c is UCS of rock, σ_t is the tensile strength of rock, W_{et} is elastic strain energy, and K_u is brittle deformation coefficient.

2.4.1.10 Hoek and Brown Classification

The rock mass strength is normally assessed by back analyzing case histories where examples of failure have been precisely documented (Sakurai, 1993). Rock mass failure

around excavation opening occurs in a form of spalling or fracturing, and back analyses can estimate the induced stresses required to cause this fracturing. Hoek and Brown (1980) proposed a complete description of brittle failure with the same criterion that can determine the rock mass instability around the excavation opening. This criterion is defined as the ratio of maximum far field stress to the UCS of rock. Table 2.20 shows the intensity of rockburst based on the Hoek and Brown classification.

Table 2 20. Rockburst intensity based on the Hoek and Brown classification (Hoek & Brown, 1980)

H-B criterion	Risk of violent rupture
$\frac{\sigma_c}{\sigma_1} \leq 0.1$	No damage
$\frac{\sigma_c}{\sigma_1} = 0.2$	Minor spalling
$\frac{\sigma_c}{\sigma_1} = 0.3$	Severe spalling
$\frac{\sigma_c}{\sigma_1} = 0.4$	Very severe spalling
$\frac{\sigma_c}{\sigma_1} = 0.5$	Stability of opening may be very difficult to achieve

However, this criterion cannot be applied to the other stress conditions or mining situations because it is based on experiences of 3 or 4 m² of tunnels in brittle rocks in South Africa’s gold mines according to the database of Ortholep and his colleagues (Ortlepp & Stacey, 1994).

2.4.1.11 Rock Mass Index (RMi)

The rock mass index was introduced as a rock mass characterization system for rock engineering purposes (Palmstrom, 1995). The main objective of the RMi is to improve the geological input data. The RMi equation is written as

$$RMi = \sigma_c \times J_p , \quad \text{Eq. 2 10}$$

Where σ_c stands for the UCS of rock, and J_p is the jointing parameter composed of the block volume and roughness, and alteration and size characteristics of joints. Based on the studies of Palmstrom (1995), the *RMi* of massive rocks is defined as follows:

$$RMi = f_a \times \sigma_c, \quad \text{Eq. 2 11}$$

Where f_a is the factor related to the scale effect of compressive strength and the range is between 0.45 and 0.55. Therefore, the competency factor can be defined as

$$C_g = \frac{RMi}{\sigma_\theta} = f_a \times \frac{\sigma_c}{\sigma_\theta}. \quad \text{Eq. 2 12}$$

Table 2.21 shows the rockburst intensity based on the value of the competency factor.

Table 2 21 Rockburst intensity based on the *RMi* (Palmstrom, 1995).

Competency factor , C_g	Failure mode
> 2.5	No rock stress-induced instability
2.5 – 1	High stress, slightly loosening
1 – 0.5	Light rockburst or spalling
< 0.5	Heavy rockburst

2.4.2 Energy Methods

The magnitude of stored strain energy within the rock mass is changed during the excavation process. Therefore, one of the effective indicators for rockburst prediction could be the release of stored strain energy of rock during the underground excavation process. Hence, rock mass-energy analysis can be used to explain the type and intensity of rockburst. In this regard, Cook (1963) conducted one of the earliest studies to show energy changes in the rock mass in underground mining when the excavation was taken place. Afterward, the researcher studied the relationship between the energy changes of rock mass and rockburst mechanism, generating an acceptable theory of elasticity for the simulation of the rock mass behavior around the excavation area. In the next section, the

important rockburst prediction methods, based on the rock stored energy, will be reviewed.

2.4.2.1 Elastic Strain Energy Index

The stored elastic energy in the rock is considered a significant way to calculate the intensity of rockburst. Kidybiński defined the elastic strain energy index as a complete stress-strain curve, as follows (Kidybiński, 1981):

$$R = \frac{W_E}{W_P}, \quad \text{Eq. 2 13}$$

Where W_E is the elastic strain energy saved before the rock failure, and W_P is the plastic strain energy consumed after rock failure. Figure 2.8 depicts the complete stress-strain curve. Based on the elastic strain energy index, rockburst intensity is categorized in Table 2.22.

Table 2 22. Energy index value (Kidybiński, 1981).

Elastic strain energy	Risk of violent rupture
$R < 2$	No rockburst
$2 \leq R < 5$	Slightly rockburst
$R \geq 5$	Severely rockburst

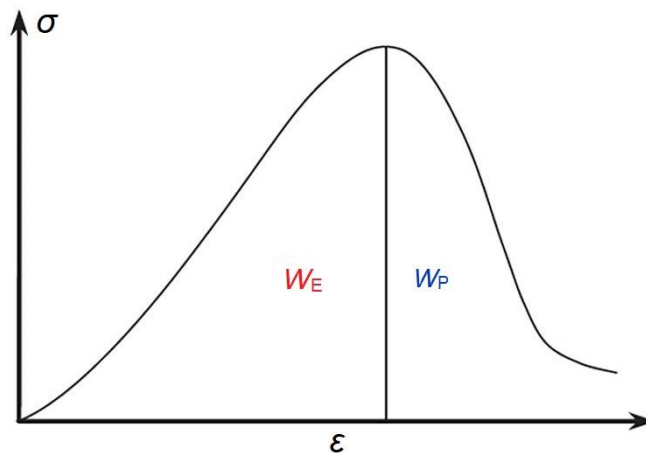


Figure 2 8. The complete stress-strain curve (Kidybiński, 1981).

2.4.2.2 Liner Elastic Energy and Burst Potential Index (BPI)

Wang and Park (2001) firstly introduce the linear elastic energy (W_{et}), which is defined as the linear elastic energy stored in the rock specimen before the rock failure point, expressed as

$$W_{et} = \frac{\sigma_c^2}{2E_u}, \quad \text{Eq. 2 14}$$

Where σ_c is the UCS of intact rock (MPa), and E_u is the elastic modulus. Table 2.23 shows the rockburst intensity based on the value of linear elastic energy.

Table 2 23. Rockburst intensity based on the linear elastic energy (Wang & Park, 2001).

Liner elastic energy	Risk of violent rupture
Weak rockburst	$W_{et} < 50 \text{ KJ/m}^3$
Moderate rockburst	$50 \text{ KJ/m}^3 < W_{et} < 100 \text{ KJ/m}^3$
Strong rockburst	$100 \text{ KJ/m}^3 < W_{et} < 200 \text{ KJ/m}^3$
Extra strong rockburst	$W_{et} > 200 \text{ KJ/m}^3$

The linear elastic energy has a relationship with the brittleness coefficient (Lee et al., 2004), as follows:

$$W_{et} = 213.94 \ln(B_i) - 321.10, \quad \text{Eq. 2 15}$$

Where B_i is the brittleness coefficient.

Singh (1988) also introduced BPI, which is defined as the ratio of the strain energy retained, E_R , to the permanent strain energy, E_D . The BPI is written in Eq. (2.16) as follows:

$$\text{BPI} = \frac{E_R}{E_D}, \quad \text{Eq. 2 16}$$

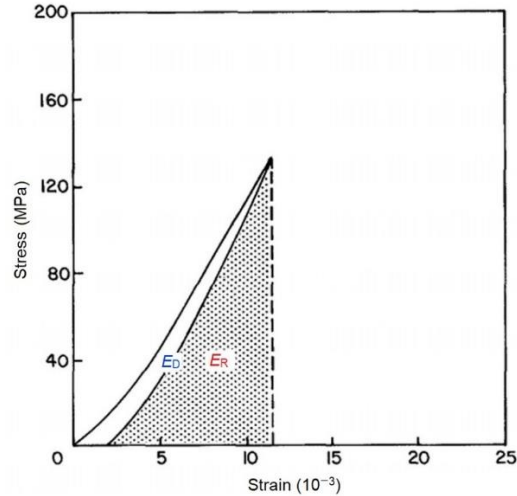


Figure 2.9. Typical stress-strain curve for loading and unloading during uniaxial compression test (Singh, 1988).

Despite the advantage of BPI criterion, achieving 80% – 90% of the rock strength with BPI is a problem because of two reasons: first, the strength can be known only in a probabilistic manner; second, the value of the index is influenced by the relative value of the load attained. Therefore, another index, called Brittleness Index Modified (BIM), was proposed to eliminate this problem (Gill et al., 1988). The BIM equation is written in Eq. (2.17) as follows:

$$\text{BIM} = \frac{A_2}{A_1}, \quad \text{Eq. 2.17}$$

Where A_2 represents the area under the loading curve, and A_1 is the area under the line corresponding to the elastic modulus of the rock (E) (Figure 2.10). When the BIM increases, additional energy is dissipating during loading, and less energy is available for violent rupture. Aubertin et al. (1994) proposed a risk classification for rockburst based on the value of the BIM, as shown in Table 2.24.

Table 2 24. BIM indicative values and risk of violent rupture (Aubertin et al., 1994).

BIM	Risk of violent rupture
Between 1.00 and 1.20	High
Between 1.20 and 1.50	Moderate
More than 1.50	Low

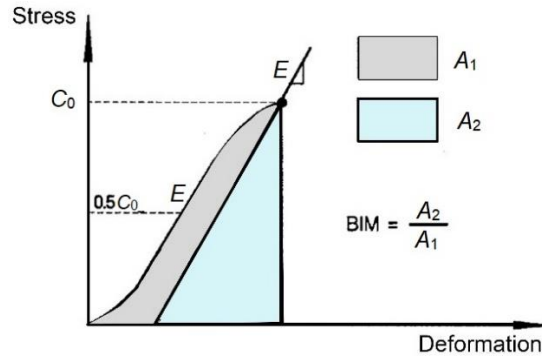


Figure 2 10. Determination of BIM with uniaxial compression tests (Aubertin et al., 1994).

Regarding the results from the comparison of the empirical and simulation methods, a new rockburst prediction index was introduced (Jiang et al., 2010), called the rockburst energy release rate (RBERR) as follows:

$$RBERR = \frac{LERR}{LESR} = \frac{U_{i \max} - U_{i \min}}{LESR} = \frac{U_{i \max} - U_{i \min}}{LESR}, \quad \text{Eq. 2 18}$$

Where LERR is the local energy release rate (LERR), and LESR is the limit energy storage rate. LERR is defined as the sudden energy release of the element; $U_{i \max}$ and $U_{i \min}$ are the peak values of elastic strain energy intensity before and after the brittle failure of the i th element, respectively, expressed as

$$\begin{cases} U_{i \max} = \frac{[\sigma_1^2 + \sigma_2^2 + \sigma_3^2 - 2\gamma(\sigma_1\sigma_2 + \sigma_2\sigma_3 + \sigma_1\sigma_3)]}{2E} \\ U_{i \min} = \frac{[\sigma_1'^2 + \sigma_2'^2 + \sigma_3'^2 - 2\gamma(\sigma_1'\sigma_2' + \sigma_2'\sigma_3' + \sigma_1'\sigma_3)']}{2E} \end{cases} \quad \text{Eq. 2 19}$$

Where σ_1 , σ_2 , and σ_3 are the three principal stresses corresponding to the peak strain energy of the element; σ_1' , σ_2' , and σ_3' are three principal stresses corresponding to the

minimum strain energy of the element; ν is the Poisson's ratio; E is Young's modulus. LERR reflects the different conditions after excavation, for example, the limited energy storage capacity of the rock mass and the different stress status in a rock mass.

2.4.2.3 Rock Mass Integrity Coefficient

This criterion is used to evaluate the rockburst intensity and defined as the ratio of rock mass elastic wave speed to the rock elastic wave (Yoon, 1994) as follows:

$$K_v = \frac{v_{pm}^2}{v_{pr}^2}. \quad \text{Eq. 2 20}$$

Table 2.25 shows the rockburst tendency based on the rock integrity coefficient.

Table 2 25. Rockburst prediction tendency based on the rock integrity coefficient (Yoon, 1994).

Rock integrity coefficient	Risk of violent rupture
$K_v < 0.5$	No rockburst
$0.5 \leq K_v < 0.6$	Weak rockburst
$0.6 \leq K_v < 0.75$	Medium rockburst
$0.75 \leq K_v < 1.0$	Strong rockburst

2.4.2.4 Seismic Energy

Spottiswoode and McGarr (1975) roposed for the first time the radiated energy of rockburst, monitored by a microseismic technique. In this regard, the relationship between rockburst radiated energy and intensity of rockburst was studied. Based on the results, the radiated energy was considered as an evaluation index for the rockburst intensity classification. Table 2.26 shows the new classification based on the common logarithms of radiant energy.

Table 2 26. Rockburst classification based on the logarithm of radiant energy (Spottiswoode & McGarr, 1975) .

Seismic method	Risk of violent rupture
No rockburst	$\lg(E/J) < 2$
Weak rockburst	$0 \leq \lg(E/J) < 2$
Moderate rockburst	$2 \leq \lg(E/J) < 4$
Intense rockburst	$4 \leq \lg(E/J) < 7$
Extremely intense rockburst	$\lg(E/J) \geq 7$

Note: $\lg(E/J)$ is the average common logarithm of the rockburst radiated energy. This radiated energy is recorded by microseismic station at the location of mining. E/J is called energy per joule and it is the unit of rockburst radiated energy.

Then, Chen et al. (2013) studied seismic energy at Jinping II Hydropower Station in China to find a new index for the seismic energy. They investigated the characteristics, magnitude, laws of the radiated energy, and the relationship between the rockburst radiated energy and intensity. From the research results, a new set of criteria for the quantitative classification of the rockburst intensity was introduced based on radiated energy and rock damage severity, as shown in Table 2.27.

Table 2 27. Rockburst intensity quantitative classification criteria based on radiated energy with rock mass failure intensity (Chen et al., 2013).

Rockburst levels	$\lg (E/J)$	Main phenomena
None	$(-\infty, 0]$	The crack occurred inside rock mass; an evident failure cannot be found on the surface of the rock mass, and the cracking sound could barely be heard; no support system and construction are affected
Weak	$(0, 2]$	Main failure type was slight spalling and slabbing in the surface surrounding rock mass; the rock mass was slightly ejected; the size of the ejected fragment was 10–30 cm; the cracking could be heard slightly, and the depth of failure was <0.5 m
Moderate	$(2, 4]$	The main failure type was severe spalling and slabbing of the surrounding rock mass; the rock mass was evidently ejected; the size of the ejected fragment was 30–80 cm; the cracking was similar to a diameter blasting and lasted for some time inside the rock mass
Intense	$(4, 7]$	A great deal of rock mass was suddenly ejected; the failure range was extensive; the size of ejected fragment was 80–150 cm; the edge of the failure zone typically has a fresh fracture plane; the rockburst is similar to an explosive
Extremely intense	$(7, \infty]$	A large block of rock mass was suddenly ejected with intensive seismically, and the stability was seriously damaged; the depth of the failure was more than 3 m

2.4.2.5 Excess Shear Stress (ESS)

Ryder firstly proposed the ESS criterion, which is based on available energy when passing from static resistance (before slip movement) to the dynamic resistance (during slip) (Ryder, 1987). The static resistance of discontinuities (T_s) can be calculated using the Mohr-Coulomb criterion as follows:

$$\tau_s = c + \mu_s \sigma_n , \quad \text{Eq. 2 21}$$

Where c is the static cohesion, σ_n is the normal stress, and μ_s is the static friction angle. Therefore, the value of ESS is obtained from the following equation (Eq. (2.22)):

$$\text{ESS} = \tau_s - |\tau| - \tau_d , \quad \text{Eq. 2 22}$$

Where τ_s is the net shear stress available to produce a seismic event, τ is the shear stress at the initiation point, and τ_d is \ at this point which is given by Eq. (2.23):

$$\tau_d = \mu \sigma_n . \quad \text{Eq. 2 23}$$

If ESS value brought by the progression of the excavation toward the discontinuity is large, then the surface of the discontinuity involved would also be large, and the seismic event would produce a large surface. However, the back analysis showed that not all positive ESS situation yielded seismic events, which may be due to the lack of accuracy of data or stress involved. Gill et al. (1994) and Ryder, (1987) noted that this lack of rockburst for positive ESS confirms the discontinuity post-peak stiffness. If the post-peak stiffness of the rock specimen is less than the load system stiffness, then the equilibrium state becomes unstable, and the failure of the rock specimen is violent. Otherwise, the equilibrium state becomes stable and the failure occurs gradually. In addition, the rock mass stiffness on both sides of the discontinuity may play a major role in this process.

2.4.2.6 Fractional Energy Release Rate (FERR)

Based on the energy release rate (ERR) and the LERR, Xiao, et al. (2016) introduced a new index as a frictional energy release rate (FERR). The ERR is an important index to evaluate the stability of the rock which has been confirmed by many researchers. The ERR can evaluate the rockburst intensity. However, the location, intensity, and scale of rockburst are not clear when the ERR is applied. Moreover, ERR is an average ERR of

tunnel excavation, and when the tunnel excavation processes, the average of ERR is not suitable to estimate the local energy released. The LERR is an index to describe the energy released from a certain element in each excavation step. However, this index is based on the elastic assumption. Therefore, the failure of rock cannot be considered. The new index (FEER) was proposed to overcome the disadvantages of ERR and LERR. The FERR can be defined as follows (Eqs. (2.24)–(2.27)):

$$\text{FERR}_i = \frac{E_i}{V_i}, \quad \text{Eq. 2 24}$$

$$\text{FV}_i = V_i, \quad \text{Eq. 2 25}$$

Where E_i and V_i are calculated by Eqs. (26) and (27), respectively:

$$E_i = \sum_{j=1}^m \text{LERR}_j \cdot V_j, \quad \text{Eq. 2 26}$$

$$V_i = \sum_{j=1}^m V_j, \quad \text{Eq. 2 27}$$

Where E_i is the total released energy of failed rock in interval i , LERR_j is the local released energy of broken element j , V_j is the volume of broken element j , V_i is the total volume of broken elements in statistic interval i , and m is the total broken elements of statistic interval i .

2.4.2.7 Burst Efficiency Ratio

Singh (1989) proposed the burst efficiency ratio as follows (Eq. 2.28):

$$\eta = \left(\frac{E_t}{E_s} \right) \times 100, \quad \text{Eq. 2 28}$$

Where E_t is the energy of rock fragments after the failures of a specimen under uniaxial compressive stress, and E_s is the maximum elastic strain energy. Table 2.28 shows the burst efficiency ratio based on the rockburst intensity.

Table 2 28. Rockburst intensity based on the burst efficiency ratio (Singh, 1989).

Rock of violence rupture	Burst efficiency
No rockburst	$\eta < 3.5\%$
Light rockburst	$3.5\% \leq \eta < 4.2\%$
Medium rockburst	$4.2\% \leq \eta < 4.7\%$
Strong rockburst	$\eta \geq 4.7\%$

2.4.3 Other Rockburst Prediction Methods

Despite the stress and energy methods of rockburst prediction, some rockburst prediction criteria that are less common than stress and energy methods exist. Goel (1994) developed an empirical method based on the rock mass number N , defined as Q with SRF = 1. The rock mass number is defined by the equation :

$$N = \left[\frac{\text{RQD}}{J_n} \right] \left[\frac{J_r}{J_a} \right] [J_w], \quad \text{Eq. 2 29}$$

Where RQD is the rock quality designation, J_n is the number of joint sets, J_r is the roughness of the most unfavourable joint or discontinuity, J_a is the degree of alteration or filling along the weakest joint and J_w is the joint water parameter. Eq. (2.29) represents that N is Barton's rock mass quality with SRF 1. N is used to avoid the problems and uncertainties in obtaining the correct rating of parameter SRF in Q method. By considering the tunnel depth (H), the tunnel span or diameter (B) and the rock mass number (N), the log-log plot between N and $HB^{0.1}$ was made by Goel and Jethwa (1995). The data points above the red line represent squeezing conditions, whereas the points below show non-squeezing conditions (Figure 2.11). The equation of line AB separates the squeezing and non-squeezing cases (Its equation is $H = (275N^{0.33})B^{-0.1}$). As can be seen from Table 2.29, these demarcation lines are defined mathematically. These equations can be used to estimate the ground conditions and fix to the tunnel alignment through a better rock mass or reduced thunnel depth to avoid squeezing conditions and related tunneling problems.

Table 2 29. Prediction of ground conditions for tunneling (Goel & Jethwa, 1995) (u_a is the tunnel closure/deformation, a is the tunnel radius in m, u_a/a is the normalised tunnel convergence in %, N is the stress free Q , J_r is the Barton's joint toughness number and J_a is the Barton's joint alternation number)

Number	Ground conditions	Equations for predicting ground conditions
1	Self-supporting	$H < (23.4 N^{0.88})B^{-0.1} \& B < 2Q^{0.4}$
2	Non-squeezing	$(23.4 N^{0.88})B^{-0.1} < H < (275 N^{0.33})B^{-0.1}$
	Minor squeezing	$(275 N^{0.33})B^{-0.1} < H < (450 N^{0.33})B^{-0.1}$
3	$(\frac{u_a}{a} < 1\%)$	$\frac{J_r}{J_a} < 0.5$
	Severe squeezing	$(450 N^{0.33})B^{-0.1} < H < (630 N^{0.33})B^{-0.1}$
4	$(\frac{u_a}{a} < 3\% \text{ to } 5\%)$	$\frac{J_r}{J_a} < 0.5$
	Very severe squeezing	$H > (630 N^{0.33})B^{-0.1}$
5	$\frac{u_a}{a} > 5\%$	$\frac{J_r}{J_a} < 0.25$

According to parameters in Table 2.29, the size of a tunnel will affect the ground condition. This is probably because as the tunnel diameter increases, the rock mass confinement decreases and therefore the rock mass strength decreases. Also, when the ratio of J_r/J_a is more than 0.5, the probability of rockburst increases as well, as shown in Figure 2.11. By looking at this graph and its equations, we can calculate the ground conditions for tunneling, the types of squeezing conditions, and the rockburst.

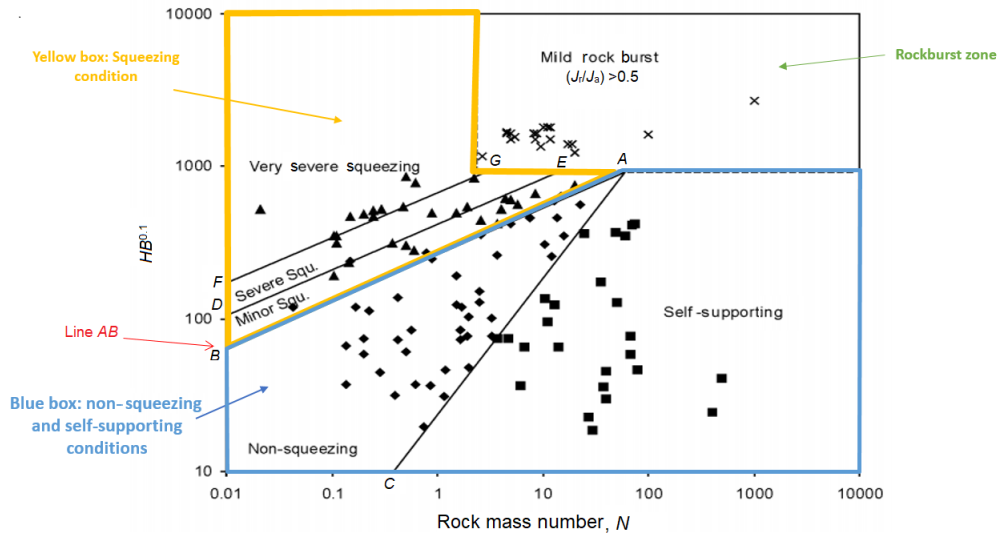


Figure 2 11. Prediction of squeezing ground condition (Goel, 1994).

Singh et al. (1997) also proposed a criterion for rockburst prediction as ground condition evaluation. This criterion is defined as a function of the rock mass quality index, the overburden thickness, and the opening width. Zhao et al. (2017) modified and proposed a new value for the rockburst intensity. The database of Qirehataer Diversion tunnel excavation in Gneissic Granite was used in this study. The location of the tunnel was 15.66 km long with a depth of 1720 m under the ground surface. Three rockburst prediction methods were used to evaluate rockburst intensity, namely, Barton, Russene, and Hoek and Brown methods (Hoek & Brown, 1980; Barton, et al., 1974; Russenes, 1974). Table 2.30 shows the results of the modified rockburst classification. The modified method is based on the revised ratio of principal stress over strength. Moreover, two prediction methods, original and modified methods, were compared with each other. The results showed that when the modified prediction methods were employed, the data interpretation had given better results than that of the original prediction method. The modified method could enhance the consistency of these three criteria.

Table 2 30. Original and modified criterion (Zhao et al., 2017).

Prediction method	Details of criterion	No rockburst	Light rockburst	Moderate rockburst	Strong rockburst	Very strong rockburst
Barton	Original prediction classification	$\frac{\sigma_c}{\sigma_1} > 5$	$2.5 < \frac{\sigma_c}{\sigma_1} < 5$		$\frac{\sigma_c}{\sigma_1} \leq 2.5$	
	Modified criterion classification	$\frac{\sigma_c}{\sigma_1} > 5$	$4 < \frac{\sigma_c}{\sigma_1} \leq 5$	$2.5 < \frac{\sigma_c}{\sigma_1} \leq 4$	$1.5 < \frac{\sigma_c}{\sigma_1} \leq 2.5$	$\frac{\sigma_c}{\sigma_1} \leq 1.5$
Russenes	Original criterion classification	$\frac{\sigma_\theta}{\sigma_c} < 0.2$	$0.2 \leq \frac{\sigma_\theta}{\sigma_c} < 0.3$	$0.3 \leq \frac{\sigma_\theta}{\sigma_c} < 0.55$	$\frac{\sigma_\theta}{\sigma_c} > 0.55$	
	Modified criterion classification	$\frac{\sigma_\theta}{\sigma_c} \leq 0.2$	$< \frac{\sigma_\theta}{\sigma_c} \leq 0.5$	$< \frac{\sigma_\theta}{\sigma_c} \leq 0.7$	$< \frac{\sigma_\theta}{\sigma_c} \leq 0.9$	$\frac{\sigma_\theta}{\sigma_c} > 0.9$
Hoek and Brown	Original prediction classification	$\frac{\sigma_c}{\sigma_v} > 7$	$\frac{\sigma_c}{\sigma_v} = 3.5$	$\frac{\sigma_c}{\sigma_v} = 2$	$\frac{\sigma_c}{\sigma_v} = 1.7$	$\frac{\sigma_c}{\sigma_v} = 0.5$
	Modified criterion classification	$\frac{\sigma_c}{\sigma_v} > 10$	$5 < \frac{\sigma_c}{\sigma_v} \leq 10$	$3.3 < \frac{\sigma_c}{\sigma_v} \leq 5$	$2.5 < \frac{\sigma_c}{\sigma_v} < 3.3$	$\frac{\sigma_c}{\sigma_v} \leq 2.5$

The other method of rockburst prediction is Rock Quality Designation (RQD) index of the rock mass, which shows the degree of rock mass integrity. RQD is a simple but useful index for rockburst prediction, developed by Tang (2000) . According to the RQD

classification system, the probability of rockburst increases with increasing the RQD index (Wang & Park, 2001; Xu, et al., 2008; Zhou, et al., 2012). Xu et al. (2008) found that the probability of rockburst is likely to occur when the RQD is more than 60% . Table 2.31 shows the classification of rock mass based on the RQD index.

Table 2 31. RQD classification (Tang, 2000).

RQD	Risk of violent rupture
<25%	No
25%–50%	Light
50%–75%	Medium
75%–90%	Strong
90%–100%	Very strong

Based on the 3D stress field analysis, Tajduś proposed several rockburst criteria for the evaluation of rockburst potential, including the energetic rockburst indicator (Tajduś, et al., 1997). This method is defined as

$$T = \frac{E_k}{E_k^0}, \quad \text{Eq. 2 30}$$

Where E_k is the accumulated energy in the rock mass, and E_k^0 is the required energy for initiating the rockburst. Hence, E_k and E_k^0 can be defined as follows:

$$E_k = V_c + E_n - L_{zv}, \quad \text{Eq. 2 31}$$

$$E_k^0 = \frac{1}{2} \rho_v V_0^2, \quad \text{Eq. 2 32}$$

Where V_c is elastic energy accumulated in the broken rock mass during rockburst, E_n is energy generated by the tremor in the rock mass, L_{zv} is used for breaking and crushing rock mass volume discharged to an opening, ρ_v is the average density of broken rock mass (2.5 t/m³), and V_0 is the average velocity of broken rock mass acting on an opening surface during rockburst (10 m/s). Therefore, the value of E_k^0 is equal to 1.25×10⁵ J/m³. Table 2.32 shows the rockburst intensity based on the energetic rockburst indicator.

Table 2 32. Rockburst occurrence based on the energetic rockburst indicator (Tajduš et al., 1997).

Energetic rockburst indicator	Risk of violent rupture
No rockburst	$T < 1$
Rockburst	$T \geq 1$

2.4.4 Literature Review on Stress, Energy, and numerical Methods of Rockburst Prediction

In rockburst occurrence, all geomechanical parameters of rock have a significant effect on rockburst occurrence. Aside from these factors, the magnitude of in situ stresses, the presence of water, and rock structure are related to the intensity, shape, and location of rockburst occurrence. As mentioned, empirical methods of rockburst are based on the analysis of rockburst from different perspectives, including stresses around the excavated rock, strength of rock, energy conversion during the excavation, and depth of excavation. These methods have been extensively used for different purposes, such as the determination of rockburst intensity in underground excavation and the utilization of these methods as input data on numerical and intelligent methods of rockburst prediction. Singh (1987) used the rock brittleness coefficient (Eq. (2.1)) to express the effect of intact rock properties on the rockburst intensity. Based on the results, brittleness, compressive and point load strengths, modulus of rigidity, and compressional wave velocity have strong influences on the Burst Proneness Index (BPI). The rockburst can occur at a certain combination of geologic and mining conditions, and the elastic characteristic plays an important role in the hard rocks. In addition, hard, brittle, and elastic rocks have a high potential for bursting. In 1988, Singh used the elastic strain energy (Eq. (2.13)) index to show a parameter that represents the energy released at the time of rock fracture and to determine the important indices and rock properties as an important factor of bursting (Singh, 1988). Based on the results, decreasing the modulus index depends on the burst-proneness index, strength, brittleness, and the strain energy stored in the rock specimens. Wang and Park (2001) studied the prediction of rockburst based on the

analysis of strain energy within the rock (Eq. (2.16)). This study focuses on the investigation of potential and tendency of rockburst during the mining at a depth of -570 m. In this regard, several empirical methods of rockburst prediction were employed as the input data of numerical modeling to determine the rockburst intensity in the Linggold gold mine in China. The results showed that numerical modeling should be employed along with the empirical methods of rockburst prediction to provide reliable results. Du et al. (2010) also used empirical methods of rockburst prediction, such as brittleness coefficient (Eq. (2.1)), deformation brittleness index (Eq. (2.2)), and elastic energy index (Eq. (2.13)) in Chengchao Iron Mine in China, for the simulation of rockburst tendency at the depth of -430 to -700 m. Moreover, tensile and UCS tests were conducted to determine the geomechanical parameters of rocks. The significant result of this study is that the probability of rockburst hazard and the critical depth of mine were identified as important factors in the mining design and rockburst prediction field. Zhou et al. (2012) employed different rockburst prediction methods, as input data of the support vector machines, for the determination and classification of long-term rockburst in underground excavations. A total of 132 rockburst events were compiled from various published studies, and five different models were investigated. The maximum tangential stress, UCS, tensile strength of the surrounding rock, rock brittleness coefficient (Eq. (2.1)), elastic strain energy index (Eq. (2.13)), and depth were regarded as the input data. On the contrary, the actual rockburst intensity was considered the output result. In several models, the stress coefficient (Eq. (2.7)) and the rock brittleness coefficient (Eq. (2.1)) were added to the input data. The results proposed that the developed models in this study can be used for the rockburst prediction, which may help to reduce the impacts of the rockbursts. Wang et al. (2015) studied the prediction of rockburst based on the fuzzy-matter elements and the empirical methods were used as the input data of fuzzy-matter elements. The study area was in Huized-Lead Zink mine in China. Zhou et al. (2016a) conducted another study on the intelligent rockburst prediction methods and selected several criteria of rockburst prediction as the input data for the cloud model with entropy weight. The entropy-cloud model was used to determine the weight of every input data. From the results, the stress coefficient, tangential stress, and the elastic energy index have shown to play a greater role compared with the brittleness coefficient, UCS, and tensile

strength of the rock in the prediction of the rockburst. Zhou et al. (2016b) conducted a study on feasibility of stochastic gradient boosting approach for the rockburst prediction. In this study, they examined a database of 254 rockburst events using stochastic gradient boosting methods (SGB) in order to categorize rockburst damage. Five factors have been evaluated, including the stress condition factor, the ground support system capacity, excavation span, geological structure, and peak particle velocity. Multiclass problems were assessed using two accuracy measures: classification accuracy rate and Cohen's Kappa. The accuracy analysis together with Kappa of the rockburst damage dataset shows that the SGB model is acceptable for predicting rockburst damage. Zhou et al. (2016c) investigated on classification of rockburst in underground projects and compared then supervised learning (SL) methods. A data set of 246 rockburst events was analyzed for rockburst classification using (SL) methods. Eight potentially relevant indicators were used to analyze the data set such as depth (H), rock mass intact coefficient (MTS), uniaxial compressive strength of rock, strain energy storage (W_{et}), stress concentration (SCF), rock brittleness index (B_1) and B_2 ($(\sigma_c - \sigma_t)/(\sigma_c + \sigma_t)$). They are considered among the most important quantifiable indicators of rockburst behavior. On the basis of their ability to learn rockburst, 11 algorithms from 10 categories of SL algorithms were evaluated, including linear discriminant analysis (LDA), quadratic discriminant analysis (QDA), partial least-squares discriminant analysis (PLSDA), naïve Bayes (NB), k-nearest neighbor (KNN), multilayer perceptron neural network (MLPNN), classification tree (CT), support vector machine (SVM), random forest (RF), and gradient-boosting machine (GBM). For multiclass problems, two accuracy measures were used: classification rate and Cohen's Kappa. Regarding to the results, GBM and RF were the most accurate models for rockburst prediction. Cai (2016) applied rockburst prediction criteria to determine the rockburst intensity in Sanshandao Gold Mine in China as a study case. They aim to develop a theory and technique for understanding the rockburst mechanism based on the analysis of disturbance energy. Results show that two conditions are necessary for the occurrence of rockburst in the underground excavation. The first one is that the rock mass must have a good condition to store strain energy, and the second one depends on geological stress conditions of the underground excavation area. Miao et al. (2016) studied the occurrence of rockburst in Sanshadoo Gold Mine in China as a case

study, and the location and intensity of rockburst during mining activity were predicted by empirical methods of rockburst prediction and numerical simulations. Hence, the main rock at a great depth of Sanshadowa Gold Mine is prone to rockburst occurrence, and the magnitude of in situ stresses is a significant factor for rockburst prediction. Xue et al. (2019) proposed a new rockburst evaluation method based on the rough set theory and extension theory. This method was applied to the underground caverns of Jiangbian Hydropower Station in China's Sichuan Province as a case study. For this study, significant methods of rockburst prediction, such as elastic strain energy index (Eq. (2.13)), rock integrity (Eq. (2.20)), rock brittleness coefficient (Eq. (2.1)), mean stress (Eq. (2.5)), and tangential stress (Eq. (2.8)) were analyzed and have been taken into the rough set theory. According to the results of the rough set theory (Xue et al., 2019), the main influential indexes and their weight were used in the extension theory to predict rockburst as a new rockburst evaluation method. Based on the results of this study, the proposed method of rockburst prediction has shown acceptable performance in real conditions. In this way, the rockburst grades and rockburst types are evaluated more comprehensively. Zhou et al. (2021) developed a hybrid system containing the firefly algorithm (FA) and an artificial neural network (ANN) to predict and classify rockburst in underground geotechnical engineering projects. A total of 196 reliable rockburst cases regarding this phenomenon were collected from deep mines and tunnels. As a result of the new hybridized model FA-ANN, the accuracy of rockburst prediction was significantly enhanced. Ahmed et al. (2017) studied the rockburst occurrence in the shaft station area of the Provence Coal Mine in South France. The mined coal had a 2.5 m thickness and a 10° dip angle. The area of the shaft station was at 1000 m depth. This study aimed to investigate the rockburst occurrence where the pillars and longwall panels excavated. Empirical methods of rockburst, such as BPI (Eq. (2.16)), rock brittleness coefficient (Eq. (2.1)), and mean stress (Eq. (2.5)) were applied to estimate rockburst tendency. Moreover, a simulation model comprising an excavation area (a large-scale finite difference numerical model regarding the area of the shaft with its irregular pillars) was employed. The results showed that vertical stress increased in the shaft station pillars due to excavation of long wall panels, and hence, the small pillars are more prone to the rockburst than the large ones. Moreover, the BPI method can be used to evaluate the risk

of rockburst in pillars. Xu et al. (2018) studied new rockburst prediction and classification methods in underground excavation. The new model was established by introducing the basic theory of ideal point methods, regarding the rockburst mechanism. The ideal-point method is an analytical method for multi-objective decision-making and can transform a multi-objective programming problem into a single-objective one. For the evaluation of rockburst in this model, the rock stress coefficient (Eq. (2.7)), rock brittleness coefficient (Eq. (2.1)), and elastic strain energy (Eq. (2.13)) were selected as significant empirical methods of rockburst prediction. A principal component analysis based on mutual information (MIPCA) for the rockburst feature selection was used to calculate a new group of parameters to eliminate any correlation between the parameters. MIPCA was used to consider weight on the selected parameters, and finally, a computer-prediction grading system for rockbursts was developed based on the proposed ideal-point model. This computer system works with measured project data, including maximum tangential stress, the UCS, and elastic energy index and shows an acceptable accuracy for rockburst prediction. Zhou et al. (2020) developed a neuro-bee intelligent system for prediction of rockburst. A hybrid technique of the artificial neural network (ANN) and artificial bee colony (ABC), namely, the neuro-bee model, was used in this study to create a sophisticated relationship between the risk of rockbursts in burst-prone grounds and its influencing factors. The indicators were the maximum tangential stress of the cavern wall (σ_{θ}), the uniaxial compressive strength (UCS) of rock, the uniaxial tensile strength of rock, the stress concentration factor (SCF) and the rock brittleness index. Based on the results, the new hybrid model provides more accurate rockburst predictions in both prediction accuracy and generalization capability when compared to other prediction methods. Ma et al. (2018) studied a novel rockburst prediction criterion based on the TBM tunnel construction of the Neelum–Jhelum (NJ) hydroelectric project in Pakistan. Empirical methods were selected to determine the new rockburst criterion (Eq. (2.1) and Hoek and Brown criterion, Section 2.4.1.10). Moreover, geomechanical parameters of rock were evaluated by considering rock strength, brittleness coefficient, quantitative GSI, the TBM construction disturbance, and the in situ stress state. The newly proposed method was defined as the ratio of rock mass strength based on the Hoek-Brown strength criterion to the maximum horizontal stress perpendicular to the

tunnel axis. Based on the results, this method could enhance the accuracy of rockburst during the excavation of underground mining. Pu et al. (2018) presented a method for rockburst prediction where no enough data for rockburst prediction exist. For this purpose, the decision tree was utilized as an intelligent method for rockburst prediction. The two Kimberlite pipes at the Diamond Mine in North Canada were selected as case study. For evaluation of rockburst, several empirical methods of rockburst prediction, such as linear elastic energy (Eq. (2.14)), rock brittleness coefficient (Eq. (2.1)), the ratio between maximum shear stress around the tunnel wall, and uniaxial tensile stress were used. The decision tree model was built for 108 samples where the rockburst occurred and its accuracy was 73% when empirical methods of rockburst were employed. By contrast, this model showed an accuracy of 93% for 132 incomplete data sample. Lee et al. (2004) focused on a new scale system of brittleness and UCS to evaluate the rockburst intensity. Hence, a relationship between the rock brittleness coefficient and UCS of intact rock was obtained:

$$UCS = 110.45 \ln (B_i) - 114.84 , \quad \text{Eq. 2 33}$$

Where B_i is the rock brittleness coefficient. The other relationship between UCS and SED was obtained as follows:

$$UCS = 10.25 SED^{0.25} , \quad \text{Eq. 2 34}$$

Moreover, SED, rock brittleness coefficient, and UCS have a significant relationship with rockburst occurrence. According to their results, the value of each rockburst class was suggested based on the three significant factors. Table 2.33 shows the rockburst intensity based on these rockburst prediction factors.

Table 2 33. Rockburst hazard based on the SED, B_i , and UCS (Lee et al., 2004) .

SED	B_i	UCS (MPa)	Rockburst hazard
<50	<5.75	<78.40	Very low
≈100	≈7.85	≈112.39	Low
≈150	≈9.87	≈138.77	Moderate
≈200	≈12.18	≈161.16	High

Wang et al. (2015) roposed a new method to predict rockburst based on the fuzzy matter-element theory. The matter-element analysis is primarily used to study the problem of incompatibility, and the improved fuzzy matter-element theory evaluation method was employed to assess water quality and showed acceptable results compared with the traditional method. For the proposed rockburst prediction method, the fuzzy matter-element theory was selected, and the rock brittleness coefficient (Eq. (2.1)), mean stress (Eq. (2.5)), impact energy tendency, and rock integrity coefficient (Eq. (2.20)) were introduced as the main influencing factors of rockburst in this model. The Huize Lead-Zinc Mine in China was selected as the study case. This method was applied to different rock strata, and finally, its results were compared with those of the empirical methods of rockburst. Based on the result, the fuzzy matter-element was very efficient for predicting rockburst intensity due to high accuracy, and this model was made based on the empirical method of rockburst. Chen et al. (2003) used the empirical methods of rockburst prediction in conjunction with the artificial neural network for prediction of rockburst. According to the results, this method has an acceptable rockburst prediction accuracy. Dong et al. (2013) performed the Random Forest (RF) method to classify rockburst and its intensity in underground rock project. The main control factors of rockburst, such as the magnitude of in situ stresses, UCS, tensile strength, and elastic energy index (Eq. (2.13)) of rocks, were selected. Therefore, the RF model and rockburst prediction methods were determined through 36 sets of rockburst predictions. The results showed that the RF model can accurately classify the rockburst intensity. Feng et al. (2012) studied the rockburst in deep tunnels in Jinping II Hydropower Project. This study

aimed to evaluate the rockburst mechanism and its seismicity and intensity before and during the excavation. Thus, laboratory tests and in situ monitoring before and after the excavation process were conducted to analyze the different types of rockburst, such as strain, fault-slip, immediate, and time-delayed rockbursts. The results showed that the evolution of rockbursts consists of generation, opening, closing, and propagation of cracks, in a form of tension, shear, or mixed failure. Rockbursts of different types, that is, strain rockbursts, strain-structure slip rockburst, and exposed different micro-cracking mechanisms in combination of tension, shear, or mixed failure, were considered. The difference with immediate rockbursts is that a quiet period of micro-seismicity before the occurrence of time-delayed rockburst exists. Wojtecki and Konicek (2016) studied the important and effective rockburst factors when the geological conditions of mining are not suitable. Based on the results, the depth of mining, dislocations, and mining remnants are important factors when the mining is located under unsuitable geological conditions. Saeidi et al. (2012) employed empirical methods of rockburst prediction in Sabzkuh Water Conveyance Tunnel as a case study. The Sabzkuh water conveyance tunnel is 11 km in length, passing through high mountains measuring 1200 m. To this end, data have been obtained from laboratory tests, literature reviews, and field studies. The results indicated that the dynamic rockburst should occur in this tunnel. Liu et al. (2013) studied the predictions of rockburst using the Cloud model that represents the overall quantitative features of the qualitative concept. In addition, the attribution weight method was used to quantify the contribution of each rockburst indicator to classification. The results of the computed weight value of the indicator showed that the stress ratio is the most important factor for rockburst occurrence, followed by the elastic strain energy index and brittleness factor. Moreover, the cloud model can predict the rockburst intensity better than the empirical methods of rockburst prediction. Yan et al. (2015) studied the mitigation of rockburst by blasting technique at Jin-ping-I (JPI) and Jin-ping-II (JPPII), which are two large hydropower stations. To this end, the elastic strain energy index (Eq. (2.13)) was used to evaluate rockburst for different excavation footages. Based on the results, the stress-relief blasting method can effectively decrease the stress concentration of the surrounding rocks and reduce the risk of rockbursts. Furthermore, they mentioned that the space between two adjacent relief holes must be less than 2 m in the design of

stress-relief blasting to ensure the stress relief effect. In addition, decreasing the excavation footage should be used to control the blasting excavation disturbance in the underground excavation. Guo et al. (2018) studied the effect of saturation time on the coal burst liability indexes. The coal seam water infusion can be used as a suitable technique for rockburst mitigation. To study its effects, they used the strain energy index as one of the empirical methods of rockburst tendency. The results showed that the strain energy index and other factors related to the rockburst tendency decreased as the saturation time increased. Jiang et al. (2010) used the LERR (Eq. (2.18)) at the Jinping tunnel to determine the conditions causing rockburst. The results showed that the LERR can satisfactorily evaluate the rockburst risk. Afraei et al. (2018) studied those predicting variables with significant effects on the rockburst. They used 188 distinct case histories. For each case history, the predictor variables were overburden thickness, maximum tangential stress in the boundary of opening, UCS of rock, the tensile strength of rock, stress ratio (Eq. (2.7)), brittleness ratio (Eq. (2.1)), elastic strain energy index (Eq. (2.13)), and one of the four defined classes (none or not-occurred, weak, moderate, and strong) for the qualitative dependent variable of rockburst intensity. The results showed that the predicting variables, such as the maximum tangential stress, stress ratio, elastic strain energy index, tensile strength, and UCS of rock, have significant roles in the rockburst phenomenon. However, the predicting variables, such as overburden thickness, the tensile strength, and brittleness ratio, have no significant effect on the rockburst phenomenon based on case histories. Liu et al., (2015) reported that if the value of UCS is between 100 and 400 MPa, and the rock mass has a high tendency for rockburst. Li and Jimenez (2018) proposed a novel empirical method for a long-term rockburst prediction based on the logistic regression. This model was tested using a database of case histories extracted from the literature and technical report on the underground project. Five possible input parameters, such as tunnel depth, H , maximum tangential stress, elastic energy index (Eq. (2.13)), the UCS of rock (UCS), and the uniaxial tensile strength of rock, were adopted to estimate the probability of rockburst. Last, the results of the new model were compared with those of empirical methods of rockburst. According to the results, the rockburst probability increases with increasing the excavation depth; therefore, *elastic energy index* and UCS have a similarly significant

influence on rockburst occurrence. Li et al. (2017) studied rockburst prediction using incomplete data from Bayesian networks. The five parameters, namely, buried depth in the tunnel, maximum tangential stress (MTS), uniaxial tensile strength, UCS, and elastic energy index, were used to construct the Bayesian network with tree augmented Naïve Bayes classifier structures. Therefore, the novel application of Bayesian network showed acceptable rockburst prediction performance based on the five parameters. Manouchehrian and Cia (2017) investigated the influence of weak planes, such as faults, joints, and dykes, on the occurrence of rockburst in a tunnel subjected to static loads. To this end, they used Abaqus 2D to simulate dynamic rock failure in deep tunnels. The results presented that the rockburst around discontinuities was more violent and the failure zone around the excavation zone was larger. Furthermore, the velocity and the released energy near the discontinuities were higher in comparison with the absence of discontinuities. Therefore, the effect of discontinuities on the rockburst occurrence must be considered in underground excavation. Fakhimi et al. (2016) studied the pillar burst by using the soft loading. To this end, the UCS test was used on sandstone samples to compute the accumulation of the strain energy and find the rupture point of samples. The numerical modeling was also utilized for the rockburst simulation. The effects of different parameters involved in the dynamic rock fracture and strainburst, such as the loading system stiffness, the rock strength, the pillar dimensions, and the rock loading system interface friction coefficient, were considered. According to the results, the pillar diameter and its UCS have an important effect on the induced kinetic energy during a strainburst.

2.4.5 Discussion

The rockburst prediction approaches can be categorized as empirical, experimental, analytical, intelligent, and numerical methods. Although none of these methods is completely effective or complete, each has its own strengths and limitations. Different assessment indices or indicators are used in empirical methods, having become widely used. It's easy and feasible to employ these methods, which have been shown to be effective in numerous cases. Among stress estimation methods, the rock brittleness coefficient and tangential stress criteria show the most reliable results in predicting the

intensity of rockbursts. They use simple indicators based on a rock mass parameters, which can be evaluated by experimental tests and give realistic values. To predict the intensity of a rockburst, energy methods are more commonly employed than stress methods. Since the results of these methods can be compared to the seismicity data collected from the excavation and the surrounding area, this can provide a clearer insight into the causes of the rockburst. The other reason of using energy methods is that the occurrence of rockburst is closely related to the energy evolution of the rock mass, which includes energy storage, dissipation, and release. Therefore, the criteria based on energy are more likely to reflect rockburst proneness than others. The criteria with multiple indicators, such as the five-factor criterion, have gained favor because it is able to measure rockburst intensity by taking into account more indicators and more significant parameters of the rock. On the other hand, there are some deficiencies with using empirical criteria to predict rockbursts. The majority of empirical criteria are based on a common concept, that is, the ratio of stress to strength, indicating that rockburst is formed by compression. Criteria thresholds are generally determined by the analytical and statistical aspects of the area where rockbursts were observed, or by engineering expertise (Zhou et al., 2012; Feng et al., 2013). In contrast, different scholars use different parameters as evaluation criteria, and the classification of rockburst intensity also differ between them. For example, Kidybinski (1981) proposed that the elastic strain energy index (W_{et}) is recommended to be greater than 5, which indicates a tendency of a strong rockburst. However, on the basis of the experimental results for the Sudbury area (Ontario, Canada) hard rock samples, Singh (1987) proposed that $W_{et} < 10$ is for no or low rockburst intensity. The multiplicity of rockburst criteria made front-line engineers obsessed with discriminating the level of the kickoff of a rockburst disaster (Zhou et al., 2018). Moreover, various conditions of geomechanical and geological conditions have been taken into consideration when developing the criteria. Many criteria consider only one component of stress. Strain and stress are second-order tensor variables. Accordingly, estimating rock mass stability based on one extracted component is unreasonable, since the surrounding rock mass is usually under biaxial or triaxial stress conditions, and the strength and deformation properties of rocks are highly affected by multiple stress conditions and the nature of the rock itself. Due to this uncertainty, a

universal and practical criterion cannot be identified, and it is necessary to analyze the results of various prediction criteria in depth. Especially, when the empirical criteria are applied, it would be best to specify a range of potential input parameters rather than a single input point, because this would reflect the involved uncertainties. In some empirical rockburst methods like the mean stress index or strength index, the magnitude of principal in situ stress is factored into the equation. The magnitude of in situ stresses in excavation at great depth below surface are estimated rather than the exact value of field stresses. As a result, using these types of empirical methods creates uncertainty, which must be considered during the design and excavation of mines. Also, there are many rockburst reports around the world, however, only a small number of those cases have been described with available or reported data for different representative factors or predictor variables. In each dataset, the values of the following predictor variables are included as: the overburden thickness of the opening in meter, the maximum tangential stress in boundary of opening, the uniaxial compressive strength of rock, the tensile strength of rock, the ratio of the maximum tangential stress to the uniaxial compressive strength of rock (stress ratio), the ratio of the uniaxial compressive to the tensile strength of rock (brittleness ratio), and the ratio of the elastic energy stored to the dissipated energy (elastic energy index). These documents do not include the detailed descriptions of geological, geomechanical, or technological conditions, any associated seismic events, or any other information factor that affects rockbursts. Furthermore, it is a fact that geological, geomechanical, and technological conditions are difficult to quantify into tangible predictor variables. As for the predictor variables, the maximum tangential stress and stress ratio have been obtained by using different approaches (determination based on in situ measurements or estimating using analytical solutions or numerical models). It is obvious that different methods produce different results. Also, one of the other significant parameters is rock texture, which can strongly influence the petrophysical and mechanical properties of a rock, including its uniaxial compressive strength, elastic properties, and shear strength. Mineral composition, crystal size, rock fabric, alteration degree, grain size and grain shape, weathering, and anisotropy are the most important factors affecting the strength and deformation properties of intact rocks. Also, the discontinuities in the rock, such as macro and micro fractures, bedding planes,

schistosity, and faults, make it weaker and control its overall behavior. Accordingly, it appears to be important to understand how rock texture and rock properties interact and subsequently how intensity relates to rockbursts. The rockburst empirical criteria should be developed based on the above factors and validated by a real database. As an outstanding advantages of empirical criteria and in comparison with other rockburst prediction methods like intelligent or numerical methods, they are not highly dependent on the data preprocessing procedure and training parameters. Moreover, stress and energy criteria are widely used in numerical and intelligent methods as the input data. In contrast with numerical methods, which have many limitations in predicting rockbursts behavior, including the complexity of rockbursts, the difficulties in modeling the transition from continuous to discontinuous behavior, and the limitations of the small displacement rule, the empirical criteria are able to predict rockburst intensity in a straightforward way.

2.5 Summary and Conclusion

Rock mass failure is an important issue in the underground excavation. The risk of rock mass failure increases as the depth of the excavation increases. The presence of an excavation induces an increase of the tangential stress and a decrease of the radial stress, leading to the occurrence of rockburst as an important failure process of brittle and hard rock. The spalling and slabbing forms of rockburst are often observed in underground excavations. Empirical methods have shown acceptable results. However, none of these methods is completely valid, and all of the prediction methods have their own advantages and disadvantages. As mentioned earlier, the predicted rockburst intensity varies considerably from one model to another. The empirical methods are based on one or two stress indices, and the scholar index for all of them is totally different. The energy and stress methods have shown acceptable performance for the evaluation of rockburst tendency. Recent studies developed the rockburst prediction intensity and found the safest rockburst analysis. Typically, one or several rockburst methods are selected, depending on the level of in situ and induced stresses, type of the rock mass, excavation methods, properties of the rock mass, location of tunnel or mine, and dynamic disturbance and experimental instrument in the laboratory. Moreover, the stress and

energy methods have been used as a part of the input data in numerical or intelligent methods. According to the literature review, rock mass brittleness, tangential stress, and Hoek and Brown criteria, as the stress methods of rockburst prediction, are used more among the other stress methods, while the elastic strain energy and linear elastic energy are used as the energy methods of rockburst prediction. However, The ERR cannot determine the intensity, location, and scale of rockburst. Therefore, the new method, FERR, was proposed to help the mining engineering understand the location and scale of rockburst in the underground excavation. However, FERR cannot evaluate the intensity of rockburst. According to the literature, maximum tangential stress, elastic strain energy index, and uniaxial compressive stress and tensile strength are highly efficient in rockburst prediction. Aside from the empirical methods, using numerical modeling is efficient to verify the results of empirical methods with the numerical method. Moreover, the geological structure of mining and the existence of discontinues, such as fault and methods of excavation, have a significant effect on the occurrence of rockburst. For example, delay-rockburst occurs after the excavation because the level of tangential induced stress does not reach to the strength of rock mass. The value of tangential stress reaches the rock mass strength, and rock failure occurs due to the blasting or machine excavation in underground mining or the existence of discontinues. Hence, the external parameters should be considered.

Empirical methods rely on various evaluation indices or indicators, which have become widely accepted. Empirical criteria are easy to employ as they have been shown to be effective in numerous research projects. Simplesness and ease of use are the main advantages of the rockburst empirical criterion and classification method, and mine engineers have used it to identify rockburst events. In the early stages of a project, empirical methods are commonly used to determine the quality of the rock mass and the rockburst of underground openings. Rockburst events are primarily predicted by factors related to stress and energy indexes. These factors are easily determined by the geomechanical laboratory test like uniaxial compressive test, triaxial test and brazillian test. So, these methods could be applied to identify the high risk zone during the excavation. Although predictions of rockburst have received much attention from the

research community, many questions remain unanswered. Investigating the following issues may be of interest in the future:

(1) The empirical methods of rockburst are based on the static condition, but there is no method of predicting the effect of dynamic loads on the indicator. Dynamic loads can be formed as extra energy to the excavation area and can increase the energy stored in the rock. It is necessary to develop the methods that take dynamic loads into account.

(2) The stress and energy methods of rockburst are based on interpolation of curves and generally have little physical significance, and their validation with real data is limited. By making a large database of rockburst events from all available databases, applying empirical methods to them, and confirming those predictions with real rockburst events, researchers might be able to develop more accurate prediction methods for rockburst.

(3) In the field, rockburst occurrence is strongly related to in situ stress conditions, lithology, excavation depth, rock texture, hydrogeological conditions, and discontinuities surrounding the excavation zone. However, the role of rock texture (Minerals, grainsize, schistosity, etc.) in occurrence of rockbursts remains largely undetermined. So, future studies can focus on the relationship between rock texture and rockburst intensity, and suggest a number of empirical methods based on the rock texture properties.

Considering these factors, application of these techniques for rockburst prediction will be straightforward and beneficial.

Acknowledgments

The authors would like to acknowledge the funding received by a grant from Natural Sciences and

Engineering Research of Canada (NSERC) for this study.

Declaration of Competing Interest

The authors declare that they have no known competing financial interests or personal relationships that could have appeared to influence the work reported in this paper.

2.6 References

- Afraei, S., Shahriar, K., & Madani, S. H. (2018). Statistical assessment of rock burst potential and contributions of considered predictor variables in the task. *Tunnelling and Underground Space Technology*, 72(11), 250–271.
- Ahmed, S. S., ALHeib, M., Gunzburger, Y., & Renaud, V. (2017). Pillar Burst Assessment Based on Large-scale Numerical Modeling. *Procedia Engineering*, 191, 179–187.
- Aubertin, M., Gill, D. E., & Simon, R. (1994). On the Use of the Brittleness Index Modified (BIM) to Estimate the Postpeak Behavior of Rocks. Rock Mechanics Models and Measurements Challenges from Industry. *1st North American Rock Mechanics Symposium*, Austin, Texas.
- Avershin, S.G. (1959). Rock Burst, *China Coal Industry Press*, Beijing.
- Aydan Ö., & Geniş M., A. T. (2001). Assessment of Susceptibility of Rock Bursting in Tunnelling in Hard Rocks. *Modern Tunnelling Science and Technology*, 67(1), 369–380.
- Bandis, S.C. (1997). Rock characterization for Tunnelling – A Rock Engineer’s Perspective, *Feldsbau edition*, 15, 3.
- Barton, N., Lien, R., & Lunde, J. (1974). Engineering classification of rock masses for the design of tunnel support. *Rock Mechanics Felsmechanik Mécanique des Roches*, 6 (4), 189–236.
- Blake, W., & Hedley, D. G. F. (2003). Rockbursts, Case Studies from North American Hardrock Mines. Book, Chapter 1, 1–15.
- Blake., W. (1972). Rock-burst mechanics. *Colorado School Mines*, 67(1), 1–64.
- Board, M. (1996). Numerical examination of mining-induced seismicity. *ISRM International Symposium*, EUROCK 96, Turin, Italy.
- Brauner, G. (1994). Rockburst in Coal Mines and Their Prevention. Taylor & Francis Group, 1st Edition, Balkema, Netherlands.
- Brady, B. H., & Brown, E. T. (1993). Rock mechanics: for underground mining, *Kluwer Academic Publishers*, Dordrecht, Netherlands.

- Broch, E., & Sørheim, S. (1984). Experiences from the planning, construction and supporting of a road tunnel subjected to heavy rockbursting. *Rock Mechanics and Rock Engineering*, 17(1), 15–35.
- Cai, M. (2016). Prediction and prevention of rockburst in metal mines - A case study of Sanshandao gold mine. *Journal of Rock Mechanics and Geotechnical Engineering*, 8(2), 204–211.
- Cao, J.J., Hu, Q.T., & Zhang, Y.J. (2015). Coal rock gas dynamic disaster classification attribute and its prevention practice in deep mine. *Electronic Journal of Geotechnical Engineering*, 20(19), 11309–11326.
- Castro., L.A.M., Bewick, R.P., & Carter, T. (2012). An overview of numerical modelling applied to deep mining. Taylor & Francis Group, (Chapter 21).
- Chen, B.R., Feng, X.T., Li, Q.P., Luo, R.Z., & Li, S. J. (2013). Rock burst intensity classification based on the radiated energy with damage intensity at Jinping II hydropower station, China. *Mechanics and Rock Engineering*, 48(1), 289–303.
- Chen, H., Li, N., Nie, D., & Shang, Y. (2003). Prediction of rockburst by artificial neural network. *Yanshilixue Yu Gongcheng Xuebao / Chinese journal of rock mechanics and engineering*. 22 (5), 762-768
- Colson., C. M. (1950). Rockburst. Master thesis, Missouri S&T University,
- Cook, N. G. W. (1963). The basic mechanics of rockbursts. *Journal of the Southern African Institute of Mining and Metallurgy*, 64(3), 71–81.
- Dechelette, O., Josien, J.P., Revalor, R., & Jonis, R. (1984). Seismo-acoustic monitoring in an operational longwall face with a high rate of advance. *South African Institute of Mining and Metallurgy*, 83–87.
- Diederichs, M. S. (1999). *Instability of Hard Rock Masses: The Role of Tensile Damage and Relaxation* [Doctoral dissertation, University of Waterloo].
- Diederichs, M.S., Carter, T., & Martin, D. (2010). Practical rock spall prediction in tunnels. *ITA World Tunnel Congress*, Vancouver.
- Dietz, M., Oremek, G.M., Groneberg, D.A., & Bendels, M. H. K. (2018). What is a rock burst?. *Zentralblatt für Arbeitsmedizin, Arbeitsschutz und Ergonomie.*, 68(1), 45–49.
- Dong, L., Li, X., & Peng, K. (2013). Prediction of rockburst classification using Random Forest. *Transactions of Nonferrous Metals Society of China*, 23(2), 472–477.
- Dowding, C. H., & Andersson, C. A. (1986). Potential for rock bursting and slabbing in deep caverns. *Engineering Geology*, 22(3), 265–279.

- Duan, K., Ji, Y., Wu, W., & Kwok, C. Y. (2019). Unloading-induced failure of brittle rock and implications for excavation-induced strain burst. *Tunnelling and Underground Space Technology*, 84, 495-506.
- Du, Z. J., Gao, Y. T., Deng, D. Q., & Han, H. L. (2010). Rockburst Prediction of Deep Mining in Tectonic Stress Mine. *International Mining Forum*. <https://file.scirp.org/pdf/29-1.18.pdf>
- Fairhurst, C. (2003). Stress estimation in rock: a brief history and review. *International journal of rock mechanics and mining sciences*, 40, 957–973.
- Fakhimi, A., Hosseini, O., & Theodore, R. (2016). Physical and numerical study of strain burst of mine pillars. *Computers and Geotechnics*, 74, 36–44.
- Feng, X., Chen, B., Li, S., Zhang, C., Xiao, Y., Feng, G., Zhou, H., Qiu, S., Zhao, Z., Yu, Y., Chen, D., & Ming, H. (2012). Studies on the evolution process of rockbursts in deep tunnels. *Journal of Rock Mechanics and Geotechnical Engineering*, 4(4), 289–295.
- Feng, X.T., Chen, B.R., Zhang, C.Q., Li, S.J., & Wu, S.Y., (2013). Mechanism, Warning and Dynamical Control of Rockburst Evolution Process. *Science Press*, Beijing, pp. 380–391.(in Chinese)
- Fisher, J. (2013). Impact of gas emissions on the initiations of coal bumps. *The 23th World Mining Congress*, Montreal, Canada, 396–410.
- Gill, D.E., Aubertin, M., & Simon, R. (1988). Une méthodologie d'évaluation du potentiel de coups de terrain dans les mines d'Abitibi. Colloque sur le Contrôle de Terrain (AMMQ), Val d'Or, Institut de recherche Robert-Sauvé en santé et en sécurité du travail (IRSST).
- Gill, D.E., Aubertin, M., & Simon, R. (1993). A practical engineering approach to the evaluation of rockburst potential. *Proceedings of the 3rd International Symposium on Rockbursts and Seismicity in Mines*. Rotterdam, Netherlands. Rotterdam, 63–68.
- Gong, F. Q., & Li, X.. (2007). A distance discriminant analysis method for prediction of possibility and classification of rockburst and its application. *Chinese Journal of Rock Mechanics and Engineering*, 26(5), 1012–1018 (in Chinese).
- Goel, R.K. (1994). Correlations for predicting support pressures and closures in tunnels. PhD Thesis, University of Nagpur, India.
- Goel, R.K., & Jethwa. J. (1995). An empirical approach for predicting ground condition for tunneling and its practical benefits. 35th US conference on rock mechanics, 431–435.

- Grimstad, E. (1999). Experiences from excavation under high rock stress in the 24.5 km long laerdal tunnel. *Proceeding of the International Conference on Rock Engineering Techniques for Site Characterization*, 135–146.
- Guo, R., & Yu, R.C. (2002). Design of support work in drift having rockburst danger. *China Mining Magazine*, 11 (3), 23–26 (in Chinese).
- Guo, W.Y., liang.T., Yang, Z., & Zhao, T. (2018). Effect of Saturation Time on the Coal Burst Liability Indexes and Its Application for Rock Burst Mitigation. *Geotechnical and Geological Engineering*, 36(3), 589–597.
- Hawkes, I. (1966). Significance of in situ stress levels. *Proceeding of the first international congress of the international society for rock mechanics.*, 1 (3).
- He, F. (2005). Study on geological hazards in tunneling of deep-buried long tunnels at qinling-dabashan orogen of the three gorges reservoir water diversion project. Ph.D Thesis. China Academy of Geological Sciences, Beijing, China (in Chinese).
- He, M., Sousa, L.R., Miranda, T., & Zhu, G. (2015). Rockburst laboratory tests database— application of data mining techniques. *Engineering Geology*, 185(5), 116–130.
- Hedley, D. G. F., (1992). Rockburst Handbook for Ontario Hardrock Mines. *Energy, Mine and Resources*, Ottawa, Canada.
- Hoek, E., & Brown, T. (1980). *Underground Excavations in Rock*, CRC Press, London. 536.
- Holland, C.T, & Thomas, E., (1954). Coal mine bumps-some aspects of occurrence, cause, and control. *BuMines*, 35, 65–71.
- Hou, F., & Wang, M. (1989). The Rockburst Criterion and Prevention and Cure Step in the Circular Tunnel. The Application of Rock Mechanics in the Project. The Knowledge press, 195–201.
- Jiang, Q., Feng, X.T., Xiang, T.B., & Si, G.S. (2010). Rockburst characteristics and numerical simulation based on a new energy index: A case study of a tunnel at 2,500 m depth. *Bulletin of Engineering Geology and the Environment*. 69(3), 381–388.
- Jiang, Y. D., Pan, Y. S., Jiang, F. X., DOU, L. M., & Ju, Y. (2014). State of the art review on mechanism and prevention of coal bumps in China. *Journal of China Coal Society*, 39 (2), 205-213.
- Jiang, Y., Zhao, Y., Wang, H., & Zhu, J. (2017). A review of mechanism and prevention technologies of coal bumps in China. *Journal of rock mechanics and*

- geotechnical engineering*, 9, 180–194.
- Kaiser, P. K., Diederichs, M. S., Martin, C. D., Sharp, J., & Steiner, W. (2000). Underground works in hard rock tunnelling and mining. *ISRM international Symposium, Melbourne, Australia*, 841–926.
- Kaiser, P.K., Tannant, D.D., & McCreath, D. R. (1996). Canadian Rockburst Support Handbook. *Geomechanics Research Center*.
- Kaiser, P.K. (2009). Failure mechanisms and rock support aspects. Int. Consultation Report for the Key Technology of Safe and Rapid Construction for Jinping II Hydropower Station High Overburden and Long Tunnels, Jinping II, 62–71.
- Kidybiński, A. (1981). Bursting liability indices of coal. *International Journal of Rock Mechanics and Mining Sciences*, 18(4), 295–304.
- Lee, S. M., Park, B. S., & Lee, S. W. (2004). Analysis of rockbursts that have occurred in a waterway tunnel in Korea. *International Journal of Rock Mechanics and Mining Sciences*, 41, 911–916.
- Li, N., & Jimenez, R. (2018). A logistic regression classifier for long-term probabilistic prediction of rock burst hazard. *Natural Hazards*, 90(1), 197–215.
- Li, N., Feng, X., & Jimenez, R. (2017). Predicting rock burst hazard with incomplete data using Bayesian networks. *Tunnelling and Underground Space Technology*, 61, 61–70.
- Li, T., Ma, C, Zhu, M. L., & Chen, G. (2017). Geomechanical types and mechanical analyses of rockbursts. *Engineering Geology*, 222, 72–83.
- Li, T., Cai, M.F., & Wang, J.A. (2005). Discussion on relativity between rockburst and gas in deep exploitation. *Journal of China Coal Society*, 30(5), 562–567 (in Chinese).
- Li, T., Cai, M.F., & Cai, M. (2007). Earthquake-induced unusual gas emission in coalmines – A km-scale in situ experimental investigation at Laohutai mine. *International Journal of Coal Geology*, 71(2–3), 209–224.
- Li, Z.H., Wang, E.Y., Ou, J.C., & Liu, Z.T. (2015). Hazard evaluation of coal and gas outbursts in a coal-mine roadway based on logistic regression model, *International Journal of Rock Mechanics and Mining Sciences*, 80, 185–195.
- Lippmann-Pipke, J., Erzinger, J., Zimmer, M., Kujawa, C., Boettcher, M., Heerden, E., Bester, A., Moller, H., Stronik, N., & Reches, Z. (2011). Geogas transport in fractured hard rock - Correlations with mining seismicity at 3.54km depth, TauTona gold mine, South Africa. *Applied Geochemistry*, 26(12), 2134–2146.

- Liu, Y., Shu, Y., & Qin, T. (2015). Rock burst forecasting and prevention technology of thin coal seam in xinxing mine. *Electronic Journal of Geotechnical Engineering*, 20, 4233–4248.
- Liu, Z., Shao, J., Xu, W., & Meng, Y. (2013). Prediction of rock burst classification using the technique of cloud models with attribution weight. *Natural Hazards*, 68 (2), 549–568.
- Lu, C. P., Liu, Y., Zhang, N., Zhao, T., & Wang, H.,(2018). In- situ and experimental investigation of rockburst precursor and prevention induced by fault slip. *International Journal of Rock Mechanics and Mining Sciences*, 108, 86–95.
- Ma, C. S., Chen, W.Z., Tan, X.J., Tian, H.M., Yang, J.P., & Yu, J.X. (2018). Novel rockburst criterion based on the TBM tunnel construction of the Neelum–Jhelum (NJ) hydroelectric project in Pakistan. *Tunnelling and Underground Space Technology*, 81, 391–402.
- Manouchehrian, M., & Cai, M. (2017). Analysis of rockburst in tunnels subjected to static and dynamic loads. *Journal of Rock Mechanics and Geotechnical*, 9(6), 1031–1040.
- Martin, C. D., & Christiansson, R. (2009). Estimating the potential for spalling around a deep nuclear waste repository in crystalline rock. *International Journal of Rock Mechanics and Mining Sciences*, 46(2), 219–228.
- Meng, F., Zhou, H., Wang, Z., Zhang, L., Kong, L., Li, S., & Zhang, C. (2016). Experimental study on the prediction of rockburst hazards induced by dynamic structural plane shearing in deeply buried hard rock tunnels. *International Journal of Rock Mechanics and Mining Sciences*, 86, 210–223.
- Meng, F., Zhou, H., Wang, Z., Zhang, L., Kong, L., Li, S., Zhang, C., & Hu, S. (2017). Experimental study of factors affecting fault slip rockbursts in deeply buried hard rock tunnels. *Bulletin of Engineering Geology and the Environment*, 76(3),1167–1182.
- Miao, S. J., Cai, M.F., Guo, Q.F., & Huang, Z.J. (2016). Rock burst prediction based on in situ stress and energy accumulation theory. *International Journal of Rock Mechanics and Mining Sciences*, 83, 86–94.
- Misich, I., & Lang, A. (2001). Examples of rockburst damage in Western Australia. *Proceedings of the 5th international Symposium*, South African Institute of Mining & Metallurgy, 59–68.
- Neyman, B., Szecowka, Z., & Zuberek, Q. (1972). Effective methods for fighting rockburst in polish collieries. *Proceedings of the 5th international strata control*

- conference, 1–9.
- Obert., L., & Duvall., W. I. (1967). Rock mechanics and design of structures in rock. Wiley, Newyork.
- Ortlepp, W. D., & Stacey, T. R. (1994). Rockburst mechanisms in tunnels and shafts. *Tunnelling and Underground Space Technology*, 9(1), 59–65.
- Palmstrom, A. (1995). RMI-a Rock Mass Characterization System for Rock Engineering Purposes. Ph.D thesis, Oslo University, Norway.
- Pan, Y.S., & Li, Z. H.(年份?) The analytic analysis stability of rock structure in mine. Proceedings of National Conference on Solid, Mechanics, Dalian University of Technology Press, Dalian (in Chinese).
- Pan, Y.S. (2016). Integrated study on compound dynamic disaster of coal-gas outburst and rockburst. *Journal of China Coal Society*, 41, (1), 105–112.
- Phillips, W. (1944). Rock Bursts and Bumps in Coal Mines. *Transactions of the American Institute of Mining and Engineering*, 104, 55–94.
- Pu Y, Apel D B, Lingga B. (2018). Rockburst prediction in kimberlite using decision tree with incomplete data. *Journal of Sustainable Mining*, 17(3), 158–165.
- Peng, Z., Wang, Y.H., & Li, T.J. (1996). Griffith theory and rock burst of criterion *Chinese Journal of Rock Mechanics and Engineering*, 15(1), 491–495 (in Chinese).
- Ptáček, J., (2017). Rockburst in Ostrava-Karvina Coalfield. *Procedia Engineering*, 191,1144–1151.
- Qian, Q., & Zhou, X. (2011). Quantitative analysis of rockburst for surrounding rocks and zonal disintegration mechanism in deep tunnels. *Journal of Rock Mechanics and Geotechnical Engineering*, 3 (1), 1–9.
- Qiao, C.S., & Tian, Z. Y. (1998). Study of the possibility of rockburst in Dong-gua-shan Copper Mine. *Chinese Journal of Rock Mechanics and Engineering*, 17, 917–921 (in Chinese).
- Rostami, J., Kahraman, S., Naeimipour, A., & Collins, C. (2015). Rock characterization while drilling and application of roof bolter drilling data for evaluation of ground conditions. *Journal of Rock Mechanics and Geotechnical Engineering*, 7(3), 273–281.
- Russenes, B. F. (1974). Analysis of rock spalling for tunnels in steep valley sides. Master thesis. Norwegian Institute of Technology, Trondheim.
- Ryder J.A. (1987). Excess shear stress in the assessment of geologically hazardous situations. the South African Institute of Mining and Metallurgy, 88, 27–39.

- Saeidi, M., Eftekharib, E., & Taromi, C. (2012). Evaluation of Rock Burst Potential in Sabzkuh Water Conveyance Tunnel, IRAN: a Case Study. 7th Asia Rock Mechanics Symposium, Seoul, South Korea.
- Sainoki, A., & Mitri, H. S. (2014). Dynamic behaviour of mining-induced fault slip. *International Journal of Rock Mechanics and Mining Sciences*, 66, 19–29.
- Sainoki, A., & Mitri, H. S. (2016). Dynamic Modelling of Fault Slip Induced by Stress Waves due to Stope Production Blasts. *Rock Mechanics and Rock Engineering*, 49(1), 165–181.
- Sainoki, A., & Mitri, H. S. (2017). Numerical investigation into pillar failure induced by time-dependent skin degradation. *International Journal of Mining Science and Technology*, 27(4), 591–597.
- Sainoki, A., Mitri, H.S., & Chinnasane, D. (2017). Characterization of Aseismic Fault-Slip in a Deep Hard Rock Mine Through Numerical Modelling : Case Study. *Rock Mechanics and Rock Engineering*, 50(10), 2709–2729.
- Sakurai, S. (1993). Back analysis in rock engineering. *Comprehensive Rock Engineering - Excavation, Support and Monitoring*. Pergamon Press, Oxford, 4, 543–569.
- Shepherd, J, Rixon, L.K., & Griffiths, L. (1981). Outbursts and geological structures in coal mines: a review. *International Journal of Rock Mechanics and Mining Sciences & Geomechanics Abstracts*, 18(4), 267–283.
- Singh, B., & Goel, R. K. (1999). *Rock mass classification: A practical approach in civil engineering*, Elsevier, Amsterdam
- Singh, B., Goel, R.K, Jethwa, J.L., & Dube, A.K. (1997). Support pressure assessment in arched underground openings through poor rock masses. *Engineering Geology*, 48(1-2), 59–81.
- Singh, S. P. (1987). The influence of rock properties on the occurrence and control of rockbursts. *Mining Science and Technology*, 5(1), 11–18.
- Singh, S. P. (1988). Burst energy release index. *Rock Mechanics and Rock Engineering*, 21(2), 149–155.
- Singh, S. P. (1989). Classification of mine workings according to their rockburst proneness. *Mining Science and Technology*, 8(3), 253–262.
- Spalding, J.(1948). *Deep mining*, Mining publication, London, 14.
- Spottiswoode, S. M., & McGarr, A. (1975). Source parameters of tremors in a deep-level gold mine. *Bulletin of the Seismological Society of America*, 65(1), 93–112.

- Sun, X.H., & Li, T. (2011). Prevention Theory and Technology on Compound Dynamic Disaster of Deep Mining in Coal Mine, *Science Press*, Beijing.(in Chinese)
- Tajduś, A., Flisiak, J., & Cala, M., (1997). Estimation of rockburst hazard basing on 3D stress field analysis. University of Mining and Metallurgy, Kraków, Poland.
- Takla, G., Tacek, J., Holecko, J., & Konicek., P. (2005). Stress state determination and prediction in rock mass with rockburst risk in Ostrava-Karvina coal basin. *ISRM international Symposium*, Brno, Czech Republic.
- Tan, Y. A. (1988) Mechanism research and comprehensive evaluation of rockburst. Ph.D Thesis.
- Tan, Y. A. (1992). Rockbursting characteristics and structural effects of rock mass. *International Journal of Rock Mechanics and Mining Sciences & Geomechanics Abstracts*, 29(6), 402–403 *Sci. Chin*, 35(8), 981–990.
- Tang, B. Y. (2000). Rock burst control using distress blasting. Ph.D. thesis. McGill University, Montreal, Canada.
- Tang, L., & Wang, W. (2002). New rock burst proneness index. *Chinese Journal of Rock Mechanics and Engineering*, 21(6), 874–878 (in Chinese).
- Tao, Z. Y. (1988). Support design of tunnels subjected to rockbursting. *Rock Mechanics and Power Plant*, ISRM International Symposium, Madrid, Spain.
- Terzaghi, K., (1946) ‘Introduction to tunnel geology’, *Rock tunneling with steel supports*, 17-99.
- Turchaninov, I. A., Markov, G.A., Gzovsky, M.V., Kazikayev, D.M., Frenze, U.K, Batugin, S.A., & Chabdarova, U.I. (1972). State of stress in the upper part of the Earth’s crust based on direct measurements in mines and on tectonophysical and seismological studies. *Physics of the Earth and Planetary Interiors*, 6(4), 229–234.
- Vasak, P., Suorineni, F.T., Kaiser, P.K., & Thibodeau, D. (2004). Hazard map approach using space-time clustering analysis of mine-induced microseismicity. CIM conference. Edmonton, Canada.
- Wang, Y.H., Li, W.D., Li, Q.G., Xu, Y., & Tan, G. H. (1998). Method of fuzzy comprehensive evaluations for rockburst prediction. *Chinese Journal of Rock Mechanics and Engineering*, 17(5). 493–501 (in Chinese).
- Wang, C., wu, A., Lu, h., Bao, T., & Liu, X. (2015). Predicting rockburst tendency based on fuzzy matter-element model’, *International Journal of Rock Mechanics and Mining Sciences*, 75, 224–232.
- Wang, J. A., & Park, H. D. (2001). Comprehensive prediction of rockburst based on

- analysis of strain energy in rocks. *Tunnelling and Underground Space Technology*, 16(1), 49–57.
- Wang, K., & Du, F. (2019). The classification and mechanisms of coal gas compind dynamic disaster: a preliminary discussion. *Journal of Mining and Mineral Engineering*, 10(1), 68–84.
- Wojtecki, Ł., & Konicek, P. (2016). Estimation of active rockburst prevention effectiveness during longwall mining under disadvantageous geological and mining conditions. *Journal of Sustainable Mining*, 15(1), 1–7.
- Wu, Y.K., & Zhang, W. B. (1997). Prevention of rockbursts in coal mines in China. *Proceedings of the 4th International Symposium on Rockbursts and Seismicity in Mines*, Rotterdam, 361–366.
- Xiao Q H, Liu J G, & Lei S X (2016). A new method for calculating energy release rate in tunnel excavation subjected to high in situ stress. *Perspectives in Science*, 7, 292–298.
- Xu C, Liu X L, Wang Z E, Zheng Y L, & Wang S J. (2018). Rockburst prediction and classification based on the ideal-point method of information theory. *Tunnelling and Underground Space Technology*, 81(1), 382–390.
- Xu, J., Jiang, J., Xu, n., Liu, Q., & Gao, Y. (2017). A new energy index for evaluating the tendency of rockburst and its engineering application. *Engineering Geology*, 230, 46–54.
- Xu, M. G., Yao, G., & Yang, Z.O. (2008). Investigation of comprehensive rockburst prediction during deep mining. *Boundaries of Rock Mechanics: Recent Advances and Challenges for the 21st Century*. 851–856.
- Xue Y G, Li Z Q, Li S C, Qiu D H, Tao Y F, Wang L, Yang W M, & Zhang K (2019). Prediction of rock burst in underground caverns based on rough set and extensible comprehensive evaluation. *Bulletin of Engineering Geology and the Environment*, 78(1), 417–429.
- Yan, P., Zhao, Z., Lu, W., Fan, Y., Chen, X., & Shan, Z. (2015). Mitigation of rock burst events by blasting techniques during deep-tunnel excavation. *Engineering Geology*, 188, 126–136.
- Yang, J.P., Chen, W.Z., & Zhao W.S.(2017). Geohazards of tunnel excavation in interbedded layers under high in situ stress. *Engineering Geology*, 230, 11–22.
- Yoon, J. S. (1994). *Tunnel Engineering*, 160–162.
- Zanski, J. *Podziemna Eksploologia* (1964). *Zloc. Katowice*, 8, English translation.

- Zhang, M., Xu, Z.H., Pan, Y.S., & Zhao, Y.S. (1991). A unified instability theory of rock burst and outburst. *Journal of China Coal Society*, 16 (4), 48–53 (in Chinese).
- Zhang, G., Chen, J., & Hu, B. (2003). Prediction and control of rockburst during deep excavation of a gold mine in China. *Chinese Journal of Rock Mechanics and Engineering*, 22(10), 1607–1612 (in Chinese).
- Zhang, J.J., & Fu, B. (2008). Rockburst and its criteria and control. *Chinese Journal of Rock Mechanics and Engineering*, 27(10), 2034–2042 (in Chinese).
- Zhang, C. Q, Feng, X. T, Zhou, H., Qiu S L & Wu W P. (2013). Rockmass damage development following two extremely intense rockbursts in deep tunnels at Jinping II hydropower station, southwestern China. *Bulletin of Engineering Geology and the Environment*, 72(2), 237–247.
- Zhao, G., Wang, D., Gao, B., & Wang, S. (2017). Modifying rock burst criteria based on observations in a division tunnel. *Engineering Geology*, 216, 153–160.
- Zhou, X. P., Qian, Q. H., Yang, H. Q. (2011). Rock burst of deep circular tunnels surrounded by weakened rock mass with cracks. *Theoretical and Applied Fracture Mechanics*, 56(2), 79–88.
- Zhou, J., Li, X.B., & Shi, X.Z., (2012). Long-term prediction model of rockburst in underground openings using heuristic algorithms and support vector machines. *Safety Science*, 50(4), 629–644.
- Zhou, K. P., Lin, y., Deng, h. W., Li, J. L., & Liu, C. J.(2016a). Prediction of rock burst classification using cloud model with entropy weight. *Transactions of Nonferrous Metals Society of China* (English Edition), 7, 1995–2002.
- Zhou, J., Shi, X. Z., Huang, R. D., Qiu, X. Y., & Chong, C. H. E. N. (2016b). Feasibility of stochastic gradient boosting approach for predicting rockburst damage in burst-prone mines. *Transactions of Nonferrous Metals Society of China*, 26(7), 1938–1945.
- Zhou, J., Li, X., & Mitri, H. S. (2016c). Classification of rockburst in underground projects: comparison of ten supervised learning methods. *Journal of Computing in Civil Engineering*, 30(5), 04016003.
- Zhou, J., Li, X.B., Mitri, H. S. (2017). A critical survey of empirical methods for evaluating rockburst potential. 15th IACMAG', 19–23 October, China.
- Zhou, J., Lia, X., & Mitri, H.S.,(2018). Evaluation method of rockburst: State-of-the-art literature review. *Tunnelling and Underground Space Technology*, 81, 632–659.
- Zhou, J., Li, E., Wang, M., Chen, X., Shi, X., & Jiang, L. (2019). Feasibility of stochastic

- gradient boosting approach for evaluating seismic liquefaction potential based on SPT and CPT case histories. *Journal of Performance of Constructed Facilities*, 33(3), 04019024.
- Zhou, J., Guo, H., Koopialipoor, M., Armaghani, D. J., & Tahir, M. M. (2021). Investigating the effective parameters on the risk levels of rockburst phenomena by developing a hybrid heuristic algorithm. *Engineering with Computers*, 37(3), 1679–1694.
- Zhou, J., Koopialipoor, M., Li, E., & Armaghani, D. J. (2020). Prediction of rockburst risk in underground projects developing a neuro-bee intelligent system. *Bulletin of Engineering Geology and the Environment*, 79(8), 4265–4279.
- Zhu, W.C., Li, Z.H., Zhu, L., & Tang, C.A. (2010). Numerical simulation on rockburst of underground opening triggered by dynamic disturbance. *Tunnelling and Underground Space Technology*, 25(5), 587–599,
- Zhu, G.A., Dou, L.M., Cai, W., Li, Z.L., Zhang, M., Kong, Y., & Shen, W. (2016). Case study of passive seismic velocity tomography in rock burst hazard assessment during underground coal entry excavation. *Rock Mechanics and Rock Engineering*, 49(12), 4945–14955.

Chapter 3: A review on relationship between texture characteristic and mechanical properties of rock ²

Abstract

The textural characteristics of rocks influence their petrophysical and mechanical properties, including their compressive and shear strength, as well as their rheological properties, such as elasticity. Such parameters directly influence rock mass stability. The ability to evaluate both the immediate and long-term behavior of rocks based on the interaction between various parameters of rock texture and petrophysical and mechanical properties is therefore crucial to many geoenvironmental facilities. However, in laboratory tests, high-quality core samples are essential for determining rock strength and elastic parameters, which are occasionally unavailable for instance in fractured or weathered strata. Moreover, detailed rock textural characteristics may not be systematically captured or considered in rock mechanics studies. Nevertheless, the relationships between mechanical properties and textural characteristics for different types of rocks have been investigated by a number of researchers through experimental tests. Single and multivariable regression analyses are conducted between mechanical properties and textural characteristics based on the experimental test data. These regressions help estimating the geomechanical parameters of rocks by using the measured rock texture parameters, and the effect of rock texture parameters can be compared. This study focuses on the review of the effects of rock texture characteristics on geomechanical parameters and summarizes the regression equations between them. The main outcome involves realizing a comprehensive overview on the topic of rock texture parameters and their effects on the mechanical behavior of rocks. Failure criteria of anisotropic rocks, namely continuous and discontinuous criteria, is also discussed. This study provides a comparison of these methods, describes their equations, and discusses their advantages and disadvantages.

Keywords: Rock texture characteristic, Failure criteria of anisotropic rocks, Quantitative mineralogy and petrography, Mechanical properties of rock

² Askaripour M, Saeidi A, Rouleau A, Mercier-Langevin P., MDPI journal (Published)

3.1 Introduction

Rock behavior under in-situ stresses is an essential element to be considered when undertaking earth engineering studies (Zhang, 2006). However, a rock mass is generally substantially heterogeneous with contrasting types of rocks; therefore, it cannot be regarded as a homogeneous medium. Furthermore, a single rock type can have distinct textural properties (e.g., mineral species, grain size, shape, and orientation). Thus, understanding the influence of rock texture on its geomechanical behavior is crucial. Rock behavior is related to petrophysical properties, such as density, ultrasonic P-wave velocity, magnetic susceptibility, electric resistivity, and magnetic remanence, and to mechanical properties, such as uniaxial compressive strength (UCS), tensile and shear strength, and elastic properties, e.g., Young's modulus and Poisson's ratio (Tapponnier and Brace, 1976). The mechanical properties and the composition of the rocks are commonly used to obtain critical information, such as rock or slope instability, failure mechanism, strength-deformation characteristic assessment, and other engineering purposes (Miskovsky, 2004). Moreover, the most influential factors on the strength and deformation behaviors of intact rocks include mineral composition, crystal size, rock fabric, grain size and shape, hydrothermal alteration, weathering, and anisotropy. (Saroglou et al., 2004). Discontinuities in the rock, such as macro- and micro-fractures, bedding planes, schistosity, and faults, contribute to its weakening and largely control its overall stress response. Anisotropy is primarily caused by schistosity, foliation, cleavage. At high metamorphic grade, a rock can become layered, substantially heterogeneous and deformed. In sedimentary rocks, different grain or clast sizes characterize bedding planes and lamination (Shakoor and Bonelli, 1991). Metamorphic rocks are generally physically weaker than magmatic rocks (e.g., Přikryl, 2006; Sun et al., 2017). Increasing microporosities along the grain boundaries and simplifying grain relationships result in decreasing strength properties (Song et al., 2021). The main literature reviews reveal that textural characteristics of the rock are major factors controlling variations in their geomechanical properties and their behavior in different engineering works.

Available information regarding the concept of rock textural characteristics in a rock mechanics context and the current definitions of geometrical features of rock is reviewed

in this paper. The effect of rock textural characteristics on geomechanical parameters, including changes in mineralogy, is then discussed. An assessment of the influence of grain size, density, porosity, and anisotropy on geomechanical parameters and their regression analyses is also presented. An introduction and a brief discussion on failure models of anisotropic rock based on continuous versus discontinuous criteria and their advantages and disadvantages are provided in the last section of this paper. Finally, key gaps in the understanding of rock textures versus rock mechanics are identified, and potential avenues for future research are highlighted.

3.2 Rock textural characteristics

The texture of a rock is a crucial factor in defining its geomechanical properties, including its strength. Rock texture has been defined as “*the degree of crystallinity, grain size or granularity and the fabric or geometrical relationship between the constituents of a rock*” (Williams et al., 1982). The drillability, cuttability, and machinability of rocks are affected by four categories of rock characteristics, namely textural, mechanical, structural, and weathering (Table 3.1).

Table 3 1. Classifications of rock characteristics (Adapted Williams et al., 1982).

Rock characteristics	Parameters
Textural characteristics	Grain size, shape and orientation, packing density, texture coefficient, mineral content, cement type and degree of cementation, porosity, grain boundary or contact relationships,
Mechanical characteristics	Strength, hardness, abrasiveness, density, pore pressure
Structural characteristics	Joints, fractures, cleavages, foliations, faults, folds, bedding, banding, and schistosity
Weathered characteristics	Alteration and water content

The geometrical relationships of the rock-forming minerals define its texture. The geometrical features of mineral grains can be obtained from visual inspection of a rock and the study of samples under the microscope (using thin-sections) and through different automated, combined analytical element mapping methods (Schulz et al., 2020). Rock texture is generally considered a qualifier, and different geometrical features are considered in quantifying the texture of a rock, as summarized in Table 3.2.

Table 3 2. Rock textural parameters (The parameters are adapted from the mentioned references)

Feature	Definition	Formula	References	Parameters
Packing density (P_d)	Ratio of the sum of the grain length encountered along a traverse across a thin section to the total length of the traverse	$P_d = \frac{\sum L_i}{TL} \times 100\%$	Kahn (1956)	L_i is the length of each grain along the traverse line, TL is the traverse length.
Packing proximity (P_p)	Ratio of the number of grains to grain contacts	$P_p = \frac{\sum g_i}{t} \times 100\%$	Kahn (1956)	g_i is the number of grain-to-grain contact, t is the total length of the traverse
<i>Index of interlocking (g)</i> :	Compares the area of the grain and its perimeter, which contacts neighboring grains	$g = \frac{1}{n} \sum \frac{L_{pi}}{\sqrt{A_i}}$	Dreyer, (1973)	n is number of grains considered, L_{pi} is a portion of the grain perimeter which contacts neighboring grains, A_i is the area of exposed grain section
<i>Index of grain size homogeneity (t)</i>	A non-directional fabric parameter that defines the grain size distribution of the rock	$t = \frac{A_{avg}}{\sqrt{\sum (A_i - A_{avg})^2}}$	Dreyer, (1973)	A_{avg} is the average grain cross-section (area), A_i is the area of individual grain
Grain contact	Ratio to its own total length of the length of contact a grain has with its neighbors	$GC = \frac{L}{\sum L_n} \times 100\%$	Dobereiner and De Freitas (1986)	L is the length of grain contact, L_n is the total length of grain surface
Grain shape	Sphericity: Ratio between grain volume and the smallest circumscribing sphere	$Sphericity = \frac{R_i}{R_c}$	Krumbein (1941)	R_i is grain volume,
	Roundness: Ratio of curvature of a grain's edges to overall grain shape	$Roundness = \frac{4 * Grain\ area}{\pi * Grain\ length}$	Wadell (1932)	R_c is the smallest circumscribing sphere
				AW is the area weighting (grain packing density), N_0 is the number of grains with aspect ratio less than 2.0,

Texture coefficient (TC)	Analyze grain shape parameters, such as circularity and elongation, orientation of grains, and degree of grain packing (proportion of grains and matrix)	$TC = AW \left[\left(\frac{N_0}{N_0+N_1} * \frac{1}{FF_0} \right) + \left(\frac{N_0}{N_0+N_1} * AR_1 * AF_1 \right) \right]$	Howarth and Rowlands (1986)	N_1 is the number of grains with aspect ratio larger than 2.0, FF_0 is the arithmetic mean of form factor of all N_0 grains, AR_1 is the arithmetic mean of aspect ratio of N_1 grains, and AF_1 is the angle factor orientation computed for all N_1 grains.
Area weighting	Reflects intergranular space	$AW = \frac{\text{Total grain areas within the reference area boundary}}{\text{Total area enclosed by the reference area boundary}}$	Howarth and Rowlands (1986)	-
Strong cement over matrix index (SCMI)	Ratio of total strong cement over matrix in sandstone	$SCMI = \frac{(\% \text{ Calcitic Cement} + \% \text{ Siliceous Cement})}{\% \text{ Matrix}} \times 100(\%)$	Vutukuri et al. (1974)	-
Strong cement over total cement (SCTC)		$SCTC = \frac{\% \text{ Calcitic Cement} + \% \text{ Siliceous Cement}}{\% \text{ Total Cement}} \times 100 (\%)$	Vutukuri et al. (1974)	-
Strong over weak contact (SOWC)	Represents how well the grains are interlocked and cemented	$SOWC = \frac{[S_u + (G-C)]}{T_a + L_o + (G-V) + (G-M)}$	Taylor (1950)	S_u is the ratio of sutured contact to total contact type (%); T_a is the ratio of tangential contact to total contact type (%); L_o is the ratio of long contact to total contact type (%); $G-C$ is the ratio of grain-to-cement contact to total contact nature (%); $G-V$ is the ratio of grain-to-void contact to total contact nature (%); $G-M$ is

		the ratio of grain-to-matrix contact to total contact nature (%).
Foliation Index (FIX)	$FIX = \frac{\sum(P_L)_\perp}{\sum(P_L)_\parallel}$	Tsidzi (1986) $\sum(P_L)_\perp$ and $\sum(P_L)_\parallel$ are the sum of the number of grain boundaries parallel and perpendicular to the mineral fabric from all measured line transections
Porosity	$n = \frac{V_p * 100}{V}$	Al-Harathi et al. (1999) V_p is specimen pore volume, V is specimen bulk volume
Density	$\rho_d = \frac{M_s}{V}$	Al-Harathi et al. (1999) M_s is oven-dried grain mass of the specimen, and V is specimen bulk volume.

The geometrical features presented in Table 3.2 are briefly explained herein. Packing density, or the relative amount of space occupied by grains in a given area, has been correlated with strength properties (Bell, 1987). The packing proximity, which is also provided as a relative value, helps quantify the immediate contact intensity of grains; a value of 100 indicates that all grains are in contact. The other parameter is the index of interlocking, which quantifies the importance of grain–grain relationships and comprises both elements of packing density and proximity. Zorlu et al. (2004) concluded the presence of a linear relationship between packing density and uniaxial compressive strength (UCS) of the rock. The UCS value of a rock increases by raising packing density. High interlocking index values indicate a high complexity of the grain boundaries. Grain size distribution is defined by the index of grain size homogeneity, as a non-directional fabric parameter. (Dreyer, 1973). The grain size homogeneity index increases with the dominance of one grain size group and therefore provides an indication of the heterogeneity level in the rock considering granulometry. Measurements such as grain length (major axis), width (minor axis), perimeter, and area can be used to quantify grain shape (Cox and Budhu, 2008). Příkryl (2006) suggested that grain size and shape can be identified by using the parameters given in Table 3.3. With recent developments in computer technology, other grain form characterization methods, including some automated ones, have emerged. Table 3.4 summarizes a few popular ways of classifying grains by their shape. However, these methods are not comprehensively reviewed in this paper, and readers are referred to the cited articles. To evaluate the rock fabric for purposes of rock mechanics, the texture coefficient (TC) was developed (Howarth and Rowlands, 1986). Quantitative characteristics of grain shape like circularity, elongation, orientation, and degree of grain packing can be captured by this dimensionless quantitative index (proportion of grains and matrix). Area weighting (AW) reflects space of intergranular in sedimentary rocks. For igneous rocks, AW equals 1 (Howarth and Rowlands, 1986). The area weighting is based on the grain packing density within the reference boundary. Tsidzi (1986) proposed foliation intensity index based on the modal percentage of the platy prismatic grains and their corresponding shape factors to quantify foliation intensity (FIX).

Table 3.3. Grain Shape and Size Characterization Methods (Adapted from Cox, 2008).

Shape characteristic	Definition	Comment
Sphericity (Krumbein, 1941)	Ratio of grain volume to that of the smallest circumscribing sphere	<ul style="list-style-type: none"> ▶ 2D chart developed to facilitate application ▶ Measurement relates to form $\frac{3}{4}$ ▶ Measurement in computer programs differ from the original definition
Roundness (Wadell, 1932)	Ratio of the curvature of grain edges/corners to overall grain	<ul style="list-style-type: none"> ▶ 2D chart developed to facilitate application ▶ Measurement relates to angularity and texture ▶ Measurement in computer programs differ from the original definition
Fourier series (Ehrlich and Weinberg, 1970)	Shape (wave of the profile) estimated by the expansion of the periphery radius as a function of angle of the grain's center of gravity by Fourier series	<ul style="list-style-type: none"> ▶ Unable to analyze highly irregular or re-entrant particles correctly
Fourier descriptors Beddow and Vetter (1977)	Calculation of shape descriptors from the Fourier series coefficients 2D value ranging from 0 to 1; describes	<ul style="list-style-type: none"> ▶ Problems with other Fourier series methods are overcome (i.e., re-entrant particles) ▶ Applies FFT algorithm and utilizes boundary information only ▶ Highly dependent on segment lengths chosen to measure profile

Fractal dimension (Kaye, 1982)	the capability of a rugged boundary to occupy void space	► Measurement is related to roughness or texture of grain rather than form
--	--	--

Table 3 4. Summary of the basic microstructural parameters measured by the petrographic image analysis of thin sections (Adapted from Howarth and Rowlands; 1987; Prikryl, 2006).

Parameters	Symbol	Computation	Meaning of parameters for real grains
Area	A_i	Number of pixels defining the object	Cross-section area
Perimeter	L_P	Length of all edge pixels outlining the object	Length of grain boundary
Major (minor) axis length	$D_{max},$ D_{min}	Distance between the two points defining the major axis	-
	$MajX_1,$ $MajX_2,$ $MajY_1,$ $MajY_2$ are the X, Y coordinates of the endpoints	$D_{max} = \sqrt{(MajX_2 - MajX_1)^2 - (MajY_2 - MajY_1)^2}$	
Slope of mineral principal axes	$MajAS$	Angle of the major or minor axes from a horizontal reference line $MajAS = \alpha \tan \frac{MajY_2 - MajY_1}{MajX_2 - MajX_1}$	-
Equivalent diameter	D_{equiv}	$D_{equiv} = \frac{4A_i}{\pi}$	Grain size

		Shape of an object as it moves from a circle to a line	Shape of the grain cross- section
Compactness	C	$C = \frac{L_p^2}{A_i}$	section
Shape (form) factor	SF	$SF = \frac{4\pi A_i}{L_p^2}$	Circularity of grain cross- section
Aspect ratio	AR	$AR = \frac{D_{max}}{D_{min}}$	Grain ellipticity
Grain boundary smoothness	GBS	$GBS = \frac{L_{Pel}}{L_{P_{real}}}$	Deviation of grain shape from the smooth surface

The size distribution of crystals (in igneous and metamorphic rocks), grains (in sedimentary and occasionally metamorphic rocks), and occasional fragments and clasts (1000 mm to 10 mm; in sedimentary and volcanic rocks comprising clasts of previously formed rocks) is one of the most commonly quantified aspects of rock texture (Higgins, 2006). The size of a crystal or grain is a measure of the space it occupies. A linear measure of size is generally used in geological applications. Figure 3.1 represents quantitative textural methods that can be used at different scales of interest.

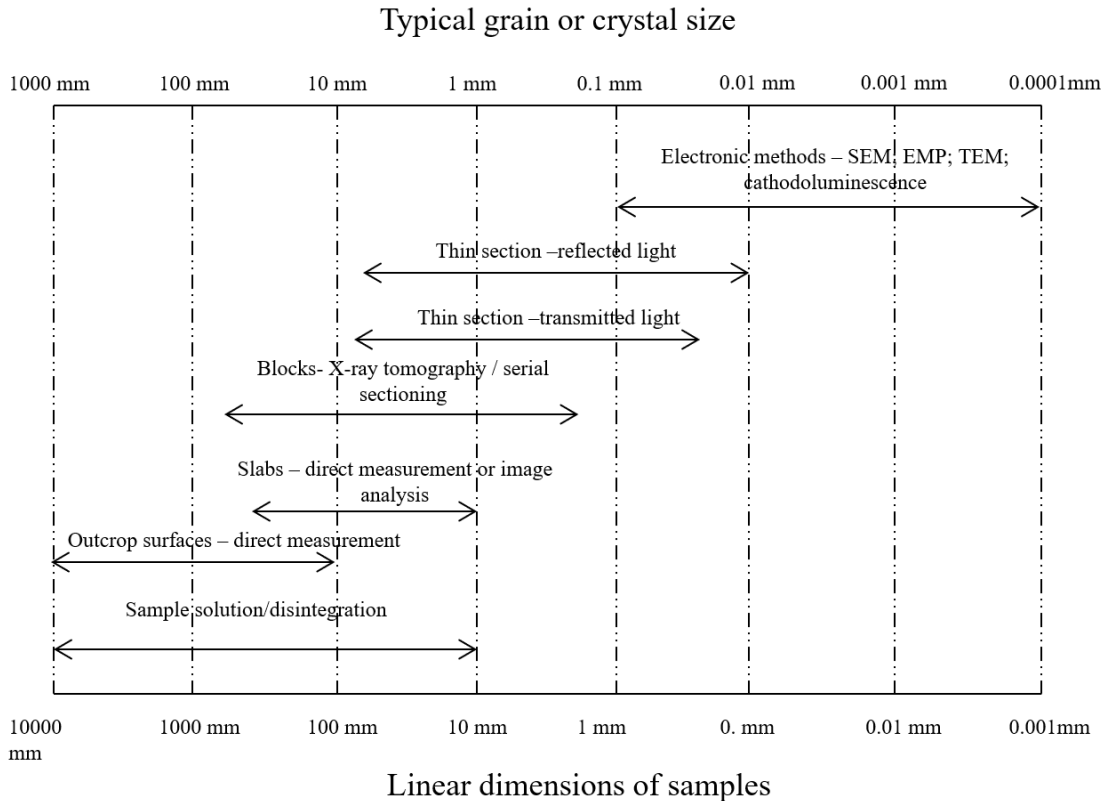


Figure 3.1. Measurements of crystal or grain size by analytical methods (Higgins, 2006).

Weathering is another vital parameter of rock texture. The weathering or alteration process is conducted via mechanical, chemical, and biological actions, which significantly affects the engineering properties of rock mass. Some of the significant effects of weathering/alteration on rock include reductions in strength, density, and volumetric stability as well as increments in deformability, porosity, and weatherability. Rocks can show no weathering or be completely weathered, which can relatively be quantified using visual criteria as summarized in Table 3.5.

Table 3 5. Degree of weathering of the rock (Hack and Price, 1997)

Term	Description
Unweathered/unaltered	Outer fracture planes may be stained or discolored, but no visible signs of alteration can be seen.
Slightly weathered /altered	Fractures may have thin fillings of altered material and are stained or discolored. It is possible for the discoloration to extend outward from the fracture planes as far as 20% of the fracture spacing (i.e., less than 40% of the core is discolored).
Medium weathered/altered	Fractures are discolored for a distance greater than 20% of the fracture spacing between them (i.e., generally large part of the rock). Altered material may fill fractures. (Except in poorly cemented sedimentary rocks) The core does not have a friable surface, and its original texture has been preserved.
Highly weathered/altered	Discoloration takes place throughout the rock. The surface of the core is friable and usually pitted due to the washing out of highly altered minerals by drilling water. Although much of the original rock texture has been preserved, grains have separated.
Totally weathered/altered	There is discoloration in the rock, and the core has a similar external appearance to soil. Despite the rock texture being partially preserved, the grains are completely separated.

The anisotropy of rock also has a major influence on its geomechanical properties. Rock anisotropy is due to the presence of cleavage, foliation, bedding planes, schistosity, joints, micro or macro fissures, or any other directional or planar feature caused by variations in mineral composition, grain size, crystal size, fabric, porosity, and weathering. Fabric-dependent anisotropy plays an important role in realization the

mechanical behavior of schistose or foliated rocks because such planar fabrics create mechanically weak discontinuities. Anisotropy in a rock can be primary (i.e., developed as the rocks are formed) or secondary (i.e., due to transformations or modifications to the rock after its formation in response to superimposed geological events, such as deformation, metamorphism, and alteration/weathering).

3.2.1 Primary structure

Primary structures are similar to micro-geological characteristics observed during the formation of various rocks. These features are influenced by the following: rock fabric anisotropy, texture, schistosity, and fissility. Microscopic features are usually related to grain size and can be found mostly on the microscopic scale. The anisotropic nature of rock is observed as follows. (1) Anisotropy in foliated metamorphic rocks, such as slate, schist, gneisses, or phyllites, may be caused by a natural orientation in the flat/long minerals or banding. (2) Anisotropic behaviors are frequently observed in stratified sedimentary rocks, including sandstone, shale, and sandstone-shale alteration, because of the presence of bedding planes. Anisotropy is mainly due to the sedimentation processes in various layers (strata) or different minerals with various grain sizes. (3) Anisotropy can also be displayed by igneous rocks exhibiting flow structures similar to porous rhyolites due to weathering (Matsukura et al., 2002).

3.2.2 Secondary structures

Secondary structures are also known as the macroscale features of rocks, which are defined by one word as “discontinuities.” The term “discontinuities” is frequently used to refer to all structure breaks within geologic materials with a low or zero tensile strength. These discontinuities are defined as follows: (1) cracks and fractures, (2) bedding planes, and (3) shear planes and faults (Salager et al. 2013). The highest degree of anisotropy is mainly observed in metamorphic rocks (Ramamurthy et al., 1993). The anisotropic form is associated with a single set of discontinuities or weakness planes (Al-Harhi, 1999). Most foliated metamorphic rocks contain fabric with preferentially parallel arrangements of flat or elongated minerals. The original rock fabric with a directional structure is modified by metamorphism. Foliation induced by the nonrandom

orientation of macroscopic minerals, parallel fractures, or microscopic mineral plates, produces particularly direction-dependent rock properties (Tien and Kuo, 2001). The anisotropy is also viewable in bedded sedimentary rocks, such as siltstone, sandstone, shale, or sandstone–shale (Ajalloeian and Lashkaripour, 2000). These metamorphic and sedimentary rocks, which are known as transversely isotropic rocks, are inherently anisotropic (Ramamurthy et al., 1993; Behrestaghi et al., 1996; Nasserri et al., 2003; Heng et al., 2015). Transverse isotropy implies the presence of an axis of rotational symmetry at each point in the rock, and the rock has isotropic properties in the plane normal to that axis, namely the plane of transverse isotropy (Amadei 1996).

Singh et al. (1989) described the concepts of the “type of anisotropy” and “anisotropy ratio.” Based on the origin of the anisotropy curves, three types of anisotropy are distinguished qualitatively: “U type,” “Undulatory type,” and “Shoulder type” (Figure 3.2).

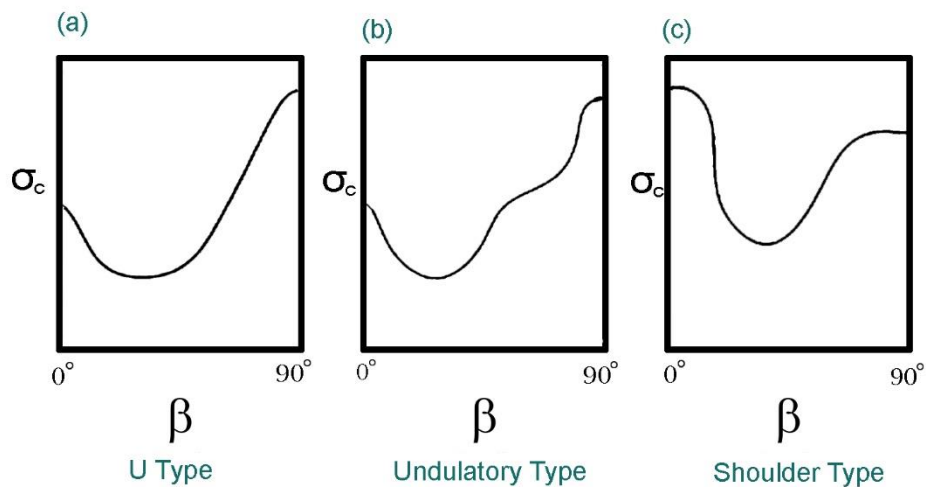


Figure 3.2. Classification of anisotropy for transversely isotropic rocks (After Singh et al., 1989; β is foliation angle, and σ_c is uniaxial compressive strength of rock)

The concept of “anisotropy ratio” was presented for quantifying anisotropy in rocks, which is defined as the ratio of UCS of the rock at $\beta = 90^\circ$ to the minimum strength observed over the range of β from 0 to 90° (Figure 3.3) which is written in Eq. 3.1 as follows:

$$I\sigma_c = \frac{\sigma_{ci(90^\circ)}}{\sigma_{ci(min)}} \tag{Eq. 3.1}$$

Where β is the foliation angle with the load direction.

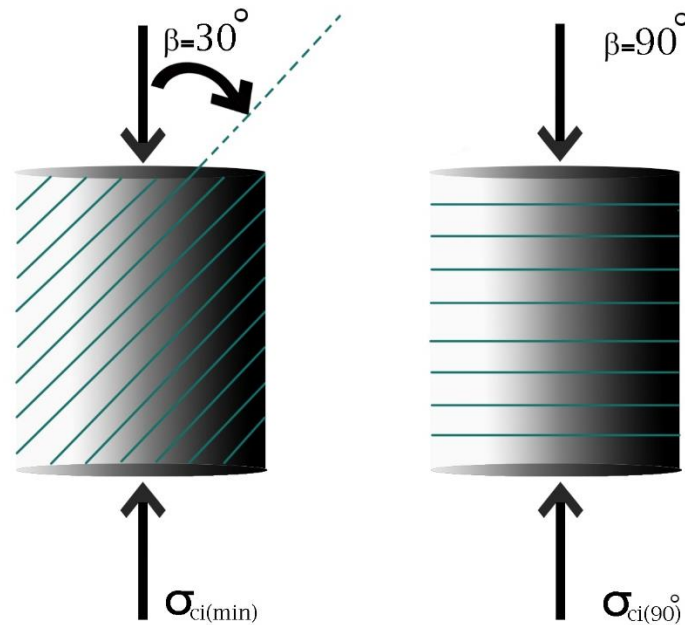


Figure 3.3. Minimum and maximum orientation of UCS of anisotropic intact rock.

Table 3.6 shows the experimental classification of anisotropic rocks based on anisotropy ratios.

Table 3.6. Anisotropy classification according to uniaxial compressive strength for different fine-grained rocks (Ramamurthy, 1993).

Anisotropy ratio	Class	Rock type
1.0–1.1	Isotropic	Sandstone
>2.1–2.0	Weakly anisotropic	Sandstone–Shale
>2.0–4.0	Moderately anisotropic	Shale–Slates–Phyllites
>4.0–6.0	Highly anisotropic	Slates–Phyllites
>6.0	Very highly anisotropic	Slates–Phyllites

The point load strength anisotropy index was initially proposed by ISRM (1981). The index $I\alpha_{(50)}$ is given as follows:

$$I\alpha_{(50)} = \frac{I_{s(50)perpendicular}}{I_{s(50)parallel}}, \quad \text{Eq. 3.2}$$

Where both $I_{s(50)}$ are the point load indexes which are perpendicular and parallel to the foliation planes at the axial and diametrical point load tests. The studies revealed that Due to the splitting through these weakness planes, the lowest point load value is found when loading parallel to the foliation planes (Saroglou and Tsiambaos 2007,a). A classification of anisotropic rocks was proposed by ISRM (1981) based on the point load strength index, $I\alpha_{(50)}$, as given in Table 3.7, while a similar classification was proposed by Tsidzi (1990).

Table 3 7. Anisotropy classification based on point load index (ISRM, 1985)

Degree of point load strength anisotropy ($I\alpha_{(50)}$)	Descriptive term
1	Isotropic
1–2	Low–moderately anisotropic
2–4	Highly anisotropic
> 4	Very highly anisotropic

Another way to determine the degree of anisotropy is to use wave velocity anisotropy of intact rock. Tsidzi (1997) proposed a velocity anisotropy index, VA, based on tests performed on metamorphic rocks, which is described by Eq. 3.3.

$$VA = \frac{V_{max} - V_{min}}{V_{mean}} (\%), \quad \text{Eq. 3 3}$$

Where $V_{(max)}$ is the maximum ultrasonic wave velocity, $V_{(min)}$ is the minimum velocity, and $V_{(mean)}$ is the mean velocity. The classification of anisotropy based on this index is given in Table 3.8.

Table 3 8. Anisotropy classification according to ultrasonic wave velocity (Tsidzi, 1997).

Degree of velocity anisotropy (VA%)	Descriptive term
< 2	Isotropic
2–6	Fairly anisotropic

6–20	Moderate anisotropic
20–40	Highly anisotropic
>40	Very highly anisotropic

Saroglou and Tsiambaos (2007,a) proposed another classification of anisotropic rocks based on uniaxial compressive strength index (I_{σ_c}), longitudinal velocity index (I_{V_p}) (the parameter plays an important role in determining the control gain) and diametrical point load index (I_d). This classification is presented in Table 3.9.

Table 3 9. Suggested classes for the classification of anisotropic rocks (Saroglou and Tsiambaos, 2007,a)

Anisotropy classification	Strength index ($I\sigma_c$)	Longitudinal velocity index (I_{Vp})	Diametrical point load index (I_d)
Isotropic	$I\sigma_c \leq 1.1$	-	$I_d = 1.0$
Fairly anisotropic	$1.1 < I\sigma_c \leq 2.0$	$I_{Vp} \leq 1.5$	
Moderate anisotropic	$2.0 < I\sigma_c \leq 3.0$	$1.5 < I_{Vp} \leq 2.0$	$1.0 < I_d \leq 2.0$
Highly anisotropic	$3.0 < I\sigma_c \leq 5.0$	$I_{Vp} > 2.0$	$2.0 < I_d \leq 4.0$
Very highly anisotropic	$I\sigma_c > 5.0$	-	$I_d > 4.0$

The aforementioned parameters define different aspects of rock texture; their relationship with mechanical properties of rock has been studied by many researchers. The mineral composition, grain shape and size, density, porosity, and foliation degree of the rock all influence its mechanical properties more than the other rock texture parameters (Onodera and Asoka, 1980). Therefore, the effect of these parameters on the mechanical properties of the rock will be discussed in the following section.

3.3 Relationships between rock textural characteristics and mechanical properties

The mechanical properties of a rock largely depend on its petrographic or textural characteristics. Some quantitative associations between rock petrographic characteristics and mechanical properties have been found. Therefore, the effect of these relationships and their extent on the mechanical characteristics of rock must be well understood as a proper frame of reference if good rock cores are unavailable for reliable tests to characterize a rock mass.

3.3.1 Mineral composition

The mechanical properties of the rock are markedly influenced by their mineralogical properties (Vutukuri et al., 1974). The strongest rocks are generally those that contain quartz as a binding material, followed by calcite (a carbonate species) and ferrous minerals (such as hematite and chromite), whereas rocks that have clays and phyllosilicates (sheet silicates) for binding materials are weak (Yılmaz et al. (2011). Several authors have investigated the links between the mineral composition and geomechanical properties of different rock types. Figure 3.4 shows the main work of experimental/empirical and numerical/simulation methods for the evaluation of the effect of mineralogy and texture parameters on geomechanical parameters of rock between 1960 and 2021. This chart represents the studies on sedimentary rock (yellow box), igneous rock (blue box), and metamorphic rock (red box). Red and green dashed lines indicate the nature of the study, that is, a substantial focus on geomechanical or rock texture. Researchers have recently provided increasing attention to the topic of using simulation methods for the prediction of rock behavior with different mineralogical assemblages.

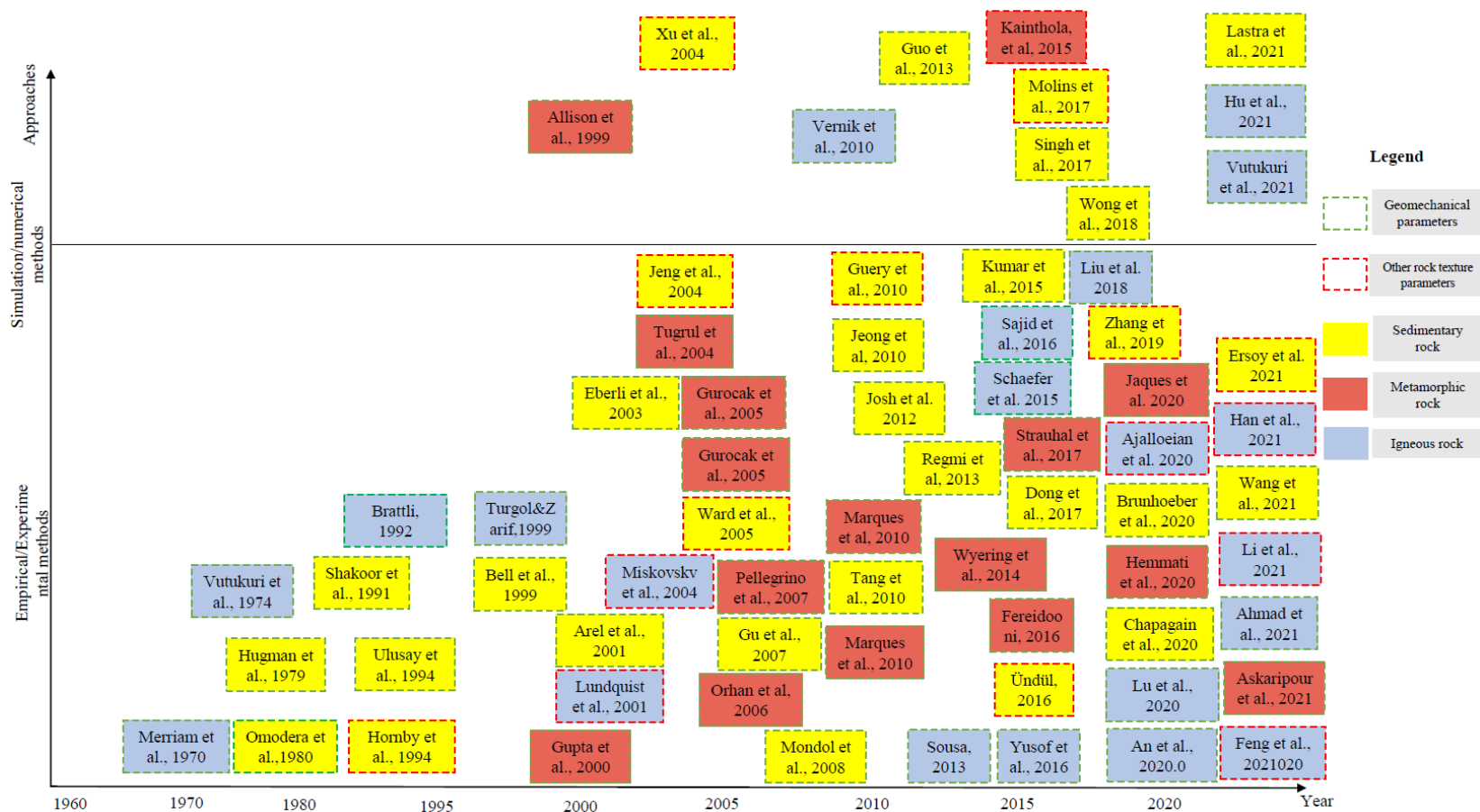


Figure 3.4. Main work on the effect of rock mineralogy on the geomechanical parameters of rock.

The relationship between geomechanical properties of the rock and quartz-to-feldspar ratio (QFR) was investigated by Tuğrul and Zarif (1999), Sousa (2013), and Yusof (2016), as presented in Table 3.10.

Table 3 10. Regression equations between mechanical properties and quartz-to- feldspar ratio (QFR) (σ_c , I_{s50} , and σ_t are in Mpa)

Equation	Mineral type	Correlation	References
$\sigma_c = 121.02 \times QFR + 115$ $\sigma_t = 19.54 \times QFR + 15$	Granite rocks	0.79	Tuğrul and Zarif (1999)
$\sigma_c = -437.67 \times QFR + 384.82$	Granite rocks	0.54	Sousa (2013)
		0.37	
$\sigma_c = 26.632 \times QFR + 24.459$ $\sigma_t = -.0957 \times QFR + 7.685$ $I_{s50} = 51.65 \times QFR + 69.49$	Granite rocks	0.39 0.16	Yusof (2016)

The main factors that affect the UCS of rocks based on their microtexture are mineral content, groundmass, and porosity, according to Undül (2016). Table 3.11 represents regression equations between the rock texture characteristic of the rock and mechanical properties where σ_u ultimate strength in MPa.

Table 3 11. Regression equations between mechanical properties and some aspect of rock texture characteristics.

Equation	Reference	Parameters	R ²
		D: mineral content of dolomite (%)	
$\sigma_u = 0.90D + 2.07M + 269$	Hugman and	M: mineral content of microcrystalline carbonate	0.73
$\sigma_u = 1.07D + 2.29M + 258$	Friedman (1979)	σ_u is in MPa	0.87
<i>Impact value</i> (%)		M = Mica (%)	0.73
$= 55.13 + 0.50M$	Miskovsky et al.		0.64
<i>Abrasion value</i> (%)			0.71
$= 3.07 - 0.032Q$	(2004)	Q = Quartz (%)	
<i>Abrasion value</i> (%)			
$= 3.0006 - 0.0137F$		F = Feldspar (%)	
		<i>Camf.</i> = Amphibole content (%)	
$UCS = 97.058 \frac{C_{plg} + C_{amf}}{C_{grm}} + 125.12$	Ündül (2016)	<i>CGrM</i> = Groundmass content for all types of compositions%	0.37
		<i>Cplg.</i> = Plagioclase content%	
		C_{grm}^1 = Groundmass content values obtained from specimen only of andesitic composition%	
$UCS = 219.75 \frac{C_{plg} + C_{amf}}{C_{grm}^1} + 35.728$	Ündül (2016)		0.66
$UCS = -7.5966C_b + 202.93$	Ündül (2016)	C_b = Biotite content%	0.56
$v = 0.0882 \frac{C_{plg} + C_{amf}}{C_{grm}} + 0.134$	Ündül (2016)		0.56

$v = 0.1191 \frac{C_{plg} + C_{amf}}{C_{grm}^1} + 0.1099$	Ündül (2016)		0.66
$v = 0.3047 \frac{C_{plg} + C_{amf}}{C_{grm}^2} + 0.0709$	Ündül (2016)	C_{grm}^2 = Groundmass content values obtained from the specimen of only rhyodacite composition	0.61

Multiple input interactions have been studied using multiple regression analysis (Ündül, 2016). The linear multiple models for uniaxial compressive strength and Young's modulus are provided in Table 3.12.

Table 3 12. Some significant multiple regression equations (Ündül,2016) (C_{plg} . is plagioclase content in %, C_{amf} . is amphibole content in %, C_{GrM} . is groundmass content for all types of composition in %, M_{felds} . is the mass fraction of total feldspar minerals in %, M_q . is the mass fraction of quartz in %. n_t is total porosity, F_{opa} . is Feret's diameter of opaque minerals in mm, F_{bio} . is Feret's diameter of biotite in mm, LOI is loss-on-ignition values in %, E is Young's modulus (Gpa), and UCS is the uniaxial compressive strength of rock in Mpa)

Equation	Correlation
$UCS = 191.887 \left(\frac{C_{plg} + C_{amf}}{C_{grm}} \right) + 155.341M_{felds} + 836.322M_q - 147.441$	0.811
$UCS = 108.151 \left(\frac{C_{plg} + C_{amf}}{C_{grm}} \right) - 13.448LOI - 16.017n_t + 219.914$	0.810
$E = 10.268 \left(\frac{C_{plg} + C_{amf}}{C_{grm}} \right) - 7.64LOI - 1.953n_t + 58.069$	0.826
$E = 7.690 \left(\frac{C_{plg} + C_{amf}}{C_{grm}} \right) - 42.543F_{opa} - 11.618F_{bio} + 54.776$	0.806

3.3.2 Grain size, density, and porosity

Grain size varies from very fine (125–250 μm) to coarse-grained (1–2 mm) size. Previous laboratory experiments have extensively investigated the relationships between mechanical and mean grain size and demonstrated that grain size has a significant mechanical influence. Brace (1961) realized that rocks with fine mineral grains have high mechanical strength, implying that grain size has an impact on mechanical properties. Hoek (1965) suggested that high stress is necessary to cause failures on grain boundaries in rocks with a tightly interlocking structure. Mendes et al. (1966) discovered that the mineralogical properties of granite samples correlate well with mechanical properties, and samples with fine grains have high strength. Willard and McWilliams (1969) revealed that mineral cleavage, microfracture, and grain boundaries influence the ultimate strength of rock as well as the direction of crack propagation. Hartley (1974) indicated that intergranular bonding had a major impact on the mechanical features of sandstones and concluded that it is possible to determine mechanical properties by counting the contacts between grains and by looking at the type of grains. Onodera and Asoka (1980) indicated that strength is significantly reduced as the grain size in igneous rock increases. Singh (1988) investigated the relationship of the mean grain size of the rock on UCS and fatigue strength. The fatigue strength of the rock has an inverse relationship with its mean UCS because the uniaxial compressive strength varied with different grain sizes. Shakoor and Bonelli (1991) indicated that sandstone density, percent absorption, total pore volume, and grain-to-grain content are all closely related to compressive strength, tensile strength, and Young's modulus values. The compressive strength, tensile strength, and Young's modulus were all high in the sandstone with high densities, low percent absorption, low total pore volume, and high percentages of saturated contacts. In addition, the percentage of angular grains had only weak influence on strength and elastic properties. Ulusay et al. (1994) concluded that grain size, packing proximity, percent grain-to-grain contacts, and grain-to-matrix contacts have the largest impact on Young's modulus. Young's modulus rises with the increase of the first three parameters. Increased grain-to-matrix contacts reduce stiffness; therefore, Young's modulus is inversely related to grain-to-matrix contacts. The relationship between these parameters is presented in Table 3.13. Akesson et al. (2001) showed that abrasion and fragility are dependent on

the grain size despite the important role of the shape and arrangement of the minerals. Tugrul and Zarif (1999) found linear equations between UCS and grain size of granite rock. Ündül (2016) concluded that the UCS decreases as total porosity increases. Furthermore, Young's modulus decreases as the grain size of biotite rises. According to French et al. (2001), a linear relationship exists between the mean grain size and the hardness value. The mean grain size increases with mean hardness while the normative hardness decreases with grain size. Decreasing mean grain size improves resistance to wearing and impact forces. Raisänen (2003) indicated that abrasion value is linearly related to grain size. Considering the sedimentary rock, all strength properties decrease with increasing porosity. Research on coal rocks reveals a linear decrease in the UCS with an increase in porosity (Price, 1960). Yusof and Zabidi (2016) indicated that the uniaxial strength relationship is indirectly proportionate to the size of the grain, thereby decreasing with the increase in grain size. The researchers found the regression equations between mechanical properties and grain size of the rock mostly through experiments. Table 3.14 represents the regression equations between grain size and mechanical parameters of rocks.

Table 3 13. Relationship between some aspects of rock texture (Ulusay et al.,1994) (Unit weight in KN/m³, point load index in MPa, quality index in %, porosity in %, uniaxial compressive strength in MPa, Young's Modulus in (GPa), mean grain size in mm, all petrographic characteristics given as independent variables are in percent)

Relationship	Prediction equation	Correlation coefficient
Unit Weight (y)		
Mean grain size (x)	$y = 25.77 - 1.21x$	-0.54
Rock fragment (x)	$y = 26.08 - 0.017x$	-0.54
Percent matrix (x)	$y = 25.03 + 0.03x$	0.53
Point Load Index (y)		
Round grain (x)	$y = 4.43 - 0.78x$	-0.68
Angular grain (x)	$y = 3.55 + 0.08x$	0.69
Sutured contacts (x)	$y = 1.87 + 0.07x$	0.55
Rock fragment (x)	$y = 4.14 - 0.02x$	-0.52

Grain to void (x)	$y = 3.53 - 0.13x$	-0.61
Quality Index (y)		
Packing proximity (x)	$y = 85.48 - 0.33x$	-0.55
Grain to grain (x)	$y = 84.37 - 0.32x$	-0.55
Grain to matrix (x)	$y = 55.57 + 0.25x$	0.53
Rock fragment (x)	$y = 71.82 - 0.28x$	-0.74
Percent matrix (x)	$y = 55.06 + 0.46x$	0.68
Porosity (y)		
Mean grain size (x)	$y = 2.31 + 2.38x$	0.56
Degree of sorting (x)	$y = 1.67 + 2.15x$	0.65
Grain to void (x)	$y = 2.62 + 0.17x$	0.59
Rock fragment (x)	$y = 1.61 + 0.04x$	0.59
Uniaxial Compressive Strength (y)		
Round grain (x)	$y = 97.17 - 1.6x$	-0.71
Angular grain (x)	$y = 61.96 + 1.59x$	0.70
Sutured contacts (x)	$y = 33.37 + 2.04x$	0.82
Young's Modulus (y)		
Mean grain size (x)	$y = 6.4 + 4.13x$	0.70
Packing proximity (x)	$y = -0.98 + 0.11x$	0.86
Grain to grain (x)	$y = -0.71 + 0.11x$	0.887
Grain to matrix (x)	$y = 9 - 0.74x$	-0.75
Poisson's ratio (y)		
Packing density (x)	$y = 0.44 - 0.0024x$	-0.77
Packing proximity (x)	$y = 0.375 - 0.002x$	-0.90
Grain to grain (x)	$y = 0.364 - 0.002$	-0.86

Table 3 14. Regression equations between geomechanical properties and mean grain size (Adapted from Ulusay et al. 1994). (σ_c is unconfined compressive strength in MPa; σ is compressive strength in MPa; D_{mean} is the mean grain size of all consisting minerals in mm; $D_{\text{mean}}^{\text{quartz}}$, $D_{\text{mean}}^{\text{plagioclase}}$, and $D_{\text{mean}}^{\text{K-feldspar}}$ mean are respectively the mean grain sizes of quartz, plagioclase, and K-feldspar minerals in mm; P is the confining pressure in MPa; a and b are empirically determined constants that depend on mean grain size.)

Equation	Minerals	Correlation	References
$\sigma_c = 128.52 * D_{mean}^{quartz} + 248$		$R^2 = 0.81$	
$\sigma_c = 54.73 * D_{mean}^{plagioclase} + 204$		$R^2 = 0.83$	Tuğrul A, Zarif (1999)
$\sigma_c = 21.12 * D_{mean}^{k-feldspar} + 20$	Granitic rock	$R^2 = 0.91$	
$\sigma_c = -1.29 * Log (D_{mean}) + 5.38$		$R^2 = 0.71$	Přikryl (2001)
$\sigma_c = 32.57 * \frac{1}{\sqrt{D_{mean}}} + 147.99$	Marble	$R^2 = 0.96$	Wong et al. (1996)
$\sigma = \sigma_c + a(D_{mean}) * [1 - e^{-b(D_{mean})*p}]$	Different lithology	$R^2 = 0.71$	Hareland (1993)

Porosity also plays a significant role in the geomechanical parameters of rock. Bell and Lindsay (1999) reported the highly significant porosity relationship with UCS and tensile strength. The UCS and tensile strength decrease as porosity increases. According to Tugrol and Zarif (1999), the total porosity and dry unit weight are linearly related. As porosity increases, the dry unit weight decreases. Fahy and Guccione (1979) suggested a correlation, which combines the compressive strength of rocks with the percentages of cement, and its mean grain size is as follows (Eq. 3.4):

$$UCS = 167.7 - 0.52 (total\ percent\ cement) - 320.9 (mean\ grain\ size), \text{ Eq. 3.4}$$

Where UCS is in MN/m², and mean grain size is in mm.

Shakoor and Bonelli (1991) studied the effect of the petrographic characteristics of sandstone on the mechanical properties of the rocks and reported that sandstones with high density, low absorption percentage, low total pore volume, and high percentage of sutured contacts exhibited high values of compressive strength, tensile strength, and Young's modulus. They proposed several empirical equations for the relationships of petrographic characteristics of sandstone to the mechanical properties of rocks, as written in Table 3.15.

Table 3 15. Regression equations for prediction geomechanical properties (Shakoor and Bonelli, 1991) (uniaxial compressive strength in psi, density in pcf, tensile strength in psi, Young's modulus $\times 10^6$ in psi, absorption in %, total pore volume in cc/gm, sutured contacts in %)

Relationship	Prediction equation	Correlation
Uniaxial compressive strength (y)	$y = 668.2x - 83366$	0.98
Density (x)		
Tensile strength (y)		
Density (x)	$y = 30.1x - 3734$	0.98
Young's modulus (y)		
Density (x)	$y = 0.1635x - 21.25$	0.91
Uniaxial compressive strength (y)	$y = 3117.5x + 26915$	-0.97
Absorption (x)		
Tensile strength (y)		
Absorption (x)	$y = -168.8x + 1363$	-0.97
Young's modulus (y)		
Absorption (x)	$y = -0.8125x + 6.075$	-0.93
Uniaxial compressive strength (y)	$y = -13217\log x - 5581$	-0.98
Pore volume (x)		
Tensile strength (y)		
Pore volume (x)	$y = -811\log x - 501$	-0.98
Young's modulus (y)		
Pore volume (x)	$y = -4.381\log x - 3.531$	-0.97
Uniaxial compressive strength (y)	$y = 2354.6x - 28637$	0.70
Sutured contacts (x)		
Tensile strength (y)		
Sutured contacts (x)	$y = 95.7x - 1120$	0.72

Young's modulus (y)

Sutured contacts (x) $y = 0.5273x - 6.91$ 0.89

Chatterjee and Mukhopadhyay (2001) developed a series of equations to link petrophysical to geomechanical rock properties. The samples were collected from the basement rocks of Krishna-Godavari and Cauvery basins in India. These equations are presented in Table 3.16.

Table 3 16. Regression analysis of core samples in the Krishna-Godavari and Gauvery basins (Chatterjee and Mukhopadhyay, 2001) (Uniaxial compressive strength in Mpa, Dry density in kg/m³, Tensile strength in MPa, effective porosity in %, Young's modulus in GPa)

Basin	Parameters related	Regression equation and correlation
Krishna-Godavari	Uniaxial compressive strength (y), dry density (x)	$y = 55.27x - 100.72, R^2 = 0.89$
	Uniaxial compressive strength(y), tensile strength (x)	$y = 10.33x^{0.89}, R^2 = 0.94$
	Uniaxial compressive strength (y), effective porosity (x)	$y = 64.23 e^{-0.085x}, R^2 = 0.92$
	Young's modulus (y), uniaxial compressive strength (x)	$y = 8.43e^{0.029x}, R^2 = 0.95$
	Uniaxial compressive strength (y), dry density (x)	$y = 37.47x - 63.11, R^2 = 0.98$
Gauvery	Uniaxial compressive strength (y), tensile strength (x)	$y = 6.89x + 5.39, R^2 = 0.93$
	Uniaxial compressive strength (y), effective porosity(x)	$y = 34.44e^{-0.044x}, R^2 = 0.87$
	Young's modulus (y), uniaxial compressive strength (x)	$y = 3.73e^{0.064x}, R^2 = 0.91$

Tamrakar et al. (2007) studied the relationship of many petrographic characteristics of rock with geomechanical properties. The samples were sandstone from the foothills of the Himalayas. These equations are presented in Table 3.17.

Table 3 17. Prediction model of multiple regression for physical and mechanical indexes (Tamrakar et al., 2006) (SHH is Schmidt hammer hardness, UCS is uniaxial compressive strength in MPa, DOI is the degree of induration, PLI is point load index in Mpa, porosity in %, G-C in %, G-V in %, Cc in %, E_s is Secant modulus in GPa, E_t is the tangent modulus in GPa. P_{dry} is dry density in Kg/m³, and P_{sat} is saturated density in Kg/m³.)

Predictor	Constant	Equation and correlation coefficient
Density (ρ_{dry})	C _c P _{cc} M _z SCTC Void SCMI	$\rho_{dry} = 1910 + 456SCTC - 17.16 Void + 1.52SCMI - 4.60CC + 3.34 P_{cc} + 67.84 M_z$ $R^2 = 0.76$
Saturated Density (ρ_{sat})	SCTC SCMI Void C _c P _d P _{cc}	$\rho_{sat} = 2440 + 318.6SCTC + 0.22SCMI - 5.15Void - 4.27C_c - 4.11P_d + 5.67P_{cc}$ $R^2 = 0.66$
Porosity (n)	SCTC Void SOWC G-C G-V C _c	$n = 7.93 - 5.10SCTC + 0.82 Void - 1.00SOWC + 0.04 G - C + 0.17 G - V - 0.08 C_c$ $R^2 = 0.66$
SHH*	Void Ψ_p	$SHH = -32.80 - 1.32 Void + 95.68\psi_p$ $R^2 = 0.23$
PLI* (I _{s50})	Void SCTC SOWC G_V Lo	$I_{s50} = 1.62 - 0.19Void - 0.06SCTC + 0.23SOWC + 0.04G_V - 0.002Lo$ $R^2 = 0.49$
UCS*	Void SOWC G_V Lo C _c	$UCS = 29.26 - 3.17Void + 3.50SOWC + 0.76G_V + 0.10Lo + 0.12C_c$ $R^2 = 0.48$

Secant modulus (E_s)	Void SOWC Lo G_V	$E_s = 0.70 - 0.05Void + 0.05SOWC - 0.001Lo + 0.03G_V$ $R^2 = 0.31$
Tangent Modulus (E_t)	Void SOWC Lo G_V	$E_t = 0.84 - 0.06Void + 0.05SOWC - 0.001Lo + 0.03G_V$ $R^2 = 0.38$
Modulus ratio (MR)	Void SCTC G-G Pd	$MR = 14 + 1.58Void - 6.30SCTC + 0.06G_G + 0.19P_d$ $R^2 = 0.21$

Ündül (2016) indicated that phenocrysts (i.e., conspicuous crystals that are substantially larger than the matrix in magmatic and volcanic rocks) and groundmass are regarded as the main factors influencing crack propagation. An increase in phenocryst content leads to an increase in radial strain and an increase in Poisson's ratio. Cracks tend to align parallel to the applied load as the groundmass content (low phenocryst content) increases. Increased groundmass reduces the Poisson's ratio compared to samples with high phenocryst contents. Table 3.18 presents empirical equations that show how petrophysical properties and microtextural variables are related.

Table 3 18. Linear regression between mechanical properties and some aspects of crock texture (Ündül, 2016) (M_g is the mass fraction of quartz (%), n_t is total porosity, CGrM is the groundmass content for all types of compositions, C_{grm}^1 is the groundmass content values obtained only from the specimen of andesitic composition, ν is Poisson's ration, E is Young's modulus (GPa), C_{grm}^2 is groundmass content values obtained only from the specimen of rhyodacite composition, $A_{ngopa.}$ is the angularity of opaque minerals, $F_{opa.}$ is Feret's diameter of opaque minerals (mm), F_{bio} is Feret's diameter of biotite (mm), $P_{opa.}$ is the perimeter of opaque minerals, LOI is an indicator of the weathering stage of rock(%), and UCS is uniaxial compressive strength (MPa).

Equation	Correlation coefficient
$UCS = 5.2455M_q + 102.36$	0.47
$UCS = -13.531n_t + 246.23$	-0.64
$v = -0.0026C_{grm} + 0.3406$	-0.62
$v = -0.0038C_{grm}^1 + 0.4078$	-0.72
$v = -0.0038C_{grm}^2 + 0.444$	-0.88
$E = -6.6561LOI + 52.326$	-0.55
$E = -57.69F_{apa} + 58.573$	-0.72
$E = -18.502P_{apa} + 55.578$	-0.69
$E = -26.325F_{bio} + 52.743$	-0.66
$E = 106.78Ang_{opa} + 36.92$	0.63

3.3.3 Texture coefficient (TC)

The texture coefficient has often been used to quantify the characteristics of rock texture. In this approach, rock material textures depend on the geometrical relation between the mineral grains and the matrix (Ozturk et al., 2014). Rocks comprising hard minerals tend to have rough surface texture and high strength properties (Räisänen et al., 2003). Soft minerals are clay minerals and organic matters. The rest of the rock-forming minerals are hard minerals. To define texture coefficient, Howarth and Rowlands (1986) considered morphological characteristics such as grain size, grain shape, grain orientation, porosity, and matrix materials. Table 3.19 represents the linear regression equations between UCS and TC of rocks, which are extracted from different studies. Various types of rocks show a linear increase in UCS as the texture coefficient increases, except for fault breccia (i.e., broken or partly disaggregated rocks in a fault zone). Ersoy and Waller (1995) found a positive linkage between UCS and texture coefficient for various sedimentary and igneous rocks. A strong link for sandstone, siltstone, marl, shale, and limestone has been validated by Ozturk et al., (2014). Most experiments have shown that UCS increases linearly by raising the texture coefficient for various rock forms (Ozturk et al. (2004); Ersoy and Waller, 1995). However,

contradictory correlations are found between TC and strength (Alber and Kahraman, 2009). Possible explanations for contradictory correlations may be as follows. Complicated rock texture characteristics cannot be effectively expressed as a coefficient of texture by one index. For example, Fault breccia, which comprises broken mineral grains filled with a fine-grained matrix, may have substantially different mineral properties than other types of rocks, such as sandstone, limestone, and granite, resulting in different relationships between UCS and grain size.

Table 3 19. Linear empirical equations between UCS and TC (σ_c is uniaxial compressive strength in MPa; σ_t is indirect tensile strength in MPa; TC is texture coefficient)

Equation	Mineral type	Correlation	Reference
	Sandstone, siltstone,		
$\sigma_c = 70.83 \times TC$ + 12.83	marl, shale, limestone	0.76	Ozturk et al.
$\sigma_c = 72.37 \times TC$ + 10.38	Limestone	0.87	(2004)
$\sigma_c = 106.51 \times TC$ + 7.46	Sandstone, siltstone, marl, shale	0.93	
$\sigma_c = -131.86 \times TC$ + 86.20	Fault breccia	0.90	Alber and Kahraman, 2009
$\sigma_t = 8.75 \times TC$ - 3.32	Sandstone, limestone, siltstone,	0.69	Ersoy and Waller, 1995
$\sigma_c = 110.01 \times TC$ - 46.12	granite, diorite	0.62	
$\sigma_c = 96.40 \times TC$ - 56.48	Saturated rock material	0.91	Howarth and Rowlands (1986)
$\sigma_c = 104.80 \times TC$ - 55.14	Dry rock material	0.92	

3.3.4 Rock anisotropy

The anisotropy of rock influences rock behavior in engineering analysis. Aagaard (1976) investigated the effect of foliation angle on the diametrical point load index of two gneisses and mica schist rocks. The point load index decreases as the foliation angle of rock increases. Behrestaghi et al. (1996) indicated that quartzitic and chlorite schists with a low amount of mica represent high tensile and UCS at all foliation angles. Nasseri et al. (1997) studied the impact of anisotropy on the UCS of quartzitic, chlorite, quartz mica, and biotite schists. They showed that all samples displayed maximum strength when $\beta = 90^\circ$ due to uniform distribution of stress throughout the anisotropy planes compared with that when the foliations are inclined. AL-Harthi (1998) studied 10 large blocks of Ranyah sandstone, which had two sets of discontinuities instead of one set of discontinuities. Because of the superimposed effects of bedding and microfissures, an anisotropy curve in the form of a W curve was obtained (Figure 3.5).

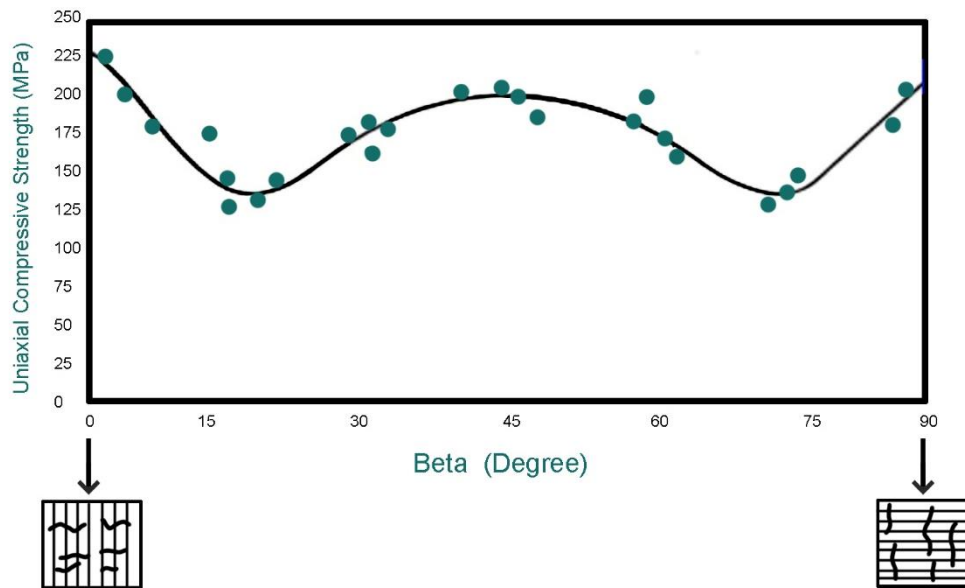


Figure 3.5. Correlation between the UCS of Ranyah sandstone and angle of orientation β (AL-Harthi, 1998)

Khanlari et al. (2014) noted that metamorphic foliation angles of samples could influence rock strength directly. The lowest rock strength was observed when the angle of foliation was from 0° to 30° . By contrast, the maximum value of rock strength is achieved when the foliation angle was 90° . Ali et al. (2014) investigated the behavior

of banded amphibolite rocks in terms of strength and deformation anisotropy. The results showed that under UCS test, the amphibolite has a U-shaped anisotropy with maximum strength at $\beta = 90^\circ$, and minimum strength is reported when $\beta = 30^\circ$. The results of the elastic deformation test show the absence of a relationship between microstructure features of subtype amphibolite (rock metamorphosed at high temperature and pressure) rocks that control modulus “shape anisotropy.” The researcher also studied the relationship between the anisotropy and tensile strength of the rock. Several researchers have demonstrated that fractures in brittle materials can occur due to a tensile stress. Therefore, the tensile strength is an important aspect of the failure resistance of rock. Hobbs (1963) reported that the maximum tensile strength is obtained when the angle of foliation is perpendicular to the load direction. This phenomenon indicates that tensile strength is larger in low degrees of anisotropy than that in high degrees of anisotropy. The low value may be attributed to low cohesion between rock materials or the presence of microcracks that directly connect to the anisotropy.

Shear strength refers to the strength of a rock or structural failure when the rock fails in shear. The rock that encounters a shear load slides along a plane, failing parallel to its direction. The effect of anisotropy on the shear strength of the rock has been researched over the last decades. McCabe and Koerner (1975) investigated the relationship between the anisotropy of mica schist samples and the shear strength parameters of the rock. The Mohr–Coulomb criterion was used to assess the relationship between rock anisotropy, cohesion, internal friction, and shear strength. The results indicated that the shear intensity value varied with the angle of foliation. The maximum and minimum values for shear strength were recorded when the foliation angle was $\beta = 30^\circ$, $\beta = 70^\circ$, and $\beta = 50^\circ\text{--}59^\circ$. Furthermore, increasing the degree of foliation and the size of the mica flake decreased cohesion and the internal friction angle. Strength anisotropy remains important in the presence of confined conditions, as evidenced by a large number of triaxial tests on Delabole slates (Brown et al., 1977) and Himalayan schists (Nasser et al., 2003). With increasing confining pressures, strength anisotropy decreases. (Donath, 1966). Ramamurthy et al. (1993) investigated the anisotropy behavior of phyllites. The compressive strength of phyllites increases non-linearly at all

orientation angles of the rock anisotropy. The results indicated that variation in cohesion with σ_3 at a particular β is exactly the opposite of that in internal friction. For example, cohesion increases and internal friction decreases when σ_3 increases, and vice versa. Moreover, the variation in cohesion with σ_3 at a particular β is significant, whereas the variation in internal friction is insignificant. Nasser et al. (1997) noted that maximum and minimum strength values for quartzitic, chlorite, and quartz mica schists are observed at $\beta = 90^\circ$ and $\beta = 30^\circ\text{--}45^\circ$, respectively. Maximum strength values for quartzitic and chlorite schists were observed at $\beta = 90^\circ$ throughout the range of confining pressures. The minimum strength is commonly 30° to 45° . However, quartzitic schist shows a 30% strength improvement at $\beta = 30^\circ$ due to confinement. For chlorite schist, this improvement is 15%, and for quartz mica schist it is 10%. Heng et al. (2015) studied the effect of anisotropy orientations on the shear strength and failure mechanisms of some shale samples. The results demonstrated that the angle between the bedding planes and the coring orientation is an important factor in strength, cohesion, and internal friction and reached the maximum and minimum values of shear strength at $\beta = 60^\circ$ and $\beta = 0^\circ$, respectively.

The foliation angle in anisotropic rock strongly affects the geomechanical parameters of rock, wherein rock strength is a crucial aspect in the design of rock structures. The representative failure criteria is necessary for the analysis of these structures' stability. Therefore, the failure criteria of anisotropic rock will be discussed in the next section.

3.4 Failure criteria of anisotropic rocks

Many constitutive models, as well as the failure criteria that study rock behavior under loading, are associated with rock strength anisotropy. A failure criterion can be defined according to Ambrose (2014): *“A Failure criterion is an equation that defines, either implicitly or explicitly, the value of the maximum principal stress that will be necessary in order to cause the rock to fail, which in the case of brittle behavior can be interpreted as causing the rock to break along one or more failure planes.”* Each criterion has a few constants that must be calculated by the study of regression test results. The researches indicate that sedimentary and metamorphic rocks, such as shale, slate, gneiss, schist, and marble, show an intense anisotropy of strength (Ali et al., 2014;

Saeidi et al., 2014; Wong and Einstein, 2009). It also leads to a non-linear strength response due to the dependence of rock strength on direction (Tien and Kuo, 2006; Singh et al., 2015).

The assessment of the anisotropic strength behavior of different rock forms has been a difficult challenge for rock mechanical and geological engineers over the last few decades. Many failure criteria have been established as a result of these experiments to predict the behavior of anisotropic rocks under loading. Most of the introduced anisotropic rock failure standards were classified until 1998 by Duvieu et al. (1998). Ambrose (2014) then added the criteria which were developed until 2014 (Table 3.20). The failure criteria are often split into continuous and discontinuous types. The first group of criteria is called the mathematical continuous approach. A continuous body and a continuous variation in strength are presumed in these criteria. The mathematical methodology is used to define the strength anisotropy of material and the type of material symmetries. Hill (1948) proposed one of the first anisotropic criteria for frictionless materials by extending the von Mises (1928) isotropic theory. Goldenblat and Kopnov (1966) suggested a general approach. These authors proposed using tensor strengths in different orders to consider anisotropy. By modifying the Hill criterion, Pariseau (1968) proposed a commonly used criterion for geological materials that accounts for the strength difference between tensile and compressive loading, as well as the strength dependence on the mean stress. Tsai and Wu (1971) formulated the failure criteria using first- and second-order strength tensors. Boehler and Sawczuk (1970, 1977) and Boehler (1975) established a systematic and general approach in the framework of the theory of invariant tensorial functions. Relevant failure criteria for rock materials (Allirot and Boehler, 1979) and composites (Boehler and Raclin, 1982) have also been suggested. Generalizations of Mohr–Coulomb and von Mises isotropic failure criteria to orthotropic and transversely isotropic media can be found in Boehler (1975). Cazacu (1995) recently expanded the Stassi isotropic criteria to construct a new invariant failure criterion. The second group of criteria is named empirical continuous models. The strength anisotropy is simply described by the determination of variation laws as a function of the loading orientation for some material parameters used in the anisotropic criterion. Such laws of variance are entirely observational and are calibrated

using basic laboratory experiments. These models are devoid of any direct physical or mathematical background. The variable cohesion theory, which was suggested by Jaeger (1960), is one of the most representative criteria of this type. This theory extended the Mohr–Coulomb failure criterion by using a variable material cohesion with the loading orientation and a constant value of the friction. McLamore and Gray (1967) suggested a simple form of this criterion and proposed to use a variation of the friction coefficient in the same way as the cohesion. Singh et al. (1998) and Ramamurthy et al. (1988) suggested a modification to McLamore and Gray (1967) criteria by using a non-linear form of the failure envelope in the Mohr plane. In addition to the first two classes of criteria, the third set of criteria, known as “discontinuous vulnerability plane-based” models, was established. Theories in this field discussed how physical mechanisms contribute to failure processes. The fundamental idea is that the failure of an anisotropic body is caused by either bedding plane or rock matrix fractures. The single plane-of-weakness theory, which was suggested by Jaeger in 1960, is the most representative model of this group. Other criteria were proposed (Walsh and Brace, 1964; Hoek, 1964, 1983; Hoek and Brown, 1980) by considering the planes of weakness as well as the extension of modified Griffith theory (McClintock and Walsh, 1962). A new theory was also recently proposed by Duveau and Henry (1998), who introduced the use of the Barton criterion for sliding along schistosity planes. The typical discontinuous criteria of anisotropic rocks in the current study are extracted from the literature and will be briefly discussed. However, continuous models are beyond the objectives of this paper. Readers are referred to the suggested literature for additional information.

Table 3 20. Classification of widely used anisotropic failure criteria (Adabted from Ambrose, 2014)

Continuous criteria		Discontinuous criteria
Mathematical approach	Empirical approach	
Von Mises (1928)	Casagrande and Carillo (1944)	Jaeger (Single plane-of-weakness theory) (1960, 1964)
Hill (1948)		
Olszak and Urbanowicz (1956)	Jaeger (variable cohesive strength theory) (1960)	Walsh and Brace (1964)
Goldenblat (1962)	Mclamore and Gray (1967)	Murrell (1965)
Goldenblat and Kopnov (1966)	Ramamurthy, Rao, and Singh (1998)	Hoek (1964, 1983)
Pariseau (1968)	Ashour (1988)	Barron (1971)
Boehler and Sawczuk (1970, 1977)	Zhao, Liu, and Qi (1992)	Ladanyi and Archambault (1972)
Tsa and Wu (1971)	Singh et al. (1998)	Bieniawski (1974)
Boehler (1975)	Tien and Kuo (2001)	Hoek and Brown (1980)
DafaliaS (1979, 1987)	Tien, Kuo, and Juang (2006)	Smith and Cheatham (1980)
Allirot and Boehler (1979)	Tiwari and Rao (2007)	Yoshinaka and Yamabe (1981)
Nova and Sacchi (1979)	Saroglou and Tsiambaos (2007,b)	Duveau et al., (1998)
Nova (1980, 1986)		Zhang (2009)
Boehler and Raclin (1982)	Zhang and Zhu (2007)	
Raclin (1984)	Lee, Pietruszczak, and Choi (2012)	
Kaar et al. (1989)		
Cazacu and Cristescu (1995)		
Cazacu and Cristescu (1999)		
Kusabuka et al. (1999)		
Pietruszczak and Mroz (2001)		
Lee and Pietruszczak (2008)		
Mroz and Maciejewski (2011)		

Jaeger's single plane-of-weakness theory (Jaeger, 1960), which is the starting point of the discontinuous method, is regarded as the first attempt. Two distinct failure modes, namely failure along the discontinuity and that across intact materials, were presumed

to exist in this criterion (Figure 3.6). The standard Mohr–Coulomb criterion is applied to characterize the failure of bedding planes and rock matrix in this theory but employs two different sets of material constants. This criterion provides good results for slightly stratified rocks. However, the results are often undesirable in the case of extremely stratified materials. The main explanation is that the bedding planes behave similarly to rock joints, and the Mohr–Coulomb criterion is unsuitable to model the failure of such discontinuities. A plane of weakness that forms an angle β with the axis of the main principal stress is described by this theory. The angle “ β ” is defined as the “orientation angle.” The UCS envelope represents the variation of failure stress corresponding to the orientation angle.

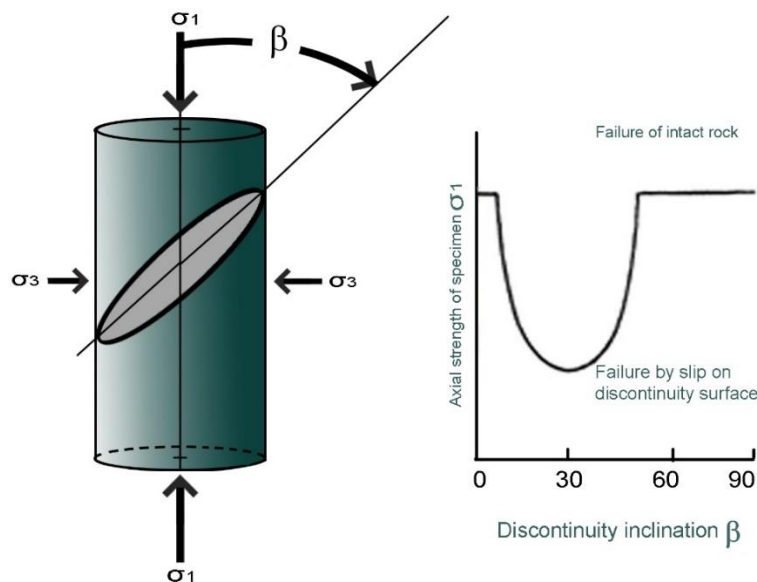


Figure 3.6. Single plane-of-weakness theory (reproduced from Saroglou and Tsiambaos 2007,b).

When the sliding along discontinuities is prevented, Jaeger's original criterion preserved rock as isotropic material by considering four parameters (Figure 3.7a). The compression strength is the same by using Jaeger's criteria at $\beta = 0^\circ$ and 90° . However, experimental data reveal that the maximal strength in certain rocks exists at $\beta = 0^\circ$, while that in other rocks occurs at $\beta = 90^\circ$. Two additional parameters have been added by other researchers to Jaeger's criterion to justify the discrepancy (e.g., Duveau and Shao, (1998) replaced the Mohr–Coulomb criteria with a non-linear model to express the strength along discontinuity (Figure 3.7b)). Table 3.21 lists the material constants

included in the modified and initial criteria. C_0 is cohesion in zero degree, $\tan \phi_0$ is friction angle in zero degree C_{90} is cohesion in 90 degree $\tan \phi_{90}$ is friction angle in 90 degree, C' and $\tan \phi'$ are cohesion and friction angle in a given degree respectively.

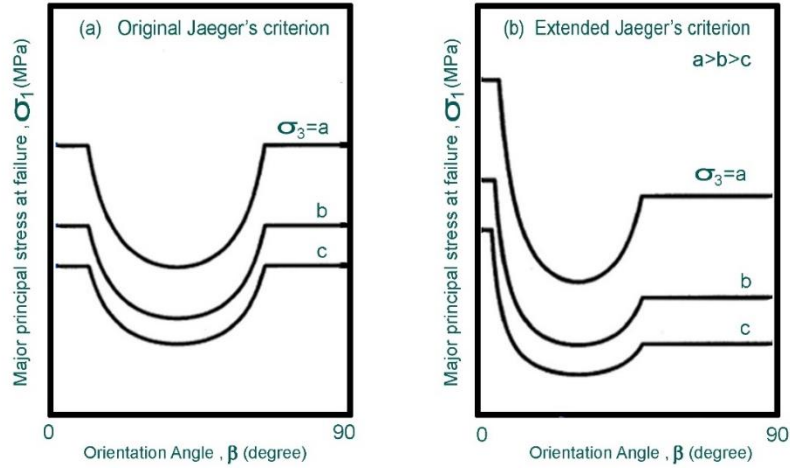


Figure 3.7. Diagram of strength variation versus β (a) original Jaeger's criterion (b) extended Jaeger's criterion (Adapted from Tien and Kuo, 2001)

Table 3.21. Material constants included in the initial and modified criteria

Criteria	Jaeger Criterion	Modified criterion
Constant parameters	$C_0, \tan \phi_0, C_{90}, \tan \phi_{90}, C', \tan \phi'$	$C_0, \tan \phi_0, C_{90}, \tan \phi_{90}, C', \tan \phi', a, b, \sigma_{c0}$

Horino and Ellickson (1970) suggested a method for calculating strength based on the Coulomb strength criterion. This criterion is written as Eq. 3.5.

$$\frac{\sigma_{1f}}{\sigma_1} = \left[\frac{(1 + \sigma_s^2)^2 - \mu_s}{\sin 2\beta - \mu_f(1 - \cos 2\beta)} \right], \quad \text{Eq. 3.5}$$

Where μ_s is the slope of the Mohr rupture envelope at low stress levels, μ_f is the coefficient of internal friction, and β is the angle of anisotropy to the vertical. These parameters can be determined from the Mohr criterion for the material and the plane-of-weakness by conventional triaxial test.

The failure of anisotropic rocks under confining pressure was discussed by Jaeger and Cook (1979). Eq. 3.6 explains the UCS of a sample with a weak plane, which is identified by cohesion C_j and friction angle ϕ .

$$\sigma_1 = \sigma_3 + \frac{2[C_j + \sigma_3 \tan(\phi_j)]}{[1 - \tan(\phi_j) \tan(\beta)] \sin(2\beta)} \quad \text{Eq. 3.6}$$

As mentioned for the single weakness plane theory (Jaeger's criterion), this theory is sufficient for predicting strength when the rock behaves anisotropically due to the existence of a single plane of weakness. However, the theory does not properly explain the strength behavior of intact rock with intrinsic anisotropy due to the presence of bedding or foliation, as in the case of siltstones, schists, and gneisses. Consequently, the Hoek–Brown failure criterion was developed in 1980 for assessing intact rock quality and rock mass strength in isotropic conditions to predict the strength of intact anisotropic rock. Hoek and Brown (1980) proposed the adjustment of the value of the analytical criterion's constants m and s based on the direction of the foliation plane relative to the principal loading axis, β . This criterion is defined as Eq. 3.7:

$$\sigma_1 = \sigma_3 + \sigma_{ci} \left(m \frac{\sigma_3}{\sigma_{ci}} + S \right)^\alpha, \quad \text{Eq. 3.7}$$

Where σ_3 is the minor principal stress, σ_1 is the major principal stress, σ_{ci} is the uniaxial compressive strength, and m , s , and α are material constants; m is equal to m_i , $\alpha = 0.5$, and $s = 1$ when the rock is intact.

Saroglou and Siambaos (2007,b) introduced a new parameter (k_β) to the Hoek and Brown criterion for the influence of strength anisotropy. Consequently, the quality of intact anisotropic rock under loading in various planes of anisotropy can be calculated. This criterion is defined as in Eq. 3.8:

$$\sigma_1 = \sigma_3 + \sigma_{c\beta} \left(K_\beta m_i \frac{\sigma_3}{\sigma_{c\beta}} + 1 \right)^{0.5}, \quad \text{Eq. 3.8}$$

Where $\sigma_{c\beta}$ is the uniaxial compressive strength at an angle of loading β , and k_β is the parameter describing the anisotropy effect. Based on the anisotropic index (α_β), this model describes the triaxial strength behavior of rocks. It is necessary in the model to estimate the uniaxial compressive strength at a given angle. Consequently, a mathematical equation is developed to predict the variation of uniaxial compressive strength of anisotropic rocks. The model is as follows:

$$\sigma_1 = \sigma_3 + \sigma_{c\beta} \left(m_i \frac{\sigma_3}{\sigma_{ci}} + S \right)^{\alpha_\beta}, \quad \text{Eq. 3.9}$$

Where α_β is the anisotropic index that determines the curvature of the failure envelope. In order to apply the failure criterion, the UCS ($\sigma_{c\beta}$) and anisotropic index (α_β) need to be known for the a given orientation β (Eqs. 3.10 and 3.11), as well as the strength parameter m_i .

$$\sigma_{c\beta} = \sigma_{c0} - (\sigma_{c0} - \sigma_{cmin}) \left[\sin\left(\frac{\beta}{\theta} 90^\circ\right) \right]^m \quad 0^\circ \leq \beta \leq \theta, \quad \text{Eq. 3 10}$$

$$\sigma_{c\beta} = \sigma_{c90} - (\sigma_{c90} - \sigma_{cmin}) \left[\cos\left(\frac{\beta-\theta}{90^\circ-\theta} 90^\circ\right) \right]^n \quad \theta < \beta \leq 90, \quad \text{Eq. 3 11}$$

Where $\sigma_{c\beta}$ is the uniaxial compressive strength of anisotropic rocks, σ_{cmin} is the minimum value of uniaxial compressive strength, and m and n are constants. Considering model verification, they also consequently presented a “general” relationship between α_β and $\sigma_{c\beta}$.

$$\alpha_\beta = 1.5 - \left(\frac{\sigma_{c\beta}}{\sigma_{ci}} \right)^b. \quad \text{Eq. 3 12}$$

Each of their approaches, however, requires a range of tests and/or a lot of curve-fitting. Hill (1948) proposed a substantially general criterion for anisotropic materials that can be expressed as a quadratic function. As such, it extends von Mises's isotropic criterion. Von Mises and Hill's criteria assume the strength of materials to be independent of hydrostatic stresses and may be suitable for metals and composite materials, but may not be applicable directly to geological materials because most geological materials are dependent on hydrostatic stresses in their strength behavior. Taking the effects of hydrostatic stresses into account, Pariseau (1968) and Cazacu et al. (1995) extended Hill's criterion. They are applicable to real 3D stress cases; they can be numerically implemented and express the strength considering stresses invariance. A generalized failure criterion for transversely isotropic rocks has been proposed by Nova (1980, 1986). According to Hill and Nova, strength continuously varies with orientation angle. The continuous model is referred to herein. It is, however, inapplicable for the shoulders and undulatory rocks, and especially for rocks that have discontinuities in their structure.

Tien and Kuo (2006) presented a new failure criterion for the transversely isotropic rocks. Two distinct failure modes are considered: failure occurs by sliding along the discontinuities, and a non-sliding mode wherein the failure is controlled by the rock material (Eq. 3.13). The developed criterion comprises seven material parameters:

cohesion and the friction angle of the discontinuity (cw, fw), Hoek–Brown’s parameters and the transversal anisotropy parameter (n).

$$\frac{S_{1(\beta)}}{S_{1(90^\circ)}} = \frac{\sigma_{1(\beta)} - \sigma_3}{\sigma_{1(90^\circ)} - \sigma_3} = \frac{K}{\cos^4 \beta + K \sin^4 \beta + 2n \sin^2 \beta \cos^2 \beta}, \quad \text{Eq. 3 13}$$

where $S_{1(\beta)} = E_{y \varepsilon y f}$, $S_{1(90^\circ)} = E_{(90^\circ) \varepsilon y f}$, and $K = \frac{E_{(0^\circ)}}{E_{(90^\circ)}} = \frac{S_{1(0^\circ)}}{S_{1(90^\circ)}}$.

Rafiai (2011) proposed a new criterion for the prediction of intact rock and rock mass failure under the polyaxial state of stresses (Eq. 3.14). According to the following relationship between effective principal stresses, rock failure in triaxial loading conditions can be demonstrated empirically:

$$\frac{\sigma_1}{\sigma_c} = \frac{\sigma_3}{\sigma_c} + \frac{1+A \left(\frac{\sigma_3}{\sigma_c}\right)}{1+B \left(\frac{\sigma_3}{\sigma_c}\right)} - r, \quad \text{Eq. 3 14}$$

Where σ_c is the UCS of intact rock, A and B are dimensionless constants that depend on the rock propertires ($A \leq B \leq 0$). The parameter, r, indicates how much the rock mass has been fractured according to its strength. For intact rock, $r = 0$; for heavily jointed rock masses, $r = 1$.

The other proposed criterion for rock failure in the polyaxial state of stresses can be expressed by the following relation between effective principal stresses.

$$\frac{\sigma_1}{\sigma_c} = \frac{\sigma_1^{trx}}{\sigma_c} + \sqrt{C \frac{\sigma_2 - \sigma_3}{\sigma_1^{trx}} \exp\left(-\frac{\sigma_2 - D\sigma_3}{\sigma_1^{trx}}\right)}, \quad \text{Eq. 3 15}$$

Where C and D are constants, and σ_1^{trx} is the rock strength in the triaxial state of stresses ($\sigma_2 = \sigma_3$) as presented below.

$$\frac{\sigma_1^{trx}}{\sigma_c} = \frac{\sigma_3}{\sigma_c} + \frac{1+A \left(\frac{\sigma_3}{\sigma_c}\right)}{1+B \left(\frac{\sigma_3}{\sigma_c}\right)} - r. \quad \text{Eq. 3 16}$$

Saeidi et al. (2014) proposed a modified failure criterion to determine the strength of transversely isotropic rocks by considering the rock failure criteria proposed by Rafiai (2011) for the triaxial failure criterion. An index, which can be measured as a strength reduction parameter due to rock strength anisotropy, was obtained through the modification process. The modified criterion is as follows:

$$\sigma_1 = \sigma_3 + \sigma_{c\beta} \left[\frac{1+A \left(\frac{\sigma_3}{\sigma_{c\beta}}\right)}{\alpha+B \left(\frac{\sigma_3}{\sigma_{c\beta}}\right)} \right], \quad \text{Eq. 3 17}$$

Where $\sigma_{c\beta}$ is the UCS of transversely intact isotropic rock at anisotropy orientation, α is the strength reduction parameter related to the rock anisotropy, and A and B are constant parameters. Several transversely isotropic rocks were compared using the modified Hoek-Brown and Ramamurthy criteria. Consequently, the modified failure criteria proposed can be used to predict the strength of transversely isotropic rocks.

3.5 Discussion

The mechanical and physical characteristics of rocks are important aspects of engineering purposes. Such properties can be influenced by the rock petrographic characteristics, including composition and texture, which result from the environment of formation (e.g., sedimentation, diagenesis, metamorphism, and weathering). The current review indicates that mineral composition is the most dominant feature of rock strength. The amount of quartz and feldspar can affect its strength. A high percentage of quartz strengthens the rocks, while the presence of feldspar can reduce strength, especially if the feldspar is present as phenocrysts. However, feldspar is susceptible to alteration (hydrothermal or weathering) and further reduces the strength of the rocks once altered to secondary minerals. In addition, rock strength can be reduced with the presence of the mica minerals, a common component of fine-grained sedimentary rocks and altered volcanic and magmatic rocks. The presence of mica minerals diminishes the rock strength. Weathering grade also affects the strength of the rock despite its small size.

Anisotropy is the other essential factor that can affect rock strength. The minimum value is usually around $\beta = 30^\circ$ based on the overall evaluation and interpretation of the experimental results, and the maximum failure strength is either at $\theta = 0^\circ$ or $\theta = 90^\circ$. Anisotropic rocks become increasingly ductile as confining pressure is raised in triaxial tests. When anisotropic rocks are subjected to uniaxial and triaxial compression tests, the orientation of the loading and the confining pressure influence the failure modes. Two kinds of failure modes are distinguishable, namely: (1) sliding failure mode, where plane discontinuity is predominant, and (2) non-sliding failure mode, where the material strength dominates.

The third important parameter is grain size. The size of the pores is proportional to the grain size. These pores can reduce the strength of rocks. The degree of interlocking in a granitic rock affects its strength. The presence of anhedral–subhedral grains will reduce rock strength. Meanwhile, euhedral can increase strength because it is well-formed with sharp faces. Some researchers argue that strength may not strongly depend on grain size despite the correlations between mechanical properties and the size of mineral grains.

For the analysis of rock stability, it is necessary to apply a representative failure criterion. The strength of the rock is affected by its anisotropy; thus, stability analysis of anisotropic rocks requires representative failure criteria. From a qualitative viewpoint, the two methods (continuous and discontinuous) use various hypotheses and techniques. An overall study of mechanical behaviors of materials revealed that mathematical continuous models propose a general and systematic method using anisotropic strength tensors. These models have an invariant formulation considering the substance symmetry groups. Their calibration only requires a few laboratory experiments, and their numerical implementation is simple and reliable. However, the theoretical calibration procedure suggested in these models cannot be used in reality because performing the necessary laboratory experiments is always difficult, and employing a numerical optimal fitting system is often important. Moreover, in strongly anisotropic rocks, such as schists, the discontinuous aspect of the transition from rock matrix failure to schistosity plane sliding is not captured by these models. Therefore, these models generally provide excessively smooth variations of material strength. However, these models can provide excellent modeling of weakly anisotropic material failure behavior when the effect of weakness planes is not dominant. Ambrose (2014) showed that Pariseau's criterion is the most commonly used mathematical model. Empirical continuous models provide a rudimentary adaptation of isotropic strength criteria to anisotropic material by proposing empirical variation laws of model parameters with loading orientation. These models have a simple mathematical form and can be easily determined considering their parameters. However, the physical meanings of the empirical laws and the involved parameters remain unclear. In addition, a high number of laboratory tests is necessary to find reliable variation laws. These

models have the same weaknesses as the statistical continuous models for a substance with strong bedding planes. The friction angle is generally assumed constant for this group and the cohesion parameters are orientation-specific. Most equations are easy to construct and modify, and they are also straightforward to use. The comparison between mathematical and empirical criteria is represented in Table 3.22.

Table 3 22. Mathematical and empirical continuous criteria based on Ambrose (2014), Duveau, Shao, and Henry (1998), and Dehkordi (2008).

Mathematical Continuous Criteria	Empirical Continuous Criteria
<u>Definition:</u>	<u>Definition:</u>
The mathematical technique used to describe a material's strength function, taking into account the type of symmetry present in the material. From these criteria, constants are obtained.	By applying empirical laws defined by the variation of material parameters considering loading orientation, it is possible to describe the anisotropic strength using the isotropic failure criterion. Experimental data is used to determine the parameters.
<u>Representative Criterion:</u>	<u>Representative Criterion:</u>
In the theory of frictionless materials, a main and first criterion is the Hill's principle, which is an extension of Von-Mises' isotropic theory. Pariseau (1968) extended Hill's criterion for cohesive-frictional material similar to rocks.	Using variational cohesion as a function of loading orientation and constant friction, Jaeger (1960) proposed a modification of the Mohr-Coulomb criterion.
<u>Challenges:</u>	<u>Challenges:</u>
1) In order to determine the material constants, experimentation should be conducted.	1) For such a criterion to be established, there must be a large amount of experimental data and a curve-fitting procedure.
2) Analyzing the physical behavior of the material or the tested rocks gives each criterion their own perspective on anisotropy.	2) The physical and mathematical bases of such criteria are lacking.

In contrast to the continuous models, the discontinuous model of the weakness plane reveals that the material strength is inherently linked to the presence of bedding planes. The final material failure is due to two distinct mechanisms in the microscopic level: isotropic failure in the rock matrix and orientated failure along weakness planes. These models lead to simple and physically-based equations. Because of its clear physical

meaning and high level of precision, this hypothesis is widely used in engineering. In addition, these models contain a small number of parameters, and their determination is generally easy. Thus, these models are well suited to strongly anisotropic materials.

3.6 Summary and Conclusion

Assessment of the relationships between mechanical and texture characteristics of the rocks is crucial to a study or research to obtain additional information regarding the behavior of the rock. This study presents the influence of mineral composition, grain size and shape, and anisotropy effect on the mechanical properties of rock. The main influence on the mechanical characteristics of the rock lies in the variations in the quartz and feldspar contents. The difference in the quartz and feldspar contents is the principal factor influencing the mechanical properties of the rock. Rocks with a high quartz-to-feldspar ratio have high strength values. Therefore, quartz and feldspar have high control and influence over rock strength. The UCS and crack propagation are affected by opaque and altered minerals. The grain size and porosity play a significant role in mechanical properties, even more than the mineral composition. Overall, the strength and elastic modulus of rocks decrease as mean grain size increases. Several studies analyzed the link between mechanical properties and grain size of the rock mostly through experiments. Regression equations are established on the basis of experimental results to predict the mechanical performance of rock materials effectively. Anisotropy of the rock represents strong effects on its mechanical properties. Several equations are used to determine the anisotropy ratio of the rock. Many studies have attempted to establish a correlation between rock anisotropy and UCS parameters and found the strength of various kinds of rocks depended on the degree of anisotropy and direction of stresses. Moreover, the shear intensity value varies with the angle of foliation. So, several failure criteria based on continuous and discontinuous criteria have been proposed to find the strength of anisotropic rocks. It is important that the anisotropic failure criterion is easy to use for the rock engineering designer as well as capable of predicting the strength of the rock. Because its parameters can be easily understood by engineers, Mohr-Coulomb's criterion tends to be used for isotropic rocks, while Jaeger's

plane-of-weakness theory tends to be used for anisotropic rocks. Jaeger's theory has been tested in several experiments.

Many questions remain unanswered despite many available studies regarding the relationship between rock texture and mechanical properties of the rock. Investigation of the following issues may be of interest in the future.

1. The model is extracted in different geological settings or rock types. However, evidence is insufficient to obtain a precise regression analysis between geomechanical parameters of rock and rock texture characteristics. For example, most regression equations between minerals and rock strength are based on only one or two main minerals of the rock, and the influence of other significant minerals, even in low percentage, has not been fully explored. Thus, further attempts on the following aspects should be made.

2. The models, equations, and criteria should be developed to determine the influencing effect of rock texture characteristics on the mechanical properties of rocks through experimental tests and numerical simulations. Moreover, these equations or criteria should be applied to different rock types from different origins to validate these models.

3. In the field of rock strength, the stability of the rock is also related to in-situ stress conditions, excavation depth, rock texture, and hydrogeological conditions surrounding the excavation zone. Therefore, future studies can focus on the relationship between these parameters and the rock texture parameters of the rock. Considering these factors, the application of these techniques for the prediction of rock behavior will be straightforward and beneficial.

3.7 References

- Aagaard B. Strength anisotropy of rocks, M.Sc. dissertation, NTH, Trondheim, pp 104, 1976.
- Ajalloeian, R., Lashkaripour, G. R. (2000). Strength anisotropies in mudrocks. *Bulletin of Engineering Geology and the Environment*, 59(3), 195-199.
- Ajalloeian, R., Jamshidi, A., & Khorasani, R. (2020). Evaluating the Effects of Mineral Grain Size and Mineralogical Composition on the Correlated Equations Between Strength and Schmidt Hardness of Granitic Rocks. *Geotechnical and Geological Engineering*, 1-11.

- Alber, M., Kahraman, S. (2009). Predicting the uniaxial compressive strength and elastic modulus of a fault breccia from texture coefficient. *Rock Mechanics and Rock Engineering*, 42(1), 117-127.
- Allirot, D., Boehler, J. P. (1979). Evolution of mechanical properties of a stratified rock under confining pressure. *4th ISRM Congress. International Society for Rock Mechanics and Rock Engineering*.
- Ali, E., Guang, W., Weixue, J. (2014). Assessments of strength anisotropy and deformation behavior of banded amphibolite rocks. *Geotechnical and Geological Engineering*, 32(2), 429-438.
- Allison, R. J., & Bristow, G. E. (1999). The effects of fire on rock weathering: some further considerations of laboratory experimental simulation. *Earth Surface Processes and Landforms: The Journal of the British Geomorphological Research Group*, 24(8), 707-713.
- Al-Harhi, A. A. (1999). Effect of planar structures on the anisotropy of Ranyah sandstone, Saudi Arabia. *Engineering geology*, 50(1-2), 49-57.
- Ahmad, T., Rizwan, M., Hussain, Z., Ullah, S., Ali, Z., Khan, A., ... & Khan, H. A. (2021). mineralogical and Textural influence on physico-mechanical properties of selected granitoids from Besham Syntaxis, Northern Pakistan. *Acta Geodyn. Geomater*, 18, 347-362.
- Åkesson, U., Lindqvist, J., Göransson, M., Stigh, J. (2001). Relationship between texture and mechanical properties of granites, central Sweden, by use of image-analysing techniques. *Bulletin of Engineering Geology and the Environment*, 60(4), 277-284.
- Amadei, B. (1996). Importance of anisotropy when estimating and measuring in situ stresses in rock. *International Journal of Rock Mechanics and Mining Sciences and Geomechanics Abstracts* 33(3), 293-325).
- An, W. B., Wang, L., & Chen, H. (2020). Mechanical properties of weathered feldspar sandstone after experiencing dry-wet cycles. *Advances in Materials Science and Engineering*.
- Ambrose, J. (2014). Failure of anisotropic shales under triaxial stress conditions. *PhD Thesis*. Imperial College London, Department of Earth Science and Engineering.
- Arel, E., & Tugrul, A. (2001). Weathering and its relation to geomechanical properties of Cavusbasi granitic rocks in northwestern Turkey. *Bulletin of Engineering Geology and the Environment*, 60(2), 123-133.
- Ashour, H. A. (1988). A compressive strength criterion for anisotropic rock materials. *Canadian Geotechnical Journal*, 25(2), 233-237.
- Barron, K. (1971). Brittle fracture initiation in and ultimate failure of rocks: Part I—Anisotropic rocks: Theory. *International Journal of Rock Mechanics and Mining Sciences & Geomechanics Abstracts* 8, (6), 553-563.
- Behrestaghi, M. H. N., Rao, K. S., Ramamurthy, T. (1996). Engineering geological and geotechnical responses of schistose rocks from dam project areas in India. *Engineering geology*, 44(1-4), 183-201.
- Bieniawski, Z. T. (1974). Estimating the strength of rock materials. *Journal of the Southern African Institute of Mining and Metallurgy*, 74(8), 312-320.
- Beddow, J. K., Vetter, A. F. (1977). The use of classifiers in morphological analysis of articulates. *Journal of Powder and Bulk Solids Technology*, 1, 42-45.
- Bell, F. G. (1978). The physical and mechanical properties of the fell sandstones, Northumberland, England. *Engineering Geology*, 12, 1-29.

- Bell, F. G., & Lindsay, P. (1999). The petrographic and geomechanical properties of some sandstones from the Newspaper Member of the Natal Group near Durban, South Africa. *Engineering Geology*, 53(1), 57-81.
- Boehler, J. P. Sawczuk, A. (1970). Equilibre limite des sols anisotropes. *Journal de Mecanique*. 5-13
- Boehler, J. P. (1975). Contributions the oriques et expérimentales a l'etude des milieux plastiques anisotropes', *Thèse de doctorat es sciences*, Grenoble.
- Boehler, J. P. Sawczuk, A. (1977). On yielding of orientated solids, *Acta Mechanica*, 27, 185-192
- Boehler, J. P. Raclin, J. (1982). Ecrouissage anisotrope des matériaux orthotropes pré de formes. *Journal de Mecanique*. 23 - 44.
- Brown, E.T, Richards, L.R, Barr, M.V. (1977). Shear strength characteristics of Delabole slate. *Proceedings of the Conference on Rock Engineering*, Newcastle-upon-Tyne, 31–51.
- Brunhoeber, O. M., Arakkal, D., Ji, R., Miletić, M., & Beckingham, L. E. (2020). Impact of mineral composition and distribution on the mechanical properties of porous media. In *E3S Web of Conferences* (Vol. 205, p. 02006). EDP Sciences.
- Brace, W. F. (1961). Dependence of fracture strength of rocks on grain size. *The 4th US Symposium on Rock Mechanics (USRMS)*. American Rock Mechanics Association. 76, 99-103.
- Casagrande, A., & Carillo, N. (1944). Shear failure of anisotropic materials *Journal of the Boston Society of Civil Engineers*. *Contributions to Soil Mechanics*, 31(4), 1941-1953.
- Cazacu, O., & Cristescu, N. D. (1995). Failure of anisotropic compressible shale (No. CONF-950686-). University of California, Los Angeles, CA (United States).
- Cazacu, O., & Cristescu, N. D. (1999). A paraboloid failure surface for transversely isotropic materials. *Mechanics of materials*, 31(6), 381-393.
- Chatterjee, R., Mukhopadhyay, M. (2002). Petrophysical and geomechanical properties of rocks from the oilfields of the Krishna-Godavari and Cauvery Basins, India. *Bulletin of Engineering Geology and the Environment*, 61(2), 169-178.
- Chapagain, Y. P., Sapkota, S., Ghale, D. B., Bohara, N. B., Duwal, N., & Bhattarai, J. (2020). A case study on mineralogy and physico-mechanical properties of commercial bricks produced in Nepal. *SN Applied Sciences*, 2(11), 1-14.
- Chen, C. S., Pan, E., Amadei, B. (1998). Determination of deformability and tensile strength of anisotropic rock using Brazilian tests. *International Journal of Rock Mechanics and Mining Sciences*, 35(1), 43-61.
- Cox, M. R., & Budhu, M. (2008). A practical approach to grain shape quantification. *Engineering Geology*, 96(1-2), 1-16.
- Dafalias, Y.F., Popov, E.P. (1979). "A model for nonlinearity hardening material for complex loading" *Acta Mechanica*, 21, (3) 173-192.
- Dafalias, Y. F. (1987). Issues on the constitutive formulation at large elastoplastic deformations, Part 1: Kinematics. *Acta Mechanica*, 69(1), 119-138.
- Dehkordi, A. R. (2008). 3D finite element cosserat continuum simulation of layered geomaterials, *PhD Thesis*. University of Toronto, Department of Civil Engineering.
- Dreyer, W. (1972). The science of rock mechanics, part 1: the strength properties of rocks 1(2).
- Dobereiner, L., Freitas, M. D. (1986). Geotechnical properties of weak sandstones. *Geotechnique*, 36(1), 79-94.

- Donath, F. (1966). A triaxial pressure apparatus for testing of consolidated or unconsolidated materials subjected to pore pressure. *Testing Techniques for Rock Mechanics*. ASTM International.
- Duveau, G., Shao, J. F., Henry, J. P. (1998). Assessment of some failure criteria for strongly anisotropic geomaterials. *Mechanics of Cohesive-frictional Materials: International Journal on Experiments, Modelling and Computation of Materials and Structures*, 3(1), 1-26.
- Eberli, G. P., Baechle, G. T., Anselmetti, F. S., & Incze, M. L. (2003). Factors controlling elastic properties in carbonate sediments and rocks. *The Leading Edge*, 22(7), 654-660.
- Ehrlich, R., Weinberg, B. (1970). An exact method for characterization of grain shape. *Journal of sedimentary research*, 40(1), 205-212.
- Ersoy, H., Atalar, C., Sünnetci, M. O., Kolaylı, H., Karahan, M., & Ersoy, A. F. (2021). Assessment of damage on geo-mechanical and micro-structural properties of weak calcareous rocks exposed to fires using thermal treatment coefficient. *Engineering Geology*, 284, 106046
- Ersoy A, Waller M D (1995). Textural characterization of rocks. *Engineering Geology*, 39(3-4): 123-136
- Fahy, M. P., Guccione, M. J. (1979). Estimating strength of sandstone using petrographic thin-section data. *Bulletin of the Association of Engineering Geologists*, 16(4), 467- 485.
- French, W. J., Kermani, S., Mole, C. F. (2001). Petrographic evaluation of aggregate parameters. *Proceeding of the 8th Euroseminar on Microscopy Applied to Building Materials*, 4-7.
- Feng, X. T., Zhao, J., Wang, Z., Yang, C., Han, Q., & Zheng, Z. (2021). Effects of high differential stress and mineral properties on deformation and failure mechanism of hard rocks. *Canadian Geotechnical Journal*, 58(3), 411-426.
- Fereidooni, D. (2016). Determination of the geotechnical characteristics of hornfelsic rocks with a particular emphasis on the correlation between physical and mechanical properties. *Rock Mechanics and Rock Engineering*, 49(7), 2595-2608.
- Gol'denblat, I. I., Kopnov, V. A. (1965). Strength of glass-reinforced plastics in the complex stress state. *Polymer Mechanics*, 1(2), 54-59.
- Guéry, A. A. C., Cormery, F., Shao, J. F., & Kondo, D. (2010). A comparative micromechanical analysis of the effective properties of a geomaterial: effect of mineralogical compositions. *Computers and Geotechnics*, 37(5), 585-593.
- Guo, Z., Li, X. Y., Liu, C., Feng, X., & Shen, Y. (2013). A shale rock physics model for analysis of brittleness index, mineralogy and porosity in the Barnett Shale. *Journal of Geophysics and Engineering*, 10(2), 025006.
- Gu, R., & Fang, Y. (2007). Experiment study on effects of mineral composition on rheological characteristics of soft clayey soil. *ROCK AND SOIL MECHANICS-WUHAN-*, 28(12), 2681.
- Gurocak, Z., & Kilic, R. (2005). Effect of weathering on the geomechanical properties of the Miocene basalts in Malatya, Eastern Turkey. *Bulletin of Engineering Geology and the Environment*, 64(4), 373-381.
- Gupta, A. S., & Rao, K. S. (2000). Weathering effects on the strength and deformational behaviour of crystalline rocks under uniaxial compression state. *Engineering Geology*, 56(3-4), 257-274.

- Hack, R., & Price, D. (1997). Quantification of weathering. *Proceedings engineering geology and the environment, Athens*, 145-150.
- Han, Q., Gao, Y., & Zhang, Y. (2021). Experimental Study of Size Effects on the Deformation Strength and Failure Characteristics of Hard Rocks under True Triaxial Compression. *Advances in Civil Engineering, 2021*
- Hartley, A. (1974). A review of the geological factors influencing the mechanical properties of road surface aggregates. *Quarterly Journal of Engineering Geology*, 7(1), 69-100.
- Hareland, G., Polston, C. E., White, W. E. (1993, December). Normalized rock failure envelope as a function of rock grain size. *International journal of rock mechanics and mining sciences and geomechanics abstracts*, 30 (7), 715 - 717).
- Heng, S., Guo, Y., Yang, C., Daemen, J. J., Li, Z. (2015). Experimental and theoretical study of the anisotropic properties of shale. *International Journal of Rock Mechanics and Mining Sciences*, 74, 58-68.
- Hemmati, A., Ghafoori, M., Moomivand, H., & Lashkaripour, G. R. (2020). The effect of mineralogy and textural characteristics on the strength of crystalline igneous rocks using image-based textural quantification. *Engineering Geology*, 266, 105467
- Higgins, M. D. (2006). Quantitative textural measurements in igneous and metamorphic petrology. Cambridge university press.
- Hill, R. (1948). A theory of the yielding and plastic flow of anisotropic metals. *Proceedings of the Royal Society of London. Series A. Mathematical and Physical Sciences*, 193(1033), 281-297.
- Howarth, D. F., Rowlands, J. C. (1986). Development of an index to quantify rock texture for qualitative assessment of intact rock properties. *Geotechnical Testing Journal*, 9(4), 169-179.
- Howarth, D. F., Rowlands, J. C. (1987). Quantitative assessment of rock texture and correlation with drillability and strength properties. *Rock Mechanics and Rock Engineering*, 20(1), 57-85.
- Hobbs, D. W. (1964, May). The tensile strength of rocks. In *International Journal of Rock Mechanics and Mining Sciences and Geomechanics Abstracts*, 1 (3), 385 -396).
- Horino, F. G., Ellickson, M. L. (1970). A method for estimating strength of rock containing planes of weakness. US Department of Interior, Bureau of Mines. (7449).
- Hornby, B. E., Schwartz, L. M., & Hudson, J. A. (1994). Anisotropic effective-medium modeling of the elastic properties of shales. *Geophysics*, 59(10), 1570-1583.
- Hoek, E., (1964). Fracture of anisotropic rock. *J. Afr. Inst. Min. Metall.*, 64 (10), 501-518.
- Hoek, E. (1965). Rock fracture under static stress conditions. *CSIR report*, Pretoria.
- Hoek, E., Brown, E. T. (1980). Empirical strength criterion for rock masses. *Journal of the geotechnical engineering division*, 106(9), 1013-1035.
- Hoek, E. (1983). Strength of jointed rock masses. *Geotechnique*, 33(3), 187-223.
- Hou, Y., Sun, W., Huang, Y., Ayatollahi, M. R., Wang, L., Zhang, J. (2017). Diffuse interface model to investigate the asphalt concrete cracking subjected to shear loading at low temperature. *Journal of Cold Regions Engineering*, 31(2), 29-38.
- Hugman, R. H. H., Friedman, M. (1979). Effects of texture and composition on mechanical behavior of experimentally deformed carbonate rocks. *AAPG Bulletin*, 63(9), 1478-1489.

- ISRM. (1981). Rock characterization, testing and monitoring, ISRM suggested methods. *Pergamon Press*, Oxford, U.K.
- ISRM. (1985). Commission on Testing Methods. Suggested method for determining Point Load Strength (revised version). *International Journal of Rock Mechanics*, (22), 51-60.
- Jaeger, J.C., (1960). Shear failure of transversely isotropic rock. *Geology Magazine*, (97), 65 - 72.
- Jaeger, J. C., Cook, N. G., (1979). Fundamentals of rock mechanics. 3rd edition, *Chapman and Hall*, Book.
- Jaques, D. S., Marques, E. A. G., Marcellino, L. C., Leão, M. F., Ferreira, E. P. S., & dos Santos Lemos, C. C. (2020). Changes in the Physical, Mineralogical and Geomechanical Properties of a Granitic Rock from Weathering Zones in a Tropical Climate. *Rock Mechanics and Rock Engineering*, 53(12), 5345-5370.
- Jeng, F. S., Weng, M. C., Lin, M. L., Huang, T. H. (2004). Influence of petrographic parameters on geotechnical properties of tertiary sandstones from Taiwan. *Engineering Geology*, 73(1-2), 71-91.
- Jeong, S. W., Locat, J., Leroueil, S., & Malet, J. P. (2010). Rheological properties of fine-grained sediment: the roles of texture and mineralogy. *Canadian Geotechnical Journal*, 47(10), 1085-1100.
- Josh, M., Esteban, L., Delle Piane, C., Sarout, J., Dewhurst, D. N., & Clennell, M. B. (2012). Laboratory characterisation of shale properties. *Journal of Petroleum Science and Engineering*, 88, 107-124.
- Kahn, J. S. (1956). The analysis and distribution of the properties of packing in sand-size sediments: 1. On the measurement of packing in sandstones. *The journal of Geology*, 64(4), 385-395.
- Kainthola, A., Singh, P. K., Verma, D., Singh, R., Sarkar, K., & Singh, T. N. (2015). Prediction of strength parameters of himalayan rocks: a statistical and ANFIS approach. *Geotechnical and Geological Engineering*, 33(5), 1255-1278.
- Kaye, B. H., BH, K. (1982). Review of new methods for characterize the shape and texture of fine particle.. *Journal of Powder and Bulk Solids Technology*, 6 (2), 1-4.
- Khanlari, G. R., Heidari, M., Sepahigero, A. A., Fereidooni, D. (2014). Quantification of strength anisotropy of metamorphic rocks of the Hamedan province, Iran, as determined from cylindrical punch, point load and Brazilian tests. *Engineering geology*, 169, 80-90.
- Krumbein, W. C. (1941). Measurement and geological significance of shape and roundness of sedimentary particles. *Journal of Sedimentary Research*, 11(2), 64-72.
- Kumar, V., Sondergeld, C., & Rai, C. S. (2015). Effect of mineralogy and organic matter on mechanical properties of shale. *Interpretation*, 3(3), SV9-SV15.
- Kusabuka, M., Takeda, H., Kojo, H., & TONEGAWA, T. (1999). Anisotropic yield function for rocks and evaluation of material parameters. *Doboku Gakkai Ronbunshu*, 631, 205-220.
- Ladanyi, b., Archambault, G., (1972), Evaluation of shear strength of a jointed rock mass, *Proceeding 24th Int. Geological Cong. Montreal*, 249-270.
- Lastra, G., Jokovic, V., & Kanchibotla, S. (2021). Understanding the impact of geotechnical ore properties and blast design on comminution circuits using simulations. *Minerals Engineering*, 170, 107001.
- Lee, Y. K., & Pietruszczak, S. (2008). Application of critical plane approach to the prediction of strength anisotropy in transversely isotropic rock masses. *International Journal of Rock Mechanics and Mining Sciences*, 45(4), 513-523.

- Lee, Y. K., Pietruszczak, S., & Choi, B. H. (2012). Failure criteria for rocks based on smooth approximations to Mohr–Coulomb and Hoek–Brown failure functions. *International Journal of Rock Mechanics and Mining Sciences*, 56, 146-160.
- Li, Q., Li, J., Duan, L., & Tan, S. (2021). Prediction of rock abrasivity and hardness from mineral composition. *International Journal of Rock Mechanics and Mining Sciences*, 140, 104658.
- Liu, J., Ding, W., Wang, R., Wu, Z., Gong, D., Wang, X., ... & Jiao, B. (2018). Quartz types in shale and their effect on geomechanical properties: An example from the lower Cambrian Niutitang Formation in the Cen'gong block, South China. *Applied Clay Science*, 163, 100-107.
- Lundqvist, S., Göransson, M. (2001). Evaluation and interpretation of microscopic parameters vs. mechanical properties of Precambrian rocks from the Stockholm region, Sweden. *Proceedings of the eighth Euroseminar on microscopy applied to building materials*, Athens, Department de Geologie, Athens, 13-20.
- Lu, Y., Li, C., He, Z., Gao, M., Zhang, R., Li, C., & Xie, H. (2020). Variations in the physical and mechanical properties of rocks from different depths in the Songliao Basin under uniaxial compression conditions. *Geomechanics and Geophysics for Geo-Energy and Geo-Resources*, 6(3), 1-14
- Marques, E. A. G., Barroso, E. V., Menezes Filho, A. P., & Vargas Jr, E. D. A. (2010). Weathering zones on metamorphic rocks from Rio de Janeiro—Physical, mineralogical and geomechanical characterization. *Engineering Geology*, 111(1-4), 1-18.
- Matsukura, Y., Hashizume, K., Oguchi, C. T. (2002). Effect of microstructure and weathering on the strength anisotropy of porous rhyolite. *Engineering Geology*, 63(1-2), 39-47.
- McLamore, R., Gray, K.E., (1967). The mechanical behavior of transversely isotropic sedimentary rocks. *Transition in American Society of Mechanical Engineering*, Series B, 62 - 76.
- McCabe, W. M.; Koerner, R. M. (1975). High pressure shear strength investigation of an anisotropic mica schist rock. *International Journal of Rock Mechanics and Mining Sciences & Geomechanics*, 12 (8), 219-228.
- McClintock, F.A. Walsh, J.B. (1962). Friction on Griffith Cracks in Rocks under Pressure. *ASME*, (2),1015-1021.
- Mendes, F. M., Aires-Barros, L., Rodrigues, F. P. (1966). The use of modal analysis in the mechanical characterization of rock masses. In *1st ISRM Congress*. International Society for Rock Mechanics and Rock Engineering. (1), 217–223.
- Merriam, R., Rieke III, H. H., Kim, Y. C. (1970). Tensile strength related to mineralogy and texture of some granitic rocks. *Engineering Geology*, 4(2), 155-160.
- Miskovsky, K., Duarte, M. T., Kou, S. Q., Lindqvist, P. A. (2004). Influence of the mineralogical composition and textural properties on the quality of coarse aggregates. *Journal of Materials Engineering and Performance*, 13(2), 144-150.
- Molins, S., Trebotich, D., Miller, G. H., & Steefel, C. I. (2017). Mineralogical and transport controls on the evolution of porous media texture using direct numerical simulation. *Water Resources Research*, 53(5), 3645-3661.
- Mondol, N. H., Jahren, J., Bjørlykke, K., & Brevik, I. (2008). Elastic properties of clay minerals. *The Leading Edge*, 27(6), 758-770.
- Mróz, Z., & Maciejewski, J. (2011). Critical plane approach to analysis of failure criteria for anisotropic geomaterials. In *Bifurcations, instabilities and degradations in geomaterials* (pp. 69-89). Springer, Berlin, Heidelberg.

- Murrell, S. A. F. (1965). The effect of triaxial stress systems on the strength of rocks at atmospheric temperatures. *Geophysical Journal International*, 10(3), 231-281.
- Nasseri, M. H., Rao, K. S., Ramamurthy, T. (1997). Failure mechanism in schistose rocks. *International Journal of Rock Mechanics and Mining Sciences*, 34(3-4), 219-223.
- Nasseri, M. H. B., Rao, K. S., Ramamurthy, T. (2003). Anisotropic strength and deformational behavior of Himalayan schists. *International Journal of Rock Mechanics and Mining Sciences*, 40(1), 3-23.
- Nova, R. (1980). The failure of transversely isotropic rocks in triaxial compression. *International Journal of Rock Mechanics and Mining Sciences & Geomechanics Abstracts* 17 (6), 325-332.
- Nova, R. (1986). An extended Cam Clay model for soft anisotropic rocks. *Computers and Geotechnics*, 2(2), 69-88.
- Nova, R., Sacchi, G. (1982). A generalized failure condition for orthotropic solids. In *Mechanical Behavior of Anisotropic Solids/Comportment Mécanique des Solides Anisotropes* 623-641. Springer, Dordrecht.
- Olszak, W., Urbanowski, W. (1956). The plastic potential and the generalized distortion energy in the theory of non-homogeneous anisotropic elastic-plastic bodies. *Arch. Mech. Stos*, 8(4), 671-694.
- Onodera, T.F.; Asoka Kumara, H.M. (1980). Relation between texture and mechanical properties of crystalline rocks. *Bulletin of the International Association of Engineering Geology*, (22), 173-177
- Orhan, M., Işık, N. S., Topal, T. A. M. E. R., & Özer, M. U. S. T. A. F. A. (2006). Effect of weathering on the geomechanical properties of andesite, Ankara–Turkey. *Environmental Geology*, 50(1), 85-100.
- Ozturk, C. A., Nasuf, E., Bilgin, N. (2004). The assessment of rock cutability, and physical and mechanical rock properties from a texture coefficient. *Journal of the Southern African Institute of Mining and Metallurgy*, 104(7), 397-402.
- Ozturk, C. A., Nasuf, E., Kahraman, S. A. İ. R. (2014). Estimation of rock strength from quantitative assessment of rock texture. *Journal of the Southern African Institute of Mining and Metallurgy*, 114(6), 471-480.
- Pariseau, W. G. (1968). Plasticity theory for anisotropic rocks and soil. *The 10th US Symposium on Rock Mechanics (USRMS)*.
- Pellegrino, A., & Prestininzi, A. (2007). Impact of weathering on the geomechanical properties of rocks along thermal–metamorphic contact belts and morpho-evolutionary processes: The deep-seated gravitational slope deformations of Mt. Granieri–Salincriti (Calabria–Italy). *Geomorphology*, 87(3), 176-195.
- Pietruszczak, S., Mroz, Z. (2001). On failure criteria for anisotropic cohesive-frictional materials. *International journal for numerical and analytical methods in geomechanics*, 25(5), 509-524.
- Přikryl, R. (2001). Some microstructural aspects of strength variation in rocks. *International Journal of Rock Mechanics and Mining Sciences*, 38(5), 671-682.
- Přikryl, R. (2006). Assessment of rock geomechanical quality by quantitative rock fabric coefficients: limitations and possible source of misinterpretations. *Engineering Geology*, 87(3-4), 149-162.
- Price, N. J. (1960), The compressive strength of coal measure rocks. *Colliery Engineering*, 37.437, 283-292.

- Raclin, J. (1984). Contributions théoriques et expérimentales à l'étude de la plasticité, de l'érouissage et de la rupture des solides anisotropes (Doctoral dissertation).
- Räisänen, M., Kupiainen, K., Tervahattu, H. (2003). The effect of mineralogy, texture and mechanical properties of anti-skid and asphalt aggregates on urban dust. *Bulletin of Engineering Geology and the Environment*, 62(4), 359-368.
- Rafiai, H. (2011). New empirical polyaxial criterion for rock strength. *International Journal of Rock Mechanics and Mining Sciences*, 48(6), 922-931.
- Ramamurthy, T., Venkatappa Rao, G., Singh, J. (1988). A strength criterion for anisotropic rocks. *Australia-New Zealand Conference on Geomechanics, 5th, Sydney* 80 (11)e.
- Ramamurthy, T. (1993). Strength Modulus Responses of Anisotropic Rocks. *Compressive Rock Engineering*, (1), 313-329.
- Regmi, A. D., Yoshida, K., Dhital, M. R., & Devkota, K. (2013). Effect of rock weathering, clay mineralogy, and geological structures in the formation of large landslide, a case study from Dumre Besei landslide, Lesser Himalaya Nepal. *Landslides*, 10(1), 1-13.
- Saeidi, O., Vaneghi, R. G., Rasouli, V., Gholami, R. (2013). A modified empirical criterion for strength of transversely anisotropic rocks with metamorphic origin. *Bulletin of Engineering Geology and the Environment*, 72(2), 257-269.
- Saeidi, O., Rasouli, V., Vaneghi, R. G., Gholami, R., Torabi, S. R. (2014). A modified failure criterion for transversely isotropic rocks. *Geoscience Frontiers*, 5(2), 215-225.
- Salager, S., François, B., Nuth, M., Laloui, L. (2013). Constitutive analysis of the mechanical anisotropy of Opalinus Clay. *Acta Geotechnica*, 8(2), 137-154.
- Saroglou, H., Marinos, P. Tsiambaos, G. (2004). The anisotropic nature of selected metamorphic rocks from Greece. *Journal of the Southern African Institute of Mining and Metallurgy*, 104 (4) , 217-222.
- Saroglou, H., Tsiambaos, G. (2007,a). Classification of anisotropic rocks. *11th ISRM Congress*. International Society for Rock Mechanics and Rock Engineering.
- Saroglou, H., Tsiambaos, G. (2007,b). A modified Hoek–Brown failure criterion for anisotropic intact rock. *International Journal of Rock Mechanics and Mining Sciences*, 45(2), 223-234.
- Sajid, M., Coggan, J., Arif, M., Andersen, J., & Rollinson, G. (2016). Petrographic features as an effective indicator for the variation in strength of granites. *Engineering Geology*, 202, 44-54.
- Schaefer, L. N., Kendrick, J. E., Oommen, T., Lavallée, Y., & Chigna, G. (2015). Geomechanical rock properties of a basaltic volcano. *Frontiers in Earth Science*, 3, 29.
- Schulz, B., Sandmann, D., and Gilbricht, S., 2020, SEM-Based Automated Mineralogy and Its Application in Geo- and Material Sciences: Minerals, v. 10, doi:10.3390/min10111004
- Shakoor, A. bonelli, R.E. (1991). Relationship between petrographic characteristics, engineering index properties, and mechanical properties of selected sandstones. *Bulletin of the Association of Engineering Geologists*, 28(1), 55-71.
- Singh, J., Ramamurthy, T. Venkatappa, R. G., (1989). Strength anisotropies in rocks. *Geo technique*. 19(2) 147- 166.
- Singh, S. K. (1988). Relationship among fatigue strength, mean grain size and compressive strength of a rock. *Rock Mechanics and Rock Engineering*, 21(4), 271-276.
- Single, B., Goel, R. K., Mehrotra, V. K., Garg, S. K., & Allu, M. R. (1998). Effect of intermediate principal stress on strength of anisotropic rock mass. *Tunnelling and Underground Space Technology*, 13(1), 71-79.

- Singh, R., Umrao, R. K., Ahmad, M., Ansari, M. K., Sharma, L. K., & Singh, T. N. (2017). Prediction of geomechanical parameters using soft computing and multiple regression approach. *Measurement*, 99, 108-119.
- Smith, M. B.; Cheatham Jr, J. B. (1980). An anisotropic compacting yield condition applied to porous limestone. *In International Journal of Rock Mechanics and Mining Sciences & Geomechanics Abstracts* 17 (3), 159-165).
- Sousa, L. M. (2013). The influence of the characteristics of quartz and mineral deterioration on the strength of granitic dimensional stones. *Environmental earth sciences*, 69(4), 1333-1346.
- Song, Z., & Zhang, J. (2021). The effect of confining pressure on mechanical properties in coal and rock: review and new insights. *Arabian Journal of Geosciences*, 14(23), 1-22.
- Strauhal, T., Zangerl, C., Fellin, W., Holzmann, M., Engl, D. A., Brandner, R., Tessadri, R. (2017). Structure, mineralogy and geomechanical properties of shear zones of deep-seated rockslides in metamorphic rocks (Tyrol, Austria). *Rock Mechanics and Rock Engineering*, 50(2), 419-438.
- Sun, W., Wang, L., & Wang, Y. (2017). Mechanical properties of rock materials with related to mineralogical characteristics and grain size through experimental investigation: a comprehensive review. *Frontiers of Structural and Civil Engineering*, 11(3), 322-328.
- Tapponnier, P., Brace, W. F. (1976, April). Development of stress-induced microcracks in Westerly granite. *International Journal of Rock Mechanics and Mining Sciences and Geomechanics Abstracts*, 13 (4), 103-112.
- Tamrakar, N. K., Yokota, S., Shrestha, S. D. (2007). Relationships among mechanical, physical and petrographic properties of Siwalik sandstones, Central Nepal Sub-Himalayas. *Engineering Geology*, 90(3-4), 105-123.
- Tang, A. M., & Cui, Y. J. (2010). Effects of mineralogy on thermo-hydro-mechanical parameters of MX80 bentonite. *Journal of Rock Mechanics and Geotechnical Engineering*, 2(1), 91-96.
- Taylor, J. M. (1950). Pore-space reduction in sandstones. *AAPG bulletin*, 34(4), 701-716.
- Tien, Y. M., Kuo, M. C. (2001). A failure criterion for transversely isotropic rocks. *International Journal of Rock Mechanics and Mining Sciences*, 38(3), 399-412.
- Tien, Y. M., Kuo, M. C., & Juang, C. H. (2006). An experimental investigation of the failure mechanism of simulated transversely isotropic rocks. *International journal of rock mechanics and mining sciences*, 43(8), 1163-1181.
- Tiwari, R. P., & Rao, K. S. (2007). Response of an anisotropic rock mass under polyaxial stress state. *Journal of materials in civil engineering*, 19(5), 393-403.
- Tsai, S.W., Wu, E.M. (1971). A general theory of strength for anisotropic materials. *Journal of composite materials*, 5(1), 58-80.
- Tsidzi, K. E. N. (1986). A quantitative petrofabric characterization of metamorphic rocks. *Bulletin of the International Association of Engineering Geology* (1), 3-12.
- Tsidzi, K. E. N. (1990). The influence of foliation on point load strength anisotropy of foliated rocks. *Engineering Geology*, 29(1), 49-58.
- Tsidzi, K. E. N. (1997). Propagation characteristics of ultrasonic waves in foliated rocks. *Association of Engineering Geology*, (56), 103-113.
- Tuğrul, A. (2004). The effect of weathering on pore geometry and compressive strength of selected rock types from Turkey. *Engineering geology*, 75(3-4), 215-227.

- Tuğrul, A., Zarif, I. H. (1999). Correlation of mineralogical and textural characteristics with engineering properties of selected granitic rocks from Turkey. *Engineering geology*, 51(4), 303-317.
- Ulusay, R., Türeli, K., & Ider, M. H. (1994). Prediction of engineering properties of a selected litharenite sandstone from its petrographic characteristics using correlation and multivariate statistical techniques. *Engineering Geology*, 38(1-2), 135-157.
- Ündül, Ö. (2016). Assessment of mineralogical and petrographic factors affecting petro-physical properties, strength and cracking processes of volcanic rocks. *Engineering geology*, 210, 10-22.
- Vernik, L., & Kachanov, M. (2010). Modeling elastic properties of siliciclastic rocks. *Geophysics*, 75(6), E171-E182.
- Vutukuri, V.S. Lama, R.D. Saluja, S.S. (1974). Handbook on Mechanical Properties of Rocks, Testing Techniques and Results. *Trans Technical Publications*, Clausthal, Germany. 280.
- Walsh, J. B., Brace, W. F. (1964). A fracture criterion for brittle anisotropic rock. *Journal of Geophysical Research*, 69(16), 3449-3456.
- Wang, Y., Sun, J., Liang, Z., Huang, S., & Wang, Y. (2021). Experimental Study on the Mechanical Properties of Triaxial Compression of White Sandstone under the Coupling Action of Chemical Corrosion and Temperature. In *IOP Conference Series: Earth and Environmental Science* 692(4), 042009.
- Wadell, H. (1932). Volume, shape, and roundness of rock particles. *The Journal of Geology*, 40(5), 443-451.
- Ward, C. R., Nunt-Jaruwong, S., & Swanson, J. (2005). Use of mineralogical analysis in geotechnical assessment of rock strata for coal mining. *International journal of coal geology*, 64(1-2), 156-171.
- Wyering, L. D., Villeneuve, M. C., Wallis, I. C., Siratovich, P. A., Kennedy, B. M., Gravley, D. M., & Cant, J. L. (2014). Mechanical and physical properties of hydrothermally altered rocks, Taupo Volcanic Zone, New Zealand. *Journal of Volcanology and Geothermal Research*, 288, 76-93.
- Williams, H., Turner, F. J., Gilbert, C. M. (1982). *Petrography: An introduction to the study of rocks in thin section*. Second edition, W.H. Freeman and company, San Francisco, Book.
- Willard, R. J., McWilliams, J. R. (1969). Microstructural techniques in the study of physical properties of rock. In *International Journal of Rock Mechanics and Mining Sciences and Geomechanics Abstracts* 6 (1), 1-12).
- Wong, R. H., Chau, K. T., Wang, P. (1996). Microcracking and grain size effect in Yuen Long marbles. *International journal of rock mechanics and mining sciences and geomechanics abstracts*. 33 (5), 479-485).
- Wong, L. N. Y., Peng, J., & Teh, C. I. (2018). Numerical investigation of mineralogical composition effect on strength and micro-cracking behavior of crystalline rocks. *Journal of Natural Gas Science and Engineering*, 53, 191-203.
- Xu, T., & Pruess, K. (2004). *Numerical simulation of injectivity effects of mineral scaling and clay swelling in a fractured geothermal reservoir* (No. LBNL-55113). Lawrence Berkeley National Lab. (LBNL), Berkeley, CA (United States).
- Yılmaz, N. G., Goktan, R. M., & Kibici, Y. (2011). An investigation of the petrographic and physico-mechanical properties of true granites influencing diamond tool wear performance, and development of a new wear index. *Wear*, 271(5-6), 960-969.

- Yoshinaka, R., & Yamabe, T. (1981), A strength criterion of rocks and rock masses. ISRM International Symposium. OnePetro.
- Yusof, N. Q. A. M., Zabidi, H. (2016). Correlation of mineralogical and textural characteristics with engineering properties of granitic rock from Hulu Langat, Selangor. *Procedia Chemistry*, 19, 975-980.
- Zhao, Q. D., Liu, Z. S. and Qi, L., 1992. Strength criteria for anisotropic rocks and experimental studies. paper SPE 25302.
- Zhang, G. Q. (2009). Rock failure with weak planes by self-locking concept. *International Journal of Rock Mechanics and Mining Sciences*, 46(6), 974-982.
- Zhang, F., An, M., Zhang, L., Fang, Y., & Elsworth, D. (2019). The role of mineral composition on the frictional and stability properties of powdered reservoir rocks. *Journal of Geophysical Research: Solid Earth*, 124(2), 1480-1497.
- Zhang L. (2006). "Engineering Properties of Rocks." *John Hudson. Elsevier, Geo-Engineering Book Series*, (4), 226–30.
- Zhang, L., & Zhu, H. (2007). Three-dimensional Hoek-Brown strength criterion for rocks. *Journal of Geotechnical and Geoenvironmental Engineering*, 133(9), 1128-1135.
- Zorlu, K., Ulusay, R. E. Ş. A. T., Ocakoglu, F., Gokceoglu, C. A. N. D. A. N., Sonmez, H. (2004). Predicting intact rock properties of selected sandstones using petrographic thin-section data. *International Journal of Rock Mechanics and Mining Sciences*, 41, 93-98.

Chapter 4: Evaluation of the effect of mineralogy on the point load compressive strength of rock ³

Abstract

The geomechanical parameters depend on the mineral composition of a rock, and play the important roles in the stability of underground structures. This research investigates the effect of rock-forming minerals in metamorphic rocks on the point load index (PLI). The axial and diametrical PLIs of over 1300 metamorphic rock specimens from a mine site were carefully measured. The mineralogy of a subset of samples representative of the principal lithologies present at the mine was established; the remaining samples were statistically grouped and attributed to specific lithologies based on similar mineralogical characteristics. Multivariable statistical methods are used to evaluate the effect of minerals on PLIs for different rock units. The principal component regression results of PLIs highlights the distinct influence of silicate and phyllosilicate minerals on PLI. Quartz, feldspar, amphibole, and epidote present positive influence on the axial and diametrical PLIs. Chlorite, sericite, and white mica show negative influence on the both PLIs. One important extra finding is that rock texture also strongly influences the PLI, because anisotropy, common in metamorphic rocks, negatively impacts the diametrical PLI of these rock core specimens obtained from drill holes perpendicular to the rock foliation.

Keywords: Underground instability; Metamorphic rocks; Point load index; Multivariable statistical analysis

4.1 Introduction

The mechanical properties of a rock, which largely depend on petrophysical properties, are important parameters that must be considered when rock mass failure is a potential issue in works, such as the drilling of wells, extraction of deep mining deposit, and the constriction of reservoirs (Worthington 1991). In general, rock strength is determined by two factors: the nature and condition of the rock itself, which includes

³ Askaripour M, Seyifaddini M, Saeidi A, Rouleau A, Mercier-Langevin P. Geomechanics and Engineering (Under journal review).

its texture, as well as factors related to sample preparation and test procedures (Gupta and Rao 2000, Liu *et al.* 2005, Tugrul 2004). For several decades, rock properties have been studied both physically and mechanically, and results have shown the close relationship between these two parameters (Zhang *et al.* 2012). Among the aforementioned factors, mineral composition influences the mechanical properties of a rock. The effect of mineralogical composition on rock strength has been studied, and research results indicate that quartz present in igneous, sedimentary, and metamorphic rocks is one of the minerals that potentially has the greatest effect on rock strength (Karaca 2012, Sousa 2013). Quartz as a very hard mineral and relatively abundant in many rock types largely contributes to the overall hardness of the rock. Numerous researchers have validated the relationship between quartz content and compressive strength of the rock (e.g., Vutukuri *et al.* 1978, Tuğrul and Zarif 1999, Yusof and Zabidi 2016). However, some other researchers argued that quartz content and strength in sandstones, which are dominantly composed of quartz, have no remarkable relationship (Bell 1978, Fahy 1979, Shakoor and Bonelli 1991). Similar inconsistent findings were also reported for phyllosilicates, which are common rock-forming minerals but much less resistant than quartz (Tugrul and Zarif, 1999). Merriam *et al.* (1970) studied the relationship between tensile strength and quartz percentage in rocks. Their results indicate that a higher relative abundance of quartz equals higher rock competency. The quartz-to-feldspar ratio (QFR) and mechanical properties have also been studied. When comparing granitic rocks, the uniaxial compressive strength (UCS) and the tensile strength increase linearly with QFR (Tugrul and Zarif 1999). Rocks with higher QFR values are generally stronger, according to Yusof and Zabidi (2016). Nevertheless, Sousa (2013) stated that QFR or quartz content cannot be directly related to unconfined compressive strength, and strength decreases with QFR. Prikryl (2001) indicated that the abundance of quartz and feldspar affects rock strength, that is, a high quartz percentage strengthens the rock, whereas feldspar has the opposite effect. Shakoor and Bonelli (1991) studied the relationship between the petrographic characteristics and mechanical properties of different sandstones. He concluded that the presence of quartz and a higher percentage of sutured contacts have good correlation with mechanical properties, whereas a high relative abundance of cement has weak association with rock strength. Keikha and Keykha (2013) indicated that UCS and tensile strength improve

when the quartz to plagioclase ratio increases. Hugman and Friedman (1979) performed mineralogical analysis, evaluated the effect of mineralogy on the UCS of carbonate rocks with intermediate dolomite and micrite contents (Yule marble, Solenhofen limestone, Hasmark dolomite, and Blair dolomite), and the best-fit plane estimated the approximate ultimate strength. When dolomite and microcrystalline carbonate are present in rocks, their ultimate strength increases. As Brattli (1992) explored, minerals have a significant influence on the resistance of igneous rock to fracture and abrasion. The results showed impact, abrasion, and durability are positively correlated with the content of feldspar, mica, and amphibole whereas the values of pyroxene are negatively related to those factors. Impact value is more affected by feldspar content than abrasion value. Lundqvist and Göransson (2001) evaluated the correlation of mechanical properties with mineral content in Precambrian rocks from Stockholm, Sweden. Researchers discovered a distinct relationship between mica content and abrasion resistance that is, mica content could decrease abrasion resistance. Iron- and magnesium-rich aggregates represent better resistance to fragmentation and abrasion. Miskovsky *et al.* (2004) found that impact values are linearly correlated, that is, abrasion value linearly decreases with the increase in feldspar and quartz contents.

The studies cited above focused on one or very few rock-forming minerals and did not incorporate detailed information nor took into account other minerals present in rock. This lack of information about mineralogy, especially about the minerals of felsic and mafic rocks, could make the mechanical behavior of rock difficult to investigate, as composition and texture can vary considerably in a rock mass. More importantly, the effect of mineralogy on the point load index (PLI) has not been studied. In most of the mentioned studies, the effect of each mineral was studied individually, but the interaction or cumulative influence of all minerals on rock strength were not studied. The mechanical properties of rock with the same mineralogical composition may vary because of textural variations. Therefore, research on the mineral composition of rock, rock texture and structures, and the influence of minerals on rock mechanics are needed to develop better knowledge and tools in evaluating rock mass behavior in complex but very common geological settings. Additionally, due to the high cost of the thin section test, it isn't feasible to perform it on all of the selected samples for geomechanical

testing, which come from different excavation areas. Thus, it is imperative to find a simple way to determine the composition of samples from different mine sites.

In order to fill this knowledge gap, an entirely new method was developed to achieve all mineralogy of each lithological unit of the boreholes. Using this innovation, the remaining samples were grouped into lithologies, based on similar geochemical characteristics. Then, we have analyzed the mineralogy of a series of samples from mafic (silica-poor) and felsic (silica-rich) volcanic rocks that have been hydrothermally altered by ore-forming fluids and then deformed and metamorphosed during later tectonic events. The samples were tested for their point load compressive strength along two different orientations, either normal or parallel to the schistosity. Results of the point load tests (PLTs) were correlated with the minerals, the mineral assemblages and the anisotropy of the rock samples using multivariate statistical analysis to determine the factors with the greatest influence on rock strength.

4.2 Westwood mine

Westwood mine is situated in Doyon property, which is 2.5 kilometers east of the former Doyon gold mine in Bousquet Township, approximately 40 kilometers east of Rouyn-Noranda, and 80 kilometers west of Val d'Or in northwestern Québec, Canada. This area is approximately 420 km northwest of Montreal (Figure 4.1). Westwood mine is owned and operated by IAMGOLD Corporation and was put into production in 2013.



Figure 4. 1. Westwood mine location

Several thousand meters of drill core were available for sampling, and large amounts of geological and geotechnical data were acquired on the core and in drill holes. The extensive underground development also provides substantial amounts of information about geology and geomechanics. The rocks hosting the Westwood deposit vary remarkably in composition and are complexly intercalated often at the meter-scale. The strata are now vertical and lithological contacts are parallel with penetrative schistosity because of regional deformation. Numerous contact parallel and high-angle ductile to brittle faults crosscut the units. All the units were affected to some extent by ore-forming hydrothermal alteration that caused the breakdown of primary minerals, such as feldspar, into phyllosilicates and clays, which were later recrystallized to coarser phyllosilicates and silicate porphyroblasts in a matrix of fine-grained quartz and feldspar. The units are often thin and interleaved and thus create or generate differential strength in rocks within short distances, which represents a day-to-day challenge for mining operations and has caused some rock stability issues (Yergeau 2015).

Characterization of the different lithologies of the Westwood deposit is essential to understand the impact of rock quality on the geomechanical parameters of rock. The geology of this deposit is complex; the deposit comprises 16 lithological units are identified, from mafic (fragile–ductile unit) to felsic (fragile unit) with six different types of alteration, which are intersected by dykes and veins with variable composition (Yergeau 2015). Therefore, the deposit is a very heterogeneous rock mass. So, the Westwood mine was selected because of its unique features in terms of different lithologies with different minerals, an increasing degree of rock metamorphism with increasing excavation depth, and reports of rock mass failure in terms of rock burst. In this study, metamorphic rock specimens were collected from four boreholes with several lithological units, namely, R19016-18, R19018-18, R19200, and R19239 (Table 4.1).

Table 4. 1. Description of the lithological units sampled by the boreholes

Borehole number	Unit Number	Sublevel number	Composition	Volcanic facies	Borehole length
R19016-18	4.2	4.2.0	Andesite to dacite	Massive breccia dykes and sills	264 m
	4.3	4.3.0	Rhyolite to rhyolite	Massive breccia dykes and sills	
	4.4	4.4.0	Basalt to basaltic andesite	Massive, brecciated, mono/polygenic lapilli blocks	
		4.4.1	Gabbro	Gabbro–basalt	
	5.1	5.1.2	Andesite to dacite	Massive, brecciated, polygenic lapilli blocks	
		5.1.3	Basalt to basaltic andesite	Massive sills	
		5.1.4	Dacite	brecciated, massive, and volcaniclastic monogenic lapilli block	
	5.4	5.4.0	Basalt	Sill (border)	
	3.3	3.3.0	Basalt to basaltic andesite	Solid and volcaniclastic mono/polygenic lapilli blocks	
	4.2	4.2.0	Andesite to dacite	Massive breccia dykes and sills	

R19018- 18	4.3	4.3.0	Rhyodacite to rhyolite	Massive breccia dykes and sills	
				Massive, brecciated, mono/polygenic lapilli blocks	185 m
	4.4	4.4.0	Basalt to basaltic andesite		
		4.4.1	Gabbro	Gabbro–basalt	
		5.1.2	Andesite to dacite	Massive, brecciated, polygenic lapilli blocks	
	5.1				
		5.1.3	Basalt to basaltic andesite	Massive sills	
				Brecciated, massive, and volcanoclastic monogenic lapilli block	
		5.1.4	Dacite		
		5.4	5.4.0	Basalt	Sill (border)
	2.0	2.0.0	Rhyolite	Massive sills	
				Solid and volcanoclastic mono/polygenic lapilli blocks	
	3.3	3.3.0	Basalt to basaltic andesite		
R19200				Solid and volcanoclastic mono/polygenic lapilli blocks	99.5 m
	3.3	3.3.1	Basalt		
	4.2	4.2.0	Andesite to dacite	Massive breccia dykes and sills	
	4.3	4.3.0	Rhyodacite to rhyolite	Massive breccia dykes and sills	

			Tonalite	Massive intrusive ± brecciated Solid and volcaniclastic	
	2T	2T			
R19239	3.3	3.3.0	Basalt to basaltic andesite	mono/polygenic lapilli blocks	
	4.2	4.2.0	Andesite to dacite	Massive breccia dykes and sills	160 m
	4.3	4.3.0	Rhyodacite to rhyolite	Massive breccia dykes and sills Massive, brecciated,	
	4.4	4.4.0	Basalt to basaltic andesite	mono/polygenic lapilli block	
		4.4.1	Gabbro	Gabbro–basalt	

The metamorphic rock specimens selected along the rock core obtained from these boreholes were subjected to PLTs and to petrographical description, in order to obtain the point load index (PLI) and observable minerals of the lithological units.

4.3 Methodology

A methodology was developed in this paper for the study of the effect of mineralogy on the point load compressive strength of rock (Figure 4.2).

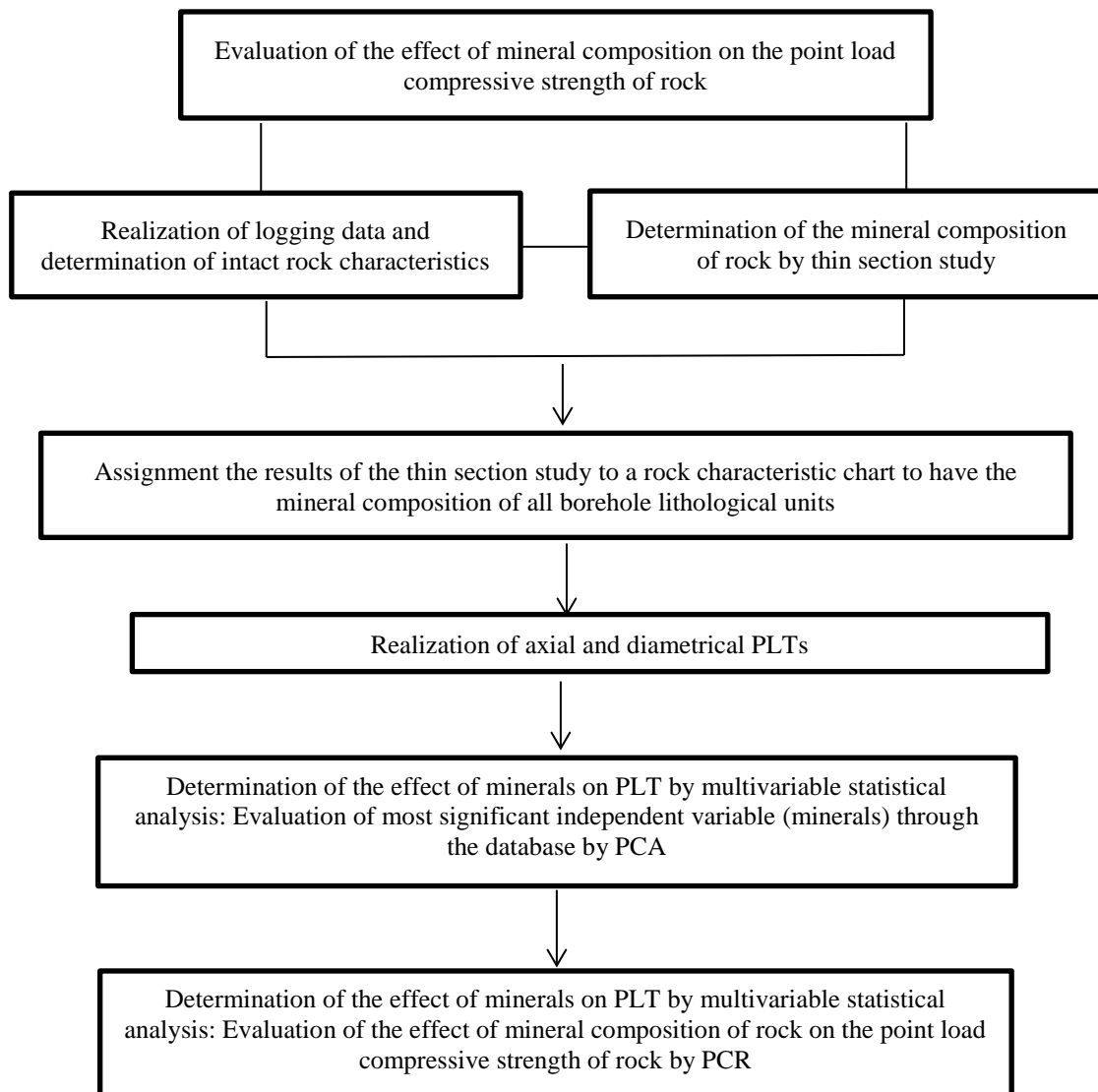


Figure 4. 2 Methodology used to evaluate the effect of rock mineral composition on the point load compressive strength of rock

This study reports data on the core samples collected from four different boreholes in Westwood mine (Table 4.1). Thin section study, geotechnical core logging data, and charting rock characteristics for the determination of observable minerals were performed. Axial and diametrical PLTs were undertaken in each meter of boreholes to estimate the PLI of rocks. Then, the results of the thin section study were assigned to the rock characteristic chart to make a large database that includes the mineralogy and axial and diametrical PLIs of all metamorphic rock specimens. This database is classified into two main groups: mafic and felsic rocks. Principal component analysis (PCA) and principal component regression (PCR) were carried out as multivariable statistical analyses to clarify the role of each mineral on axial and diametrical PLIs. PCA was applied to find the most relevant minerals among the database, and PCR was used to find out the effect of the mineralogy of mafic and felsic rocks on axial and diametrical PLIs. The methodology and data interpretation are explained in the following sections.

4.3.1 Assessment of borehole logging data

Geotechnical core logging has been developed to record the mechanical and structural properties of rock cores. The core logging method requires the core to be grouped into logging intervals that are unique geotechnical domains or design domains within a particular rock type. The geotechnical domains are determined by grouping together rocks with similar geotechnical characteristics.

In this study, four boreholes (Table 4.1) were logged and fixed interval domain logging data (unit by unit) were chosen to perform geotechnical core logging. The rocks were grouped into these domains, and then each relevant parameter required for geotechnical evaluation was logged. The total length of the logged boreholes is 708 m. The selected parameters include foliation orientation, roughness, acid reaction, magnetism, color, and observable minerals. Foliation orientation was evaluated based on the angle of foliation relative to the core axis. A rock mass characteristic chart based on the geotechnical core logging results was proposed by the authors (Figure 4.3). This proposed chart was designed to determine the observable minerals in lithological units and their properties, such as color, roughness, and other parameters. This chart is important for the determination of observable minerals in each lithological unit of a

borehole. Subsequently, the observable minerals in each lithological unit were recorded (fixed interval domain logging data). This important part of the proposed chart enabled us to assign the results of thin section study to each lithological unit of the boreholes.

Hole ID:				
From:				
To:				
Homogeneity:				
Colour:				
Hardness :				
Magnetism (0-5):				
Acid reaction (Y/N):				
Grain size:				
Schistosity (0-5):				
Alteration				
Metamorphisim				
Observable mineral:	(No/Mineral/Porphyre) %:	Orientation:	Granulometry	
Quartz				
Feldspaths				
Sericite				
Muscovite				
Chlorite				
Biotite				
Epidote				
Amphiboles				
Grenat				
Kyanite				
Sulfures				
Texture :				

Figure 4. 3. Proposed rock characteristic chart

A total of 164 rock characteristic charts were prepared for all the lithological units of the boreholes. The mineralogy of each lithological unit was coupled to its relevant thin section study results, as discussed in Section 4.4.3.

4.3.2 Assessment of rock mineralogy

The mineralogy composition and textural characteristics of the rocks were studied by using thin sections. A petrographic microscope was carried out to examine thin sections of the rock specimens for determination of their mineralogy. The samples for thin section study were collected from different locations of Westwood mine and not

from the mentioned boreholes in Table 4.1. It will be represented in section 4.3.3 that how these samples were assigned to mentioned units of boreholes in Table 4.1. The units 4-3-0, 4-4-0, 4-4-1, 5-1-3, 3-3-0, 3-3-1 are mafic rocks like basalt, lapilli tuf and gabbro-basalt whereas the units 5-1-4, 4-2-0, 2-0-0, 2T are felsic rocks like tonolite and dacite. Quartz, feldspar, amphibole, plagioclase, white mica, epidote, chlorite, carbonate, sericite, and garnet were detected by thin section study (Table 4.2). The most common minerals in the mica group were muscovite and biotite. The trace minerals included apatite, tourmaline, magnetite, and pyrite. All the samples are foliated as well. Figure 4.4 represents the minerals of the selected samples.

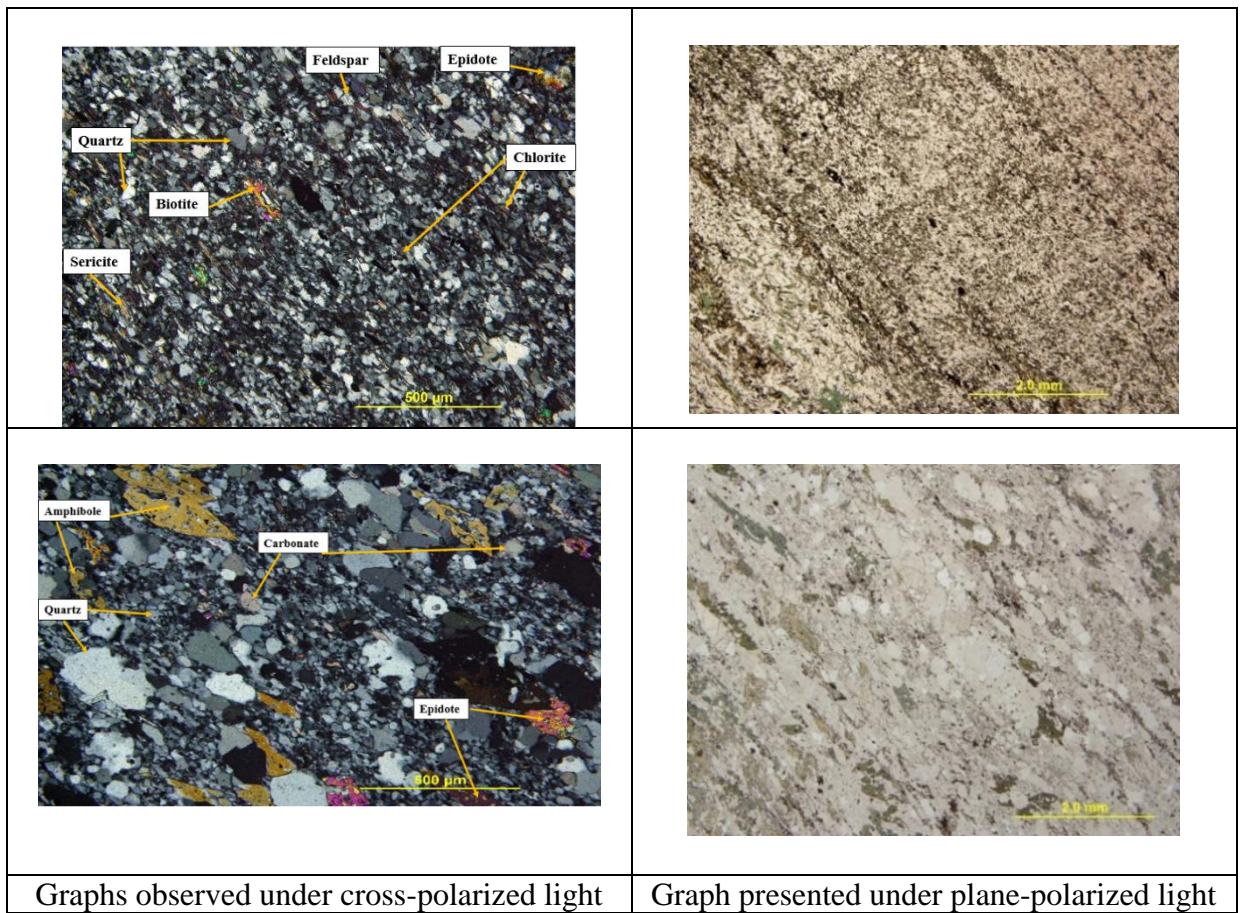


Figure 4. 4. Thin section photomicrographs of rock samples

Table 4. 2 Mineralogy of samples (All minerals in %, Q is quartz, Chl is chlorite, Car is carbonate, Ser is sericite, Epi is epidote, Amp is amphibole, Plag is plagioclase, Feld is feldspar, Bi is biotite, WM is white mica, Gar is garnet, Apa is apatite, Tou is tourmaline).

Samples			Mineralogy (%)													
Borehole ID	Unit	Rock type	Quartz	Chlorite	Carbonate	Sericite	Epidote	Amphibole	Plagioclase	Feldspar	Biotite	White mica (Muscovite)	Garnet	Apatite	Tourmaline	Opaque
R19218-19	U4-4-1	Gabbro-Basalt	10	-	-	11	31	45	3	-	-	-	-	-	-	-
R18281-17	U5-1-3	Basalt	5	25	-	58	-	-	-	10	-	-	-	-	-	2
R19218-19	U4-4-0	Tuff lappillis	35	21	8	10	-	-	-	5	-	20	-	-	-	1
R18110-17	U5-1-2	Andesite	40	2	2	20	1	-	5	20	-	5	-	-	-	5
R18110-17	U5-1-3	Basalt	35	31	-	10	1	-	-	20	3	-	-	-	-	-
R18110-17	U5-1-2	Andesite	10	10	-	32	5	-	-	40	-	3	-	-	-	-
R19217-19	U3-3-0	Tuff lappillis	40	3	-	25	12	-	-	-	-	5	-	-	1	14
R18281-17	U5-1-4	Dacite	50	10	-	20	-	-	3	15	-	2	-	-	-	-
R19164-19	U4-3-0	Dacite	58	10	-	20	9	-	-	-	-	-	-	-	-	3
R18281-17	U5-1-2	Andesite	10	9	-	30	-	-	-	41	5	-	-	-	-	5
R19197-19	U4-2-0	Dacite	70	-	1	-	-	-	-	1	8	10	-	-	-	-
R18281-17	U5-1-3	Basalt	30	5	-	55	-	-	-	10	-	-	-	-	-	5
R18110-17	U5-1-4	Dacite	10	25	-	25	30	-	10	-	-	-	-	-	-	-
R19197-19	U3-3-1	Basalt	20	-	10	15	-	30	-	21	1	-	-	-	1	2
R19199-19	U4-2-0	Dacite	57	5	7	-	-	15	-	-	10	6	-	-	-	-
R19163-19	U3-3-1	Basalt	15	20	-	40	5	-	-	-	-	20	-	-	-	-
R19163-19	U4-3-0	Dacite	59	23	2	-	1	-	-	2	5	8	-	-	-	-
R19163-19	U3-3-0	Basalt	20	13	35	10	20	2	-	-	-	-	-	-	-	-
R19163-19	U4-4-0	Tuff lappillis	47	10	-	25	11	-	6	-	-	-	-	-	-	1
R19162-19	U4-2-0	Dacite	49	18	6	25	1	-	-	-	-	-	-	-	-	1
R19026-18	U4-3-0	Dacite	51	10	-	15	13	1	8	-	1	-	-	-	-	1
R18776-18	U2-0-0	Tuff lappillis	50	3	3	1	-	-	-	25	3	15	-	-	-	-
R19017-18	U4-3-0	Dacite	30	27	-	10	2	-	-	-	-	26	-	-	-	5
R19017-18	U4-4-0	Tuff lappillis	15	20	-	39	15	-	-	0	-	6	-	-	-	5
R19017-18	U4-3-0	Dacite	51	7	-	8	1	-	-	20	-	10	-	-	-	3
R19017-18	U4-4-1	Gabbro-Basalt	10	7	-	15	20	20	-	26	-	-	-	-	-	2
R18844-18	2T	Tonolite	20	10	-	20	5	-	-	37	1	-	-	-	-	7
R18844-18	U4-2-0	Dacite	30	20	-	1	5	-	-	27	15	-	-	-	-	2
R18843-18	U4-2-0	Dacite	19	20	-	15	5	-	-	38	-	-	-	-	-	3

4.3.3 Assignment of thin section results to borehole units

The rock characteristic chart enabled us to determine information about the texture and observable minerals of rock in each lithological unit of the boreholes. By using this chart, the visual minerals of each units of boreholes could be identified. Thin section study could not be applied for each meter of borehole because the boreholes are very long, the cost is high, and the analysis is time consuming. Thus, we developed a methodology to assign the observable minerals from the rock characteristic chart to the results of the thin section study as illustrated in Figure 4.5. The assignment was accurate because the minerals, color, unit number, rock type, texture, schistosity degree, and roughness of the rock were also considered to match the sections. If both results were similar, the determined minerals from the thin section were assigned to the entire relevant lithological unit. If not, we tried the next thin section. The mineralogy of all lithological units of the boreholes in Table 4.1 was determined through this method.

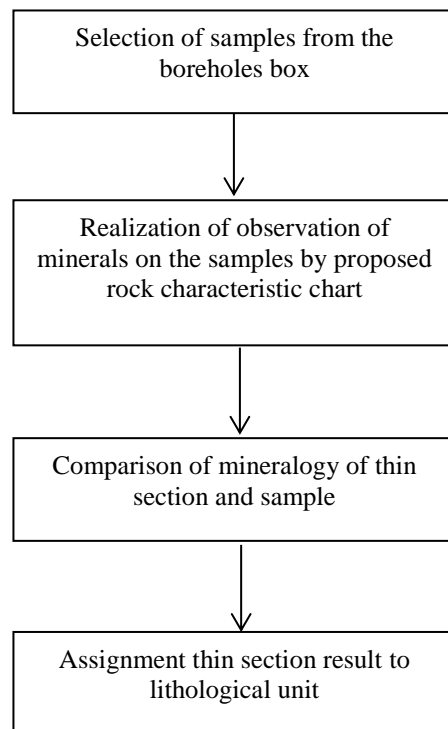


Figure 4. 5. Assignment of thin section results to each intact rock sample

4.3.4 Point load test (PLT)

The benefit of PLT is that it provides much of the same information at a lower cost than UCS. PLT is an interesting alternative to UCS because it can provide similar data at a lower cost. This test was standardized by the Franklin in 1985. In this study, axial and diametrical PLTs were carried out. Uncorrected point load strength index can be calculated using PLT, which must be corrected to the standard equivalent diameter of 50 mm (I_{s50}). I_{s50} was determined by the following equation (Eq.4.1) where P is load (in MN) and D_e^2 is the equivalent core diameter (in mm).

$$I_{s50} = \frac{P}{D_e^2} \quad \text{Eq. 4 1}$$

In this study, axial and diametrical PLTs were carried out for each meter of the mentioned boreholes in Table 4.1. A total of 1380 PLTs were done, and corresponding PLIs were calculated by Eq.4.1. The mineralogy of rock (lithological units) was determined by PLT. We were able to determine the effect of rock mineralogy on PLI by having this large database of the PLI and mineralogy of each lithological unit.

4.3.5 Determination of the effect of minerals on PLT by multivariable statistical analysis

It was identified in the literature review that there had been no quantitative assessment of the mineral composition's effect on rock strength. In line with the objective of this article, the effect of rock mineralogy on the axial and diametrical point load compressive strengths of rock (PLI) was evaluated using multivariable statistical analysis. The term “multivariate statistics” includes all statistics where more than two variables are analyzed simultaneously. Multivariable statistical analysis was used because the effect of minerals on the PLI of rock is multidimensional and related to more than one mineral.

PCA and PCR were selected for multivariable statistical analysis. PCA was used to extract the most relevant minerals among several minerals in the database, and PCR was used to determine the effect of rock mineralogy on axial and diametrical PLIs. These statistical methods (Figure 4.6) are explained in the following sections.

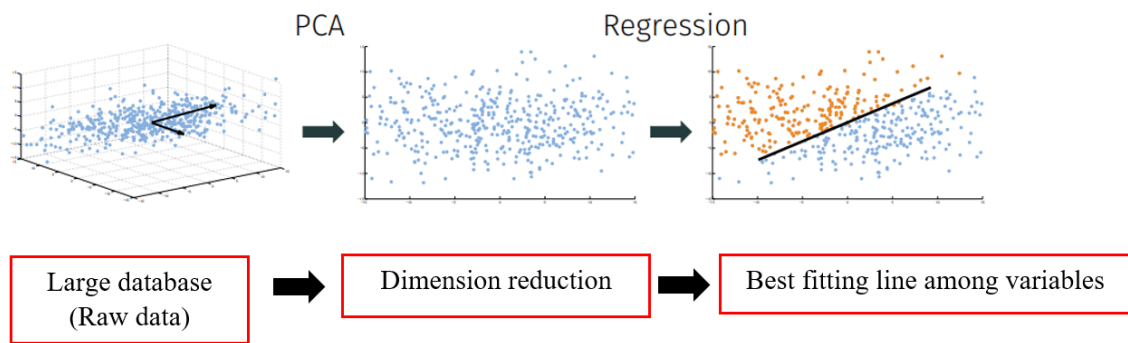


Figure 4. 6. Simple schematic of the applied multivariable statistical method

4.3.5.1 Step 1: Evaluation of most significant independent variable (minerals) through the database by PCA

There is an increasing tendency in many disciplines to use large datasets. It is crucial that such datasets be reduced in a way that can be analyzed, such that most of the information can still be interpreted. The PCA is among the oldest and most widely used of the statistical techniques developed for this purpose. With PCA, dominant patterns in a data matrix are identified through a complement of score and loading plots. In other words, PCA is a statistical technique that uses a single set of variables to determine which variables are correlated among themselves (Tabachnick and Fidell, 1996). Factors or components are often used to describe the underlying correlations between variables (Liang *et al.* 2011, Morissette *et al.* 2014).

In this study, PCA was used to explore the pattern among variables to identify important variables (minerals) to make subsequent data reduction possible. The database was classified into two main groups: felsic and mafic rocks. Then, the effect of minerals on these two groups was evaluated by PCR.

4.3.5.2 Step 2: Evaluation of the effect of mineral composition of rock on the point load compressive strength of rock by PCR

PCR is a method that combines linear regression and PCA to determine the quantitative relationship between variables. An independent variable with a high correlation degree can be aggregated into a principal component with the PCA. The PCA converts correlated variables into an uncorrelated set of principal components because principal components are independent. The "best" regression equation is achieved by estimating standard errors as high as possible using uncorrelated principal

components. Finally, a general linear regression equation was generated from the "best" equation. According to the study of Liu X *et al.* (2003), the steps of PCR are as follows:

1. Run stepwise regression with all independent variables X including a dependent variable Y to find p independent variables with statistical significance ($P < 0.05$) and check whether the p independent variables have multicollinearity or not.

2. Transform correlated variables into uncorrelated principal components by using p independent variables and calculate the information quantities of each set of principal components

3. Calculate the standardized dependent variable, the p standardized independent variables, and the p principal components according to Eqs. (4.2) to (4.4) to prepare p standardized PCR equations.

$$Y' = \frac{(Y - \bar{Y})}{S_Y} / S_Y, \quad \text{Eq. 4 2}$$

$$X'_i = \frac{(X_i - \bar{X}_i)}{S_{X_i}} / S_{X_i} \quad (i = 1, \dots, p), \quad \text{Eq. 4 3}$$

$$C_i = C_{i1}X'_1 + C_{i2}X'_2 + \dots + C_{ip}X'_p \quad (i = 1, \dots, p), \quad \text{Eq. 4 4}$$

Where Y' stands for the standardized dependent variable, Y is the dependent variable, S_Y is the standard deviation of the dependent variable, \bar{Y} is the mean of the dependent variable, X'_i is the i th standardized independent variable, X_i is the i th independent variable, \bar{X}_i is the mean of the i th independent variable, S_{X_i} is the standard deviation of the i th independent variable, C_i is the i th principal component, and a_{ij} is the coefficient of the principal component matrix (the matrix consists of C_i and X'_i).

4. Begin with the first principal component to build the standardized PCR equation, then include each principle component one by one to get m standardized PCR equations as represents in Eq.(4.5). Verify that all the principal components are independent of one another, then, by comparing the adjusted R^2 and standard error of estimate of each standardized PCR equation, select the "best" standardized PCR equation in Eq (4.5).

$$\hat{Y}'_j = \sum B'_i C_i \quad (j = 1, \dots, m \leq p; \quad i = 1, \dots, K \leq p) \quad \text{Eq. 4 5}$$

Where \hat{Y}'_j is the estimate of the j th standardized PCR equation and B'_i is the i th standardized partial regression coefficient of the standardized PCR equation.

5. Utilize Eq. (4.6) to the “best” standardized PCR equation to yield the standardized linear regression equation after sorting it out as shown in Eq. (4.6):

$$\hat{Y}' = \sum b'_i X'_i \quad (i = 1, \dots, K \leq p) \quad \text{Eq. 4 6}$$

Where \hat{Y}' is the estimate of the standardized linear regression equation and b'_i is the i th standardized partial regression coefficient of the standardized linear regression equation.

6. The coefficients and constants for partial regression are given in Eqs. (4.7) and (4.8):

$$b_i = b'_i \left(\frac{L_{yy}}{L_{x_i x_i}} \right)^{\frac{1}{2}} \quad (i = 1, \dots, K \leq p) \quad \text{Eq. 4 7}$$

$$b_0 = \bar{Y} - \sum b_i \bar{X}_i \quad (i = 1, \dots, K \leq p) \quad \text{Eq. 4 8}$$

7. Finally, convert the standardized linear regression equation to the general linear regression equation as shown in Eq. (4.9). According to this equation, PCR provides the best line fitting among the extracted components.

$$\hat{Y} = b_0 + \sum b_i X_i \quad (i = 1, \dots, K \leq p) \quad \text{Eq. 4 9}$$

Where b_i is the i th partial regression coefficient of the general linear regression equation, L_y is the sum of the squares of dependent variable Y , L_{x_i} is the sum of squares of the i th independent variable X_i , and b_0 is the constant of the general linear regression equation.

In this study, PCR was carried out for mafic and felsic rocks separately to evaluate the effect of mineral composition on the PLI of rock.

4.4 Data preparation

The collected data from geotechnical logging are explained and the PLT results are presented in this section.

4.4.1 Point load compressive strength of rock

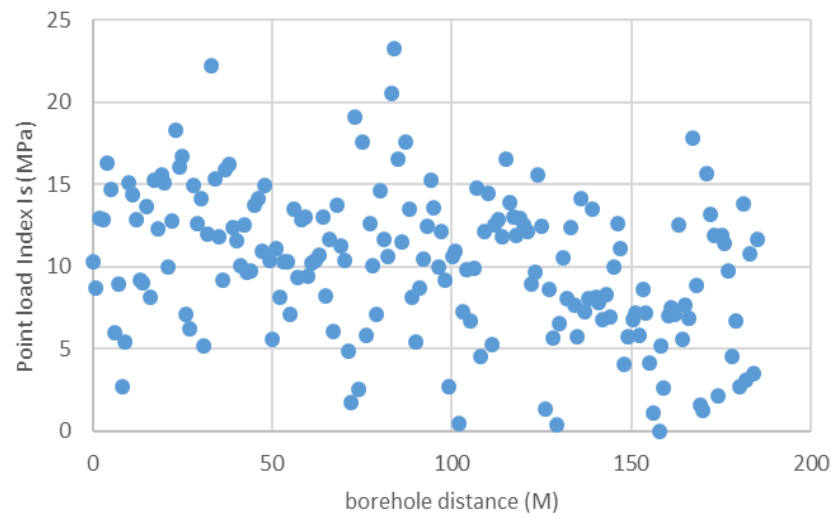
Point load compressive strength was selected as the indicator of rock strength. Axial and diametrical PLTs were applied for each meter of the boreholes. Table 4.3 presents the number of tests for each unit of borehole, and Figure 4.7 shows the values of the PLI along the boreholes. For the metamorphic rock specimens from the lithological units of the boreholes, the foliation orientation was evaluate based on the between the foliation plane and the axe of the rock core. Foliation angle was around 75° – 90° . In this study, the number of PLT depends on the length of the lithological unit where axial and diametrical PLTs were carried out in each meter. A total of 1380 PLTs were done. Figure 4.7 represents the distribution of the axial and diametrical PLIs of the selected metamorphic rock specimens. The average axial PLI is greater than the diametrical PLI because of the direction of load in the sample. The load was applied parallel to the rock core axis in the axial PLT; and applied perpendicular to the core axis, i.e. sub-parallel to the schistosity of the sample, in the diametrical PLT. The diameter of samples was 47mm.

Table 4. 3. Number of PLT in each unit of boreholes

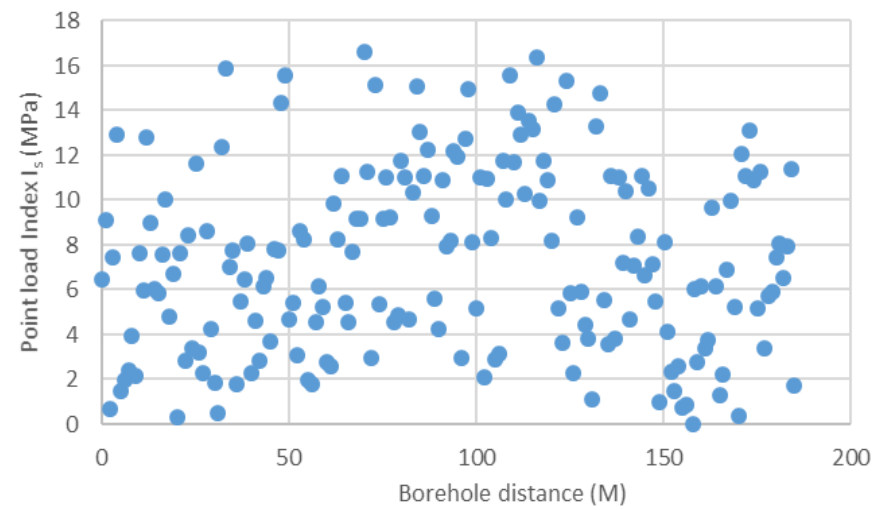
Borehole details		Number of PLT		
Borehole number	Unit	Axial	Diametrical	Total
	U3-3-0	2	2	
	U4-2-0	22	22	
	U4-3-0	21	21	
	U4-4-0	86	86	
R19016-18	U4-4-1	15	15	550
	U5-1-2	63	63	
	U5-1-3	28	28	
	U5-1-4	2	2	
	U5-2-1	6	6	
	U5-4-0	30	30	
	U4-2-0	20	20	
	U4-3-0	14	14	

	U4-4-0	90	90	
R19018-18	U4-4-1	5	5	360
	U5-1-2	16	16	
	U5-1-3	4	4	
	U5-1-4	5	5	
	U5-4-0	26	26	
	U3-3-0	62	62	
	U4-2-0	8	8	
	U4-3-0	1	14	296
R19239-19	U4-4-0	61	61	
	U4-4-1	10	10	
	2T	6	6	
	U2-0-0	23	23	
	U3-3-0	23	23	
R19200	U3-3-1	29	29	174
	U4-2-0	12	12	

Axial point load index - R19016-18



Diametrical point load index R19016-18



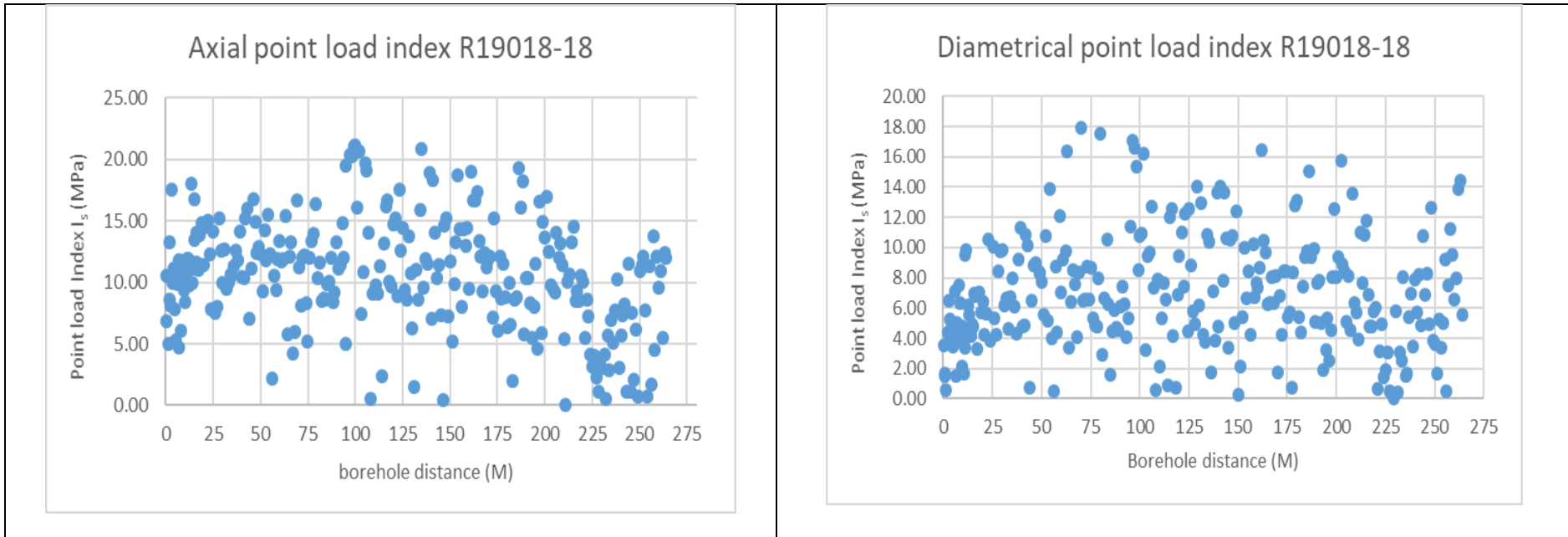


Figure 4. 7. Distribution of axial and diametrical point load indexes

4.4.2 Prerequisite to multivariable statistical analysis

The most important minerals within the database were identified to assess the minerals that affect PLI. PCA was the first technique used in multivariable statistical analysis. PCA and PCR were applied separately for the two groups of rock, felsic and mafic rocks. The statistical analyses were conducted in the SPSS software (Liu X *et al.* 2003).

PCA can only be performed once all assumptions and prerequisites have been met via a series of checks and diagnostics. It is also important to follow this step to ensure precision of the results and apply the method in the most appropriate way.

4.4.2.1 Linearity testing

The assumption that two variables are linearly related is called linearity (Tabachnick and Fidell 1996), because PCA relies on Pearson correlation coefficients and it does not take into account non-linear relationships. Due to the exploratory nature of the study, we only examined the scatter plot to assess linearity between pairs of continuous variables. An oval-shaped scatter plot results when both variables are linearly related. A non-linear relationship between two variables results in a curved scatter plot. The scatter plots of two random minerals (chlorite and white mica) are presented in Figure 4.8 as an example. Many charts display a scatter pattern with no clear correlation. This result indicated that the correlations among variables in this dataset are weak and no scatter plot presents a visible curvature. Therefore, the linearity assumption among continuous variables is adequate for this study. All the mineral graphs in this study were plotted against each other. Garnet showed a constant value against all minerals. Therefore, this mineral was removed from the subsequent study.

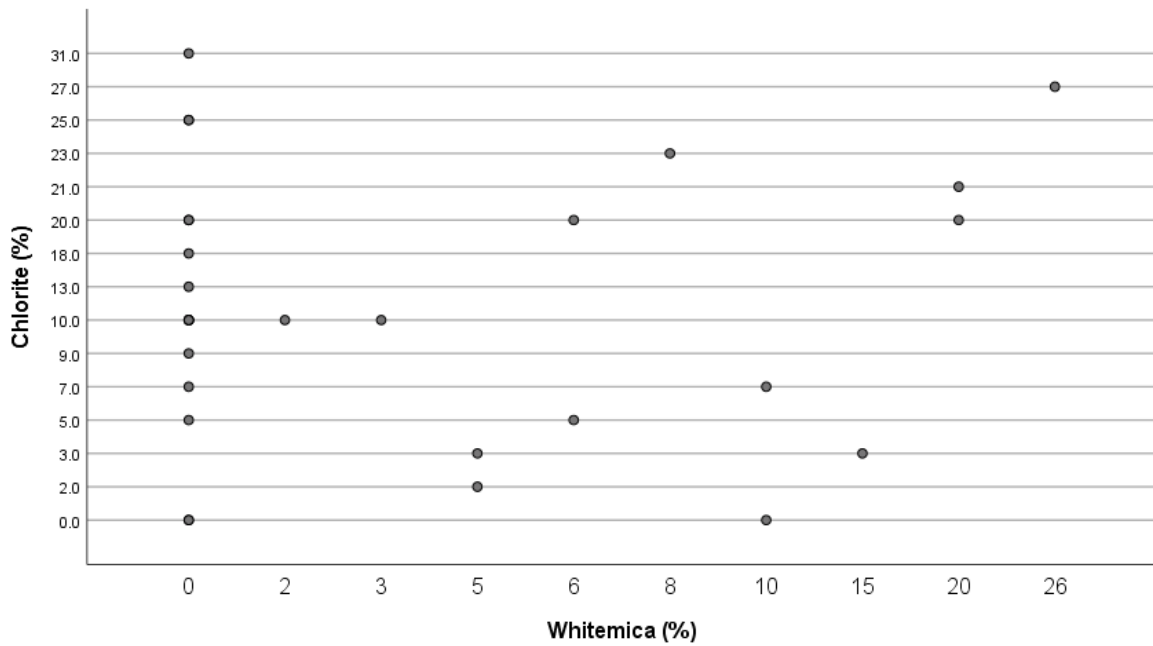


Figure 4. 8. Scatter plot matrix of chlorite – white mica for linearity testing

4.4.2.2 Multicollinearity verification

If the variables in a dataset are highly correlated, then it is referred to as multicollinearity, which is a problem in a correlation matrix. Variables with multicollinearity are highly correlated ($R^2 > 0.9$). Extreme multicollinearity introduces bias into the analysis results and dictate the real result (Tabachnick and Fidell 1996). A further investigation of the variance of inflection factor (VIF) for each variable may confirm the existence of multicollinearity. VIF is what extends a particular variation to contribute to multicollinearity. A VIF below 4.4 indicates no multicollinearity among factors, whereas a VIF between 3 and 10 indicates high correlation that may be problematic. A VIF above 10 implies that the regression coefficients are poorly estimated because of multicollinearity. The VIF value for each independent variable was calculated through Eq. (4.10):

$$VIF = \frac{1}{1-R_i^2} \quad \text{Eq. 4 10}$$

Figure 4.9 shows that the VIF values of all the variables are less than 4, which indicates that multicollinearity does not exist. Therefore, multicollinearity does not pose any problem in this study

<table border="1"> <thead> <tr> <th>Constant</th> <th>VIF</th> </tr> </thead> <tbody> <tr><td>Chlorite</td><td>1.199</td></tr> <tr><td>Carbonate</td><td>1.293</td></tr> <tr><td>Sericite</td><td>2.268</td></tr> <tr><td>Epidote</td><td>1.294</td></tr> <tr><td>Amphibole</td><td>1.817</td></tr> <tr><td>Feldspar</td><td>1.589</td></tr> <tr><td>Plagioglase</td><td>1.308</td></tr> <tr><td>Biotite</td><td>1.614</td></tr> <tr><td>White mica</td><td>1.277</td></tr> </tbody> </table>	Constant	VIF	Chlorite	1.199	Carbonate	1.293	Sericite	2.268	Epidote	1.294	Amphibole	1.817	Feldspar	1.589	Plagioglase	1.308	Biotite	1.614	White mica	1.277	<table border="1"> <thead> <tr> <th>Constant</th> <th>VIF</th> </tr> </thead> <tbody> <tr><td>Quartz</td><td>3.059</td></tr> <tr><td>Carbonate</td><td>1.319</td></tr> <tr><td>Sericite</td><td>3.204</td></tr> <tr><td>Epidote</td><td>1.373</td></tr> <tr><td>Amphibole</td><td>2.289</td></tr> <tr><td>Feldspar</td><td>3.659</td></tr> <tr><td>Plagioglase</td><td>1.3</td></tr> <tr><td>Biotite</td><td>1.536</td></tr> <tr><td>White mica</td><td>1.291</td></tr> </tbody> </table>	Constant	VIF	Quartz	3.059	Carbonate	1.319	Sericite	3.204	Epidote	1.373	Amphibole	2.289	Feldspar	3.659	Plagioglase	1.3	Biotite	1.536	White mica	1.291	<table border="1"> <thead> <tr> <th>Constant</th> <th>VIF</th> </tr> </thead> <tbody> <tr><td>Quartz</td><td>3.996</td></tr> <tr><td>Chlorite</td><td>1.598</td></tr> <tr><td>Sericite</td><td>2.85</td></tr> <tr><td>Epidote</td><td>1.357</td></tr> <tr><td>Amphibole</td><td>2.132</td></tr> <tr><td>Feldspar</td><td>3.646</td></tr> <tr><td>Plagioglase</td><td>1.361</td></tr> <tr><td>Biotite</td><td>1.622</td></tr> <tr><td>White mica</td><td>1.275</td></tr> </tbody> </table>	Constant	VIF	Quartz	3.996	Chlorite	1.598	Sericite	2.85	Epidote	1.357	Amphibole	2.132	Feldspar	3.646	Plagioglase	1.361	Biotite	1.622	White mica	1.275	<table border="1"> <thead> <tr> <th>Constant</th> <th>VIF</th> </tr> </thead> <tbody> <tr><td>Quartz</td><td>1.496</td></tr> <tr><td>Chlorite</td><td>1.01</td></tr> <tr><td>Sericite</td><td>1.208</td></tr> <tr><td>Epidote</td><td>1.523</td></tr> <tr><td>Amphibole</td><td>2.325</td></tr> <tr><td>Feldspar</td><td>3.587</td></tr> <tr><td>Carbonate</td><td>2.411</td></tr> <tr><td>Biotite</td><td>1.251</td></tr> <tr><td>White mica</td><td>1.501</td></tr> </tbody> </table>	Constant	VIF	Quartz	1.496	Chlorite	1.01	Sericite	1.208	Epidote	1.523	Amphibole	2.325	Feldspar	3.587	Carbonate	2.411	Biotite	1.251	White mica	1.501
Constant	VIF																																																																																		
Chlorite	1.199																																																																																		
Carbonate	1.293																																																																																		
Sericite	2.268																																																																																		
Epidote	1.294																																																																																		
Amphibole	1.817																																																																																		
Feldspar	1.589																																																																																		
Plagioglase	1.308																																																																																		
Biotite	1.614																																																																																		
White mica	1.277																																																																																		
Constant	VIF																																																																																		
Quartz	3.059																																																																																		
Carbonate	1.319																																																																																		
Sericite	3.204																																																																																		
Epidote	1.373																																																																																		
Amphibole	2.289																																																																																		
Feldspar	3.659																																																																																		
Plagioglase	1.3																																																																																		
Biotite	1.536																																																																																		
White mica	1.291																																																																																		
Constant	VIF																																																																																		
Quartz	3.996																																																																																		
Chlorite	1.598																																																																																		
Sericite	2.85																																																																																		
Epidote	1.357																																																																																		
Amphibole	2.132																																																																																		
Feldspar	3.646																																																																																		
Plagioglase	1.361																																																																																		
Biotite	1.622																																																																																		
White mica	1.275																																																																																		
Constant	VIF																																																																																		
Quartz	1.496																																																																																		
Chlorite	1.01																																																																																		
Sericite	1.208																																																																																		
Epidote	1.523																																																																																		
Amphibole	2.325																																																																																		
Feldspar	3.587																																																																																		
Carbonate	2.411																																																																																		
Biotite	1.251																																																																																		
White mica	1.501																																																																																		
(a) Variance of inflection factor (Dependent variable is quartz)	(b) Variance of inflection factor (Dependent variable is chlorite)	(c) Variance of inflection factor (Dependent variable is carbonate)	(d) Variance of inflection factor (Dependent variable is plagioclase)																																																																																
<table border="1"> <thead> <tr> <th>Constant</th> <th>VIF</th> </tr> </thead> <tbody> <tr><td>Quartz</td><td>2.927</td></tr> <tr><td>Chlorite</td><td>1.621</td></tr> <tr><td>Carbonate</td><td>1.19</td></tr> <tr><td>Epidote</td><td>1.366</td></tr> <tr><td>Amphibole</td><td>1.37</td></tr> <tr><td>Feldspar</td><td>2.289</td></tr> <tr><td>Plagioglase</td><td>1.378</td></tr> <tr><td>Biotite</td><td>1.365</td></tr> <tr><td>White mica</td><td>1.27</td></tr> </tbody> </table>	Constant	VIF	Quartz	2.927	Chlorite	1.621	Carbonate	1.19	Epidote	1.366	Amphibole	1.37	Feldspar	2.289	Plagioglase	1.378	Biotite	1.365	White mica	1.27	<table border="1"> <thead> <tr> <th>Constant</th> <th>VIF</th> </tr> </thead> <tbody> <tr><td>Quartz</td><td>3.902</td></tr> <tr><td>Chlorite</td><td>1.624</td></tr> <tr><td>Carbonate</td><td>1.325</td></tr> <tr><td>Sericite</td><td>3.194</td></tr> <tr><td>Amphibole</td><td>2.295</td></tr> <tr><td>Feldspar</td><td>3.748</td></tr> <tr><td>Plagioglase</td><td>1.249</td></tr> <tr><td>Biotite</td><td>1.603</td></tr> <tr><td>White mica</td><td>1.291</td></tr> </tbody> </table>	Constant	VIF	Quartz	3.902	Chlorite	1.624	Carbonate	1.325	Sericite	3.194	Amphibole	2.295	Feldspar	3.748	Plagioglase	1.249	Biotite	1.603	White mica	1.291	<table border="1"> <thead> <tr> <th>Constant</th> <th>VIF</th> </tr> </thead> <tbody> <tr><td>Quartz</td><td>3.344</td></tr> <tr><td>Chlorite</td><td>1.652</td></tr> <tr><td>Carbonate</td><td>1.27</td></tr> <tr><td>Sericite</td><td>1.955</td></tr> <tr><td>Epidote</td><td>1.401</td></tr> <tr><td>Feldspar</td><td>2.749</td></tr> <tr><td>Plagioglase</td><td>1.288</td></tr> <tr><td>Biotite</td><td>1.579</td></tr> <tr><td>White mica</td><td>1.273</td></tr> </tbody> </table>	Constant	VIF	Quartz	3.344	Chlorite	1.652	Carbonate	1.27	Sericite	1.955	Epidote	1.401	Feldspar	2.749	Plagioglase	1.288	Biotite	1.579	White mica	1.273	<table border="1"> <thead> <tr> <th>Constant</th> <th>VIF</th> </tr> </thead> <tbody> <tr><td>Quartz</td><td>1.575</td></tr> <tr><td>Chlorite</td><td>1.408</td></tr> <tr><td>Carbonate</td><td>1.159</td></tr> <tr><td>Sericite</td><td>1.776</td></tr> <tr><td>Epidote</td><td>1.174</td></tr> <tr><td>Amphibole</td><td>1.252</td></tr> <tr><td>Plagioglase</td><td>1.384</td></tr> <tr><td>Biotite</td><td>1.622</td></tr> <tr><td>White mica</td><td>1.263</td></tr> </tbody> </table>	Constant	VIF	Quartz	1.575	Chlorite	1.408	Carbonate	1.159	Sericite	1.776	Epidote	1.174	Amphibole	1.252	Plagioglase	1.384	Biotite	1.622	White mica	1.263
Constant	VIF																																																																																		
Quartz	2.927																																																																																		
Chlorite	1.621																																																																																		
Carbonate	1.19																																																																																		
Epidote	1.366																																																																																		
Amphibole	1.37																																																																																		
Feldspar	2.289																																																																																		
Plagioglase	1.378																																																																																		
Biotite	1.365																																																																																		
White mica	1.27																																																																																		
Constant	VIF																																																																																		
Quartz	3.902																																																																																		
Chlorite	1.624																																																																																		
Carbonate	1.325																																																																																		
Sericite	3.194																																																																																		
Amphibole	2.295																																																																																		
Feldspar	3.748																																																																																		
Plagioglase	1.249																																																																																		
Biotite	1.603																																																																																		
White mica	1.291																																																																																		
Constant	VIF																																																																																		
Quartz	3.344																																																																																		
Chlorite	1.652																																																																																		
Carbonate	1.27																																																																																		
Sericite	1.955																																																																																		
Epidote	1.401																																																																																		
Feldspar	2.749																																																																																		
Plagioglase	1.288																																																																																		
Biotite	1.579																																																																																		
White mica	1.273																																																																																		
Constant	VIF																																																																																		
Quartz	1.575																																																																																		
Chlorite	1.408																																																																																		
Carbonate	1.159																																																																																		
Sericite	1.776																																																																																		
Epidote	1.174																																																																																		
Amphibole	1.252																																																																																		
Plagioglase	1.384																																																																																		
Biotite	1.622																																																																																		
White mica	1.263																																																																																		
(e) Variance of inflection factor (Dependent variable is sericite)	(f) Variance of inflection factor (Dependent variable is epidote)	(g) Variance of inflection factor (Dependent variable is amphibole)	(h) Variance of inflection factor (Dependent variable is feldspar)																																																																																
<table border="1"> <thead> <tr> <th>Constant</th> <th>VIF</th> </tr> </thead> <tbody> <tr><td>Quartz</td><td>4.202</td></tr> <tr><td>Chlorite</td><td>1.568</td></tr> <tr><td>Carbonate</td><td>1.367</td></tr> <tr><td>Sericite</td><td>2.755</td></tr> <tr><td>Epidote</td><td>1.383</td></tr> <tr><td>Amphibole</td><td>2.234</td></tr> <tr><td>Plagioglase</td><td>1.377</td></tr> <tr><td>Feldspar</td><td>4.131</td></tr> <tr><td>White mica</td><td>1.294</td></tr> </tbody> </table>	Constant	VIF	Quartz	4.202	Chlorite	1.568	Carbonate	1.367	Sericite	2.755	Epidote	1.383	Amphibole	2.234	Plagioglase	1.377	Feldspar	4.131	White mica	1.294	<table border="1"> <thead> <tr> <th>Constant</th> <th>VIF</th> </tr> </thead> <tbody> <tr><td>Quartz</td><td>4.162</td></tr> <tr><td>Chlorite</td><td>1.649</td></tr> <tr><td>Carbonate</td><td>1.344</td></tr> <tr><td>Sericite</td><td>3.207</td></tr> <tr><td>Epidote</td><td>1.394</td></tr> <tr><td>Amphibole</td><td>2.253</td></tr> <tr><td>Plagioglase</td><td>1.362</td></tr> <tr><td>Feldspar</td><td>4.09</td></tr> <tr><td>Biotite</td><td>1.62</td></tr> </tbody> </table>	Constant	VIF	Quartz	4.162	Chlorite	1.649	Carbonate	1.344	Sericite	3.207	Epidote	1.394	Amphibole	2.253	Plagioglase	1.362	Feldspar	4.09	Biotite	1.62																																										
Constant	VIF																																																																																		
Quartz	4.202																																																																																		
Chlorite	1.568																																																																																		
Carbonate	1.367																																																																																		
Sericite	2.755																																																																																		
Epidote	1.383																																																																																		
Amphibole	2.234																																																																																		
Plagioglase	1.377																																																																																		
Feldspar	4.131																																																																																		
White mica	1.294																																																																																		
Constant	VIF																																																																																		
Quartz	4.162																																																																																		
Chlorite	1.649																																																																																		
Carbonate	1.344																																																																																		
Sericite	3.207																																																																																		
Epidote	1.394																																																																																		
Amphibole	2.253																																																																																		
Plagioglase	1.362																																																																																		
Feldspar	4.09																																																																																		
Biotite	1.62																																																																																		
(i) Variance of inflection factor (Dependent variable is biotite)	(g) Variance of inflection factor (Dependent variable is white mica)																																																																																		

Figure 4. 9 Variance of inflection factor of all variables prior to PCA

4.5 Results and discussion

4.5.1 Determination of the most important variables

The PCA was run to explore the pattern among variables and to identify and distinguish “noise” variables for subsequent data reduction. Thus, the most important minerals are extracted after PCA. PCA was run first without Varimax rotation technique after data preparation. Extra variables were removed from the initial database in the first run. Varimax rotation was used in the second run to obtain the maximum loading factor of the important extracted variables. Thus, ten variables (minerals), namely, quartz, chlorite, carbonate, plagioclase, sericite, feldspar, epidote, white mica, amphibole, and biotite, were used in the first run without Varimax rotation technique. These variables were obtained from the assignment of the thin section results to the proposed rock characteristic chart. The extracted components and their associated eigenvalues and variance are shown in Tables 4.4 - 4.5 for felsic and mafic rocks respectively. The eigenvalue for a component indicates the variance of data along the new feature axes. For interpretation, factors with eigenvalues greater than 1 must be retained according to the Latent Roots Criterion (or Eigenvalue Criterion) (Meyers *et al.*, 2006). Using this criterion, four components were chosen for interpretation. The 67% of the variance in the dataset is explained by the four factors, which is considered acceptable based on a recommended range of 50% to 75% (Tabachnick and Fidell 1996). It can be interpreted that the total variance represents all variation introduced by all variables and variance indicates how much variation is “captured” by the extracted correlations among variables.

Table 4. 4 Eigenvalue and total variance of extracted components for felsic rocks

Component	Initial eigenvalues			Extraction sums of squared loadings		
	Total	% of variance	Cumulative %	Total	% of variance	Cumulative %
1	2.095	29.947	20.947	2.095	20.947	20.947
2	1.822	18.215	39.162	1.822	18.215	39.162
3	1.634	16.341	55.503	1.634	16.341	55.503
4	1.244	12.436	67.943	1.244	12.439	67.943
5	0.961	9.611	77.553			
6	0.737	7.367	84.921			
7	0.648	6.479	91.400			
8	.473	4.731	96.131			
9	0.302	3.024	99.155			
10	0.084	0.845	100			

Table 4. 5 Eigenvalue and total variance of extracted components for mafic rocks

Component	Initial eigenvalues			Extraction sums of squared loadings		
	Total	% of variance	Cumulative %	Total	% of variance	Cumulative %
1	2.105	21.048	21.048	2.105	21.048	21.048
2	1.815	18.146	39.194	1.815	18.146	39.194
3	1.622	16.215	55.409	1.622	16.215	55.409
4	1.250	12.504	67.914	1.250	12.504	67.914
5	0.955	9.550	77.464			
6	0.736	7.358	84.822			
7	0.655	6.550	91.372			
8	0.474	4.744	96.116			
9	0.296	2.957	99.073			
10	0.093	0.927	100			

Tables 4.6-4.7 present the factor loading matrix without rotation technique for felsic and mafic rocks, respectively. In PCA, factor loadings, also known as component loadings, indicate the correlation between variables (rows) and factors (columns). In this study, factor loading was interpreted to extract the important minerals in our database. A minimum loading number cut-off of 0.32 was considered, following Liu X *et al.* (2003) for the interpretation and extraction of the important minerals.

Table 4. 6 Factor loading number for felsic rocks

	Components			
	1	2	3	4
Quartz	0.917	0.085	-0.250	-0.069
Chlorite	-0.284	-0.181	0.276	-0.039
Carbonate	0.292	0.278	0.127	-0.314
Sericite	-0.427	0.133	-0.193	1.38
Epidote	0.414	0.018	0.289	-0.197
Amphibole	0.002	0.759	0.288	0.299
Feldspar	-0.249	0.726	0.008	-0.045
Plagioclase	0.082	0.132	0.14	0.195
Biotite	0.147	-0.074	0.122	-0.144
White mica	-0.141	-0.165	-0.642	0.221

In felsic rocks (Table 4.6), principal component 1 is positively correlated with quartz and epidote and negatively correlated with sericite. This positive loading number for quartz and epidote confirms the statistical similarities between them. The negative weak correlation of sericite with component 1 suggests its inverse relationship with the other extracted variables. Principal component 2 is well represented by amphibole and feldspar. The positive loading number for amphibole and feldspar confirms that these minerals play an important role in our statistical analysis. Principal component 3 is well represented by white mica. Principal component 4 has weak correlation with all variables, and its eigenvalue is more than the mentioned criterion. Thus, this component could not capture the effect of the variables. The main use of PCA is to decrease the number of variables. The results show that some variables could be considered outlier

variables. First, garnet mineral was removed because it had a constant value in the scatter plot. Then, if the minimum cut-off is 0.32, principal component 1 suggests that quartz, epidote, and sericite are statistically closely correlated and can be used to represent their effect on the PLI of rock. Amphibole, feldspar were extracted from principal component 2 because these three variables are statistically similar. Finally, white mica was determined from principal component 3. In summary, quartz, epidote, sericite, amphibole, feldspar and white mica were selected as the important variables for felsic rock, and the rest of the variables were removed from the next step of the study. These extracted minerals were considered the most important minerals in the second run of PCA with Varimax rotation.

In mafic rocks (Table 4.7), principal component 1 is positively correlated with quartz, feldspar, and epidote and negatively correlated with chlorite and white mica. Principal component 2 is well represented by amphibole, feldspar, and quartz. Principal component 3 is well represented by epidote and amphibole, and principal component 4 has weak correlation with all variables. The extracted variables are the same as those in felsic rocks but chlorite was selected instead of sericite. Therefore, quartz, epidote, chlorite, amphibole, feldspar and white mica were selected as the important variables for mafic rocks, and the rest of the variables were removed from future steps of the study. The important minerals were used in the second run of PCA with Varimax rotation to obtain the proper factor loading index for mafic rock.

Table 4. 7 Factor loading number for mafic rocks

	Components			
	1	2	3	4
Quartz	0.814	0.417	-0.042	-0.158
Chlorite	-0.532	-0.395	0.150	-0.056
Carbonate	-0.222	0.210	0.123	-0.290
Sericite	-0.222	0.210	0.123	-0.290
Epidote	0.515	-0.184	0.565	-0.070
Amphibole	0.220	0.797	0.505	0.249
Feldspar	0.412	0.674	0.168	0.012
Plagioclase	0.154	0.213	0.11	0.24
Biotite	0.197	-0.218	-0.199	-0.089
White mica	-0.365	-0.198	-0.642	-0.150

PCA was rerun using Varimax rotation after removing the outlier variables to obtain the proper component loading factor for PCR. The Varimax Rotation was chosen because it maximizes the sum of the variance of the squared loadings, where loadings represent correlations between variables and factors (Duan, 2016). Subsequently, the score loading factor and weighting factors are improved as compared with those in PCA without rotation. Six variables in felsic rock, namely, quartz, epidote, sericite, amphibole, feldspar and white mica, and six variables in mafic rocks, namely, quartz, epidote, chlorite, amphibole, feldspar and white mica, were used in the second PCA with Varimax rotation (Tables 4.8-4.9).

Table 4. 8 Eigenvalue and total variance of extracted components for felsic rocks

Total Variance Explained						
Component	Initial eigenvalues			Rotation sums of squared loading		
	Total	% of variance	Cumulative %	Total	% of variance	Cumulative %
1	1.775	25.355	25.355	1.760	25.146	25.146
2	1.547	22.105	47.461	1.505	21.494	46.641
3	1.355	19.362	66.823	1.413	20.182	66.823
4	0.996	15.806	82.629			
5	0.640	9.138	91.766			
6	0.576	8.234	100			

Table 4. 9 Eigenvalue and total variance of extracted components for mafic rock.

Total Variance Explained						
Component	Initial eigenvalues			Rotation sums of squared loading		
	Total	% of variance	Cumulative %	Total	% of variance	Cumulative %
1	2.010	28.709	28.709	1.999	28.563	28.563
2	1.566	22.370	51.079	1.427	20.385	18.949
3	1.217	17.382	68.461	1.366	19.513	68.461
4	0.820	11.712	80.173			
5	0.779	11.141	89.734			
6	0.497	8.686	100			

Three factors account for 67% and 68% of the total variance in the datasets for felsic and mafic rocks, respectively (Tables 4.8-4.9). These values are acceptable according to the recommended value of between 50% and 75% (Tabachnick and Fidell, 1996). The

factor loading matrix for felsic rock with Varimax rotation (Table 4.10) indicates that principal component 1 is positively correlated with quartz, feldspar and epidote and negatively correlated with sericite. This positive loading number for quartz and epidote confirms the statistical similarities between them. Principal component 2 is well represented by amphibole, feldspar. The positive loading number for amphibole, feldspar confirms that these minerals play an important role in our statistical analysis. Principal component 3 is well represented by white mica.

Table 4. 10 Factor loading matrix with Varimax rotation for felsic rock

	Components		
	1	2	3
Quartz	0.902	-0.090	0.045
Sericite	-0.582	-0.241	0.108
Epidote	0.545	0.137	0.128
Amphibole	-0.077	0.884	0.184
Feldspar	0.597	0.406	0.215
White mica	-0.727	0.109	-0.461

The factor loading matrix for mafic rocks with Varimax rotation (Table 4.11) shows that principal component 1 is positively correlated with quartz and epidote and negatively correlated with chlorite. Principal component 2 is well represented by amphibole, feldspar. The positive loading number for amphibole, feldspar confirms that these minerals play an important role in our statistical analysis. Principal component 3 is well represented by white mica.

Table 4. 11 Factor loading matrix with Varimax rotation for mafic rock

	Components		
	1	2	3
Quartz	0.880	-0.119	0.180
Chlorite	-0.657	0.021	0.062
Epidote	0.693	-0.094	0.129
Amphibole	-0.180	0.749	0.378
Feldspar	0.314	0.501	0.221
White mica	0.188	0.031	-0.687

The most important minerals in the databases of felsic and mafic rocks and their factor loading were obtained by PCA. The extracted weighting factors were used in PCR, as discussed in the following section.

4.5.2 Determination of the effect of each mineral on point load index by PCR analysis

The effect of rock minerals on PLI was determined by PCR. PCR was used for the four factors in our database: effects of felsic rock minerals on axial and diametrical PLIs, and effects of mafic rock minerals on axial and diametrical PLIs.

The linear regression among the extracted components could be obtained through Equations (4.2)–(4.9) in Section 4.3.5.2 Linear regression could be extracted between independent and dependent variables. Based on the four PLI values (axial and diametrical PLIs for felsic and mafic rocks), four separated linear regression were extracted to find the relationship between the minerals in felsic and mafic rocks and the PLIs.

Two line fit through the extracted components of felsic rocks (Table 4.10) as determined by (Eqs. (4.11)-(4.12):

$$PLI_{AXIAL} = 0.51 (Q) - 0.32 (Ser) + 0.2 (Epi) + 0.31 (Amp) + 0.11 (Felds) - 0.22 (WM), \quad \text{Eq. 4 11}$$

$$R^2 = 0.64$$

$$PLI_{DIAMETRICAL} = 0.38 (Q) - 0.39 (Ser) + 0.17 (Epi) + 0.3 (Amp) + 0.1 (Felds) - 0.34 (WM),$$

$$\text{Eq. 4 12}$$

$$R^2 = 0.58$$

According to the axial regression line, increasing the amount of quartz could increase the PLI of felsic rocks. Amphibole has a similar relationship with PLI. However, its effects are weaker than that of quartz. In comparison, sericite and white mica have negative effect on PLI. The reason is that white mica and quartz are sheet minerals and do not have enough hardness; therefore, they could decrease the PLI. This behavior is similar for diametrical PLI. Moreover, a notable decrease in PLI associated with sericite and white mica was noted. The minerals that have a positive effect in the axial PLT represent a less positive effect in the diametrical PLI because of the effect of schistosity,

which is nearly perpendicular to the core axis. Conversely, the minerals that have a negative effect in the axial PLT represent a more negative effect in the diametrical PLT because of the effect of schistosity. The reason is that the degree of schistosity of the tested samples was between 70° and 90°. Schistosity was parallel to load direction in the diametrical PLT. Thus, increasing the degree of schistosity can negatively affect PLI. When the schistosity of rocks is close to parallel to the force load, it would be broken easier (Dinh *et al.*, 2013).

The following linear regression lines present the effect of mafic rock minerals on the axial and diametrical PLIs of mafic rocks (Eqs. (4.13)-(4.14)).

$$PLI_{AXIAL} = 0.31 (Q) - 0.42 (Chl) + 0.18 (Epi) + 0.44 (Amp) + 0.18 (Felds) - 0.21 (WM),$$

Eq. 4 13

$$R^2 = 0.67$$

$$PLI_{DIAMETRICAL} = 0.25 (Q) - 0.48 (Chl) + 0.08 (Epi) + 0.37 (Amp) + 0.09 (Felds) - 0.38 (WM),$$

Eq. 4 14

$$R^2 = 0.61$$

Quartz and amphibole have a positive effect on the PLI of mafic rocks. Chlorite has a negative effect on axial PLI. The minerals that have a positive effect on the axial test represented a less positive effect on the diametrical test. The minerals that have a negative effect on the axial test represented a more negative effect on the diametrical tests because of the effect of schistosity on diametrical PLT. Epidote and feldspar in felsic and mafic rocks have a weak positive effect on axial and diametrical PLIs. This weak value is because of the low percentage of these minerals in the rock samples. However, despite their low percentage, these minerals have a positive effect on axial and diametrical PLIs, that is, their presence in rock can improve rock strength.

A comparison of the results between felsic and mafic rocks shows that quartz has a more positive effect on felsic rocks than on mafic rocks. Amphibole presents a more positive effect on mafic rocks than on felsic rocks. Sericite and chlorite have shown the highest negative correlation with felsic and mafic rocks because these minerals reduce rock strength. Sericite and chlorite are secondary minerals and have less strength than initial minerals.

4.6 Conclusion

Rocks consist of different minerals that influence rock behavior in underground excavation. Rock strength can be increased or decreased depending on its mineralogy. In this article, a methodology was developed to determine the effects of the mineral composition of a rock on its compressive strength via PLI. More than 1300 axial and diametrical PLTs were applied to the different lithology units of Westwood mine. A petrographic study was made on the representative samples from different drill cores to determine their mineralogy. Mineralogical assemblages were attributed to a suite of over 1300 samples from predetermined lithological units. This approach enabled us to have a large database that includes the PLI and mineral of the metamorphic rock specimens. Then, two multivariable statistical analyses, namely, PCA and PCR, were applied to this dataset. PCA was used to lower the number of variables from ten to seven by identifying the most important variables in the database and to evaluate the influence of minerals on PLI.

- The results indicate that quartz, amphibole, have a positive effect (increase) on axial and diametrical PLIs, whereas sericite and chlorite have a negative effect (decrease) on PLI.
- Metamorphic minerals, such as epidote, are associated with weak positive effects on PLI. By contrast, schistosity is an important parameter that reduces rock strength as shown in the axial and diametrical PLIs.
- Based on a few thin section results and visual minerals of samples, the methodology developed in this study could assign the mineralogy of more than 1300 samples of metamorphic rocks.
- This study fills the knowledge gap by showing how different minerals or group of minerals, and the rock texture have a major influence on rock mechanics. Thus, a rock mass made of distinct lithologies with distinct compositions and geological histories cannot be considered a homogeneous rock mass.
- The composition and mineralogy of a rock mass must be considered when designing underground work in heterogeneous geological environments.
- The methodology developed in this paper could be used in the study of other rock types to more precisely determine the influence of minerals and groups of minerals on rock mechanics.

Acknowledgments

The authors would like to thank the Natural Sciences and Engineering Research Council of Canada, IAMGOLD Corporation, and Westwood mine for supporting and funding this research (Grant number: RDCPJ 520428–17).

4.7 References

- Bell, F. G. (1978), “The physical and mechanical properties of the fell sandstones, northumberland, england”, *Engineering Geology*, 12, 1-29. [https://doi.org/10.1016/0013-7952\(78\)90002-9](https://doi.org/10.1016/0013-7952(78)90002-9).
- Brattli, B. (1992), “The influence of geological factors on the mechanical properties of basic igneous rocks used as road surface aggregates”, *Engineering Geology*, 33(1), 31-44. [https://doi.org/10.1016/0013-7952\(92\)90033-U](https://doi.org/10.1016/0013-7952(92)90033-U).
- Dinh, Q., Konietzky, H. and Herbst, M. (2013), “Brazilian tensile strength tests on some anisotropic rocks”, *International journal of rock mechanics and rock sciences*, 58, 1-7. <https://doi.org/10.1016/j.ijrmms.2012.08.010>.
- Duan, W. (2016), “An assessment of the significance of factors affecting the occurrence of rockburst damage”, Master Dissertation, University of Western, Australia.
- Fahy, M. P. and Guccione, M. J. (1979), “Estimating strength of sandstone using petrographic thin-section data”, *Bulletin of the Association of Engineering Geologists*, 16(4), 467- 485. <https://doi.org/10.2113/gseegeosci.xvi.4.467>.
- Gupta, A. S. and Rao, K. S. (2000), “Weathering effects on the strength and deformational behaviour of crystalline rocks under uniaxial compression state”. *Engineering geology*, 56(3-4), 257-274. [https://doi.org/10.1016/S0013-7952\(99\)00090-3](https://doi.org/10.1016/S0013-7952(99)00090-3).
- Hugman, R. H. H., Friedman, M. (1979), “Effects of texture and composition on mechanical behavior of experimentally deformed carbonate rocks”. *AAPG Bulletin*, 63(9), 1478-1489. <https://doi.org/10.1306/2F9185C7-16CE-11D7-8645000102C1865D>.
- Franklin, J.A. (1985), “Suggested method for determining point load strength.”, *International Journal of Rock Mechanics*, 22 (2) 51 -60. [https://doi.org/10.1016/0148-9062\(85\)92327-7](https://doi.org/10.1016/0148-9062(85)92327-7).

- Karaca, Z. (2012). "Relationship between the mechanical properties and the surface roughness of marble", *International journal of materials research*, 103 (5), 633-637. <https://doi.org/10.3139/146.110728>.
- Keikha, T. and Keykha, H. A. (2013), "Correlation between mineralogical characteristics and engineering properties of granitic rocks", *EJGE*, 18, 4055-4065. [https://doi.org/10.1016/S0013-7952\(98\)00071-4](https://doi.org/10.1016/S0013-7952(98)00071-4).
- Liu, R.X. Kuang, J. Gong, Q. and Hou, X.L. (2003), "Principal component regression analysis with spss", *Computer methods and programs in biomedicine*, 71 (2), 141-147. [https://doi.org/10.1016/S0169-2607\(02\)00058-5](https://doi.org/10.1016/S0169-2607(02)00058-5).
- Liu, H. Kou, S. Lindqvist, P. A. Lindqvist, J. E. and Akesson, U. (2005). Microscope rock texture characterization and simulation of rock aggregate properties. Research Report No. 60-1362/2004; Luleå university of technology, Sweden.
- Liang, G. Hadjigeorgious, J. and Thibodeau, D. (2011), "Evaluation of performance of support system at vale's coleman and north mine", *45th US rock mechanics and geomechanics symposium, American rock mechanics association*, San Francisco, USA. June.
- Lundqvist, S. and Göransson M. (2001). "Evaluation and interpretation of microscopic parameters vs mechanical properties of precambrian rocks from the stockholm region, sweden", *Proceedings of the 8th Euroseminar Applied to Building Materials*, Athens, Greece, June.
- Merriam, R., Rieke, H. and Kim, Y. C. (1970). "Tensile strength related to mineralogy and texture of some granitic rocks". *Engineering Geology*, 4 (2), 155-160. [https://doi.org/10.1016/0013-7952\(70\)90010-4](https://doi.org/10.1016/0013-7952(70)90010-4).
- Meyers, L.S. Gamst, G. and Guarino, A.J. (2006). *Applied Multivariable Research- Design And Interoperation*, Sage publications, California, USA.
- Miskovsky, K. Duarte, M. T. Kou, S. Q. and Lindqvist, P. A. (2004). "Influence of the mineralogical composition and textural properties on the quality of coarse aggregates". *Journal of Materials Engineering and Performance*, 13 (2), 144-150. <https://doi.org/10.1361/10599490418334>.
- Morissette, P. Hadjigeorgiou, J. Thibodeau, D. (2014). "Investigating the dynamic-load demand on support systems using passive monitoring data". *International journal of*

- rock mechanics and mining sciences*, 67, 115-126.
<https://doi.org/10.1016/j.ijrmms.2014.01.012>.
- Přikryl, R. (2001). “Some microstructural aspects of strength variation in rocks”. *International Journal of Rock Mechanics and Mining Sciences*, 38 (5), 671-682.
[https://doi.org/10.1016/S1365-1609\(01\)00031-4](https://doi.org/10.1016/S1365-1609(01)00031-4).
- Shakoor, A. and Bonelli, R.E. (1991), “Relationship between petrographic characteristics, engineering index properties, and mechanical properties of selected sandstones”, *Bulletin of the Association of Engineering Geologists*, 28 (1), 55-71.
<https://doi.org/10.2113/gseegeosci.xxviii.1.55>.
- Sousa, L. M. (2013), “The influence of the characteristics of quartz and mineral deterioration on the strength of granitic dimensional stones”. *Environmental earth sciences*, 69(4), 1333-1346. <https://doi.org/10.1007/s12665-012-2036-x>.
- Tabachnick, B.G. and Fidell, L.S. (1996). *Using Multivariable Statistics*, HarperCollins college publishers, New York, USA.
- Tuğrul, A. and Zarif, I. H. (1999). “Correlation of mineralogical and textural characteristics with engineering properties of selected granitic rocks from Turkey”. *Engineering geology*, 51 (4), 303-317. [https://doi.org/10.1016/S0013-7952\(98\)00071-4](https://doi.org/10.1016/S0013-7952(98)00071-4).
- Tuğrul, A. (2004). “The effect of weathering on pore geometry and compressive strength of selected rock types from Turkey”. *Engineering geology*, 75 (3-4), 215-227.
<https://doi.org/10.1016/j.enggeo.2004.05.008>.
- Vutukuri, V.S. Lama, R.D. and Saluja, S.S. (1978). *Handbook On Mechanical Properties Of Rocks, Testing Techniques and Results*. Trans Technical Publications, Clausthal, Germany.
- Worthington, P. F. (1991). “The direction of petrophysics: a five-year perspective”. *The Log Analyst*, 32(02), 261-274.
- Yergeau, D. (2015). “Géologie du gisement synvolcanique aurifère atypique westwood, abitibi, québec”. Ph.D. Dissertation; Université du Québec, Québec, Canada.
- Yusof, N. Q. A. M. and Zabidi, H. (2016). “Correlation of mineralogical and textural characteristics with engineering properties of granitic rock from Hulu Langat, Selangor”. *Procedia Chemistry*, 19, 975-980.
<https://doi.org/10.1016/j.proche.2016.03.144>.

Zhang, L. Ding, X. and Budhu, M. (2012), “A rock expert system for the evaluation of rock properties”, *International journal of rock mechanics and mining science*, 50, 124–132. <https://doi.org/10.1016/j.ijrmms.2012.01.00>.

Chapter 5: Effects of mineral composition on geomechanical parameters of hydrothermally altered volcanic rocks ⁴

Abstract

Mechanical properties of rocks including uniaxial compressive strength, deformation modulus, and tensile strength are important parameters in the underground structure stability in geomechanics. Textural features, such as grain size, mineral composition, and structural fabrics, affect these parameters. Therefore, understanding the interactions between parameters of mineralogy and mechanical properties of rock masses is crucial. In this study, we attempt to determine the effect of mineralogy of variably metamorphosed (recrystallized) rocks on their tensile and compressive strength. Sampling was conducted at different depths at a mine site, and the geomechanical tests were carried out in the laboratory. A random sampling method, known as inverse of cumulative distribution function method (CDF^{-1}), is applied to generate sufficient values of uniaxial compressive strength (UCS) and tensile strength values for the statistical methods. Then, two multivariable statistical methods, principal component analysis and principal component regression, are used to determine the effect of several minerals on intact rock resistance. Results show that the CDF^{-1} method could be used to develop geomechanical laboratory test database when the data for analysis are insufficient. In addition, the study highlights that quartz, amphibole, feldspar, and epidote have shown a positive influence on UCS and tensile strength of felsic and mafic rocks, whereas chlorite, sericite, and white mica have shown a negative influence on both tests.

Keywords: Metamorphic rocks, Geomechanical parameters of rock, Random sampling method, Minerals, Statistical analysis.

5.1 Introduction

In recent years, the mining industry has received substantial attention given that increasing demand for natural resources, improvements in extraction methods and metal recovery processes, and increased difficulties in finding and profitably mining near-surface resources (Lippmann et al., 2011). In underground excavation, the probability of rock

⁴ Askaripour M, Saeidi A, Mercier-Langevin P, Rouleau A, International Journal of Mining Science and Technology (Submitted)

mass failure increases due to several factors, including inherent properties of rock, such as texture characteristics, and external conditions, such as magnitude of in-situ stresses, dynamic disturbance, excavation sequence, and geological structure (Meng et al., 2017). Rock texture is a very important factor in the strength parameter; as strongly influences the strength properties of intact rock. Rock texture has been defined as “*the degree of crystallinity, grain size or granularity, and the fabric or geometrical relationship between the constituents of a rock*” (Williams et al., 1982). Consequently, a deep understanding of the effect of rock texture characteristics on the mechanical rock behavior is critical. Rock behavior is described by petro-physical (unit weights and ultrasonic P-wave velocity) and mechanical properties such as unconfined compressive strength (UCS), tensile strength, Young’s modulus, and Poisson’s ratio (Tapponnier and Brace, 1976). Rock mechanical properties and composition are often used to gather crucial information to address a various problems such as rock or slope instability, failure mechanism, strength and deformation characteristic assessment, and other engineering purposes (Miskovsky, 2004). Many studies on the effect of mineralogical composition of rock strengths have been conducted in recent decades. Merriam et al. (1970) documented a correlation between the tensile strength of granitic rock and the amount of quartz. They concluded that the tensile strength is inversely proportional to the quartz content. Hugman and Friedman (1979) utilized compressive test and mineralogical characterization to analyze carbonate rocks with intermediate dolomite and micrite content (Yule marble, Solenhofen limestone, Hasmark dolomite, and Blair dolomite). The ultimate strength of rocks increases as the content of dolomite and microcrystalline carbonate increases. Mineral cleavage and microfissures in feldspar reduce compressive and tensile strength (Onodera and Asoka Kumara, 1980). Bell and Lindsay (1999) focused on how the mineral composition of sandstone samples influenced the mechanical properties of rock. The result showed that the content of clay and quartz influenced the unconfined compressive strength. When the former’s content increases, the strength decreases, and the strength increases when the quartz’s content increases. Tugrol and Zarif (1999) studied granitic rocks and discovered that one of the most significant factors in determining rock strength is mineralogical composition. In addition, the difference between quartz and feldspar content is the most essential aspect influencing the mechanical properties of the rock. Many studies have confirmed the strong link between quartz and rock compressive strength (Gunsallus and Kulhawy, 1984). However, other scientists claimed that quartz does not influence sandstone strength (Bell, 1987; Fahy 1979; Shakoor and Bonelli 1991). The mica (a phyllo- or sheet silicate) has also been reported to have conflicting

results. According to results of Åkesson *et al.*, (2003) mica does not affect fragmentation resistance directly. However, mica that forms in plane foliation leads to crack propagation. Ündül (2016) identified mineral content, groundmass content (the matrix that holds the larger crystals (phenocrysts) in igneous rocks), and porosity as the key micro textural factors affecting the uniaxial compressive strength of the rock. UCS and crack propagation are affected by opaque and altered minerals. The UCS decreases as the amount of opaque minerals increases. However, increased ground mass phenocryst content (e.g., amphibole and plagioclase) increases UCS. Quartz and feldspar have a considerable control and impact over rock strength, according to Yusof and Zabidi's results (2016). As the percentage of quartz increased, the rock strength increased. On the contrary, due to the low percentage of quartz, the UCS also had the lowest value. Feldspar had a significant role in strength reduction. However, the studies that are mentioned above, focused on one or very few rock-forming minerals and did not incorporate detailed information about the other minerals present in the rock, especially, those of metamorphic rock. Thus, having little knowledge of mineralogy causes difficulty in investigating the mechanical behavior of rocks given that the composition and texture can be relatively variable in a rock mass and even within an otherwise compositionally homogeneous rock unit. Moreover, the mechanical properties of rocks with the same mineral composition can differ due to various textural variations. Therefore, studies on the mineral composition and its texture effects on rock mechanics are crucial to improve the knowledge of rock behavior, especially in complex geological environments. However, considering high-quality core samples for laboratory tests to estimate rock strength and elastic parameters is not always possible. As a result, the probability of finding a correlation between mineralogy and mechanical properties of the rock is limited because of the insufficient evidence to obtain a reliable regression analysis between geomechanical parameters of rock and rock texture characteristics. Therefore, understanding the interaction among various parameters of rock texture, petrophysical characteristics, and mechanical properties can be beneficial for the development of various geoenvironmental facilities and research, including methods to compensate for limited datasets.

The present study aims to determine the interactive effect of mineral composition on uniaxial compressive strength (UCS) and tensile strength of variably metamorphosed, hydrothermally altered mafic (Mg and Fe-rich), and felsic (Si-rich) volcanic rocks. The samples were tested to determine uniaxial compressive and tensile strength values. Over 200 UCS tests (81 tests for felsic rock and 137 tests for mafic rock) were conducted, and 50 Brazilian tests

were also performed (28 tests for felsic rock and 24 tests for mafic rock) on samples collected at different depths and in rocks of variable metamorphic conditions, all from the Westwood mine in Canada. In the absence of sufficient core samples for the uniaxial compressive strength (UCS) and tensile strength tests, the inverse of cumulative distribution function (CDF^{-1}) was used to generate sufficient values of UCS and tensile strength based on the distribution function of both variables. Then, two multivariate statistical methods called principal component analysis (PCA) and principal component regression (PCR) were used to determine the significant minerals that are the most significantly associated with rock strength based on the UCS and tensile strength results.

5.2 Westwood Mine

The Westwood mine is situated in northwestern Québec, Canada, 40 kilometers east of Rouyn–Noranda. This area is approximately 620 km northwest of Montreal (Figure 5.1). The Westwood mine is owned and operated by IAMGOLD Corporation and started production in 2013.



Figure 5. 1 Westwood mine location (IAMGOLD Corporation)

The rocks hosting the Westwood deposit vary remarkably in composition and are complexly intercalated often at the meter-scale. The strata are nearly vertical, and the lithological contacts are parallel with a penetrative fabric (strong foliation) because of regional deformation. Numerous contact-parallel and high-angle ductile to brittle faults crosscut the units and the ore zones. All the units were affected, to some extent, by syn-volcanic ore-forming hydrothermal alteration that caused the breakdown of primary minerals, such as feldspar, into phyllosilicates,

which were later recrystallized during regional metamorphism to coarser phyllosilicates and silicate porphyroblasts in a matrix of fine-grained quartz and feldspar. The units are often thin and interleaved; thus, it creates or generates differential strengths in rocks within short distances, representing a day-to-day challenge for mining operations and causing some rock stability issues (Yergeau, 2015; Tremblay, 2021). The lithology of the Westwood deposit must be characterized to understand the effect of rock composition on rock geomechanical parameters. This deposit has a complicated geology. The deposit comprises 16 lithological units identified from mafic (fragile–ductile unit) to felsic (fragile unit) with six different alteration types, which are intersected by dykes and veins with variable compositions (Yergeau, 2015). The Westwood mine work extends from the surface to a depth of approximately 2,200 meters below the surface, and the metamorphic conditions gradually transition from greenschist facies near the surface to the upper greenschist and to the lower amphibolite facies at depth. This metamorphism caused recrystallization of some of the previously formed alteration minerals and locally partly overprints the fabrics (regional foliation) in the rocks. Thus, the Westwood mine represents a particularly relevant case study because of its unique characteristics in terms of diversity of lithology and alteration minerals and an increasing degree of rock metamorphism with increasing depth.

5.3 Methodology

A methodology for studying the influence of mineralogy on the uniaxial compressive strength and tensile strength of rock was established (Figure 5.2).

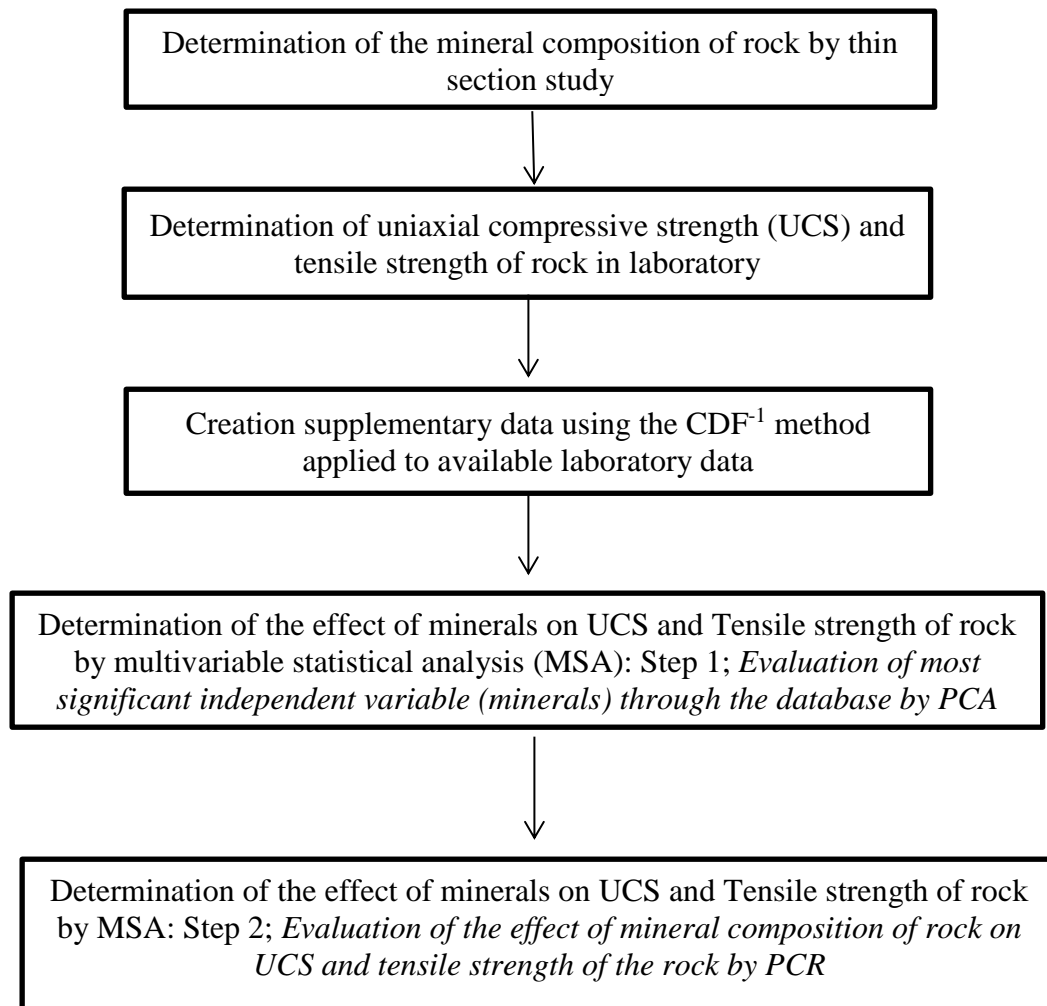


Figure 5. 2 Methodology used to assess the effect of rock mineral composition on the UCS and tensile strength of rock.

This study reports data on the metamorphosed rock core samples collected from different boreholes at the Westwood mine. Uniaxial compressive strength (UCS) test and Brazilian test were undertaken in many samples from different lithology of the deposit. Then, thin section study was performed on these samples to establish the mineralogy and petrology of the studied samples. Performing a random sampling method was appropriate due to the limited amount of

UCS and tensile strength values. The method is called CDF⁻¹ and is considered one of the most efficient and useful techniques for generating random sampling (Shadab Far and Wang, 2016). This technique provides an increased quantity of data on the tensile strength and UCS of these rocks, that is sufficient to carry multivariate statistical analysis. The database is classified into two main groups, namely, mafic (units that are rich in iron and magnesium are relatively poor in silica and tend to be more ductile than felsic rocks) and felsic rocks (units that are relatively rich in silica and tend to have a more fragile behavior). Principal component analysis (PCA) and principal component regression (PCR) were carried out as multivariate statistical analyses to clarify the role of each mineral on UCS and tensile strength and developed criteria for these rocks. PCA was applied to find the most relevant minerals among the database, and PCR was used to identify the effect of the mineralogy of mafic and felsic rocks on UCS and tensile strength. The methodology and data interpretation are explained in the following sections.

5.3.1 Assessment of rock mineralogy

The mineralogical composition and textural characteristics of the rocks were studied using thin sections and a microscope under transmitted light. A petrographic documentation was carried out to systematically document rock specimens to determine their composition, texture, and structural fabrics. Different units were sampled at different locations in the mine environment, including mafic rocks, such as basalt, lapilli tuff, and gabbro, as well as felsic rocks, such as tonalite, rhyodacite, dacite, and rhyolite. Quartz, feldspar, amphibole, muscovite, epidote, chlorite, plagioclase, carbonate, sericite, biotite, and garnet are the most common minerals (Table 5.1). White mica in this dataset represent muscovite crystals that are randomly oriented. Sericite has a similar composition (muscovitic), but a much smaller grain size and oriented in the foliation. Common trace minerals comprise apatite, tourmaline, magnetite, and pyrite. All the samples are foliated. Figure 5.3 is an example of the minerals of the felsic and mafic samples collected at the Westwood Mine.

Table 5. 1 Mineralogy of samples by thin section study (All minerals in modal %)

Samples			Mineralogy (%)													
Borehole ID	Unit	Rock type	Quartz	Chlorite	Carbonate	Sericite	Epidote	Amphibole	Plagioclase	Feldspar	Biotite	White mica (Muscovite)	Garnet	Apatite	Tourmaline	Opaque
R19218-19	U4-4-1	Gabbro-Basalt	10	-	-	11	31	45	3	-	-	-	-	-	-	-
R18281-17	U5-1-3	Basalt	5	25	-	58	-	-	-	10	-	-	-	-	-	2
R19218-19	U4-4-0	Tuff lappillis	35	21	8	10	-	-	-	5	-	20	-	-	-	1
R18110-17	U5-1-2	Andesite	40	2	2	20	1	-	5	20	-	5	-	-	-	5
R18110-17	U5-1-3	Basalt	35	31	-	10	1	-	-	20	3	-	-	-	-	-
R18110-17	U5-1-2	Andesite	10	10	-	32	5	-	-	40	-	3	-	-	-	-
R19217-19	U3-3-0	Tuff lappillis	40	3	-	25	12	-	-	-	-	5	-	-	1	14
R18281-17	U5-1-4	Dacite	50	10	-	20	-	-	3	15	-	2	-	-	-	-
R19164-19	U4-3-0	Dacite	58	10	-	20	9	-	-	-	-	-	-	-	-	3
R18281-17	U5-1-2	Andesite	10	9	-	30	-	-	-	41	5	-	-	-	-	5
R19197-19	U4-2-0	Dacite	70	-	1	-	-	-	-	1	8	10	-	-	-	-
R18281-17	U5-1-3	Basalt	30	5	-	55	-	-	-	10	-	-	-	-	-	5
R18110-17	U5-1-4	Dacite	10	25	-	25	30	-	10	-	-	-	-	-	-	-
R19197-19	U3-3-1	Basalt	20	-	10	15	-	30	-	21	1	-	-	-	1	2
R19199-19	U4-2-0	Dacite	57	5	7	-	-	15	-	-	10	6	-	-	-	-
R19163-19	U3-3-1	Basalt	15	20	-	40	5	-	-	-	-	20	-	-	-	-
R19163-19	U4-3-0	Dacite	59	23	2	-	1	-	-	2	5	8	-	-	-	-
R19163-19	U3-3-0	Basalt	20	13	35	10	20	2	-	-	-	-	-	-	-	-
R19163-19	U4-4-0	Tuff lappillis	47	10	-	25	11	-	6	-	-	-	-	-	-	1
R19162-19	U4-2-0	Dacite	49	18	6	25	1	-	-	-	-	-	-	-	-	1
R19026-18	U4-3-0	Dacite	51	10	-	15	13	1	8	-	1	-	-	-	-	1
R18776-18	U2-0-0	Tuff lappillis	50	3	3	1	-	-	-	25	3	15	-	-	-	-
R19017-18	U4-3-0	Dacite	30	27	-	10	2	-	-	-	-	26	-	-	-	5
R19017-18	U4-4-0	Tuff lappillis	15	20	-	39	15	-	-	0	-	6	-	-	-	5
R19017-18	U4-3-0	Dacite	51	7	-	8	1	-	-	20	-	10	-	-	-	3
R19017-18	U4-4-1	Gabbro-Basalt	10	7	-	15	20	20	-	26	-	-	-	-	-	2
R18844-18	2T	Tonolite	20	10	-	20	5	-	-	37	1	-	-	-	-	7
R18844-18	U4-2-0	Dacite	30	20	-	1	5	-	-	27	15	-	-	-	-	2
R18843-18	U4-2-0	Dacite	19	20	-	15	5	-	-	38	-	-	-	-	-	3

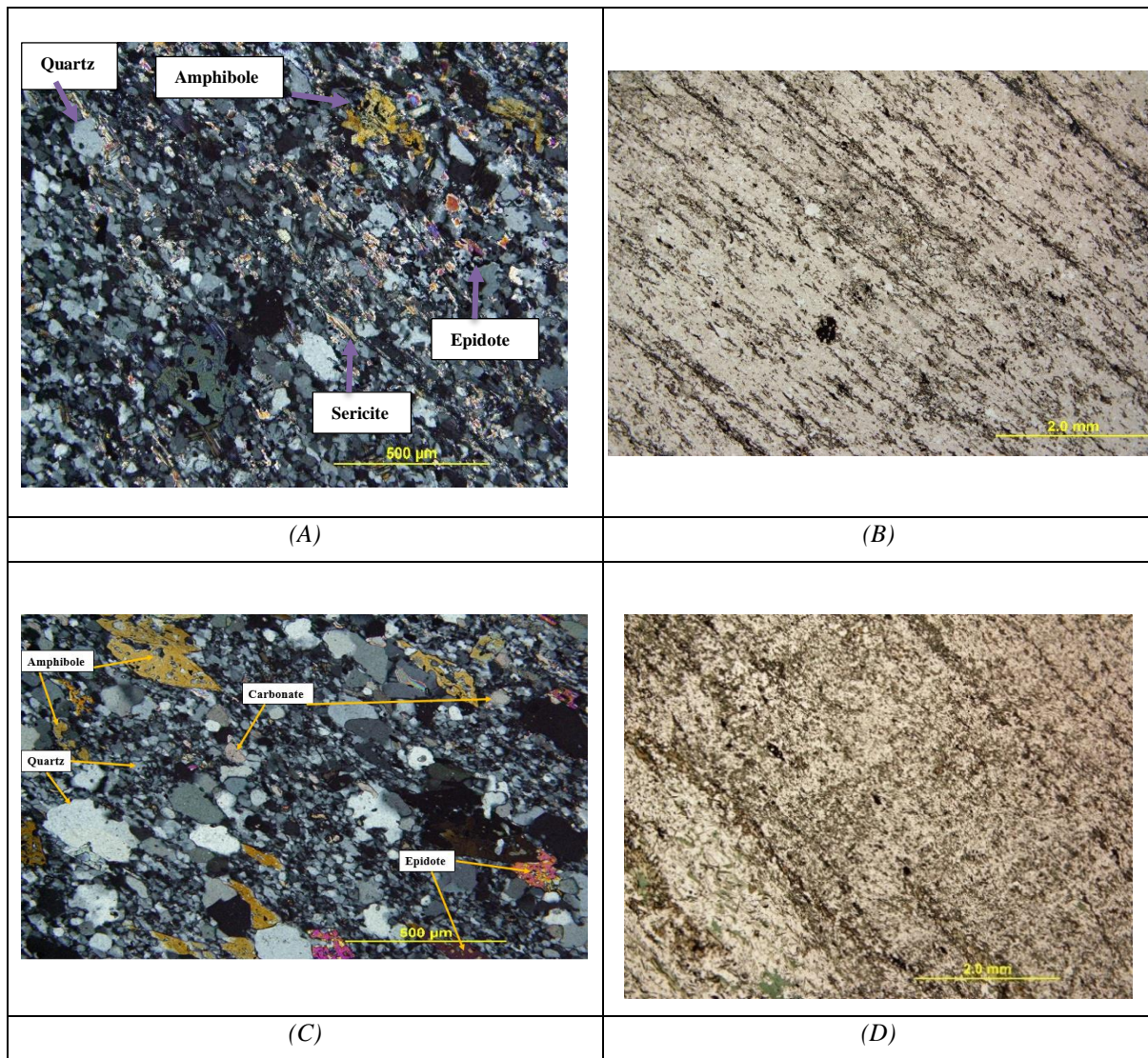


Figure 5. 3. Thin section photomicrographs of rock samples (A and B are graphs observed under polarized transmitted light and normal transmitted light of felsic rock; C and D are graph presented under polarized transmitted light and normal transmitted light of mafic rock)

5.3.2 Uniaxial compressive strength test (UCS) and Brazilian test

The UCS of more than 200 numbers of metamorphic rock samples was determined using a uniaxial compression testing machine according to the ISRM (1981) specification, 81 tests for felsic rock and 137 tests for mafic rock. The tensile strength of metamorphic rocks was determined using the Brazilian test according to ISRM 1981 (28 tests for felsic rocks and 24 tests for mafic rocks). The core samples and diameters of the samples for both tests were the same (diameter \approx 47.5mm).

5.3.3 Methods of random sampling generation

Whenever a statistical estimation is based on repeated experiments, input variables should be selected such that the data pool used in all runs of the analysis reflects the probability characteristics of the input variable. This finding indicates that the values (numbers) should be sampled according to a distribution. They also appear to be random. Many approaches are available for the generation of random samples, including the reject–accept algorithm, the inverse of the CDF⁻¹ and Markov Chain Monte Carlo simulation (MCMC) (Miranda et al., 2009). The basic building block of such sampling is the ability to generate random numbers from a uniform distribution between 0 and 1. The advantages and disadvantages of each method are different. For example, the MCMC method is generally used for complicated functions, such as Bayesian statistics. In addition, in the MCMC method, it is recommended that the proposed distribution be symmetric. The "Metropolis–Hastings" algorithm, which is usually used in case of asymmetric distributions, must be modified to use a reject -accept step. Using reject–accept methods generates considerable samples without considering the distribution function, such as normal or lognormal. This condition indicates that some samples have to be discarded, and the process takes time. The inverse of CDF is a useful and faster technique for generating samples based on the distribution function. The main advantage of the CDF is that it can be defined for any type of random variable including discrete, continuous, and mixed. This method can be used to generate random values of a variables according to its probability distribution functions, with their specific means and standard deviations. This procedure requires that the probability distribution function is pre-determined, in order to extract the mean and standard deviation of the function, which are used for generating the CDF. In this study, CDF⁻¹ was selected (Shadab Far and Wang, 2016). The steps of CDF⁻¹ are as follows:

1. Generating the CDF of the variable based on its distribution function and probability density function (normal distribution and Beta distribution)
2. Generating a set of random numbers with uniform distribution within 0 and 1.
3. Plotting the set of uniform random number on CDF graph and determining the value X' that corresponds to this probability value.

Therefore, by applying these methods, a sufficient number of samples (UCS and tensile strength values) could be generated for statistical analysis.

5.3.4 Determination of the effect of minerals on UCS and tensile strength by multivariable statistical analysis

This study aims to investigate the influence of mineral composition on rock strength considering especially the minerals that are specific to mafic and to felsic rocks. Multivariable statistical analysis is used as a tool to achieve this objective given the large number of variables. The term “multivariable statistics” includes all statistics, where more than two variables are analyzed simultaneously. Multivariable statistical analysis was used because the effect of minerals on the UCS and tensile strength of rock is multidimensional and related to more than one mineral. PCA was used to extract the most relevant minerals among several minerals in the database, and PCR was used to determine the effect of mineralogy on UCS and tensile strength.

Step 1: Evaluation of the most significant independent variable (minerals) through the database by PCA

In many disciplines the use large datasets are increasing tendency. Such datasets must be reduced in a way that most of the information remain available for interpretation. By combining scores and loading plots, a PCA extracts dominant patterns from a data matrix. With PCA, dominant patterns in a data matrix are identified through a complement of score and loading plots. In other words, PCA is a statistical technique that uses a single set of variables to determine, which variables are correlated among themselves (Tabachnick and Fidell, 1996). Extracted factors or components are often used to describe the underlying correlations between variables (Morissette et al., 2014).

In this study, the minerals were previously determined in felsic and mafic rocks. PCA was then used to explore the pattern among variables to identify important variables (minerals) to make subsequent data reduction possible. The PCA enables the extraction of important minerals among the other minerals. In the other words, an important goal of PCA is to reduce the dimensionality of such datasets, increasing their interpretability, while minimizing information loss.

Step 2: Evaluation of the effect of mineral composition of rock on the UCS and tensile strength of rock by PCR

The PCR was run after extracting the main mineral composition of mafic and felsic rocks by PCA. The main scope of this approach is that effect of minerals of geomechanical parametrs

of rock evaluate based on the linear regression equations. An independent variable with a high correlation degree can be aggregated into a principal component with the PCR. The PCR converts correlated variables into an uncorrelated set of principal components because they are independent. The “best” regression equation is achieved by estimating standard errors as high as possible using uncorrelated principal components. Finally, a general linear regression equation was generated from the “best” equation.

In this study, PCR was carried out for mafic and felsic rocks separately to evaluate the effect of mineral composition on the UCS and tensile strength of rock.

5.4 Data preparation

5.4.1 Laboratory test data for UCS and tensile strength of intact rock

Over 200 UCS tests on altered and metamorphosed volcanic rock samples, 81 tests for felsic and 137 tests for mafic rocks, plus 50 Brazilian tests that is 28 tests for felsic and 24 tests for mafic rocks. Tables AI and AII in the appendix section summarize the results of the mechanical tests conducted on felsic and mafic rocks, respectively.

5.4.2 Creation of additional data

Insufficient core samples were available for UCS and tensile strength tests to run statistical analysis. Therefore, we applied the inverse of the CDF to generate more data values. To do, the first step is to determine the probability distribution function of the variables, that are the UCS and tensile strength of felsic and mafic rocks. We assume that the real curves of UCS and tensile strength of felsic and mafic rocks follow a normal distribution. The Shapiro–Wilk test and Kolmogorov Smirnov test were used to prove this assumption (Shapiro and Wilk., 1965; Komogorov, 1933). Both tests are used to evaluate normality in statistics analysis. For these tests, a normal distribution (H_0) is the null hypothesis. The selected p-level is 0.05, which is a 95% confidence interval. The null hypothesis is rejected if the p-value is less than 0.05, and a normal distribution cannot be inferred from the data. Thus, both normality tests were run for the UCS and tensile strength of mafic and felsic rocks (Table 5.2). df is degree of freedom.

Table 5. 2 Test of normality

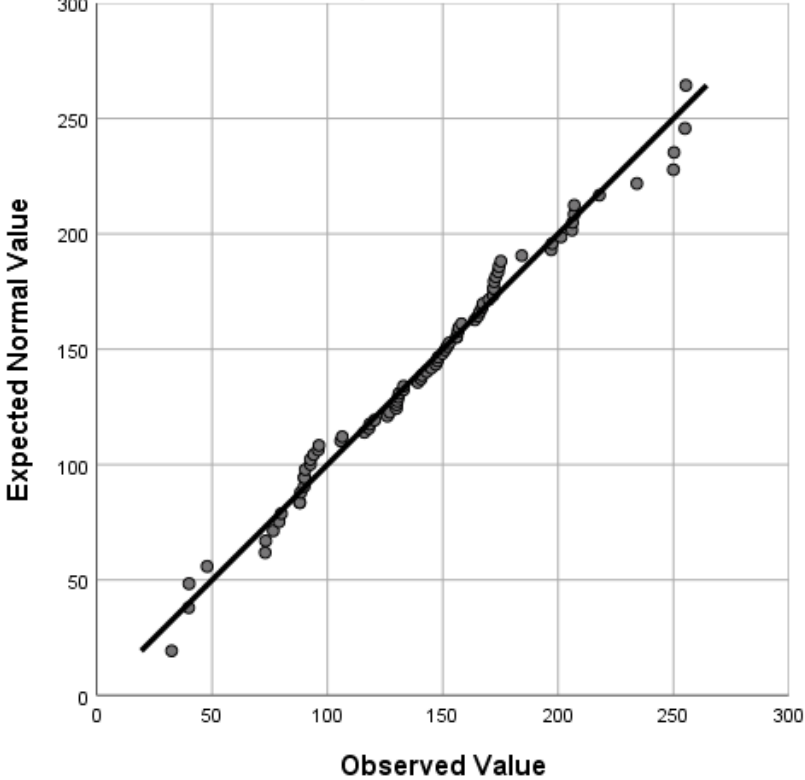
Tests of Normality						
	Kolmogorov-Smirnov			Shapiro-Wilk		
	Statistic	df	Sig.	Statistic	df	Sig.
Uniaxial compressive strength – Felsic rock	.082	81	.200	.981	81	.280
Uniaxial compressive strength – Mafic rock	.108	137	.000	.944	137	.000
Tensile strength – Felsic rock	.136	28	.198	.949	28	.189
Tensile strength – Mafic rock	.154	24	.054	.920	24	.057

Along with the normality tests, the Q-Q plots of UCS and tensile strength of mafic and felsic rocks were derived. The Q-Q plots are created by comparing two sets of quantiles. A line is drawn if both quantile sets came from the same distribution. Thus, we used the Q-Q plot to verify the probability distribution function fitting as the second verification of the probability function among the database. In our case, the solid line in the Q-Q plots represents the theoretical line of the distribution between the points. The Q-Q plots of variables are plotted in Figure 5.4. More information about the mean and standard deviation of data are provided in Table 5.3. The histogram of data is presented in Figure 5.5.

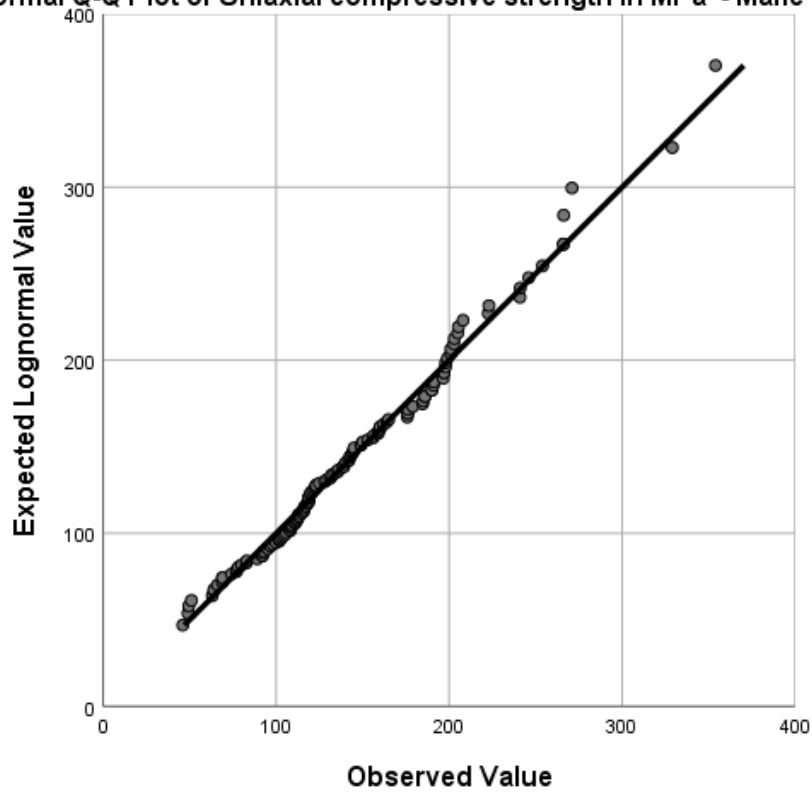
Table 5. 3 Mean and standard deviation of data

Rock type	Mean	Standard deviation
UCS (MPa) – Felsic rock	141.82	50.57
UCS (MPa) – Mafic rock	142.14	56.09
Tensile strength (MPa) – Felsic rock	18.54	5.43
Tensile strength (MPa) – Mafic rock	17.39	4.65

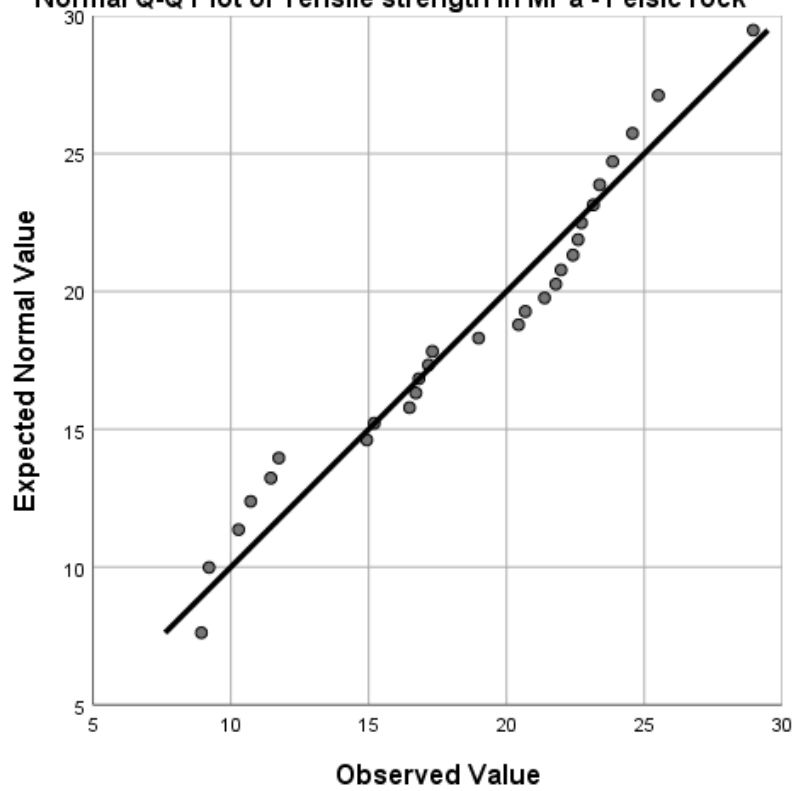
Normal Q-Q Plot of Uniaxial Compressive Strength in MPa- Felsic rock



Lognormal Q-Q Plot of Uniaxial compressive strength in MPa - Mafic rock



Normal Q-Q Plot of Tensile strength in MPa - Felsic rock



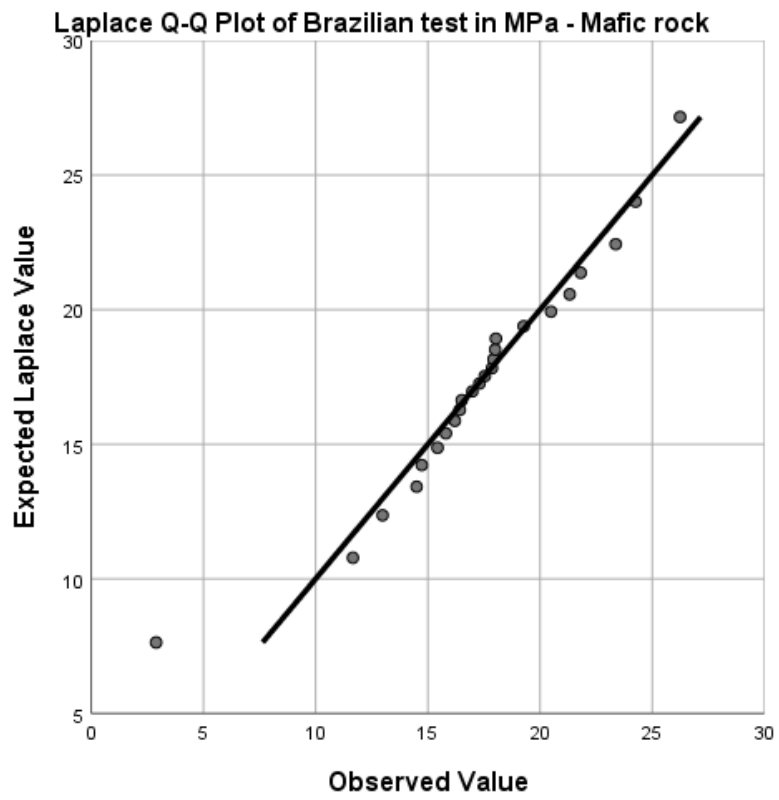
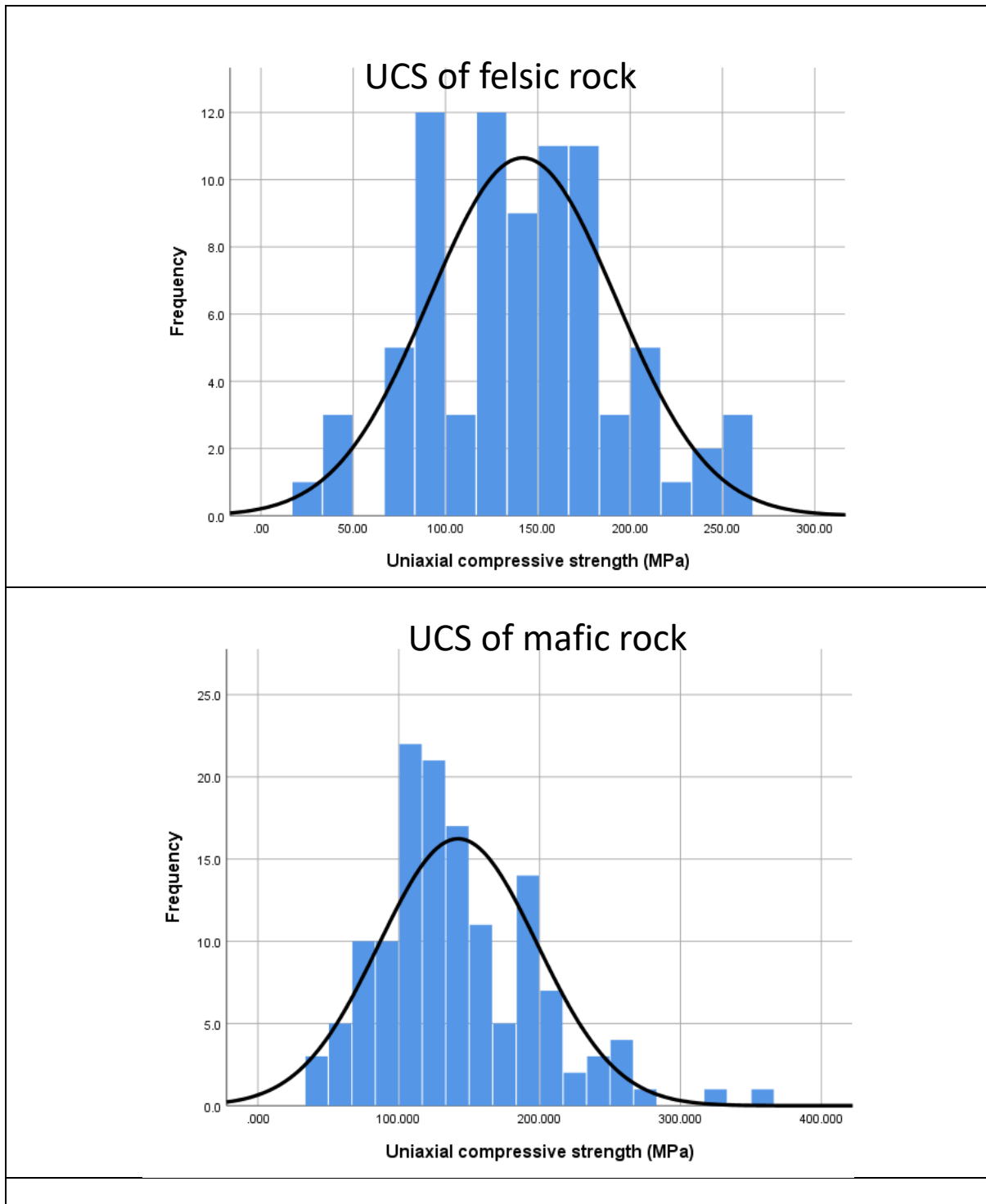


Figure 5. 4 Q-Q plot of laboratory data of felsic and mafic rocks



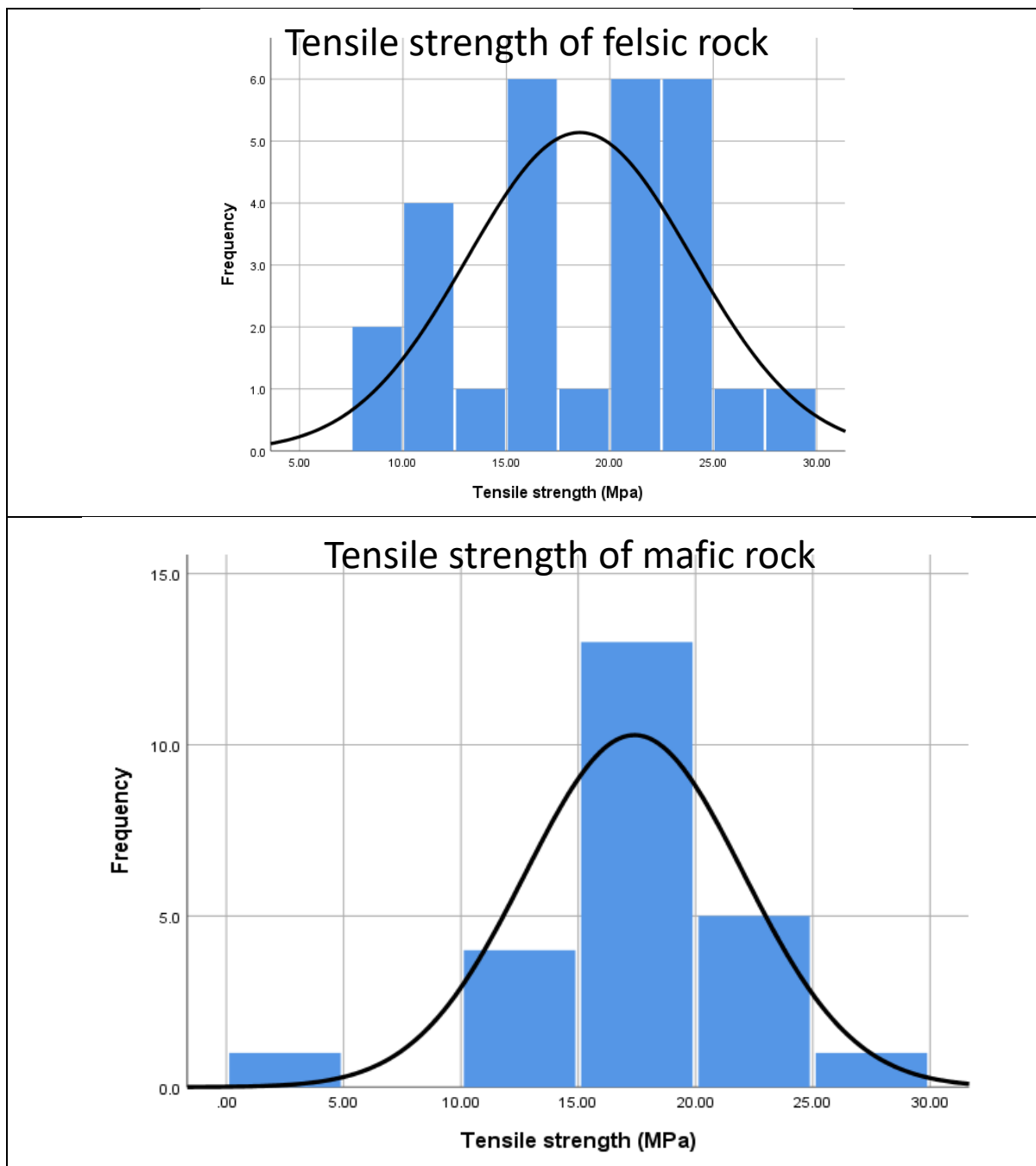


Figure 5. 5 Histogram of laboratory tests data of mafic and felsic rocks

The p-values of the UCS tests data and the tensile strength data on felsic are greater than 0.05 (Table 2). Thus, the null hypothesis of the normal distribution cannot be rejected, and the data are considered as normally distributed. However, for the UCS and tensile strength of mafic rock, the p-value is smaller than 0.05; thus, the data are not considered as following a normal distribution. The Q-Q plot and p-value were used to identify the distribution fitting the data on UCS and tensile strength of mafic rocks. Different other distribution functions were tested and

the log-normal distribution was found suitable for UCS of mafic rock (p-value is 0.07), and the Laplace distribution function was found as the most accurate since the plotted data are near the solid line (p-value is 0.11) which represents the theoretical quantile of the Laplace distribution. Therefore, the log-normal and the Laplace distribution function were selected to generate virtual random samples from their CDF.

The normal distribution and its cumulative distribution function are expressed in Eqs. 5.1 and 5.2. The Laplace distribution and its cumulative distribution function are written in Eqs. 5.3 to 5.4, and the log-normal distribution and its cumulative distribution function are written in Eqs. 5.5 to 5.6. The values of UCS and tensile strength were generated for mafic and felsic rocks by utilizing the inverse of a cumulative distribution function of each variable.

$$f(x) = \frac{1}{\sigma\sqrt{2\pi}} e^{-\frac{1}{2}\left(\frac{x-\mu}{\sigma}\right)^2}, \quad \text{Eq. 5 1}$$

$$CDF = \frac{1}{2} \left[1 + \operatorname{erf}\left(\frac{x-\mu}{\sigma\sqrt{2}}\right) \right], \quad \text{Eq. 5 2}$$

$$f_x = \frac{1}{2b} \exp\left(-\frac{|x-\mu|}{b}\right), \quad \text{Eq. 5 3}$$

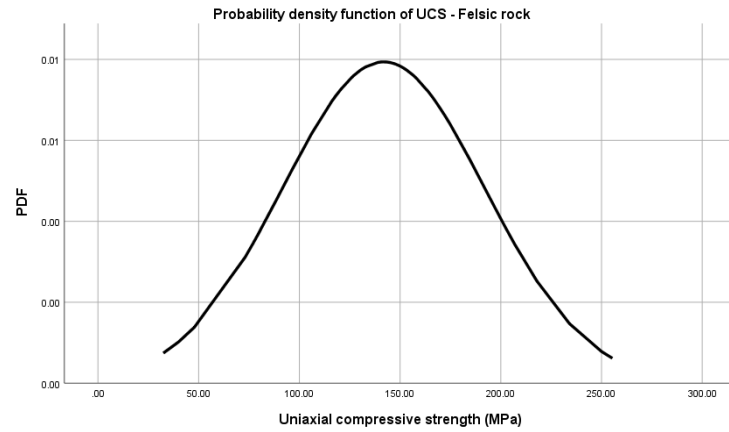
$$CDF = 1 - \frac{1}{2} \exp\left(-\frac{|x-\mu|}{b}\right) \text{ if } X \geq \mu \quad ; \text{ AND} \quad CDF = \frac{1}{2} \exp\left(\frac{|x-\mu|}{b}\right) \text{ If } X < \mu \quad \text{Eq. 5 4}$$

$$f_x = \frac{1}{x\sigma\sqrt{2\pi}} \exp\left(-\frac{(\ln x - \mu)^2}{2\sigma^2}\right), \quad \text{Eq. 5 5}$$

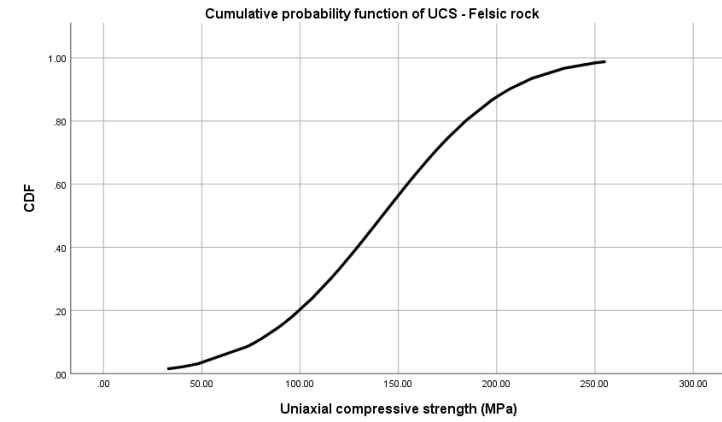
$$CDF = \frac{1}{2} \left[1 + \operatorname{erf}\left(\frac{\ln x - \mu}{\sigma\sqrt{2}}\right) \right], \quad \text{Eq. 5 6}$$

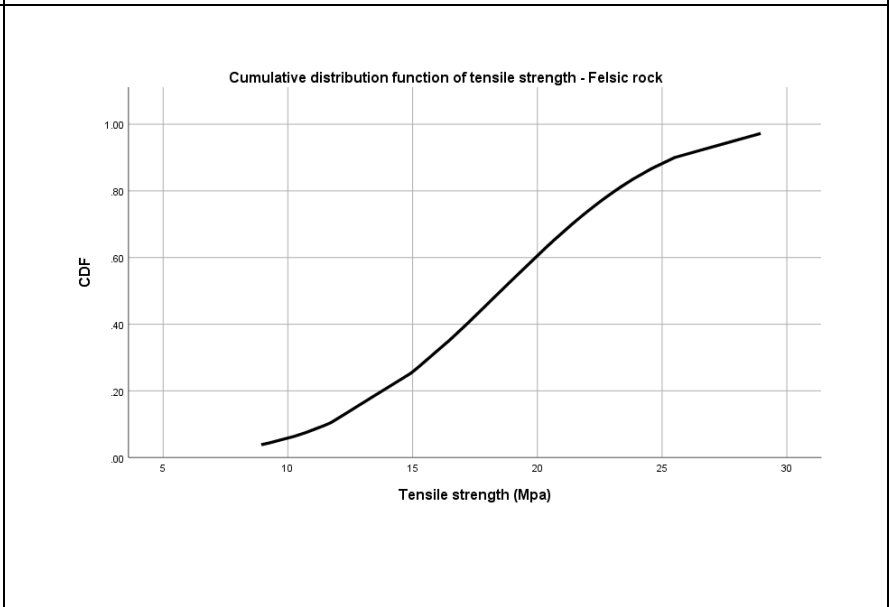
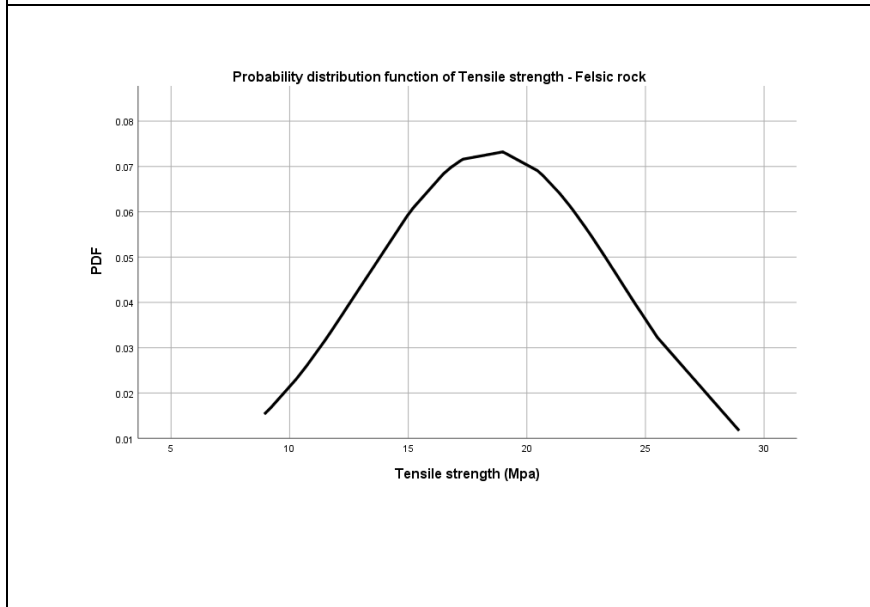
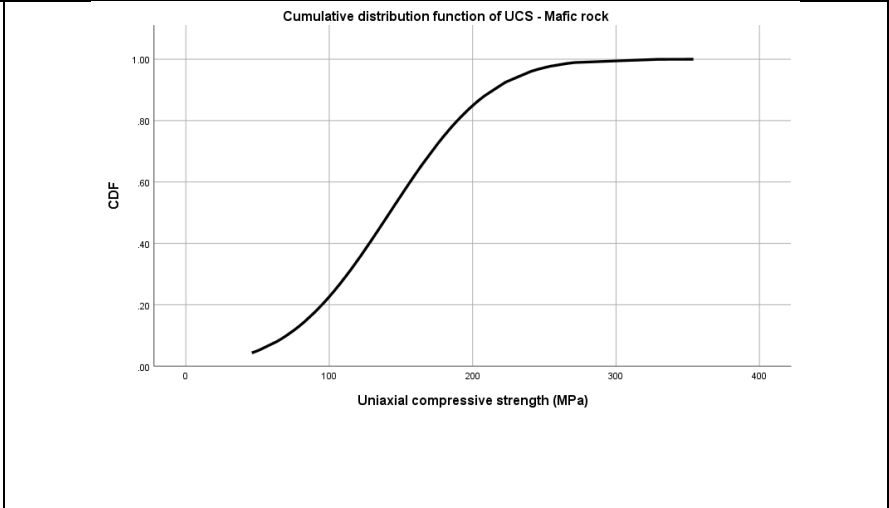
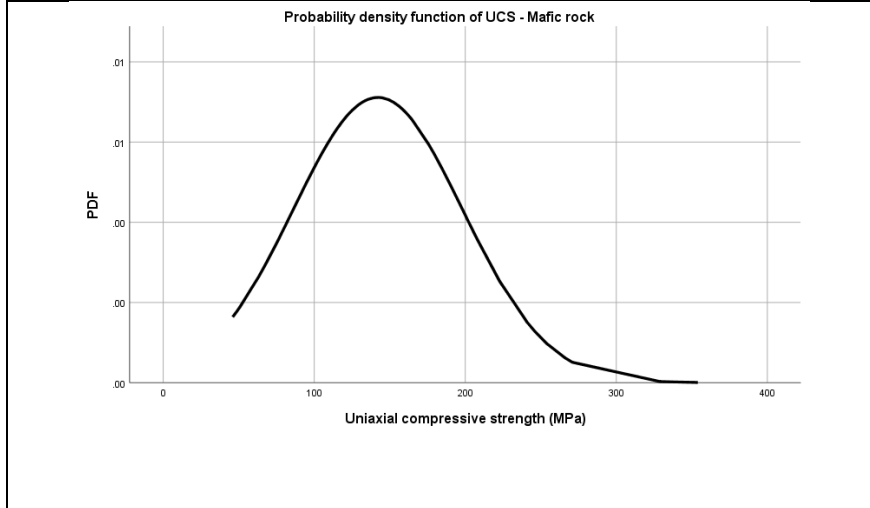
Where μ is mean, σ^2 is variance, and b is the average absolute deviation. Using these equations, the probability density functions (PDFs) and cumulative distribution functions (CDFs) of UCS and tensile strength of metamorphic rocks were generated (Figure 5.6).

Probability density function (PDF)



Cumulative distribution function (CDF)





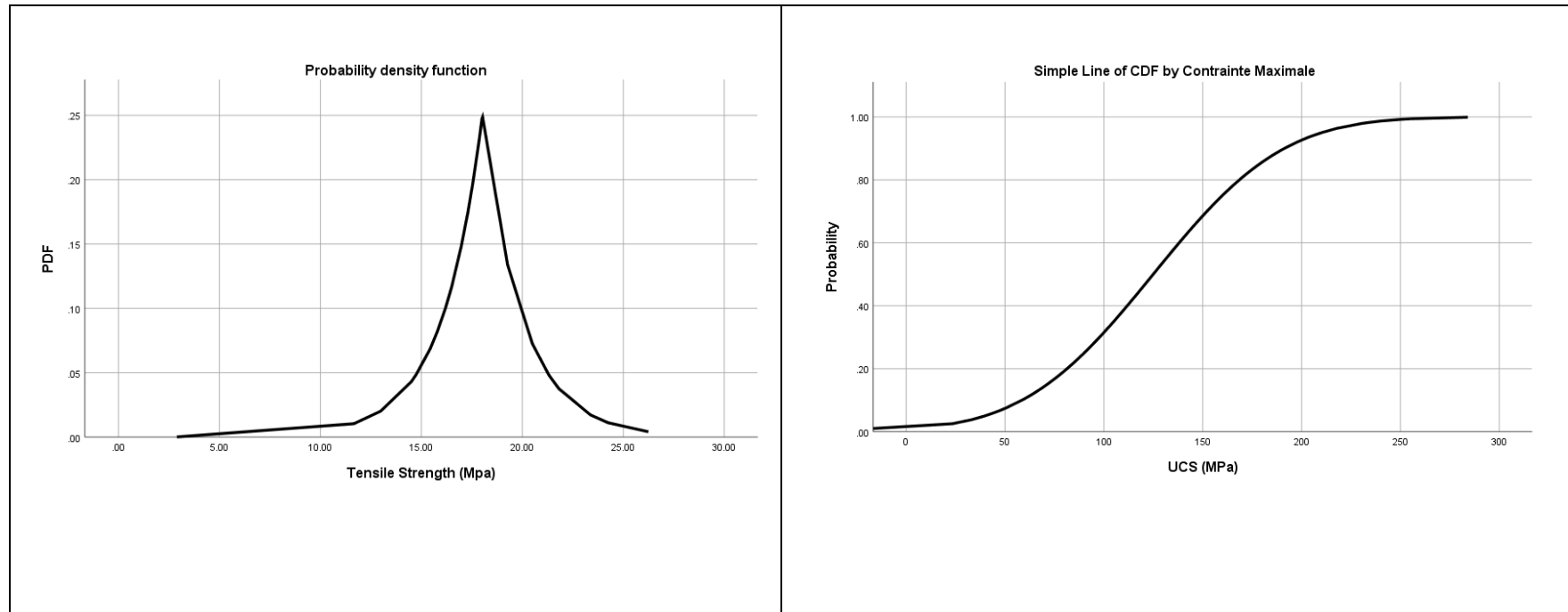


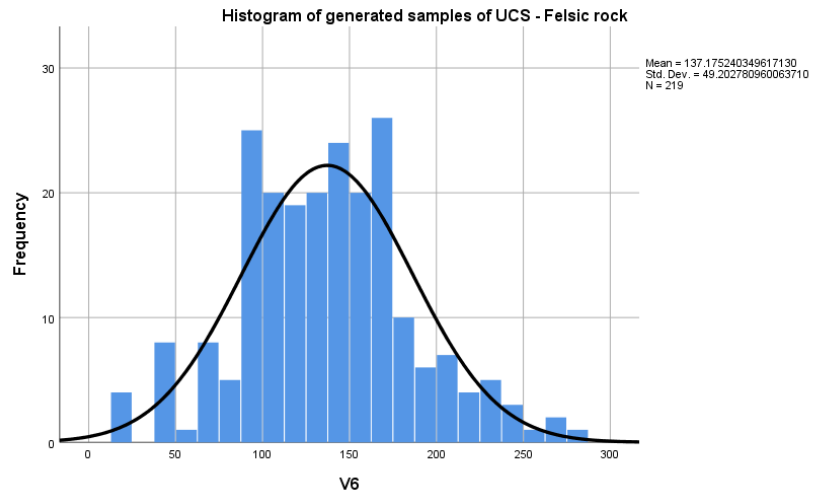
Figure 5. 6 Probability density function and cumulative distribution function of variables

This procedure has been followed to generate between 122 and 219 virtual values of UCS and tensile strength, for felsic and for mafic rocks (Table 5.4). This new data set is shown in Figure 5.7 as a series of histograms and Q-Q plots. The generated virtual values complement the values obtained in the laboratory (Table 4), in order to reach a total of 300 values for UCS and 150 for tensile strength. For example, for felsic rock, we conducted 81 tests and generated 219 samples to reach 300 samples. Figure 5.7 shows that the CDF⁻¹ generated data are most closely matched with solid lines, as shown by Q-Q plots. The solid line represents the theoretical quantile of selected distribution function like normal distribution or Laplace distribution function. This finding indicates that the generated values for UCS and tensile strength are close to those in the reality database used for generating random sampling. Two multivariate statistical analyses were now conducted to determine the correlation between the mineralogy of metamorphic rocks and the geomechanical parameters of the rock.

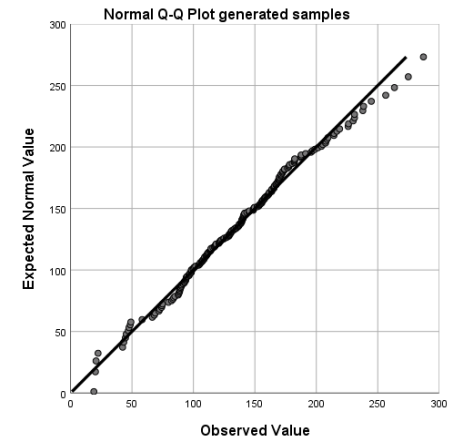
Table 5. 4 Detailed information about generated samples

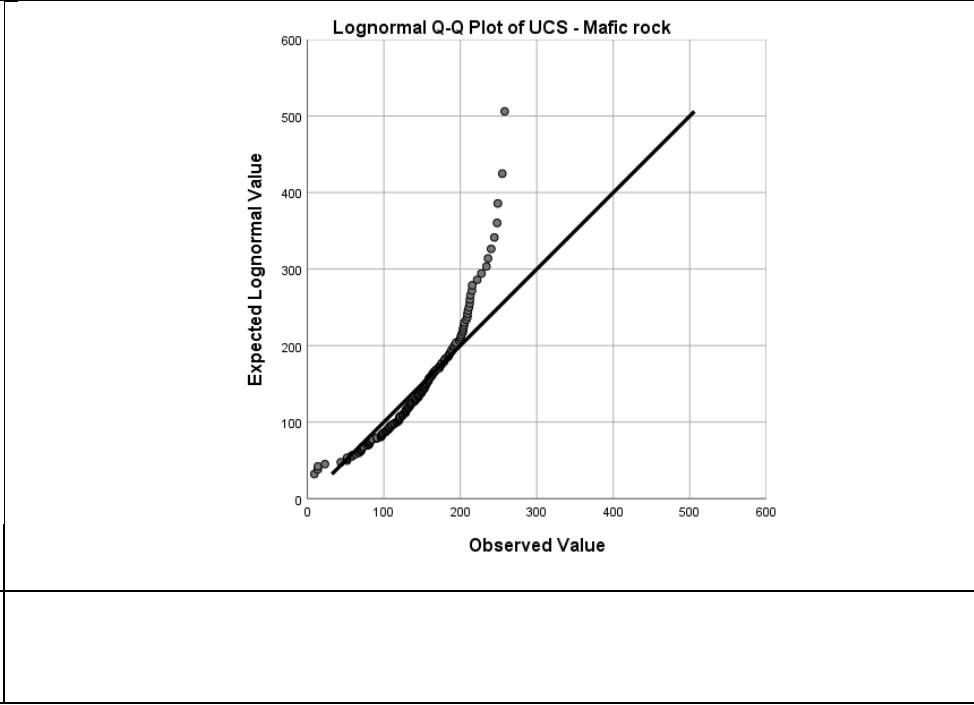
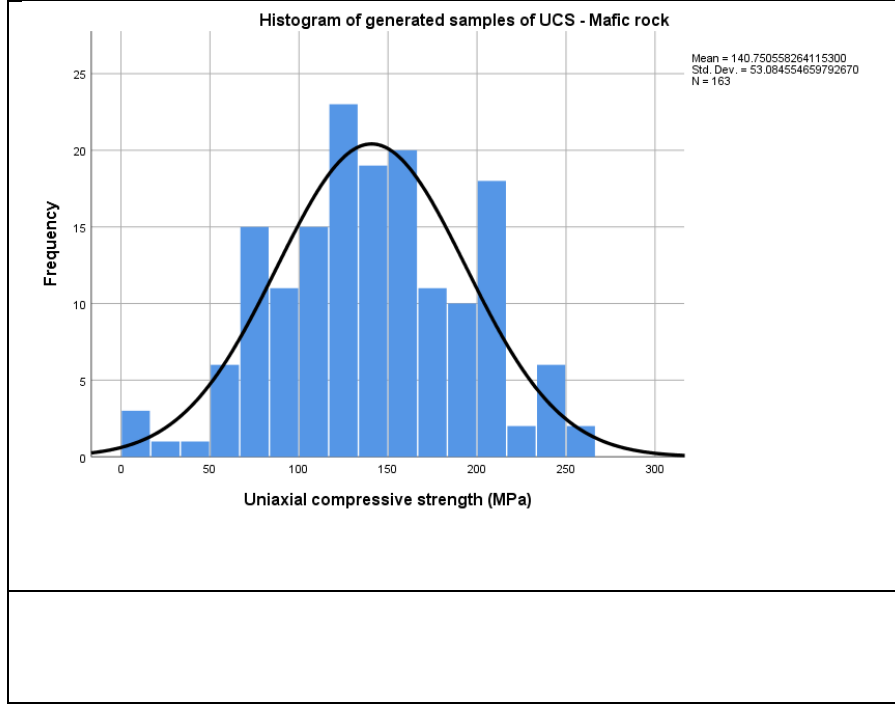
	Generated value	Laboratory test	Mean of generated value (MPa)	Standard deviation of generated value (MPa)
UCS– Felsic rock	219	81	137.17	49.20
UCS – Mafic rock	163	137	140.75	53.08
Tensile strength – Felsic rock	122	28	18.12	5.34
Tensile strength – Mafic rock	126	24	17.66	5.05

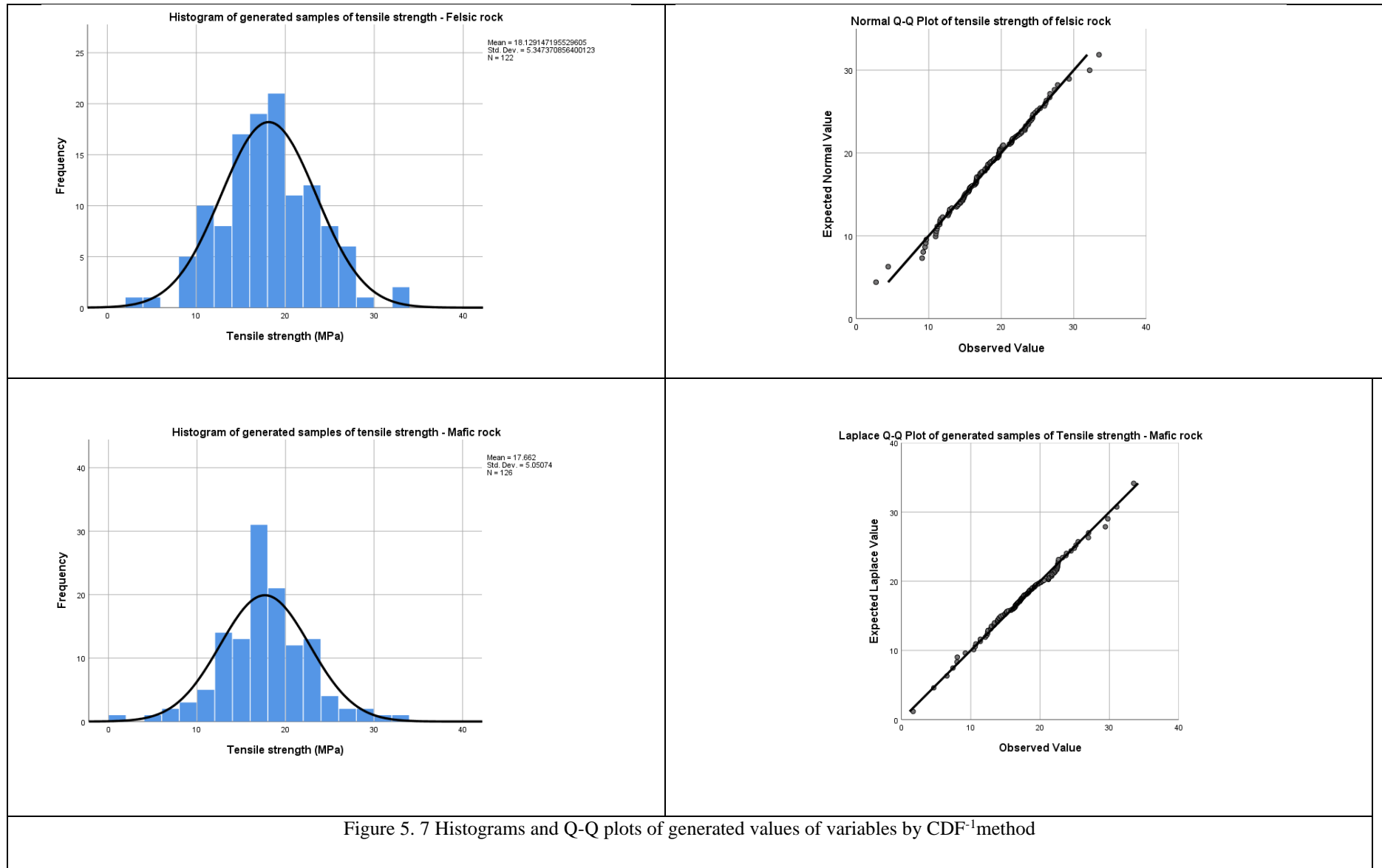
Histogram of generated samples



Q-Q plot of generated values by CDF⁻¹







5.4.3 Prerequisite to multivariable statistical analysis

PCA can only be performed once all assumptions and prerequisites have been satisfied via a series of checks and diagnostics. Linearity testing and multicollinearity verification should be conducted.

A) Linearity testing

PCA relies on Pearson correlation coefficients and it does not consider nonlinear relationships. Therefore, the assumption that two variables are linearly related is called linearity (Tabachnick and Fidell, 1996). We only examined the scatter plot to assess the linearity between pairs of continuous variables due to the exploratory nature of the study. An oval-shaped scatter plot is obtained when both variables are linearly related. A nonlinear relationship between two variables results in a curved scatter plot. The majority of plots between pairs of variables exhibits a random scatter pattern without distinctive correlation, similar to the example shown in Figure 5.8 for chlorite and white mica and no scatter plot presents a visible curvature., as an example. This result indicated that the correlations among variables in this dataset are weak. The linearity assumption among continuous variables is adequate for this study. All the mineral graphs in this study were plotted against each other. Garnet showed a constant value (zero) against all minerals. Therefore, this mineral was removed from the subsequent study.

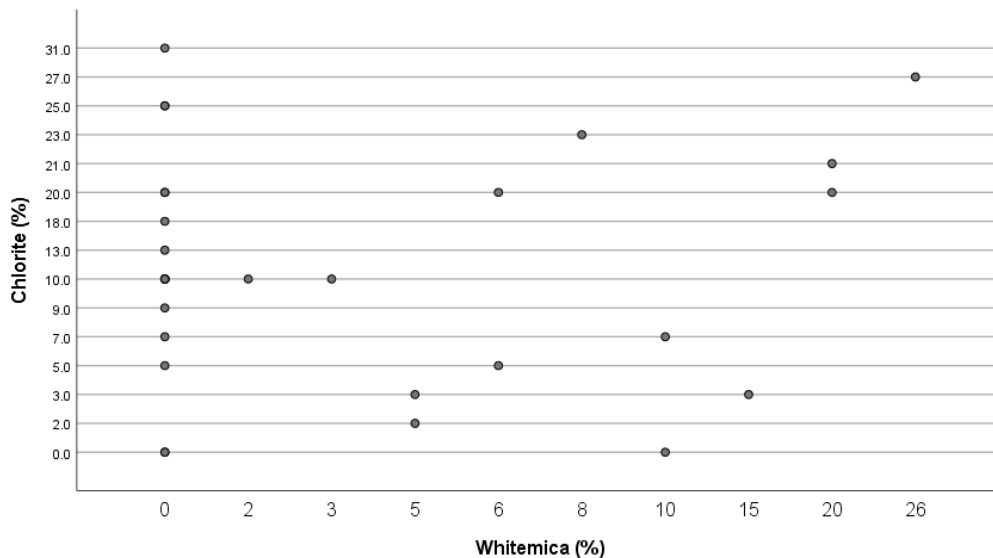


Figure 5. 8 Scatter plot matrix of Chlorite and white mica (sericite and muscovite) for linearity testing (Chl and WM) in %

B) Multicollinearity verification

If the variables in a dataset are highly correlated, then multicollinearity, which is a problem in a correlation matrix, is obtained. Variables with multicollinearity are highly correlated ($R^2 > 0.9$). Extreme multicollinearity introduces bias into the analysis results and dictates the actual result (Tabachnick and Fidell, 1996). A further investigation of the variance of inflation factor (VIF) for each variable may confirm the existence of multicollinearity. VIF extends a particular variation to contribute to multicollinearity. A VIF below 4 indicates no multicollinearity among factors, whereas a VIF between 3 and 10 indicates a high correlation that may be problematic. A VIF above 10 implies that the regression coefficients are poorly estimated because of multicollinearity. The VIF value for each independent variable was calculated as follows:

$$\text{VIF}_i = \frac{1}{1-R_i^2} \quad \text{Eq. 5 7}$$

Where R_i^2 is the coefficient of determination of the regression equation.

Figure 5.9 shows that the VIF values of all the variables are less than 4, indicating that multicollinearity does not exist and does not pose any problem in this study.

<table border="1"> <thead> <tr> <th>Constant</th> <th>VIF</th> </tr> </thead> <tbody> <tr><td>Chlorite</td><td>1.199</td></tr> <tr><td>Carbonate</td><td>1.293</td></tr> <tr><td>Sericite</td><td>2.268</td></tr> <tr><td>Epidote</td><td>1.294</td></tr> <tr><td>Amphibole</td><td>1.817</td></tr> <tr><td>Feldspar</td><td>1.589</td></tr> <tr><td>Plagioclase</td><td>1.308</td></tr> <tr><td>Biotite</td><td>1.614</td></tr> <tr><td>White mica</td><td>1.277</td></tr> <tr> <td colspan="2">A) Dependant variable: Quartz</td> </tr> </tbody> </table>	Constant	VIF	Chlorite	1.199	Carbonate	1.293	Sericite	2.268	Epidote	1.294	Amphibole	1.817	Feldspar	1.589	Plagioclase	1.308	Biotite	1.614	White mica	1.277	A) Dependant variable: Quartz		<table border="1"> <thead> <tr> <th>Constant</th> <th>VIF</th> </tr> </thead> <tbody> <tr><td>Quartz</td><td>3.059</td></tr> <tr><td>Carbonate</td><td>1.319</td></tr> <tr><td>Sericite</td><td>3.204</td></tr> <tr><td>Epidote</td><td>1.373</td></tr> <tr><td>Amphibole</td><td>2.289</td></tr> <tr><td>Feldspar</td><td>3.659</td></tr> <tr><td>Plagioclase</td><td>1.3</td></tr> <tr><td>Biotite</td><td>1.536</td></tr> <tr><td>White mica</td><td>1.291</td></tr> <tr> <td colspan="2">A) Dependant variable: Chlorite</td> </tr> </tbody> </table>	Constant	VIF	Quartz	3.059	Carbonate	1.319	Sericite	3.204	Epidote	1.373	Amphibole	2.289	Feldspar	3.659	Plagioclase	1.3	Biotite	1.536	White mica	1.291	A) Dependant variable: Chlorite		<table border="1"> <thead> <tr> <th>Constant</th> <th>VIF</th> </tr> </thead> <tbody> <tr><td>Quartz</td><td>3.996</td></tr> <tr><td>Chlorite</td><td>1.598</td></tr> <tr><td>Sericite</td><td>2.85</td></tr> <tr><td>Epidote</td><td>1.357</td></tr> <tr><td>Amphibole</td><td>2.132</td></tr> <tr><td>Feldspar</td><td>3.646</td></tr> <tr><td>Plagioclase</td><td>1.361</td></tr> <tr><td>Biotite</td><td>1.622</td></tr> <tr><td>White mica</td><td>1.275</td></tr> <tr> <td colspan="2">C) Dependant variable: Carbonate</td> </tr> </tbody> </table>	Constant	VIF	Quartz	3.996	Chlorite	1.598	Sericite	2.85	Epidote	1.357	Amphibole	2.132	Feldspar	3.646	Plagioclase	1.361	Biotite	1.622	White mica	1.275	C) Dependant variable: Carbonate		<table border="1"> <thead> <tr> <th>Constant</th> <th>VIF</th> </tr> </thead> <tbody> <tr><td>Quartz</td><td>4.162</td></tr> <tr><td>Chlorite</td><td>1.649</td></tr> <tr><td>Carbonate</td><td>1.344</td></tr> <tr><td>Sericite</td><td>3.207</td></tr> <tr><td>Epidote</td><td>1.394</td></tr> <tr><td>Amphibole</td><td>2.253</td></tr> <tr><td>Plagioclase</td><td>1.362</td></tr> <tr><td>Feldspar</td><td>4.09</td></tr> <tr><td>Biotite</td><td>1.62</td></tr> <tr> <td colspan="2">D) Dependant variable: White mica</td> </tr> </tbody> </table>	Constant	VIF	Quartz	4.162	Chlorite	1.649	Carbonate	1.344	Sericite	3.207	Epidote	1.394	Amphibole	2.253	Plagioclase	1.362	Feldspar	4.09	Biotite	1.62	D) Dependant variable: White mica	
Constant	VIF																																																																																										
Chlorite	1.199																																																																																										
Carbonate	1.293																																																																																										
Sericite	2.268																																																																																										
Epidote	1.294																																																																																										
Amphibole	1.817																																																																																										
Feldspar	1.589																																																																																										
Plagioclase	1.308																																																																																										
Biotite	1.614																																																																																										
White mica	1.277																																																																																										
A) Dependant variable: Quartz																																																																																											
Constant	VIF																																																																																										
Quartz	3.059																																																																																										
Carbonate	1.319																																																																																										
Sericite	3.204																																																																																										
Epidote	1.373																																																																																										
Amphibole	2.289																																																																																										
Feldspar	3.659																																																																																										
Plagioclase	1.3																																																																																										
Biotite	1.536																																																																																										
White mica	1.291																																																																																										
A) Dependant variable: Chlorite																																																																																											
Constant	VIF																																																																																										
Quartz	3.996																																																																																										
Chlorite	1.598																																																																																										
Sericite	2.85																																																																																										
Epidote	1.357																																																																																										
Amphibole	2.132																																																																																										
Feldspar	3.646																																																																																										
Plagioclase	1.361																																																																																										
Biotite	1.622																																																																																										
White mica	1.275																																																																																										
C) Dependant variable: Carbonate																																																																																											
Constant	VIF																																																																																										
Quartz	4.162																																																																																										
Chlorite	1.649																																																																																										
Carbonate	1.344																																																																																										
Sericite	3.207																																																																																										
Epidote	1.394																																																																																										
Amphibole	2.253																																																																																										
Plagioclase	1.362																																																																																										
Feldspar	4.09																																																																																										
Biotite	1.62																																																																																										
D) Dependant variable: White mica																																																																																											
<table border="1"> <thead> <tr> <th>Constant</th> <th>VIF</th> </tr> </thead> <tbody> <tr><td>Quartz</td><td>2.927</td></tr> <tr><td>Chlorite</td><td>1.621</td></tr> <tr><td>Carbonate</td><td>1.19</td></tr> <tr><td>Epidote</td><td>1.366</td></tr> <tr><td>Amphibole</td><td>1.37</td></tr> <tr><td>Feldspar</td><td>2.289</td></tr> <tr><td>Plagioclase</td><td>1.378</td></tr> <tr><td>Biotite</td><td>1.365</td></tr> <tr><td>White mica</td><td>1.27</td></tr> <tr> <td colspan="2">D) Dependant variable: Sericite</td> </tr> </tbody> </table>	Constant	VIF	Quartz	2.927	Chlorite	1.621	Carbonate	1.19	Epidote	1.366	Amphibole	1.37	Feldspar	2.289	Plagioclase	1.378	Biotite	1.365	White mica	1.27	D) Dependant variable: Sericite		<table border="1"> <thead> <tr> <th>Constant</th> <th>VIF</th> </tr> </thead> <tbody> <tr><td>Quartz</td><td>3.902</td></tr> <tr><td>Chlorite</td><td>1.624</td></tr> <tr><td>Carbonate</td><td>1.325</td></tr> <tr><td>Sericite</td><td>3.194</td></tr> <tr><td>Amphibole</td><td>2.295</td></tr> <tr><td>Feldspar</td><td>3.748</td></tr> <tr><td>Plagioclase</td><td>1.249</td></tr> <tr><td>Biotite</td><td>1.603</td></tr> <tr><td>White mica</td><td>1.291</td></tr> <tr> <td colspan="2">D) Dependant variable: Epidote</td> </tr> </tbody> </table>	Constant	VIF	Quartz	3.902	Chlorite	1.624	Carbonate	1.325	Sericite	3.194	Amphibole	2.295	Feldspar	3.748	Plagioclase	1.249	Biotite	1.603	White mica	1.291	D) Dependant variable: Epidote		<table border="1"> <thead> <tr> <th>Constant</th> <th>VIF</th> </tr> </thead> <tbody> <tr><td>Quartz</td><td>3.344</td></tr> <tr><td>Chlorite</td><td>1.652</td></tr> <tr><td>Carbonate</td><td>1.27</td></tr> <tr><td>Sericite</td><td>1.955</td></tr> <tr><td>Epidote</td><td>1.401</td></tr> <tr><td>Feldspar</td><td>2.749</td></tr> <tr><td>Plagioclase</td><td>1.288</td></tr> <tr><td>Biotite</td><td>1.579</td></tr> <tr><td>White mica</td><td>1.273</td></tr> <tr> <td colspan="2">D) Dependant variable: Amphibole</td> </tr> </tbody> </table>	Constant	VIF	Quartz	3.344	Chlorite	1.652	Carbonate	1.27	Sericite	1.955	Epidote	1.401	Feldspar	2.749	Plagioclase	1.288	Biotite	1.579	White mica	1.273	D) Dependant variable: Amphibole		<table border="1"> <thead> <tr> <th>Constant</th> <th>VIF</th> </tr> </thead> <tbody> <tr><td>Quartz</td><td>1.575</td></tr> <tr><td>Chlorite</td><td>1.408</td></tr> <tr><td>Carbonate</td><td>1.159</td></tr> <tr><td>Sericite</td><td>1.776</td></tr> <tr><td>Epidote</td><td>1.174</td></tr> <tr><td>Amphibole</td><td>1.252</td></tr> <tr><td>Plagioclase</td><td>1.384</td></tr> <tr><td>Biotite</td><td>1.622</td></tr> <tr><td>White mica</td><td>1.263</td></tr> <tr> <td colspan="2">D) Dependant variable: Feldspar</td> </tr> </tbody> </table>	Constant	VIF	Quartz	1.575	Chlorite	1.408	Carbonate	1.159	Sericite	1.776	Epidote	1.174	Amphibole	1.252	Plagioclase	1.384	Biotite	1.622	White mica	1.263	D) Dependant variable: Feldspar	
Constant	VIF																																																																																										
Quartz	2.927																																																																																										
Chlorite	1.621																																																																																										
Carbonate	1.19																																																																																										
Epidote	1.366																																																																																										
Amphibole	1.37																																																																																										
Feldspar	2.289																																																																																										
Plagioclase	1.378																																																																																										
Biotite	1.365																																																																																										
White mica	1.27																																																																																										
D) Dependant variable: Sericite																																																																																											
Constant	VIF																																																																																										
Quartz	3.902																																																																																										
Chlorite	1.624																																																																																										
Carbonate	1.325																																																																																										
Sericite	3.194																																																																																										
Amphibole	2.295																																																																																										
Feldspar	3.748																																																																																										
Plagioclase	1.249																																																																																										
Biotite	1.603																																																																																										
White mica	1.291																																																																																										
D) Dependant variable: Epidote																																																																																											
Constant	VIF																																																																																										
Quartz	3.344																																																																																										
Chlorite	1.652																																																																																										
Carbonate	1.27																																																																																										
Sericite	1.955																																																																																										
Epidote	1.401																																																																																										
Feldspar	2.749																																																																																										
Plagioclase	1.288																																																																																										
Biotite	1.579																																																																																										
White mica	1.273																																																																																										
D) Dependant variable: Amphibole																																																																																											
Constant	VIF																																																																																										
Quartz	1.575																																																																																										
Chlorite	1.408																																																																																										
Carbonate	1.159																																																																																										
Sericite	1.776																																																																																										
Epidote	1.174																																																																																										
Amphibole	1.252																																																																																										
Plagioclase	1.384																																																																																										
Biotite	1.622																																																																																										
White mica	1.263																																																																																										
D) Dependant variable: Feldspar																																																																																											
<table border="1"> <thead> <tr> <th>Constant</th> <th>VIF</th> </tr> </thead> <tbody> <tr><td>Quartz</td><td>4.202</td></tr> <tr><td>Chlorite</td><td>1.568</td></tr> <tr><td>Carbonate</td><td>1.367</td></tr> <tr><td>Sericite</td><td>2.755</td></tr> <tr><td>Epidote</td><td>1.383</td></tr> <tr><td>Amphibole</td><td>2.234</td></tr> <tr><td>Plagioclase</td><td>1.377</td></tr> <tr><td>Feldspar</td><td>4.131</td></tr> <tr><td>White mica</td><td>1.294</td></tr> <tr> <td colspan="2">D) Dependant variable: Biotite</td> </tr> </tbody> </table>	Constant	VIF	Quartz	4.202	Chlorite	1.568	Carbonate	1.367	Sericite	2.755	Epidote	1.383	Amphibole	2.234	Plagioclase	1.377	Feldspar	4.131	White mica	1.294	D) Dependant variable: Biotite		<table border="1"> <thead> <tr> <th>Constant</th> <th>VIF</th> </tr> </thead> <tbody> <tr><td>Quartz</td><td>1.496</td></tr> <tr><td>Chlorite</td><td>1.01</td></tr> <tr><td>Sericite</td><td>1.208</td></tr> <tr><td>Epidote</td><td>1.523</td></tr> <tr><td>Amphibole</td><td>2.325</td></tr> <tr><td>Feldspar</td><td>3.587</td></tr> <tr><td>Carbonate</td><td>2.411</td></tr> <tr><td>Biotite</td><td>1.251</td></tr> <tr><td>White mica</td><td>1.501</td></tr> <tr> <td colspan="2">D) Dependant variable: Plagioclase</td> </tr> </tbody> </table>	Constant	VIF	Quartz	1.496	Chlorite	1.01	Sericite	1.208	Epidote	1.523	Amphibole	2.325	Feldspar	3.587	Carbonate	2.411	Biotite	1.251	White mica	1.501	D) Dependant variable: Plagioclase																																															
Constant	VIF																																																																																										
Quartz	4.202																																																																																										
Chlorite	1.568																																																																																										
Carbonate	1.367																																																																																										
Sericite	2.755																																																																																										
Epidote	1.383																																																																																										
Amphibole	2.234																																																																																										
Plagioclase	1.377																																																																																										
Feldspar	4.131																																																																																										
White mica	1.294																																																																																										
D) Dependant variable: Biotite																																																																																											
Constant	VIF																																																																																										
Quartz	1.496																																																																																										
Chlorite	1.01																																																																																										
Sericite	1.208																																																																																										
Epidote	1.523																																																																																										
Amphibole	2.325																																																																																										
Feldspar	3.587																																																																																										
Carbonate	2.411																																																																																										
Biotite	1.251																																																																																										
White mica	1.501																																																																																										
D) Dependant variable: Plagioclase																																																																																											

Figure 5. 9 Variance of inflection factor of all variables prior to PCA

5.5. Results and discussion

5.5.1 Determination of the most important variables

PCA was run first without Varimax rotation technique after data preparation. Initially, extra variables were removed from the initial database in the first run. Then, Varimax rotation was

used in the second run to obtain the maximum loading factor of the important extracted variables. We used the Varimax rotation to rotate the factors to better fit the data and find the maximum loading factor (Mulaik and Cureton, 1975). Thus, ten variables (minerals), namely, quartz, chlorite, carbonate, plagioclase, sericite, feldspar, epidote, white mica, amphibole, and biotite were used in the first run without Varimax rotation technique. These variables were obtained from the assignment of the thin section results to the proposed rock characteristic chart.

The extracted components and their associated eigenvalues and variance are shown in Tables 5.5 and 5.6 for felsic and mafic rocks, respectively. Eigenvalues are the quantities that represent the variance that a principal component can explain. For interpretation, factors with eigenvalues greater than 1 must be retained according to the Latent Root Criterion (or Eigenvalue Criterion) (Meyers et al., 2006). Using this criterion, four components were selected for interpretation. A total of 67% of the variance in the dataset is explained by the four factors; this value is considered acceptable based on a recommended range of 50% to 75% (Tabachnick and Fidell, 1996). The total variance represents the variation introduced by all variables and variance, indicating how much variation is “captured” by the extracted correlations among variables.

Table 5. 5 Eigenvalue and total variance of extracted components for felsic rocks

Component	Initial eigenvalues			Extraction sums of squared loadings		
	Total	% of variance	Cumulative %	Total	% of variance	Cumulative %
1	2.095	29.947	20.947	2.095	20.947	20.947
2	1.822	18.215	39.162	1.822	18.215	39.162
3	1.634	16.341	55.503	1.634	16.341	55.503
4	1.244	12.436	67.943	1.244	12.439	67.943
5	0.961	9.611	77.553			
6	0.737	7.367	84.921			
7	0.648	6.479	91.400			
8	.473	4.731	96.131			
9	0.302	3.024	99.155			
10	0.084	0.845	100			

Table 5. 6 Eigenvalue and total variance of extracted components for mafic rocks

Component	Initial eigenvalues			Extraction sums of squared loadings		
	Total	% of variance	Cumulative %	Total	% of variance	Cumulative %
1	2.105	21.048	21.048	2.105	21.048	21.048
2	1.815	18.146	39.194	1.815	18.146	39.194
3	1.622	16.215	55.409	1.622	16.215	55.409
4	1.250	12.504	67.914	1.250	12.504	67.914
5	0.955	9.550	77.464			
6	0.736	7.358	84.822			
7	0.655	6.550	91.372			
8	0.474	4.744	96.116			
9	0.296	2.957	99.073			
10	0.093	0.927	100			

Tables 5.7 and 5.8 present the factor loading matrix without rotation technique for felsic and mafic rocks, respectively. In PCA, factor loadings, also known as component loadings, indicate

the correlation between variables (rows) and factors (columns). In this study, factor loading was interpreted to highlight the important minerals in our database. A minimum loading number cut-off of 0.32 was considered, following Liu et al. (2003) for the interpretation and extraction of the important minerals.

Table 5. 7 Factor loading number for felsic rocks

	Components			
	1	2	3	4
Quartz	0.917	0.085	-0.250	-0.069
Chlorite	-0.284	-0.181	0.276	-0.039
Carbonate	0.292	0.278	0.127	-0.314
Sericite	-0.427	0.133	-0.193	1.38
Epidote	0.414	0.018	0.289	-0.197
Amphibole	0.002	0.759	0.288	0.299
Feldspar	-0.249	0.726	0.008	-0.045
Plagioclase	0.082	0.132	0.14	0.195
Biotite	0.147	-0.074	0.122	-0.144
White mica	-0.141	-0.165	-0.642	0.221

In felsic rocks (Table 5.7), principal component 1 is positively correlated with quartz and epidote and negatively correlated with sericite. This positive loading number for quartz and epidote confirms the statistical similarities between them. The negative weak correlation of sericite with component 1 suggests its inverse relationship with the other extracted variables. Principal component 2 is well represented by amphibole and feldspar. The positive loading number for amphibole and feldspar confirms that these minerals play an important role in our statistical analysis. Principal component 3 is well represented by white mica but with a negative sign. Principal component 4 has weak correlation with all variables, and its eigenvalue is more than that of the criterion. Thus, this component could not capture the effect of the variables. PCA is mainly used to decrease the number of variables. The results show that some variables could be considered outlier variables. Garnet mineral was removed because it had a constant value in the scatter plot, as shown in Table 5.1. Then, if the minimum cut-off is 0.32, then the principal component 1 suggests that quartz, epidote, and sericite are statistically closely correlated and can be used to represent their effects on the UCS and tensile strength of felsic rock. Amphibole and feldspar were extracted from principal component 2 because these variables are statistically similar. Finally, white mica was determined from principal component 3. In summary, quartz, epidote, sericite, amphibole, feldspar, and white mica were

selected as the important variables for felsic rock, and the remaining variables were removed from the next step of the study. These extracted minerals were considered the most important minerals in the second run of PCA with Varimax rotation.

In mafic rocks (Table 5.8), principal component 1 is positively correlated with quartz, feldspar, and epidote and negatively correlated with chlorite and white mica. Principal component 2 is well represented by amphibole, feldspar, and quartz. Principal component 3 is well represented by epidote and amphibole and principal component 4 has weak correlation with all variables. The extracted variables are the same as those in felsic rocks but chlorite was selected instead of sericite. Therefore, quartz, epidote, chlorite, amphibole, feldspar, and white mica were selected as the important variables for mafic rocks, and the remaining variables were removed from the future steps of the study. The important minerals were used in the second run of PCA with Varimax rotation to obtain the appropriate factor loading index for mafic rock.

Table 5. 8 Factor loading number for mafic rocks

	Components			
	1	2	3	4
Quartz	0.814	0.417	-0.042	-0.158
Chlorite	-0.532	-0.395	0.150	-0.056
Carbonate	-0.222	0.210	0.123	-0.290
Sericite	-0.222	0.210	0.123	-0.290
Epidote	0.515	-0.184	0.565	-0.070
Amphibole	0.220	0.797	0.505	0.249
Feldspar	0.412	0.674	0.168	0.012
Plagioclase	0.154	0.213	0.11	0.24
Biotite	0.197	-0.218	-0.199	-0.089
White mica	-0.365	-0.198	-0.642	-0.150

PCA was rerun using Varimax rotation after removing the outlier variables to obtain the appropriate component loading factor for PCR. Six variables in felsic rock, namely, quartz, epidote, sericite, amphibole, feldspar, and white mica and six variables in mafic rocks, namely, quartz, epidote, chlorite, amphibole, feldspar, and white mica were used in the second PCA with Varimax rotation (Tables 5.9 and 5.10).

Table 5. 9 Eigenvalue and total variance of extracted components for felsic rocks

Total Variance Explained						
Component	Initial eigenvalues			Rotation sums of squared loading		
	Total	% of variance	Cumulative %	Total	% of variance	Cumulative %
1	1.775	25.355	25.355	1.760	25.146	25.146
2	1.547	22.105	47.461	1.505	21.494	46.641
3	1.355	19.362	66.823	1.413	20.182	66.823
4	0.996	15.806	82.629			
5	0.640	9.138	91.766			
6	0.576	8.234	100			

Table 5. 10 Eigenvalue and total variance of extracted components for mafic rocks

Total Variance Explained						
Component	Initial eigenvalues			Rotation sums of squared loading		
	Total	% of variance	Cumulative %	Total	% of variance	Cumulative %
1	2.010	28.709	28.709	1.999	28.563	28.563
2	1.566	22.370	51.079	1.427	20.385	18.949
3	1.217	17.382	68.461	1.366	19.513	68.461
4	0.820	11.712	80.173			
5	0.779	11.141	89.734			
6	0.497	8.686	100			

Three factors account for 67% and 68% of the total variance in the datasets for felsic and mafic rocks, respectively (Tables 5.9 and 5.10). These values are acceptable according to the recommended value between 50% and 75% (Tabachnick and Fidell, 1996).

The factor loading matrix for felsic rocks with Varimax rotation (Table 5.11) indicates that principal component 1 is positively correlated with quartz, feldspar, and epidote and negatively correlated with sericite and white mica. This positive loading number for quartz and epidote confirms the statistical similarities between them; both should be selected as an outcome variable. Principal component 2 is well represented by amphibole and feldspar. The positive loading number for amphibole and feldspar confirms that these minerals play an important role in our statistical analysis. Principal component 3 is well represented by white mica.

Table 5. 11 Factor loading matrix with Varimax rotation for felsic rock

	Components		
	1	2	3
Quartz	0.902	-0.090	0.045
Sericite	-0.582	-0.241	0.108
Epidote	0.545	0.137	0.128
Amphibole	-0.077	0.884	0.184
Feldspar	0.597	0.406	0.215
White mica	-0.727	0.109	-0.461

The factor loading matrix for mafic rocks with Varimax rotation (Table 5.12) shows that principal component 1 is positively correlated with quartz and epidote and negatively correlated with chlorite. Principal component 2 is well represented by amphibole and feldspar. The positive loading number for amphibole and feldspar confirms that these minerals play an important role in our statistical analysis. Principal component 3 is well represented by white mica.

Table 5. 12 Factor loading matrix with Varimax rotation for mafic rock

	Components		
	1	2	3
Quartz	0.880	-0.119	0.180
Chlorite	-0.657	0.021	0.062
Epidote	0.693	-0.094	0.129
Amphibole	-0.180	0.749	0.378
Feldspar	0.314	0.501	0.221
White mica	0.188	0.031	-0.687

The most important minerals in the databases of felsic and mafic rocks and their factor loading were obtained by PCA. The extracted weighting factors were used in PCR, as discussed in the following section.

5.5.2 Determination of the effect of each mineral on UCS and tensile strength of rock

The effects of minerals on UCS and tensile strength of the rock were determined by PCR. The linear regression among the extracted components could be obtained through

Equations (5.1)–(5.6) in Section 5.4.2. Linear regression could be extracted between independent (minerals of the rock) and dependent variables (UCS and tensile strength of the rock). Based on the four UCS and tensile strength values (for felsic and mafic rocks), four separated linear regressions were extracted to find the relationship between the minerals in felsic and mafic rocks and the geomechanical parameters of rock. In the following equations related to the felsic and mafic rocks, Q is quartz (%), Epi is the amount of epidote (%), Ser is the amount of sericite (%), Amp is the amount of amphibole, Feld is the amount of feldspar, and Wm is the amount of white mica. Two lines fit through the extracted components of felsic rocks (Table 5.10), as determined by the following:

$$\text{UCS} = 3.17 (Q) - 1.81 (\text{Ser}) + 0.81 (\text{Epi}) + 0.65 (\text{Amp}) + 0.40 (\text{Felds}) - 1.06 (\text{Wm}), \quad \text{Eq. 5 8}$$

$R^2 = 0.72$

$$\sigma_t = 0.68 (Q) - 0.29 (\text{Ser}) + 0.22 (\text{Epi}) + 0.18 (\text{Amp}) - 0.21 (\text{Felds}) - 0.1 (\text{Wm}), \quad \text{Eq. 5 9}$$

$R^2 = 0.81$

According to the UCS regression line, increasing the amount of quartz could increase the UCS of felsic rocks. Feldspar and amphibole have a similar relationship with UCS. However, their effects are weaker than that of quartz. In comparison, sericite and white mica have negative effect on UCS. The reason is that white mica and sericite are sheet minerals with weak strength; therefore, they could decrease the UCS. This behavior is similar for tensile strength values. Moreover, a notable decrease in UCS associated with sericite and white mica was noted. However, feldspar showed a different behavior in UCS and tensile strength. The value of UCS increases when the amount of feldspar minerals increases as well, but the tensile strength value decreases.

The following linear regression lines present the effect of mafic rock minerals on the UCS and tensile strength of rock.

$$\text{UCS} = 2.56 (Q) - 1.03 (\text{Chl}) + 2.31 (\text{Epi}) + 1.18 (\text{Amp}) + 1.71 (\text{Felds}) - 0.84 (\text{Wm}), \quad \text{Eq. 5 10}$$

$R^2 = 0.76$

$$\sigma_t = 0.49 (Q) - 0.28 (\text{Chl}) + 0.74 (\text{Epi}) + 0.08 (\text{Amp}) + 0.1 (\text{Felds}) - 0.25 (\text{Wm}), \quad \text{Eq. 5.11}$$

$R^2 = 0.81$

Quartz, amphibole, epidote, and feldspar positively affect the UCS of mafic rocks. Chlorite and white mica negatively affect UCS. A similar relationship for tensile strength of the rock is found when the amount of these quartz, epidote, amphibolite, and feldspar

increases.

A comparison of the results between felsic and mafic rocks shows that quartz has a more positive effect on felsic rocks than on mafic rocks. Our results indicate that the presence of quartz in rocks can improve their tensile strength. Interestingly, these results contradict the findings of Merriam et al. (1970), where high-quartz contents show little crystal intergrowth or interlocking, and quartz negatively affects the rock strength. However, more contents of quartz positively affect rock strength. The amphibole mineral presents a more positive effect on mafic rocks than on felsic rocks. Sericite and chlorite have shown the highest negative correlation with felsic and mafic rocks because these minerals reduce rock strength. Sericite and chlorite are secondary minerals and have less strength than primary minerals, such as quartz.

5.6 Evaluation of model performance

Based on a set of 44 samples, the mineralogy and geomechanical test results (19 samples for UCS of felsic rock, 11 samples for UCS of mafic rock, six samples for tensile strength of felsic rock, and eight samples for tensile strength of mafic rock) from the Westwood mine, the proposed models were used to predict the values of UCS and tensile strength by using the developed equation and the results used for evaluating the performance in estimating UCS and tensile strength of the felsic and mafic rock. The root mean square error (RMSE) is used (Eq. 5.19) for the performance analysis of the models. The RSME is used for all four developed models, and the results obtained are illustrated in Table 5.13.

$$RMSE = \sqrt{\frac{\sum_{i=1}^n (\sigma_i^t - \sigma_i^p)^2}{n}} \quad \text{Eq. 5 11}$$

Where σ_i^t and σ_i^p are the *i*th measured and *i*th predicted values, and *n* is the number of datasets.

Table 5. 13 Results of performance analysis of different models

Models	Rock type	R ²	RMSE(MPa)	Test number
Uniaxial compressive strength	Felsic	0.72	18.14	19
Uniaxial compressive strength	Mafic	0.76	19.58	11
Tensile strength	Felsic	0.71	22.31	6
Tensile strength	Mafic	0.81	17.60	8

As shown in Table 5.13, the tensile strength of mafic rocks shows a reasonable RMSE value, which is lower and better than those of the other models. Hence, the highest correlation value ($R^2=0.81$) and lowest RMSE are associated with the tensile strength of the mafic rocks, indicating its strength in predicting the tensile strength of the mafic rock. In terms of UCS prediction, the good model belongs to the felsic rock, which has a lower RMSE than the mafic rock.

5.7 Conclusion

In this article, a methodology was developed to determine the effects of the mineral composition on UCS and tensile strength of rock. A petrographic study was conducted on the representative samples from different drill cores to determine their mineralogy. More than 200 UCS tests were applied on different metamorphosed volcanic rock samples in the laboratory, and 50 Brazilian tests were carried out as well. A random sampling technique called CDF⁻¹ was applied on the database to obtain sufficient data for statistical calculations given the limitation of geomechanical laboratory tests. Then, two multivariable statistical analyses, namely, PCA and PCR, were applied to this dataset. PCA was used to reduce the number of variables from 10 to six by identifying the most important variables in the database and to evaluate the influence of minerals on UCS and tensile strength of the rock.

Our results indicate that quartz and amphibole positively affect UCS and tensile strength of the rock, whereas sericite and chlorite negatively affect UCS. In addition, metamorphic minerals, such as epidote, are associated with weak positive effects on both test values. This study fills a knowledge gap by showing how different minerals or group of minerals, as well as the rock texture have a major influence on rock mechanics. Thus, a rock mass made of distinct lithology with distinct compositions and geological histories cannot be considered a homogeneous rock mass. The composition and mineralogy of a rock mass must be considered when designing underground work in heterogeneous geological environments.

In addition, the proposed methodology could be applied to the study of other rock types to provide a more precise understanding of the influence of minerals and groups of minerals on rock mechanics.

Acknowledgments

The authors would like to thank the Natural Sciences and Engineering Research Council of Canada, IAMGOLD Corporation, and Westwood mine for supporting and funding this research (Grant number: RDCPJ 520428–17).

5.8 References

Åkesson, U., Stigh, J., Lindqvist, J. E., & Göransson, M. (2003). The influence of foliation on the fragility of granitic rocks, image analysis and quantitative microscopy. *Engineering Geology*, 68(3-4), 275-288.

Bell, F. G. (1978). The physical and mechanical properties of the fell sandstones, Northumberland, England. *Engineering Geology*, 12, 1-29.

Bell, F. G., & Lindsay, P. (1999). The petrographic and geomechanical properties of some sandstones from the Newspaper Member of the Natal Group near Durban, South Africa. *Engineering Geology*, 53(1), 57-81.

Cureton, E. E., & Mulaik, S. A. (1975). The weighted varimax rotation and the promax rotation. *Psychometrika*, 40(2), 183-195.

Fahy, M. P., Guccione, M. J. (1979). Estimating strength of sandstone using petrographic thin-section data. *Bulletin of the Association of Engineering Geologists*, 16(4), 467- 485.

Gunsallus, K. T., Kulhawy, F. H. (1984). A comparative evaluation of rock strength measures. In *International Journal of Rock Mechanics and Mining Sciences and Geomechanics Abstracts*, 21, (5), 233-248.

Hugman, R. H. H., & Friedman, M. (1979). Effects of texture and composition on mechanical behavior of experimentally deformed carbonate rocks. *AAPG Bulletin*, 63(9), 1478-1489.

Lippmann-Pipke, J., Erzinger, J., Zimmer, M., Kujawa, C., Boettcher, M., Heerden, E. Bester, A., Moller, H., Stronik, N., & Reches, Z. (2011). Geogas transport in fractured hard rock - Correlations with mining seismicity at 3.54km depth, TauTona gold mine, South Africa. *Applied Geochemistry*, 26(12), 2134–2146.

Liu, R.X. Kuang, J. Gong, Q. and Hou, X.L. (2003), “Principal component regression analysis with spss”, *Computer methods and programs in biomedicine*, 71 (2), 141-147. [https://doi.org/10.1016/S0169-2607\(02\)00058-5](https://doi.org/10.1016/S0169-2607(02)00058-5).

Meng, F., Zhou, H., Wang, Z., Zhang, L., Kong, L., Li, S., Zhang, C., & Hu, S. (2017). Experimental study of factors affecting fault slip rockbursts in deeply buried hard rock tunnels. *Bulletin of Engineering Geology and the Environment*, 76(3),1167–1182.

Merriam, R., Rieke, H. and Kim, Y. C. (1970). “Tensile strength related to mineralogy and texture of some granitic rocks”. *Engineering Geology*, 4 (2), 155-160. [https://doi.org/10.1016/0013-7952\(70\)90010-4](https://doi.org/10.1016/0013-7952(70)90010-4).

Meyers, L.S. Gamst, G. and Guarino, A.J. (2006). “*Applied Multivariable Research Design And Interoperation*, Sage publications, California, USA.

Miskovsky, K., Duarte, M. T., Kou, S. Q., Lindqvist, P. A. (2004). Influence of the mineralogical composition and textural properties on the quality of coarse aggregates. *Journal of Materials Engineering and Performance*, 13(2), 144-150.

Miranda, T., Correia, A. G., & e Sousa, L. R. (2009). Bayesian methodology for updating geomechanical parameters and uncertainty quantification. *International Journal of Rock Mechanics and Mining Sciences*, 46(7), 1144-1153.

Onodera, T.F.; Asoka Kumara, H.M. (1980). Relation between texture and mechanical properties of crystalline rocks. *Bulletin of the International Association of Engineering Geology*, (22), 173-177

Shakoor, A. bonelli, R.E. (1991). Relationship between petrographic characteristics, engineering index properties, and mechanical properties of selected sandstones. *Bulletin of the Association of Engineering Geologists*, 28(1), 55-71.

Shapiro, S. S., & Wilk, M. B. (1965). An analysis of variance test for normality (complete samples). *Biometrika*, 52(3/4), 591-611.

Tapponnier, P., Brace, W. F. (1976, April). Development of stress-induced microcracks in Westerly granite. *International Journal of Rock Mechanics and Mining Sciences and Geomechanics Abstracts*,13 (4), 103-112.

Ündül, Ö. (2016). Assessment of mineralogical and petrographic factors affecting petro-physical properties, strength and cracking processes of volcanic rocks. *Engineering geology*, 210, 10-22.

Tuğrul, A., Zarif, I. H. (1999). Correlation of mineralogical and textural characteristics with engineering properties of selected granitic rocks from Turkey. *Engineering geology*, 51(4), 303-317.

Tabachnick, B.G. and Fidell, L.S. (1996). *Using Multivariable Statistics*, HarperCollins college publishers, New York, USA.

Kolmogoroff, A. (1931). Über die analytischen Methoden in der Wahrscheinlichkeitsrechnung. *Mathematische Annalen*, 104(1), 415-458..

Williams, H., Turner, F. J., Gilbert, C. M. (1982). *Petrography: An introduction to the study of rocks in thin section*. Second edition, W.H. Freeman and company, San Francisco, Book.

Yusof, N. Q. A. M., Zabidi, H. (2016). Correlation of mineralogical and textural characteristics with engineering properties of granitic rock from Hulu Langat, Selangor. *Procedia Chemistry*, 19, 975-980.

Conclusion

The mechanical properties of a metamorphic rock, which largely depend on petrophysical properties, are important parameters that must be considered when rock mass failure is a potential issue in works, such as the drilling of boreholes and wells and extraction of deep ore deposits for example. In general, rock strength is determined by two factors: the nature and condition of the rock itself, which includes its texture, and the factors related to sample preparation and test procedures. The texture features affect the petrophysical and mechanical properties of rocks, including UCS, elastic properties, and tensile strength. Therefore, understanding the interactive effects of rock texture and petrophysical properties on the mechanical properties is crucial.

The research presented in this thesis employed a proposed chart in conjunction with the thin section study to provide a methodology to assess the individual and effects of minerals on the geomechanical parameters of intact metamorphic rock, such as PLI, UCS, and tensile strength. A methodology is developed for creating an enlarged database so that it can be used for statistical analysis based on CDF^{-1} in the case of UCS and tensile strength because of limited original data. Statistical analyses, including PCA and PCR, were used to achieve this work's objectives. The Westwood mine was used as a case study for applying the methodology. The most important findings of this thesis are presented below.

Assessing the effect of metamorphic minerals on axial and diametrical point load index using a new mineral assignment method

- The minerals of mafic and felsic metamorphic rocks were determined by thin section petrographic studies. These minerals are quartz, chlorite, carbonate, sericite, epidote, amphibole, plagioclase, feldspar, biotite, white mica, garnet, apatite, tourmaline, and opaques (mainly oxides and sulfides).
- The following minerals were omitted before running statistical analysis due to insufficient data or having a constant value: garnet, apatite, tourmaline, and opaque minerals.
- PCA could extract the most significant minerals among the database and reduce the number of database minerals from 10 to 7. Garnet, apatite, carbonate, tourmaline, and opaque were removed before running PCA. Carbonate, biotite, and plagioclase were also removed by PCA. Quartz, chlorite, sericite, epidote,

amphibole, feldspar, and white mica were extracted as the main minerals affecting the geomechanical properties of mafic and felsic rocks.

- PCR evaluated the individual effect of the minerals of metamorphic rocks on axial and diametrical PLI.
- Quartz, amphibole, and plagioclase have a positive effect (increase) on the axial and diametrical PLIs of mafic and felsic rocks.
- Sericite and chlorite have a negative effect (decrease) on PLIs.
- Schistosity is an important factor that reduces rock strength, as shown in the axial and diametrical PLIs.
- A comparison of the results between felsic and mafic rocks shows that quartz has a more positive effect on felsic rocks than on mafic rocks.
- The developed methodology (proposed mineralogy chart) could assign the results of the limited thin section study to the all mineralogy of the Westwood mine boreholes which were selected for the point load tests.

Assessing the mineral composition effect on UCS, tensile strength, and PLI

- In the absence of sufficient core samples for the UCS and tensile strength tests, CDF^{-1} was chosen as one of the random sampling methods. By using this method, enough values of UCS and tensile strength can be generated based on the distribution function of both variables.
- A higher quartz content could increase the UCS and tensile strength of felsic rocks. Feldspar and amphibole have a similar relationship with UCS and tensile strength. However, their effects are weaker than that of quartz.
- Sericite and white mica have a negative effect on the UCS and tensile strength of felsic rocks.
- Quartz, amphibole, epidote, and feldspar have a positive effect on the UCS and tensile strength of mafic rocks.
- Chlorite and white mica have a negative effect on the UCS and tensile strength of mafic rocks.
- A comparison of the results between felsic and mafic rocks shows that quartz has a more positive effect in felsic rocks than in mafic rocks.

- This study shows that the generation of random sampling by the inverse of distribution function can be applied when there is insufficient data for geomechanical laboratory tests.
- With regard to RMSE, the regression equation for the tensile strength of mafic rock could predict the strength of the rock better than the other equations.

Perspectives for future research

- Development of the empirical correlation between rock texture and geomechanical parameters of metamorphic rocks.
- Evaluation of the effect of mineralogy and rock texture (grain size, schistosity, anisotropy, ...) on rockburst occurrence.
- Development of empirical / numerical criteria for predicting rockburst in metamorphic rock in Canadian shield.

APPENDIX I: SUPPORTING INFORMATION FOR CHAPTER 4

Table A I. Results of uniaxial compressive strength and Young's modulus of felsic rock

Sample	Unit	Young's Modulus (E) in GPa	Uniaxial compressive strength (σ_c) in MPa	Tensile strength in MPa
1	U4-2-0	81	156.63	22.41
2	2T	68	250.23	15.20
3	2T	43	73.24	11.45
4	U4-2-0	59	90.41	10.28
5	U4-2-0	68	88.4	16.48
6	2T	60	140.54	16.71
7	U4-2-0	74	206.27	-
8	U2-0-0	53	130.75	18.19
9	U2-0-0	73	89.95	21.35
10	2T	75	255.39	16.82
11	U2-0-0	54	118.32	23.12
12	U2-0-0	39	39.89	-
13	2T	53	132.95	8.93
14	2T	42	96.3	14.93
15	2T	79	197.43	21.79
16	U4-3-0	72	172.25	22.72
17	U4-3-0	67	206.89	25.51
18	2T	71	129.86	10.72
19	U4-3-0	71	156	9.21
20	U4-2-0	81	147.8	20.44
21	U4-2-0	70	171.84	23.85
22	U4-2-0	79	167.42	-
23	U4-2-0	-	32.47	-
24	U4-2-0	80	174.4	-
25	U4-2-0	78	234.15	-
26	U4-3-0	71	165.29	20.68
27	U4-2-0	75	151.01	17.31
28	U4-2-0	84	139.15	-
29	U4-2-0	70	120.45	17..17
30	U4-2-0	62	217.9	22.60
31	U4-3-0	86	201.24	28.95

32	U2-0-0	53	92.65	-
33	U2-0-0	70	105.82	-
34	U4-2-0	68	163.9	24.57
35	U4-3-0	60	47.85	-
36	U4-2-0	50	149.82	-
37	U4-2-0	51	152.88	-
38	U4-2-0	57	175.17	-
39	U4-2-0	51	158.14	21.98
40	U4-3-0	61	184.27	23.38
41	U5-1-4	32	92.6	-
42	U5-1-4	40	106.4	-
43	U5-2-1	37	76.5	-
44	U5-2-1	79	130.3	-
45	U5-2-1	71.8	145	-
46	U4-3-0	57.4	152	-
47	U4-3-0	86.6	127	-
48	U4-3-0	62.8	143	-
49	U4-3-0	51.2	88	-
50	U4-3-0	58.5	116	-
51	U4-3-0	58.9	80	-
52	U4-3-0	36.4	79	-
53	U4-3-2	65.3	173	-
54	U5-1-4	53.8	94	-
55	U5-1-4	53	126	-
56	U2-0-0	57.4	170	-
57	U4-3-0	79.5	147	-
58	U4-3-0	53	133	-
59	U4-2-0	42	96	-
60	U2-0-0	53	131	-
61	U2-0-0	73	90	-
62	U4-2-0	75	255	-
63	U2-0-0	54	118	-
64	U2-0-0	39	40	-
65	U4-2-0	81	157	-
66	2T	68	250	-
67	2T	43	73	-
68	U4-2-0	59	90	-
69	U4-2-0	68	88	-
70	2T	60	141	-

71	2T	71	130	-
72	U4-3-0	71	156	-
73	U4-3-0	66	166	-
74	U4-2-0	74	206	-
75	U4-2-0	79	197	-
76	U4-3-0	72	172	-
77	U4-2-0	67	207	-
78	U4-2-0	81	148	-
79	U4-2-0	70	172	-
80	U4-2-0	79	167	-
81	U4-2-0	80	174	-

Table A II. Results of uniaxial compressive strength and Young's modulus of mafic rocks

Sample	Unit	Young's Modulus (E) in Gpa	Uniaxial compressive strength (σ_c) in MPa	Tensile strength in MPa
1	U3-3-1	71	101.92	23.37
2	U3-3-0	77	184.68	16.42
3	U4-4-1	83	109.059	2.98
4	U5-4-0	78	144.46	18.03
5	U4-4-0	83	118.85	17.86
6	U4-4-0	51	108.41	17.54
7	U4-4-0	58	122.86	14.73
8	U5-4-0	76	205.38	24.26
9	U1-1-0	82	145.01	26.24
10	U1-1-0	77	191.12	21.32
11	U1-1-0	67	175.79	15.80
12	U4-4-1	97	241.11	21.81
13	U4-4-1	97	159.01	17.30
14	U3-3-1	32	119.84	15.43
15	U3-3-1	55	131.93	16.20
16	U3-3-1	85	202.73	12.98
17	U4-4-0	94	113.09	18
18	U4-4-0	-	82.77	11.66
19	U3-3-1	69	142.61	19.27
20	U3-3-1	105	92.02	16.98
21	U3-3-1	85	160.05	17.93
22	U4-4-0	62	49.46	16.51

23	U3-3-1	64	77.42	20.49
24	U3-3-1	86	196.57	14.50
25	U3-3-1	77	200.98	-
26	U3-3-1	74	110.86	-
27	U4-4-0	80	176.09	-
28	U4-4-0	70	266.19	-
29	U4-4-0	64	156.42	-
30	U4-4-1	75	115.89	-
31	U5-4-0	37	112.1	-
32	U5-4-0	47	118.9	-
33	U5-1-3	68	197.9	-
34	U5-1-3	72	222.6	-
35	U5-1-3	75	68.9	-
36	U4-3-0	108	186	-
37	U1-1-0	101	329	-
38	U1-1-0	109	354	-
39	U5-1-3	71	179	-
40	U5-4-0	36	100	-
41	U5-4-0	83	139	-
42	U4-4-0	89	139	-
43	U3-3-1	54	123	-
44	U4-4-0	54	105	-
45	U4-4-0	117	119	-
46	U4-4-0	74	104	-
47	U4-4-0	46	95	-
48	U4-4-0	51	122	-
49	U5-1-1	62	89	-
50	U5-1-1	67	63	-
51	U3-3-0	91	125	-
52	U4-4-0	87	80	-
53	U4-4-0	118	108	-
54	U4-4-0	120	162	-
55	U4-4-0	101	95	-
56	U4-4-0	59	266	-
57	U4-4-0	74	197	-
58	U4-4-0	72	142	-
59	U5-1-3	68	103	-
60	U5-1-3	64	121	-
61	U5-4-0	21	117	-

62	U1-1-0	63	164	-
63	U3-3-0	15	51	-
64	U3-3-0	43	149	-
65	U4-4-0	68	208	-
66	U1-1-0	29	128	-
67	U4-4-0	12	46	-
68	U3-3-1	32	120	-
69	U3-3-1	55	132	-
70	U1-1-0	82	145	-
71	U1-1-0	77	191	-
72	U1-1-0	67	176	-
73	U3-3-1	71	102	-
74	U3-3-0	77	185	-
75	U3-3-1	85	203	-
76	U4-4-0	83	119	-
77	U4-4-0	51	108	-
78	U4-4-0	58	123	-
79	U4-4-1	83	109	-
80	U5-4-0	78	144	-
81	U5-4-0	76	205	-
82	U4-4-1	97	241	-
83	U4-4-1	97	159	-
84	U4-4-0	94	113	-
85	U3-3-1	69	143	-
86	U3-3-1	105	92	-
87	U3-3-1	85	160	-
88	U4-4-0	62	49	-
89	U3-3-1	64	77	-
91	U3-3-1	86	197	-
92	U3-3-1	77	201	-
93	U3-3-1	74	111	-
94	U4-4-0	80	176	-
95	U3-3-1	24	64	-
96	U4-4-0	52	113	-
97	U4-4-0	48	116	-
98	U4-4-1	39	92	-
99	U4-4-0	70	266	-
100	U4-4-0	50	142	-
101	U4-4-0	44	83	-

102	U4-4-0	64	156	-
103	U4-4-1	75	116	-
104	U4-4-0	51	131	-
105	U4-4-0	60	153	-
106	U4-4-0	67	246	-
107	U4-4-0	106	186	-
108	U4-4-0	69	140	-
109	U4-4-0	70	118	-
110	U4-4-0	65	96.6	-
111	U4-4-0	40	78.2	-
112	U4-4-0	58	133.8	-
113	U4-4-0	39	92.9	-
114	U4-4-0	87	190	-
115	U4-4-0	77	190	-
116	U4-4-0	74	199	-
117	U4-4-0	89	129	-
118	U4-4-0	62	135.7	-
119	U4-4-0	42	74.14	-
120	U4-4-0	76	139	-
121	U4-4-0	73	69	-
122	U5-1-3	68	198	-
123	U5-1-3	72	223	-
124	U5-1-3	75	69	-
125	U5-4-0	37	112	-
126	U5-4-0	47	119	-
127	U5-4-0	31	66	-
128	U5-4-0	35	64	-
129	U4-4-1	102	271	-
130	U4-4-1	49	106	-
131	U4-4-0	80	136	-
132	U4-4-0	75	254	-
133	U4-4-0	68	115	-
134	U4-4-0	65	117	-
135	U4-4-0	68	150	-
136	U5-1-3	58	98	-
137	U4-4-0	71	165	-
138	U4-4-0	70	149	-

LIST OF PUBLICATIONS

JOURNAL PAPERS

1. Askaripour M, Saeidi A, Rouleau A, Mercier-Langevin P., (2022) Rockburst in underground excavation, A review of mechanism, classification and prediction methods., **Underground space.**, (Online Published).
2. Askaripour, M., Saeidi, A., Mercier-Langevin, P., Rouleau, A. (2022). A Review of Relationship between Texture Characteristic and Mechanical Properties of Rock. **Geotechnics**, 2(1), 262-296.
3. Askaripour M, Saeidi A, Rouleau A, Mercier-Langevin P, Seyifaddini M., Evaluation of the effect of mineralogy on the point load compressive strength of the rock, **Geomechanics and Engineering** (Under journal review).
4. Askaripour M, Saeidi A, Rouleau A, Mercier-Langevin P., Effects of mineral composition on geomechanical parameters of hydrothermally altered volcanic rocks, **International Journal of Mining Science and Technology** (Submitted).

CONFERENCE PAPERS

1. Askaripour M, Saeidi A, Rouleau A, Mercier-Langevin P. Effect of metamorphic rock mineralogy on the point load index. GeoCalgary 2020.